Redundancy of Twin Steel Box Girder Bridges

Final Report

Mohammad Abedin
Armin Mehrabi
Atorod Azizinamini

Department of Civil and Environmental Engineering
Florida International University
Miami, Florida

Michel Ghosn
City College of New York

Andy Nowak
Anjan Ramesh Babu
Auburn University

Disclaimer

Technical Report Documentation Page

1. Report No.	2. Government Accession No.	3. Recipient's Catalog No.
4. Title and Subtitle **Redundancy of Twin Steel Box Girder Bridges**		5. Report Date January 2021
		6. Performing Organization Code
7. Author(s) Armin Mehrabi Michel Ghosn Atorod Azizinamini Andy Nowak Mohammad Abedin Anjan Ramesh Babu		8. Performing Organization Report No.
9. Performing Organization Name and Address Department of Civil and Environmental Engineering Florida International University, Miami, FL 33174. Department of Civil Engineering The City College of New York, New York, NY 10031. Department of Civil Engineering Auburn University, Auburn, AL 36849.		10. Work Unit No. (TRAIS)
		11. Contract or Grant No. BDV29-977-40
12. Sponsoring Organization Name and Address FDOT Research Center Phone: (850) 414-5260 605 Suwannee Street Tallahassee, Florida 32399-0450 Email: research.center@dot.state.fl.us		13. Type of Report and Period Covered Final Report: January 2018-January 2021
		14. Sponsoring Agency Code
15. Supplementary Notes		

16. Abstract

Currently, twin steel box girder bridges (TSGB) are classified as bridges with fracture critical members. Recent research results, however, demonstrated a high level of internal redundancy. The main question as to what load levels and performance measures established on a scientific basis should be used still remains unanswered. The objective of this project is to establish a design target performance and safety level for TSGB, and outline an approach for assessing the redundancy. For the purpose of this study, a simply supported single-span bridge tested at the University of Texas with a span length of 120 ft was selected as a baseline model. Weigh-in-motion data in the state of Florida was used to develop a live load model. A detailed finite element model was developed and validated to investigate the failure mode and capacity. The results showed that concrete deck bending is the dominant failure mode after a fracture occurs in one girder in the bridge. Using these results, a simple and unified yield line analysis method was developed to determine the bridge deck capacity. Furthermore, a simplified reliability analysis approach was developed to estimate the minimum criteria that the deck and intact girder should satisfy in order to ensure redundancy; that is, the bridge can carry safely a minimum level of load after a fracture in one girder until the next inspection. This analysis developed and tabulated a set of reliability indexes that could be translated to redundancy expectation based on the various levels of live load expected on the bridge between inspection intervals.

17. Key Words Twin Steel Box Girder Bridge; Fracture Critical, Redundancy, Reliability, Finite Element Analysis, Notional Bridge		18. Distribution Statement No Restriction	
19. Security Classification Unclassified	20. Security Classification (of this page) Unclassified	21. No. of Pages 172	22. Price

Executive Summary

In steel girder bridges, fatigue cracking is one of the most important phenomena affecting structural performance and integrity. In general, fatigue cracks are the result of out-of-plane distortion or other unanticipated secondary stresses at low fatigue resistance members. Development of fatigue cracking may lead in time to a full-depth fracture of one girder without noticeable bridge profile changes. It is critical to ensure that the bridge will have adequate capacity to prevent collapse until the next cycle of inspection discovers the damage. Bridges that a failure in an individual member could result in the total collapse of the structure are classified as fracture critical by AASHTO. It is required that inspection of these bridges be carried out using an "arm's length" approach, which is costly and is a drain on the state's total bridge budget.

Currently, twin steel box girder bridges are classified as bridges with fracture-critical members. However, recent research results indicate that these bridges could be redundant because of their high torsional resistance even after a full-depth fracture of one girder. The most notable study is the series of full-scale tests carried out by the University of Texas-Austin that demonstrated a high level of internal redundancy of twin steel box girder bridges. The main question as to what load level should be used and established using a scientific approach still remains as a task to be accomplished. Further, many questions remain regarding the expected failure mode of the damaged twin steel box girder bridges and the methods for assessing the bridge performance, before these bridges could be removed from the non-redundant list. An upcoming specification developed by Purdue researchers establishes a set of requirements for redundancy of twin steel box girder bridges that could be considered at the design stage to assure redundancy. This specification applies only to bridges with continuous spans.

The objective of this project was to establish a design target performance and safety level for twin steel box girder bridges, and outline a methodology and approach for assessing the redundancy of these bridges of simple and continuous spans. The Florida Bridge Inventory was statistically analyzed to determine the available range of each functional and geometric parameter like span length, number of spans, number of lanes, deck width, and radius of curvature in existing twin steel box girder bridges, and at the end, the bridge tested at the University of Texas with the span length of 120 ft was selected as a baseline model for developing information for preliminary reliability analysis of twin steel box girder bridges. Furthermore, weight-in-motion (WIM) data from 32 stations collected throughout four years (2013-2016) in the state of Florida was used to develop a live load model the bridge would be subjected to during a two-year inspection interval. The data left after filtering out vehicles less than 20-kip gross vehicle weight (GVW) were used for further analysis.

Since the controlling criteria in the design are the load effects, i.e., moment and shear created by vehicles. Each vehicle in the database was run over an influence line for the considered span length of 120 ft, and moment and shear were calculated. For a better interpretation of results, the moment

and shear produced by each vehicle were divided by the corresponding load effects of the HS-20 design truck. It was assumed that 32 WIM stations in Florida have representative truck traffic for Florida. The statistical parameters of mean maximum and coefficient of variation (CV) of live load (moment) were presented and were used for reliability analysis calculations.

A detailed finite element model was developed to simulate the local and global behavior of bridge superstructure using steel girder made composite with concrete deck slabs. The model was validated with a series of available test results on full-scale and scaled bridges. These included the full-scale University of Nebraska bridge consisting of three I-shaped steel girders, and the FIU scaled twin steel box girders. The finite element models were shown to simulate very well both the global and local behavior of the tested bridges in their intact condition as well as after one girder fracture (FIU Bridge). The University of Texas bridge was then modeled to investigate the failure mode and ultimate load-carrying capacity of the bridge subjected to truck loading after a full-depth fracture in one of the girders. Material nonlinearity and concrete damage plasticity were used to consider tensile cracking and compressive crushing of the concrete deck in the model. Contact surface was used to define the surface contact between the railings and also to consider the possibility of support uplift during the loading. Moreover, according to the results of available tests and analyses, shear studs between girders and deck slab may influence the onset of failure in the deck, and therefore, shear studs were also modeled. A large number of analyses were performed on this bridge chosen as a case study for reliability analysis.

Three tests were conducted by the University of Texas on the full-scale bridge. The first test was performed to evaluate the behavior of the bridge under loading simulated by the weight of concrete blocks (slightly over HS-20 loading and equal to 76 kips total) after a sudden fracture at the bottom flange of the exterior girder. The second test was conducted by cutting the bottom flange and 83% web of the exterior girder to study the fractured bridge behavior under the same loading as Test 1. And finally, the ultimate load test was performed to investigate the ultimate load-carrying capacity of the fractured bridge. The ultimate test was performed by increasing a uniform load applied using sand over the HS-20 truck outline area until the bridge collapsed. The finite element model was validated against these available experimental test results conducted by the University of Texas, as shown in Figure- I. In addition to global behavior, the model was capable of simulating the local behavior, including the development of the deck yield line pattern shown in Figure- II.
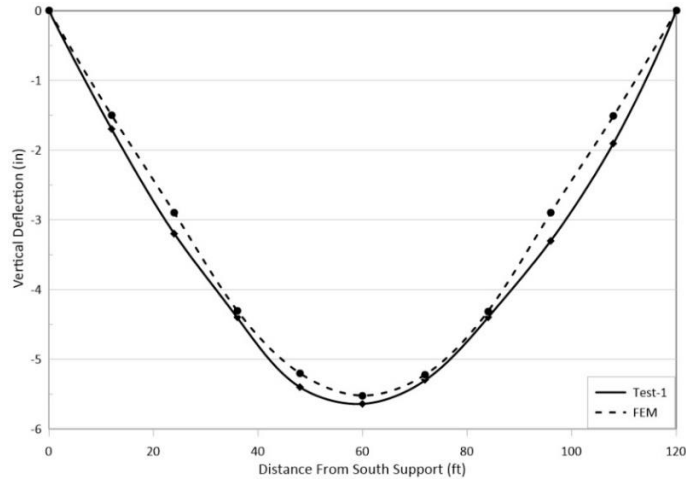
Figure- I. Comparison of the deflection curve of the first test for fractured girder obtained from experiment and FE model.
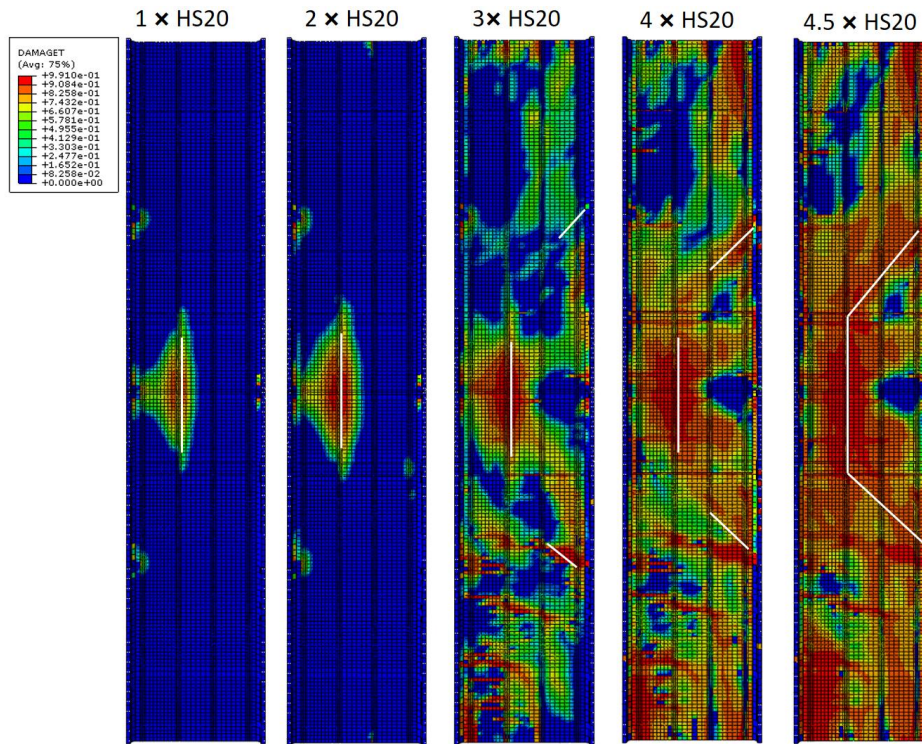
Figure- II. The yield line pattern of the deck subjected to increasing live load in the Finite Element Model. (white lines are added to reflect the idealized yield lines used in simple analysis).

After verification of the FE model, the bridge was analyzed for two scenarios of the intact and fractured bridge. The bridge was loaded in terms of an HS-20 design truck positioned at the mid-span over the fractured girder to generate maximum moment at the section with fracture (one-lane loading). In order to study the effect of truck position on the failure mode and the ultimate load-carrying capacity, the HS-20 truck was positioned in four different locations across the bridge width. The results showed that concrete deck failure is the governing failure mode of the fractured

vi

bridge subjected to truck loading at different positions. The sensitivity analysis indicated that one-way shear is the bridge failure mode when the truck is positioned closest to the intact girder, and concrete deck bending is the bridge failure mode when the truck position transversely is farthest from the intact girder. Nevertheless, the truck position at farthest from the intact girder with the concrete deck bending failure resulted in the lowest bridge load carrying capacity and was considered as the dominant failure mode.

In order to consider the effect of variation in bridge configurations and material properties, as well as truck loading configuration on the bridge failure mode, a sensitivity analysis for the deck concrete compressive, deck thickness, and truck configuration was conducted. Different concrete compressive strengths and deck thicknesses varying from 4 ksi to 6.2 ksi and 7.5 in. to 8.5 in., respectively, and three trucks with loading configurations other than the HS-20 truck were selected for this purpose, as shown in Figure- III. The C5 truck (80 kips; 36 feet long) is longer and heavier than the HS-20 design truck configuration, and the EV3 truck (86 kips; 19 feet long) that creates larger longitudinal and transverse bending moment in the bridge were selected as Florida legal and emergency vehicles. Moreover, WIM data in the state of Florida were also used for selecting a typical truck, which creates a larger moment and shear for a 120-ft simple span bridge. The selected truck, which is called here WIM Data-FL, has a gross vehicle weight of 120 kips distributed over seven axles (Class 13 based on FHWA vehicle category classification).

The results showed that variation in material properties and truck loading configuration would not change the dominant mode of failure for the twin steel box girder bridge considered in this study after a fracture in one girder. Therefore, to simplify the process and avoid the need for FE analysis for each loading case, a simple and unified yield line analysis was developed to determine the bridge load-carrying capacity subjected to different truck configurations, based on the concrete deck damage pattern observed in the FE analysis, as shown in Figure-IV. This model is an improvement to a model proposed earlier by the University of Texas that was developed based on limited test and analysis results. In this newly proposed pattern, the truck is positioned closest to the railing, where its center of gravity coincides with the mid-span over the fracture. The length of the longitudinal yield line (b) is considered equal to the truck length. To find the angle of the diagonal lines (α in Figure- IV), a parametric analysis was conducted to find an angle that results in capacity in agreement with patterns and capacity obtained from FE analysis. The results show that the simplified method with 35º gives the best average capacity ratio compared to the FE analysis. This unified pattern, however, provides a conservative estimate of the deck capacity when compared to the values obtained from nonlinear finite element analysis.
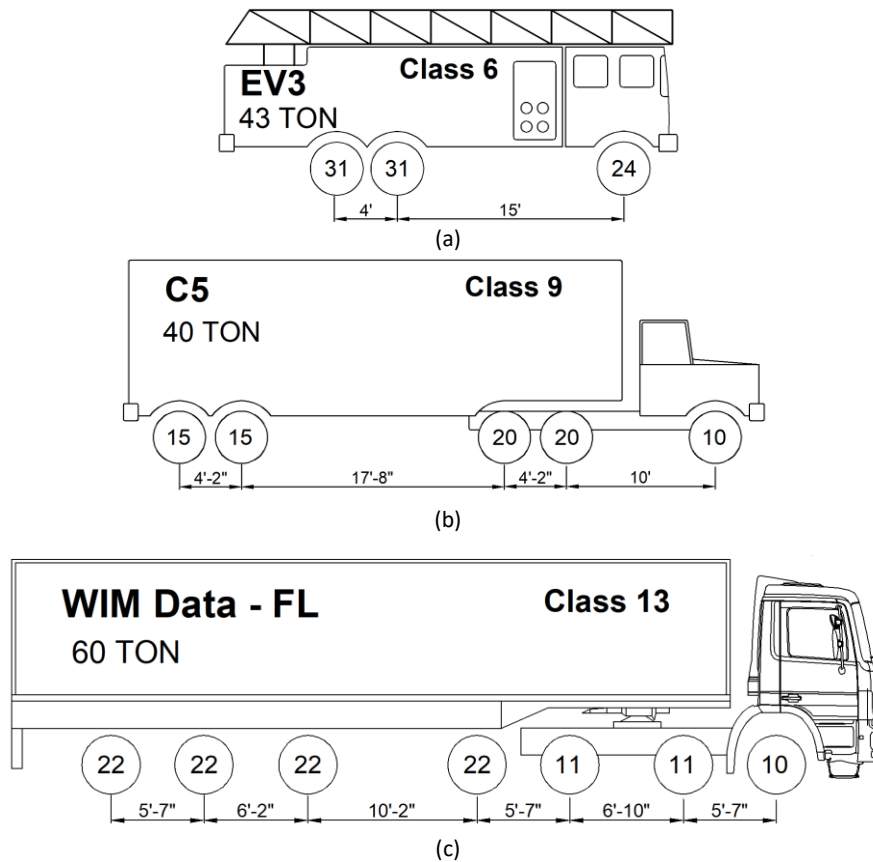
Figure- III. Vehicle loading configuration. (a) Florida Emergency Vehicle (EV3); (b) Florida legal load (C5); (c) Florida typical truck (WIM Data –FL).
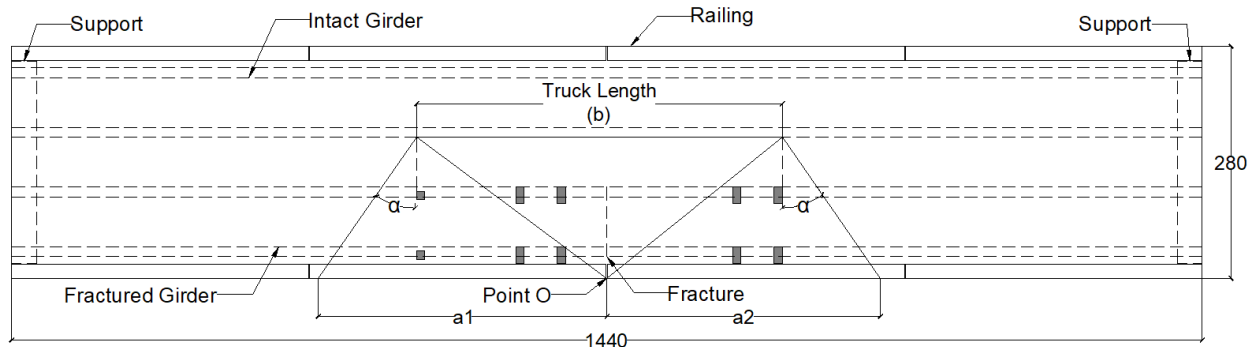

Figure- IV. Simplified yield line pattern for different loading configurations.

Moreover, a series of analyses were conducted on the bridge to investigate the behavior of the bridge in intact and damaged scenarios under dead and increasing live load. The goal was to determine the distribution of dead and live loads before and after the fracture of one girder. According to the results, the dead load moment on the intact girder increases by about 50 percent once a fracture occurs. The fractured girder has a very small stiffness at the middle (one can assume hinge or very weak spring), so it attracts only a negligible moment compared to the intact girder. The live load moment analysis for the intact bridge shows that the left girder (loaded) carries 60%,

and the right girder carries 40% of the live load. However, after the fracture, the right girder (intact) carries most of the live load (66%) because of a decrease in stiffness of the fractured girder. Nevertheless, the fractured girder is undamaged through most of its length. Because a truck's load is applied through its wheel footprint, and rear and front wheels are at a distance from the middle, the fracture girder can transfer some portion of live load (34%) through those segments as a cantilever beam. Unlike the live load, the dead load is distributed along the bridge, and the fractured girder is able to transfer a noticeable portion through its undamaged end segments.

A simplified reliability analysis of a twin steel box girder bridge superstructure and its deck was presented to estimate the minimum criteria that a deck should satisfy in order to ensure that it can transfer a minimum level of load between the box girders when one of the girders sustains a severe fracture. The recommendation was made based on meeting a reliability index target, β_{target}=2.5 over a five-year service period. In addition, a list of live load factors was provided for different target reliability levels for the case of the two-year service period. The calculations were performed assuming that the load-carrying capacity of the deck was modeled using the yield line analysis approach presented in this study that provides a conservative estimate of the deck capacity compared to FE analysis. Nevertheless, lacking any additional data, it is herein assumed that the yield line analysis would be applicable for the most heavily loaded trucks that could potentially cross a Florida twin steel box girder bridge that has sustained a severe fracture to one of its box girders. In addition to applying the recommended live load factor, the yield line analysis implies the application of a dynamic amplification factor IM=1.33, a dead load factor γ_{DL}=1.25 and a moment resistance factor for the concrete deck equal to ϕ=0.9.

A reliability analysis was carried out to estimate the reliability index corresponding to various live load levels based on the simplified yield line bending failure of the deck only. The results are presented in Table- I. The analysis of the bridge deck for the 120-ft bridge studied in this report, therefore, indicates that the bridge deck in its current configuration and concrete strength and ignoring the possible contribution of the railings to help carry some of the load will fail at a live load factor γ_{LL}=1.71 when the deck's concrete strength is set at f'$_c$=6.23 ksi as determined from the tests. This indicates that its reliability index is on the order of β=2.0 for a five-year service period, or slightly higher than that for a two-year service period. However, For the bridge to provide sufficient reliability to sustain the possible fracture of one of its two-box girders, it is important that the remaining box girder has sufficient load carrying capacity to withstand the entire live load that may cross the damaged bridge with one fractured box. This can be ensured if the bridge's box girders outside of fracture can satisfy a minimum rating factor.

Target Reliability index	5-year live load factor, γ_{LL}	2-year live load factor, γ_{LL}
3.50	2.69	2.61
3.00	2.32	2.26
2.50	2.00	1.94
2.25	1.85	1.79
2.00	1.71	1.65
1.50	1.44	1.39
1.00	1.21	1.16

The analysis of fractured bridges was repeated for two scenarios. The first scenario assumes that the fractured bridge will still be able to carry its own dead weight but transfers all the live load to the intact girder. The second scenario assumes that the load distribution follows the nonlinear FE analysis conducted in this study that the bending moment of the intact girder will increase by 50% under dead load, and 66% of the live load in the lane over the fractured girder will transfer to the intact girder. Based on the assumed scenarios, Tables II and III show the LRFR Inventory Rating Factors required for the box girder members to ensure that the bridge will be able to sustain the fracture of one box girder and yet be able to support sufficient live loading over a two-year or a five-year service period until the damage is detected. The results show that an LRFR Inventory Ratings on the order of R.F.=1.28 to 1.33 and R.F.= 1.34 to 1.38 are required for scenarios I and II, respectively, to meet a target reliability index β_{target}=2.50 should one of the two box girders fracture.

Target Reliability index, β_{target}	R.F. Inventory Rating for 5-year service life	R.F. Inventory Rating for 2-year service life
3.50	1.73	1.67
3.00	1.52	1.46
2.50	1.33	1.28
2.25	1.24	1.19
2.00	1.16	1.11
1.75	1.07	1.03
1.50	1.00	0.96
1.25	0.92	0.89
1.00	0.85	0.82

Table- III. LRFR inventory rating factors for box girders necessary for fractured bridge to meet different target reliabilities based on the second scenario.

Target Reliability index, β_{target}	R.F. Inventory Rating for 5-year service life	R.F. Inventory Rating for 2-year service life
3.50	1.74	1.69
3.00	1.55	1.51
2.50	1.38	1.34
2.25	1.30	1.27
2.00	1.23	1.19
1.75	1.15	1.12
1.50	1.08	1.05
1.25	1.01	0.98
1.00	0.95	0.92

The bridge analyzed in this study has an LRFR Inventory Rating of R.F.=2.05. Thus, the intact box girder is capable of sustaining a significant level of live loads as well as a large proportion of the dead loads that were originally carried by the fractured girder, and that the bridge failure is definitely expected to be due to the failure of the deck as explained earlier. It should be noted that in simple span steel bridges, service limit states are normally the governing design limit states, and the strength LRFR Inventory Rating is considerably greater than one and in the order of the bridge considered in this study.

TABLE OF CONTENTS

List of Figures

List of Tables

Chapter 1   Background Statement

In steel girder bridges, fatigue cracking is one of the most important phenomena affecting structural performance and integrity [1]. In general, fatigue cracks are the result of out-of-plane distortion or other unanticipated secondary stresses at low fatigue resistance members. Development of fatigue cracking may lead in time to a full-depth fracture of one girder without noticeable bridge profile changes. It is critical to ensure that the bridge will have adequate capacity to prevent collapse until the next cycle of inspection discovers the damage. Investigations on the bridge collapses show that a failure in an individual member could result in the total collapse of the structure [2].

According to the American Association of State Highway Transportation Officials (AASHTO LRFD Bridge Design Specifications) [3], "Fracture Critical members (FCMs) are steel tension members or steel tension components of members whose failure would be expected to result in the collapse of the bridge." It is required that inspection of these bridges be carried out using "arms-length" approach, which is costly and is a drain on the State's total bridge budget [4, 5]. Currently, twin steel box girder bridges are classified as bridges with fracture critical members. Specifically, the tension bottom flange in the twin steel box girder bridges is categorized as a fracture critical element. Inspection of tension bottom flanges over a busy roadway is costly, time-consuming, and causes traffic disruption and potential safety hazards. It may also take the inspectors as long as two years to detect the fracture, rendering the bridge potentially unsafe for a long duration [6, 7].

Studies on the fracture critical bridges indicate examples of steel bridges that survived even after a full-depth fracture in one of the girders [8]. The results demonstrated a high level of internal redundancy and secondary load paths in the bridge systems that have not been considered in the design procedure [9–16]. The US-52 bridge over the Mississippi River, the Neville Island bridge on I-79 in Pittsburgh, and the Brandywine River bridge on I-95 in Wilmington are examples of bridges with a full-depth fracture in one of the girders that remained in service with a static deflection [17, 18].

Recent research results indicate that twin steel box girder bridges could be redundant because of their high torsional resistance even after a full-depth fracture of one girder. The most notable study is the series of full-scale tests carried out by the University of Texas-Austin [19, 20] that demonstrated a high level of internal redundancy of twin steel box girder bridges. A study carried out by HNTB on the two box girder structures in the Marquette Interchange, through non-linear numerical analysis, also demonstrated the high level of internal and structural redundancy of twin steel box girder bridges [21]. NCHRP project 12-87 [11] includes an objective, "(1) develop a methodology to quantify when a steel bridge system is considered FC based on loads, existing conditions, material properties, and bridge configurations, and (2) recommend AASHTO specifications using the methodology in the design of new bridges and the evaluation of existing

bridges". NCHRP 12-87 has recently developed a series of recommendations and requirements for twin steel box girder bridges to be considered non-fracture critical.

The main question as to what load level should be used and established using a scientific approach still remains as a task to be accomplished. Further, many questions remain on the level of performance expected from damaged twin steel box girder bridges and behavior in between inspection cycles before twin steel box girder bridges could be removed from the non-redundant list. Additional efforts are spearheaded by Texas DOT for the use of "simple" method to assess the redundancy of twin steel box girder bridges, which oftentimes are difficult to meet because of the level of conservatism involved. It is, however, promising that FHWA has been more receptive to the idea of removing twin steel box girder bridges from the non-redundant list. There will be some complementary and overlap among the ongoing two limited studies cited above and this project. This should provide a more compelling reason for FHWA and more credible justifications and verifications to consider removing twin steel box girder bridges from the non-redundant list. In conclusion, this study, with the composition of the research team assembled, will be very influential in resolving this long-standing and challenging issue, namely the redundancy of twin steel box girder bridges.

An additional relevant project related to twin steel box girder bridges is a limited numerical study being carried out at Purdue University with limited funding provided by the National Steel Bridge Alliance (NSBA). To date, this study has analyzed a few twin steel box girder bridges and has developed automated meshing that could be used in conjunction with detail three-dimensional non-linear finite element analyses.

The most comprehensive recent study is a project performed at Florida International University and sponsored by Florida Department of Transportation entitled "Managing Florida's Fracture Critical Bridges - Phases I & II," FDOT Research Project Number BDV29-977-17 [22]. These extensive experimental, field testing, numerical and analytical studies have shown that a high level of redundancy exists in twin steel box girder bridges. Major conclusions from this study include:

a) Twin steel box girder bridges have a capacity after the complete fracture of the tension flange on one girder
b) Punching shear capacity of the deck is the weak link. Results of FDOT sponsored work indicates that damaged twin steel box girder bridges do not have the mechanism to transfer high wheel loads below the deck, and punching shear of the deck will take place before any other failure type. We should also note that very seldom the bridge sees loads that are designed for, and almost impossible to see the kind of wheel loads that would result in a failure. This important observation is completely absent in recent works conducted by Texas, NCHRP, or Purdue work.

What remains to be accomplished is to take advantage of existing knowledge and conduct the necessary additional work to fill in the knowledge gap and develop a sound methodology, approach, and tools that State DOTs could use to evaluate redundancy of twin steel box girder bridges and eliminate them from the fracture critical list.

The existing guidelines in the AASHTO LRFD Bridge Design specification as well as the June 20, 2012 memorandum (FHWA is in the process of issuing an update on this memorandum) issued by FHWA and very recent discussions with FHWA, and the recently completed NCHRP 12-87 research project allows and provides a roadmap for assessing the redundancy of twin steel box girder bridges.

The commentary for Section 6.6.2 of the *AASHTO LRFD Bridge Design Specifications* provides general guidelines that can be used to evaluate the performance of bridges with Fracture Critical members. The challenge in evaluating redundancy of the twin steel box girder bridges is that it is implied that each bridge in the State inventory should be analyzed individually before it can be removed from the fracture critical list. In this study, the notional bridge approach will be used, as explained later.

Chapter 2   Project Objectives

The objective of this project is to establish a design target performance and safety level for twin steel box girder bridges, outline a methodology and approach for assessing the redundancy of the twin steel box girder bridges, assess the redundancy of a bridge using the recommended approach, and summarize the findings to present the results to FHWA.

For establishing bridge loading and response criteria, and minimum acceptable methods and requirements for analysis, a series of tasks as per the original proposal were conducted and deliverables were submitted as separate reports for each task. This Final Report compiles all previous reports in an organized manner supplemented by Executive Summary and Summary and Discussions.

Chapter 3   Development of "Equivalent" or Notional Twin Steel Box Girder Bridge

The FDOT sponsored project performed earlier by FIU has developed a preliminary approach to develop an "Equivalent" simple or continuous span bridge that could represent a series of twin steel box girder bridges. This approach and conceptual steps for developing a notional bridge are summarized as follows.

The most reliable method for checking the redundancy of twin steel box girder bridges is conducting a detailed nonlinear finite element model and checking the critical limit states and the minimum load levels that bridges can carry before these limit states are reached. However, checking the redundancy of all twin steel box girder bridges within the inventory of a given state requires a significant amount of financial, labor, and computer recourses. Moreover, future bridges may have different characteristics than the current bridges, and their redundancy needs to be evaluated by developing a new finite element model.

The notional approach proposed by the earlier FIU study suggested reducing the level of efforts by subdividing all twin steel box girder bridges within the state inventory into several groups based on their main characteristics, and developing a notional simple or continuous span twin steel box girder bridge that would represent each group. By evaluating the redundancy of the notional bridge using a detailed nonlinear finite element model, all bridges within the group under consideration can also be evaluated. Moreover, the redundancy of any new bridge can be evaluated by comparing its characteristics to the presented notional bridges.

The grouping criteria are determined based on the geometrical characteristics of the bridge, including the type of bridge, designed lane-load number, maximum span length, number of spans, radius of curvature, and cross-section. Based on these factors, bridges of interest can be categorized into several groups. Once select bridges are categorized into groups, a notional bridge model that can represent all the bridges within each group needs to be developed.

By developing a calibrated finite element model for the notional bridge representing each group, the analysis results such as the ultimate load-carrying capacity and maximum deflection can be calculated to check against redundancy criteria. As a result, if the notional bridge model satisfies the redundancy criteria and is classified as redundant, all the bridges within that group will also be categorized as redundant. If the criteria are not satisfied, bridges in that group can be divided into smaller subgroups, and the process to find a group that meets the redundancy criteria can be repeated. This approach has the potential ability to classify all the bridges into redundant or non-redundant groups.

3.1 Florida Bridge Inventory

At the request of FIU researchers, FDOT Research Office provided an inventory of steel box girder bridges in the state of Florida. As it was stated earlier, the functional and geometric parameters of bridges that have an effect on the ultimate load-carrying capacity and maximum deflection need to be considered for developing a notional bridge for each group of bridges in the inventory. As a result, the Florida Bridge Inventory was statistically analyzed to determine the available range of each functional and geometric parameter. According to the Florida Bridge Inventory, as of 2016, there are approximately 12,900 bridges in Florida, including 1200 steel bridges, of which 140 are steel box girder bridges, with the majority being two-box girder bridges. Three hundred ninety steel bridges currently are classified as Fracture Critical. Table 3-1 and Figure 3-1 show the distribution of bridges based on the number of box girders that varies from a single girder to nine girders. Single box girder bridges, regardless of their configurations, are classified as fracture critical bridges and are excluded from this study. If a twin steel box girder bridge group is determined to be redundant, bridges with three or more box girders with the same characteristic would be automatically determined to be redundant. Hence, statistical analysis of the inventory in this study will be performed over all available two-box girder bridges. Detailed information obtained from the Florida Bridge Inventory is presented in Appendix A.

Table 3-1. Distribution of bridges: Number of the box girder.

No. of Box Girders	1	2	3	4	≥5	Total
No. of Bridges	3	85	33	7	12	140
Percentage	2%	61%	24%	5%	9%	
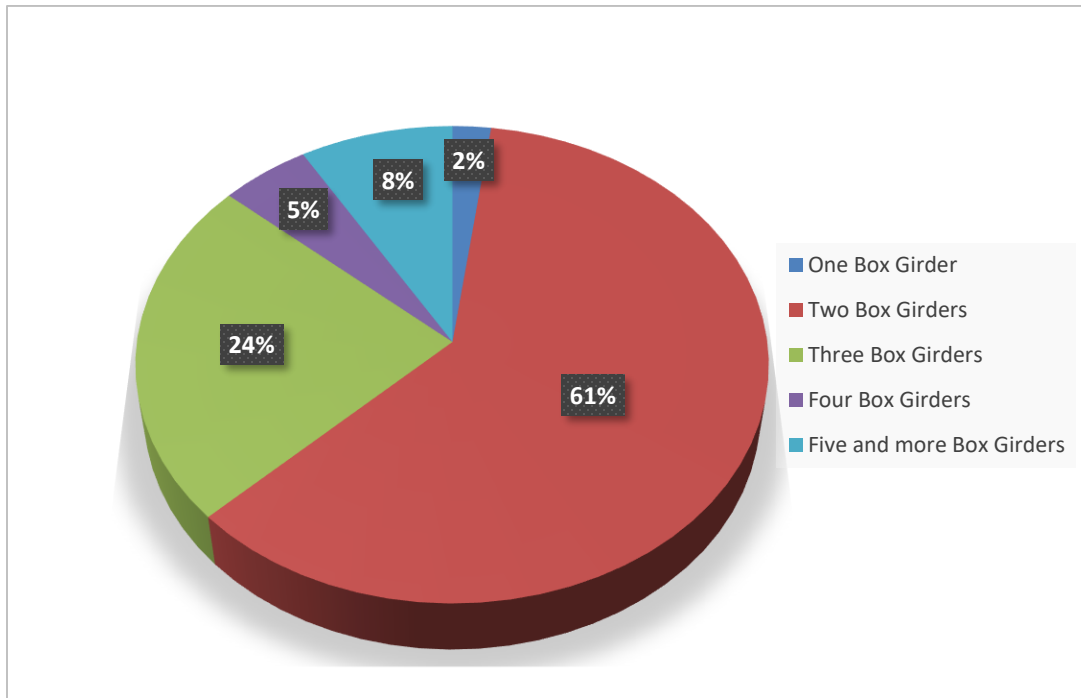
Figure 3-1. Distribution of bridges: Number of box girders.

6

3.1.1 Maximum Span Lengths and Number of Spans

The span lengths and the number of spans for a bridge are normally determined in design based on parameters such as the topography of the site, configuration of other roads beneath or around the bridge, environmental issues, architectural plans, structural systems, and construction methods. In a multi-span bridge, span lengths and the number of piers are usually determined for optimum configuration. However, by considering environmental effects and construction difficulties for the piers, longer spans with fewer foundations may be the preferred solution. Figure 3-2 shows the distribution of maximum lengths of span for Florida's twin steel box girder bridges divided into five main groups. The span lengths vary from 113 ft to 372 ft, with a large majority of bridges having a span between 150~250 ft.

Figure 3-3 shows the distribution of bridges based on the number of the span. As can be seen, most of the bridges have more than three spans, and there are only five simple span bridges of this type in the state of Florida. The number of spans, consequently the continuity of spans, plays a defining role in the maximum deflection and ultimate load capacity of a bridge. This is especially important since one fractured girder in a span within a multi-span bridge can carry the load as a cantilever beam. As a result, the stiffness of continuous bridges after fracture is much higher than simple span bridges with the same characteristics. The worst fracture scenario in a multi-span bridge is a fracture in the middle of the first or last span, i.e., exterior spans. Because in this case, the fractured girder can act as a cantilever beam just on one side. Accordingly, and for simplicity, a two-span continuous bridge can be considered to represent all multi-span bridges conservatively.

	100 ≤Span<150	150≤Span<200	200≤Span<250	250≤Span<300	300≤Span<400
No. of Bridges	10	28	28	15	4
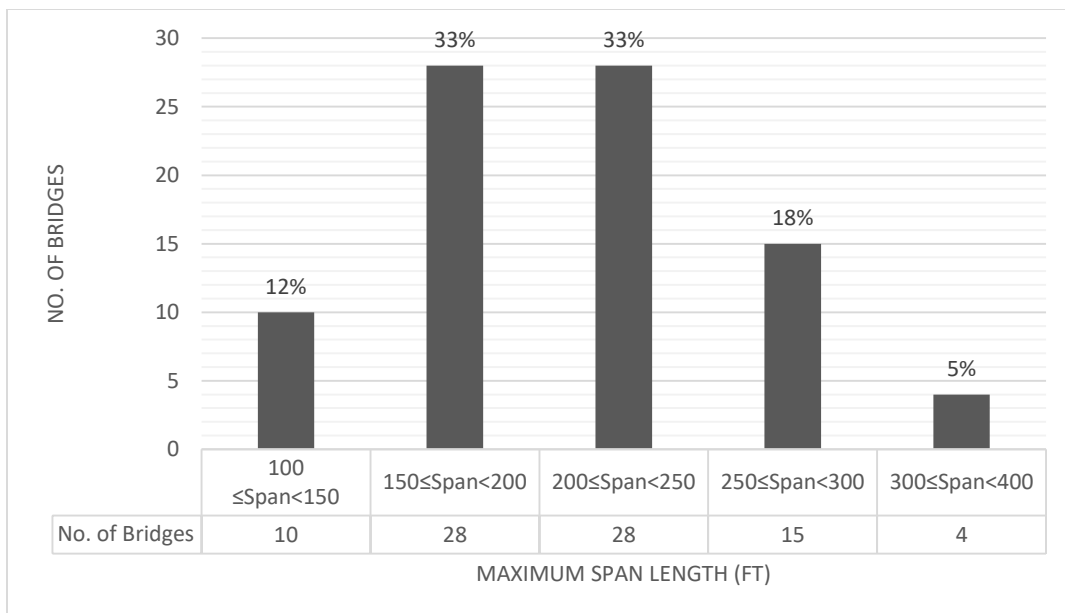
Figure 3-2. Distribution of bridges: Length of max. Span (ft).
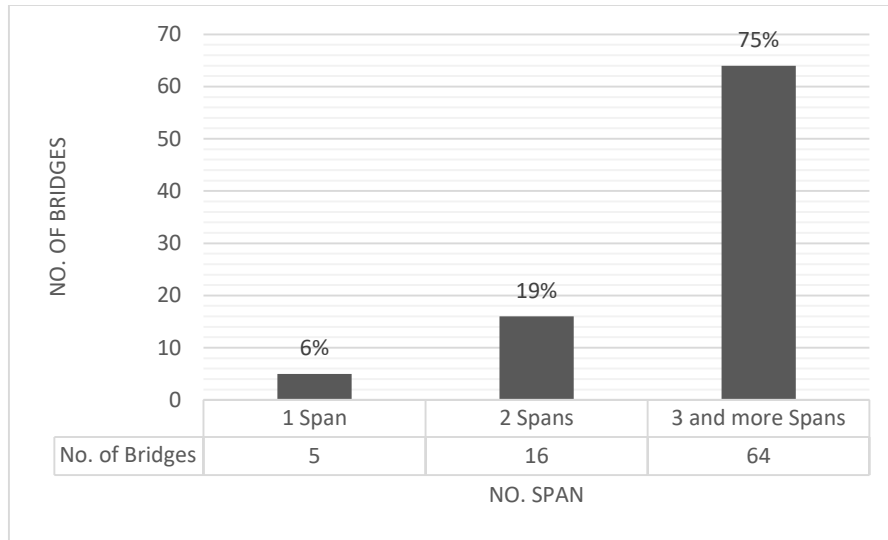
Figure 3-3. Distribution of bridges: Number of the span.

3.1.2 Number of Lanes

The number of lanes is determined based on parameters such as average annual daily traffic (ADTT), the desired level of service, percent of trucks and peak hour factor (PHF), and the number of lanes in the connecting roadway. Loading configuration for the design and evaluation of a bridge depends on the number of lanes, therefore making it another effective parameter in redundancy evaluation. As shown in Figure 3-4, statistical analysis over the Florida bridge inventory shows that 92% of twin steel box girder bridges have 1 or 2 lanes, which are generally used for overpass roadways. Therefore, because of their lower percentage number, bridges with 3 or 4 lanes, for the time being, are not considered in the grouping criteria. Also, for all the remaining single and double-lane bridges, 2-lane bridges will be used conservatively in the grouping process.
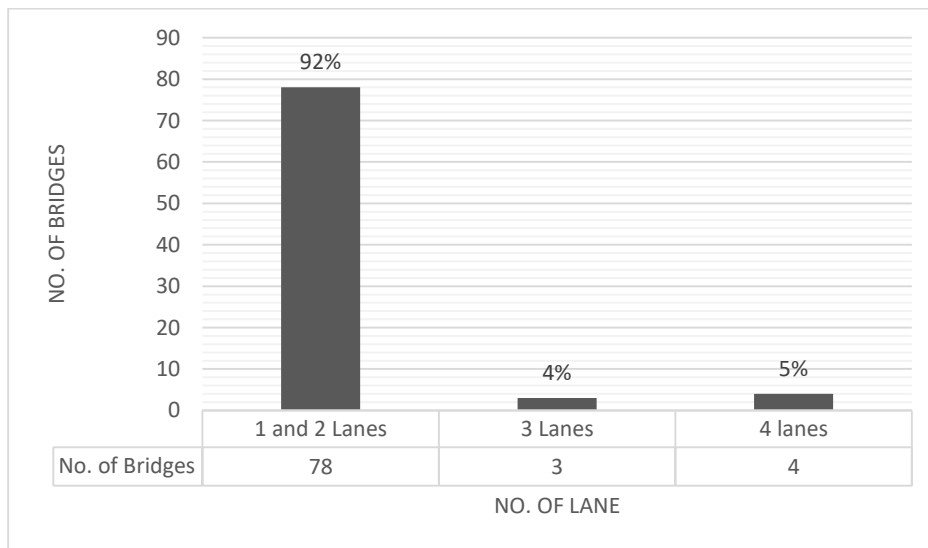
Figure 3-4. Distribution of bridges: Number of lanes.

8

3.1.3 Deck Width

A typical lane width is 12 ft; however, the actual width can vary based on the type of roadway, whether it is a principal arterial, rural highway, or residential street, or whether it is in a straight or curved span. Further, the lane closest to a raised median or in a ramp may be extra wide to allow for some distance between the vehicle and the median. Deck width includes the lane widths plus shoulders, curbs, and railings, and the larger the lane width, the more critical will be the effect of eccentric loading (over fractured girder). Road width is normally 2 to 3 ft smaller than deck width. Analysis of inventory bridges shows that the deck width varies within a range for a certain number of lanes. For example, deck width for a two-lane bridge varies between 40 ft and 50 ft. For this study, the deck width is not considered a parameter (variable). For simplicity, it will be attempted to use in analysis a typical width that would represent the majority of two-lane bridges. It is also realized that the design of a specific bridge, including dimensions and spacing of the girders, have already taken into account the deck width, therefore renders it to be a dependable variable. Figure 3-5 shows the distribution of bridges based on the deck width.
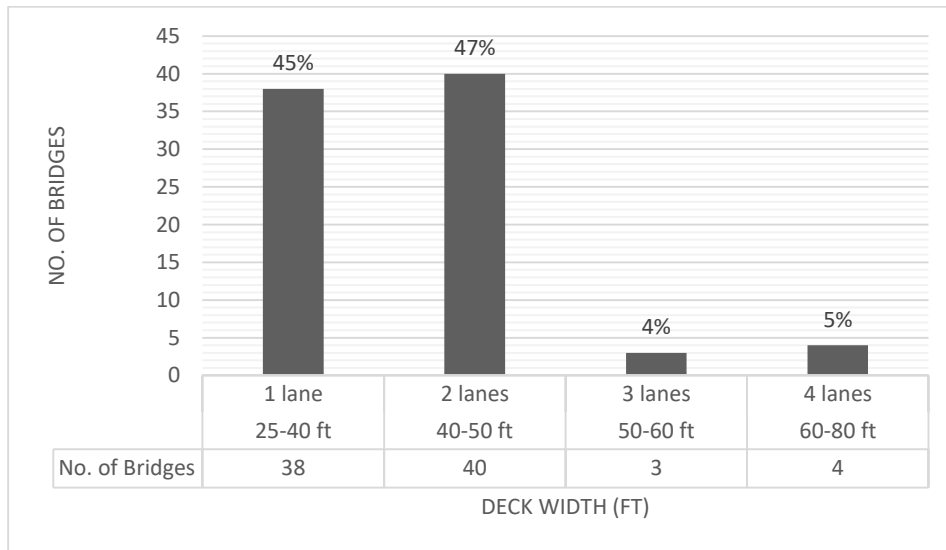
Figure 3-5. Distribution of bridges: Deck width.

3.1.4 Radius of Curvature

Whilst straight highway bridges are the ideal configuration when the design is concerned; bridge layouts may need to be curved due to the site topology, existing obstacles, and roadway function (ramps). The minimum radius of curvature, as shown in Figure 3-6, is normally determined based on parameters such as design speed, slide friction factor, lateral acceleration, super-elevation, steel constructability, functional adequacy, space availability, etc. As the radius of curvature of a bridge decrease, the torsional moment increases due to the eccentricity of gravity loads relative to the line of support. This torsional moment is significant even for a short span bridge.

9

Because of this, steel box girder bridges, because of their high torsional resistance, are mainly used for ramp and curved overpass highway bridges. In cases where one girder is fractured, torsional resistance would decrease significantly; as a result, loading eccentricity due to curvature will negatively affect the ultimate load capacity and serviceability of the bridge and cannot be ignored.
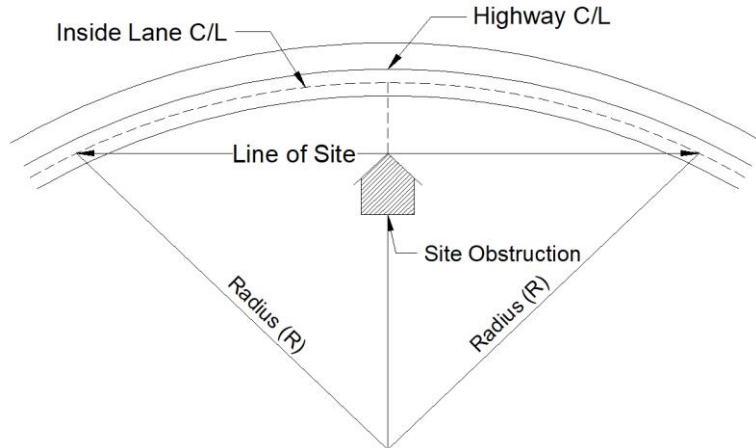
Figure 3-6. The radius of curvature.

According to the AASHTO LRFD, the horizontal radius of curvature measured to the centerline of the girder web shall not be less than 150 ft. In addition, the radius shall not be less than 1000 ft when the flange thickness exceeds 3.0 in or the flange width exceeds 30.0 in. Table 3-2 shows the available minimum radius of curvature for each span group that would be used for grouping representing the most critical combination of span length and curvature.

Table 3-2. Distribution of loading eccentricity based on bridge curvature.

Length of Max. Span (ft)	100-150	150-200	200-250	250-300	300-400
Available Min. radius of curvature (ft)	175	280	400	490	774

3.1.5   *Parameters to Be Considered in Grouping*

Based on analyzing Florida Bridge Inventory, it can be concluded that the only number of spans (single span or two continuous spans), maximum span length, the radius of curvature, and cross-section are the parameters with the highest impact and will be considered for grouping criteria. Other parameters will be assumed constant for notional bridges. In this research, the deck is assumed to have two lanes, and the width of the deck is assumed to be a typical value most used within the inventory for 2-lane bridges. For this stage of the investigation, skewness at supports will not be considered as one of the parameters, i.e., supports are assumed to be perpendicular to the longitudinal axis of the bridge.

For the initial grouping, all bridges in the inventory are divided into two main groups of simple and two continuous spans. In the latter case, the fractured girder in a multi-span bridge can still carry loads as a cantilever beam from one side; as a result, the stiffness of these bridge after fracture is higher than simple span bridges with the same characteristics. Also, a two continuous-span bridge can represent all other multi-span bridges conservatively. Each of these two main groups can be divided into five subgroups based on the maximum span length presented in Figure 3-2 to form 10 main initial groups. The range of radius of curvature for each span length group can be determined according to the available radius of curvature in the inventory.

Once geometric parameters of the notional bridge for each group are determined, design details of a set of similar inventory bridges will be obtained from FDOT. The notional finite element model for each group will then be developed based on these design details and analyzed to evaluate the ultimate load-carrying capacity and the maximum deflection to span length ratio for the intact bridge. The load-carrying capacity and deflection will be used to define the level of over or under capacity design as well as the deflection to span ratio and to assure that the cross-sections are a true representation for bridge configuration.

Finally, the notional finite element model representing each group with the minimum available radius of curvature for that group can be developed for the fractured girder condition. The models can be analyzed under the loading condition obtained from reliability analysis. The results can be compared to the redundancy criteria (Ultimate limit state and serviceability limit states) to find if a notional bridge with the minimum allowable radius of curvature will meet the redundancy criteria. If the notional bridge representing a group with the minimum radius of curvature satisfies the redundancy criteria, then all bridges in that group will be identified as redundant. Otherwise, the radius of curvature will be increased incrementally until the redundancy criteria are met. Accordingly, the referenced bridge group can be divided into subgroups based on the radius of curvature that would satisfy the redundancy criteria. Since the groups cover wide ranges of span length with different radius of curvature, it is likely that some groups with large span will not meet the redundancy criteria even for a straight bridge. For such cases, the bridge group can then be divided into subgroups with varying span lengths in each group to determine redundant and non-redundant subgroups based on their span length. Figure 3-7 presents the initial grouping for the notional bridge concept to be considered in the redundancy analysis.
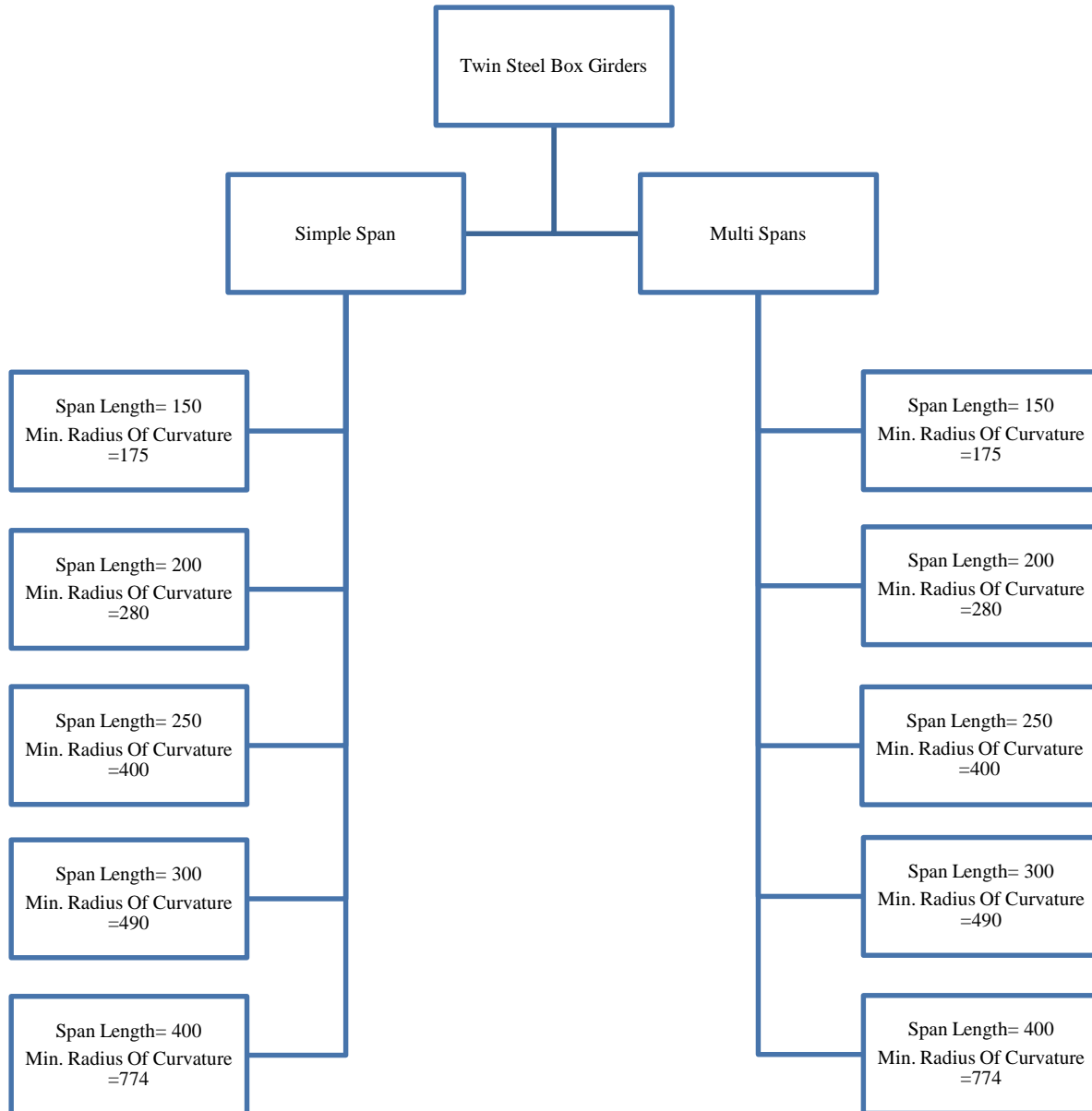
Figure 3-7. Initial notional bridges.

Chapter 4   Development of Loading and Criteria for Redundancy Verification

Previous studies have investigated the redundancy of twin steel box girder bridges using more or less an arbitrary load level [13], [23–25]. Arbitrarily selecting the load level that the damaged twin steel box girder bridges should be able to carry has been frequently questioned. Therefore, there is a need to develop more rational approaches to establish the load level and application method that the damaged bridge should carry for proper evaluation. Further, there may also be a need to develop additional performance criteria, such as deflection limits for damaged bridges. The concept of damaged twin steel box girder bridges being able to deflect without collapse is a desirable mode of behavior since it will be detectable. This task may involve establishing the target safety level or reliability index. Two approaches may be considered to establish the target reliability level. One approach will consist of seeking the bridge owner's input on an appropriate safety level. The other approach will be to establish the safety level inherent in redundant bridges. The reliability analysis of twin steel box girder bridges and discussions over the level of live loads are presented in Chapter 8.

4.1   Proposed Live Load Model

In the new generation of design codes, safety reserve is provided by means of load and resistance factors determined by the reliability-based calibration process [26]. The code calibration requires the knowledge of statistical parameters of load and resistance. It is important to know the expected maximum load, its statistical parameters on the load side. However, these statistical parameters depend on location as they are site-specific, considered time period, and Average Daily Truck Traffic (ADTT). On the resistance side, respective statistical parameters are also needed. While in the case of evaluating the redundancy of new design methods and concepts, risk and reliability-based assessment is important before it is implemented in the design codes.

The objective of the proposed live load model is to develop a state-specific bridge live load model that may be expected on the bridge at fracture state for Florida. Since the bridges are inspected every two years, the evaluation period is limited to the inspection period. The analysis includes weigh-in-motion (WIM) data from 31 stations collected throughout four years (2013-2016) in the state of Florida. The obtained data included 136 million vehicles in total. After applying filtering criteria to eliminate lightweight vehicles, about 20% of the data were eliminated. The initial investigation of Redundancy of Twin Steel Box Girder Bridges was limited to 120 ft span length and evaluation (return) period of two years. The statistical parameters, mean (μ) and standard deviation (σ) for maximum moment and shear, are developed for 120 ft span and two year return period for ADTT's ranging from 250 to 10,000.

4.1.1   WIM Database

The WIM data used in this study contained data from the years 2013 – 2016 and was obtained from FHWA. The WIM stations in Florida are shown in Figure 4-1. The WIM data were obtained in 4 different traffic data monitoring formats that are in the Traffic Monitoring Guide (TMG) [27]. The truck weight data format was used as it contains information such as, but not limited to, the number of axles, the spacing between axles, axle weights and gross vehicle weight (GVW), and exact time of measurement for each recorded vehicle at each location. The data was available from 31 WIM stations out of 32 WIM stations that are currently in Florida. Table 4-1 shows the WIM stations co-ordinates, number of lanes, and directions of each WIM station used in this study.

4.1.2   WIM Data Filtering

Long-term WIM data collection can be affected by errors in recording due to various reasons such as malfunction and improper vehicle positioning on the sensor. More reasons for the need of WIM data filtering is discussed in the literature [28, 29]. Some of the errors are inevitable but using the proper filtering criteria can eliminate the improper recordings, thus eliminating the under or overestimation of loads and design. It was observed that the data obtained from FHWA was filtered through the Traffic Monitoring Analysis System (TMAS) Quality Control (QC) checks [30]. Only vehicles with a GVW of less than 20 kips were eliminated from the obtained database. Vehicles with GVW less than 20 kips limit do not cause much damage to bridges and pavements [31]. Table 4-2 shows the number of records and days that are available for each WIM station that is considered in this study. The number of records is a total number of vehicles that were recorded in both directions and all the lanes.

14
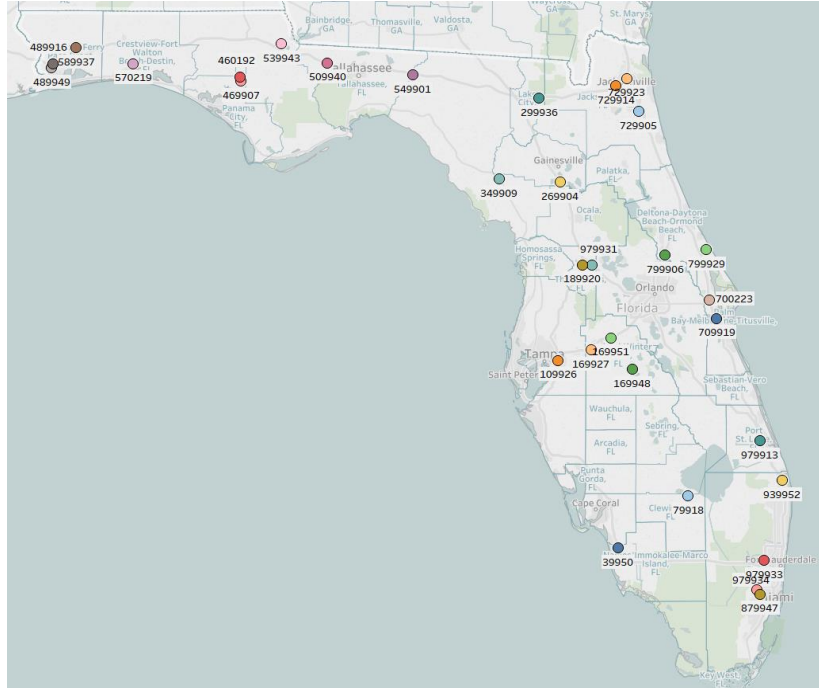
Figure 4-1. WIM stations in Florida.

4.1.3 *Initial Data Analysis*

The data left after filtering out vehicles less than 20 kip GVW are used for further analysis. The Cumulative Distribution Function (CDF) of GVWs are plotted on probability paper in Figure 4-2 for the year 2014. Each curve on the plot is data from each WIM station in Florida. Since the controlling criteria in the design are the load effects, i.e., moment and shear created by vehicles. Each vehicle in the database is run over an influence line for the considered span length of 120 ft, and moment and shear are calculated. For a better interpretation of results, the moment and shear produced by each vehicle are divided by the corresponding load effects of the HS-20 design truck. Figure 4-3 shows the CDF plot for the moment ratio of 120 ft span length for the year 2014. Traffic in WIM location 46907 is heavier compared to the rest of the WIM locations in Florida. Figure 4-4 shows the CDF plot for a shear ratio of 120 ft span length for the year 2014. The moment and shear ratios have the same type of distribution.

15

Table 4-1. WIM stations coordinates and summary of direction and lanes.

Serial Number	WIM Station ID	Latitude	Longitude	No. of directions	Lanes per direction
1	39950	26.29169	-81.74247	2	2
2	79918	26.75402	-81.05527	2	1
3	109926	27.95868	-82.32668	2	2
4	169927	28.05314	-82.00487	2	1
5	169948	27.87893	-81.59732	2	1
6	169951	28.15774	-81.81207	2	2
7	189920	28.80083	-82.08849	2	2
8	269904	29.52316	-82.3098	2	1
9	299936	30.25178	-82.51512	2	1
10	349909	29.55195	-82.90068	2	1
11	460192	30.43572	-85.4465	1	1
12	469907	30.39721	-85.43494	2	1
13	489916	30.54356	-87.28171	2	1
14	489949	30.50989	-87.29086	2	1
15	509940	30.55474	-84.59297	2	1
16	539943	30.71949	-85.03963	2	1
17	549901	30.45142	-83.75296	2	1
18	570219	30.54796	-86.49696	0	0
19	589937	30.68388	-87.05378	1	1
20	700223	28.49352	-80.84429	0	0
21	709919	28.32957	-80.77445	2	1
22	729905	30.13464	-81.53441	2	2
23	729914	30.35666	-81.76062	2	2
24	729923	30.42235	-81.65637	2	2
25	799906	28.8875	-81.27905	2	2
26	799929	28.932	-80.87713	1	2
27	879947	25.87349	-80.3491	2	2
28	939952	26.89359	-80.13425	2	2
29	979913	27.24645	-80.34639	2	1
30	979931	28.79909	-81.99811	2	1
31	979933	26.17933	-80.30672	2	2
32	979934	25.91205	-80.38156	2	2

Table 4-2. Summary of a number of records and days for each available year of WIM data.

WIM Station ID	YEAR							
	2013		2014		2015		2016	
	No. of records	No. of days	No. of records	No. of days	No. of records	No. of days	No. of records	No. of days
39950	1,152,871	365	1,356,465	365	1,414,695	333	1,668,626	364
79918	599,433	353	740,377	362	722,516	333	649,578	365
109926	1,533,003	365	1,174,407	365	242,309	70	0	0
169927	360,962	359	328,987	315	302,534	333	186,515	214
169948	499,291	365	606,877	364	594,815	333	623,310	366
169951	2,225,227	365	2,420,670	365	2,007,969	333	1,974,743	301
189920	2,225,050	365	2,430,585	365	1,546,895	261	0	0
269904	1,999,877	365	2,046,124	365	1,500,610	303	0	0
299936	1,365,149	365	1,453,450	364	1,254,093	321	1,659,298	365
349909	108,567	365	87,509	361	99,140	272	0	0
460192	17,441	365	21,403	365	23,644	270	0	0
469907	172,215	247	290,228	365	265,738	331	304,625	365
489916	246,460	365	192,958	363	148,237	299	0	0
489949	1,071,839	365	1,230,179	365	1,204,885	333	1,407,113	366
509940	38,054	365	45,605	362	34,849	272	3,521	30
539943	55,129	363	68,009	357	54,411	302	24,070	122
549901	1,458,382	365	450,154	107	0	0	0	0
570219	0	0	0	0	0	0	0	0
589937	26,044	350	8,059	97	0	0	0	0
700223	0	0	0	0	0	0	0	0
709919	1,237,832	365	1,321,028	354	1,308,070	333	1,502,369	366
729905	2,632,309	365	2,702,871	336	2,694,015	333	2,155,516	366
729914	627,877	125	2,239,028	364	2,146,196	333	2,489,478	366
729923	2,287,335	355	12,998	5	738,075	91	0	0
799906	1,764,788	365	1,834,224	364	1,354,705	330	569,544	145
799929	24,512	365	25,226	365	21,278	270	0	0
879947	445,005	175	753,381	334	945,805	333	1,092,731	364
939952	1,528,004	363	1,633,682	365	1,476,551	333	1,698,537	364
979913	1,095,237	365	1,301,554	365	1,319,373	333	1,583,223	366
979931	1,284,042	334	1,497,063	364	1,492,759	333	1,786,579	366
979933	564,712	365	120,175	63	0	0	208,530	91
979934	1,437,970	359	1,628,987	365	1,702,749	333	1,926,311	365
SUM	30,084,617	-	30,022,263	-	26,616,916	-	23,514,217	-
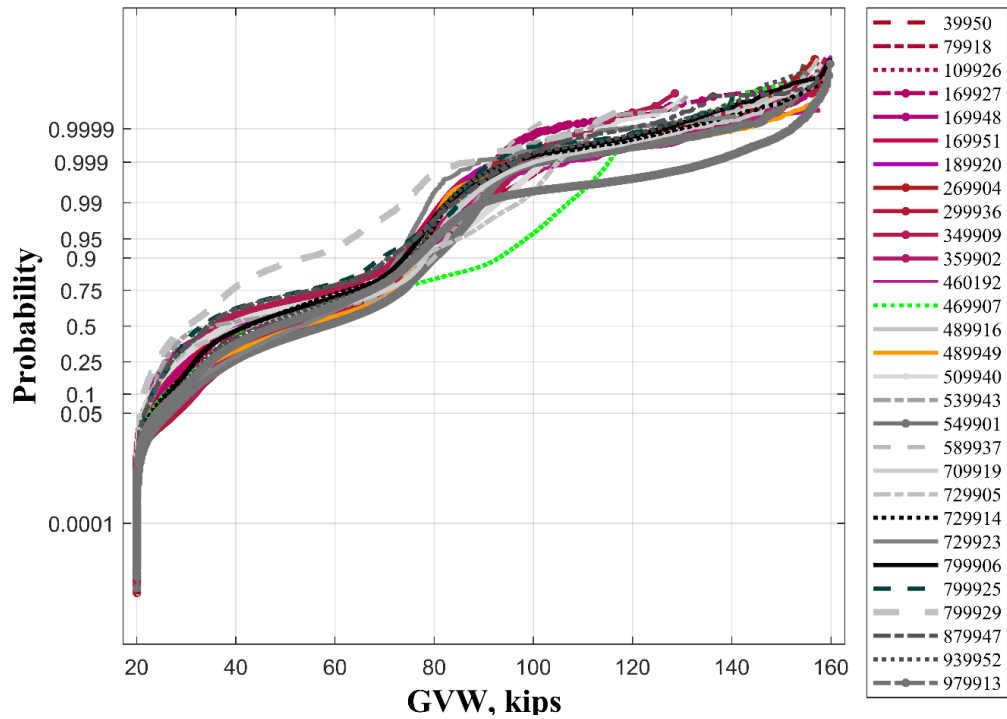
Figure 4-2. CDF plot of GVW of all WIM stations in Florida for the year 2014.
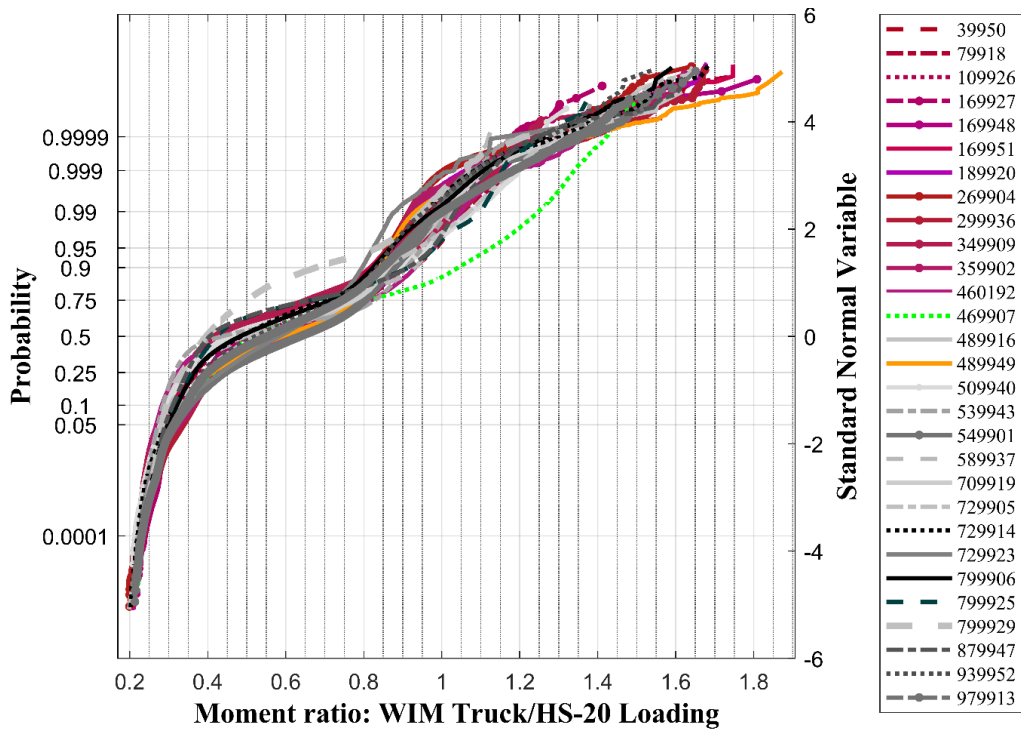
Figure 4-3. CDF plot of moment ratio of all WIM stations in Florida for the year 2014.
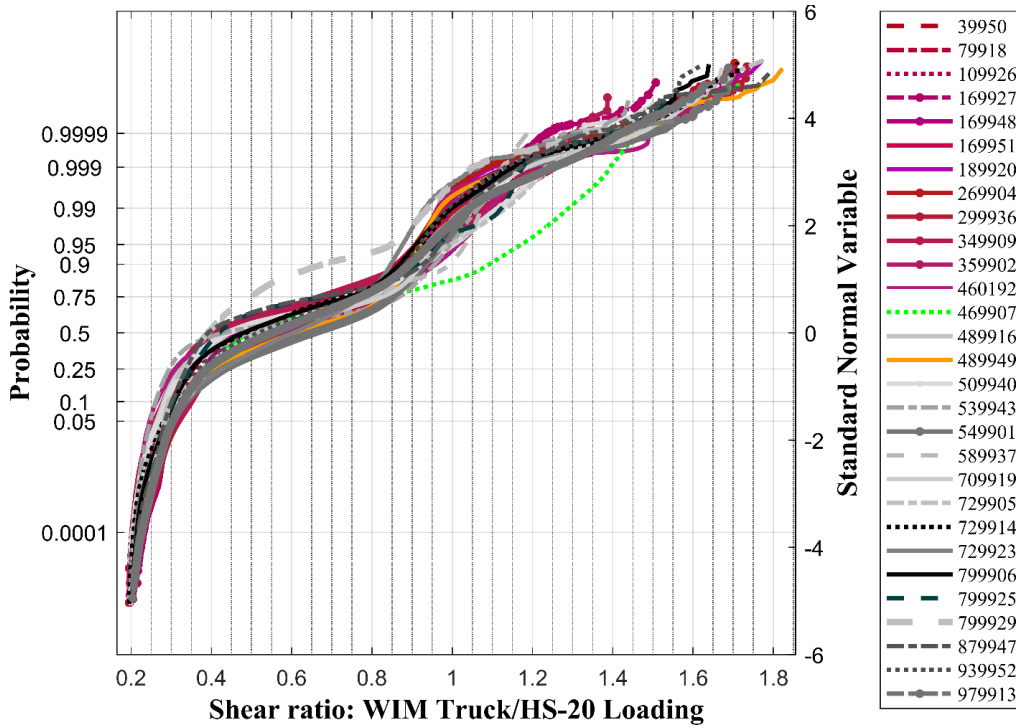
Figure 4-4. CDF plot of the shear ratio of all WIM stations in Florida for the year 2014.

4.1.4 Maximum Moment for Different Load Periods

The maximum moment is a random variable, and it depends on the period of time considered, ADTT, and span length. In this report, the period of time of two years and a span length of 120 ft is considered. The ADTTs are varied from 250 to 10,000. The mean value of the maximum moment is determined for each WIM station traffic data for different ADTTs. More information about the procedure is discussed in Kulicki, J.M et al. [28]. For each CDF, the vertical coordinate of the maximum moment (Zmax) is given by Equation (1). The vertical coordinates for different ADTT's are shown in Figure 4-5 (a) for normal probability scale and standard normal variable scale.

$$Z_{max} = \Phi^{-1}\left(\frac{1}{N}\right) \tag{1}$$

where, Φ^{-1} = inverse standard normal distribution function. N = number of records for the period, T (in days), and certain ADTT as shown in Equation (2)

$$N = T * ADTT \tag{2}$$

The mean maximum moment can be directly obtained from the graph by reading the moment ratio (horizontal axis) with the corresponding vertical coordinate for the considered time period. The values for larger coordinates were projected or extrapolated as appropriate. For an easier interpretation, the vertical coordinates for different ADTT's are plotted on the probability paper along with CDF's for years 2013-2016 in Figure 4-5(a) to Figure 4-8(a). The mean maximum

19

moments of each WIM station traffic data are plotted on probability paper in Figure 4-5(b) to Figure 4-8(b).

4.1.5 Statistical Parameters

It is assumed that 32 WIM stations in Florida have representative truck traffic for Florida. The statistical parameters of mean maximum and coefficient of variation (CV) of live load (moment) are shown in Table 4-3. The mean of these maximum values can be considered as the mean maximum for Florida based live load model. These statistical parameters can be further used for reliability analysis calculations. At this stage, the statistical parameters are calculated only for moments.

Table 4-3. Statistical parameters of live load moments for different ADTT.

ADTT	Year 2013		Year 2014		Year 2015		Year 2016		All years averaged	
	μ	CV	μ	CV	μ	CV	μ	CV	μ	CV
250	1.51	0.07	1.51	0.08	1.50	0.06	1.51	0.04	1.51	0.06
1,000	1.60	0.09	1.61	0.09	1.59	0.07	1.61	0.05	1.60	0.07
2,500	1.66	0.10	1.67	0.10	1.64	0.07	1.66	0.05	1.66	0.08
5,000	1.70	0.11	1.71	0.11	1.69	0.07	1.71	0.05	1.70	0.09
10,000	1.75	0.11	1.76	0.12	1.73	0.08	1.75	0.06	1.74	0.09
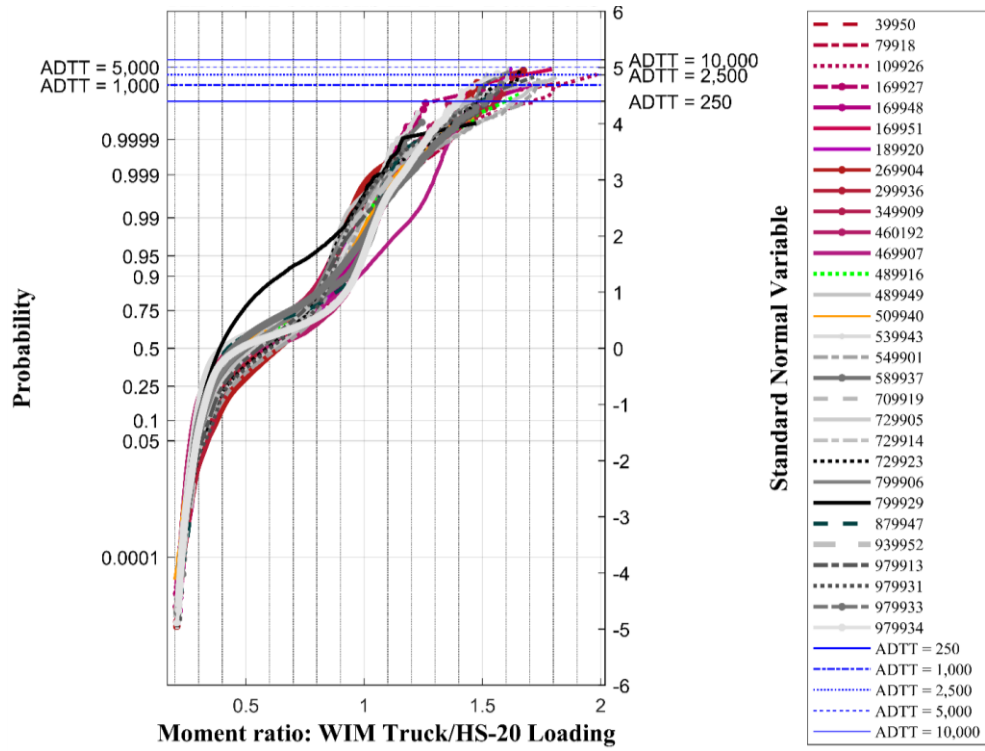
(a)
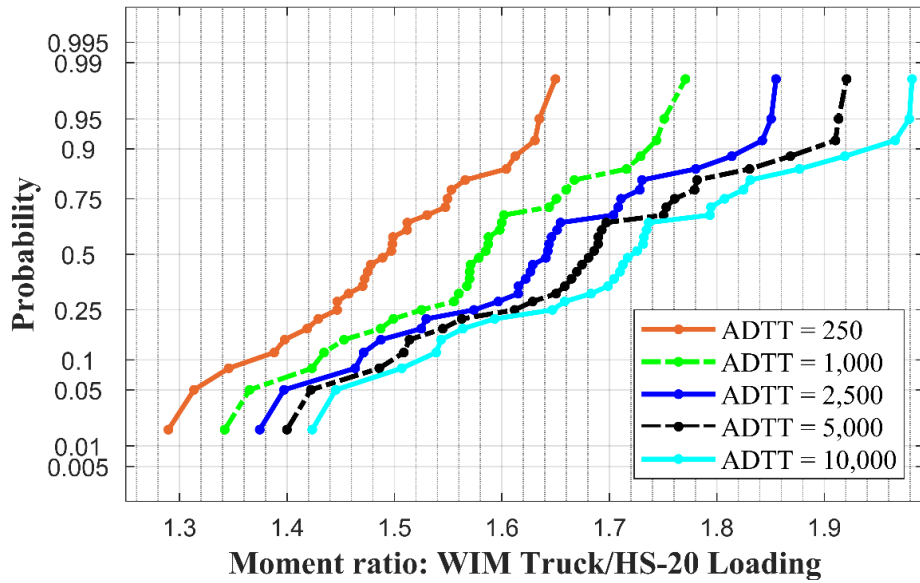
(b)

Figure 4-5. CDF plot for the year 2013: (a) Vertical coordinates for different time periods; (b) Mean maximum moment ratios for different ADTT.

21

(a)

(b)
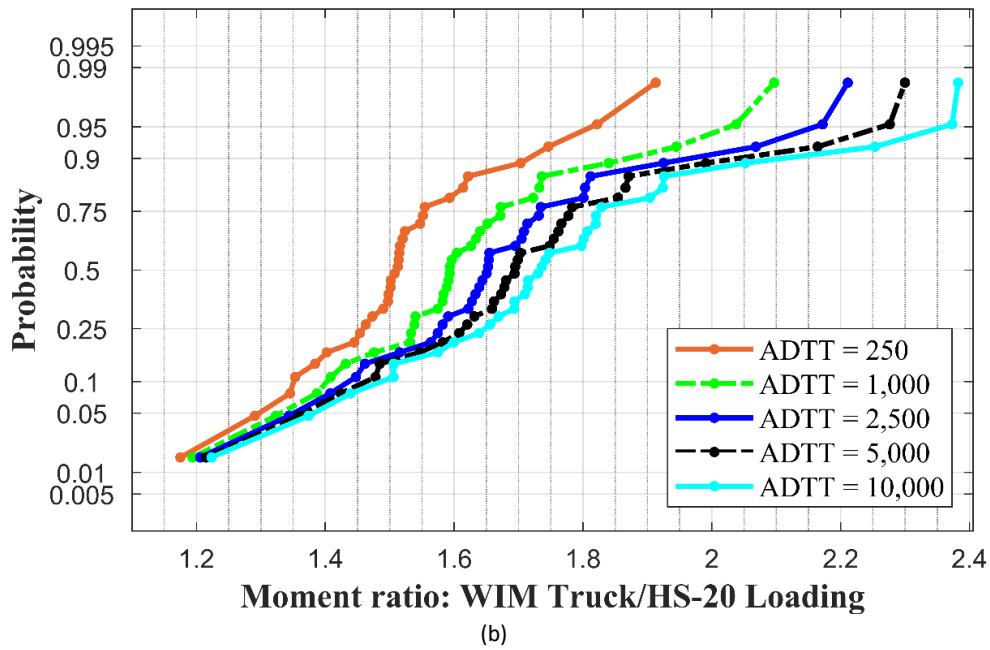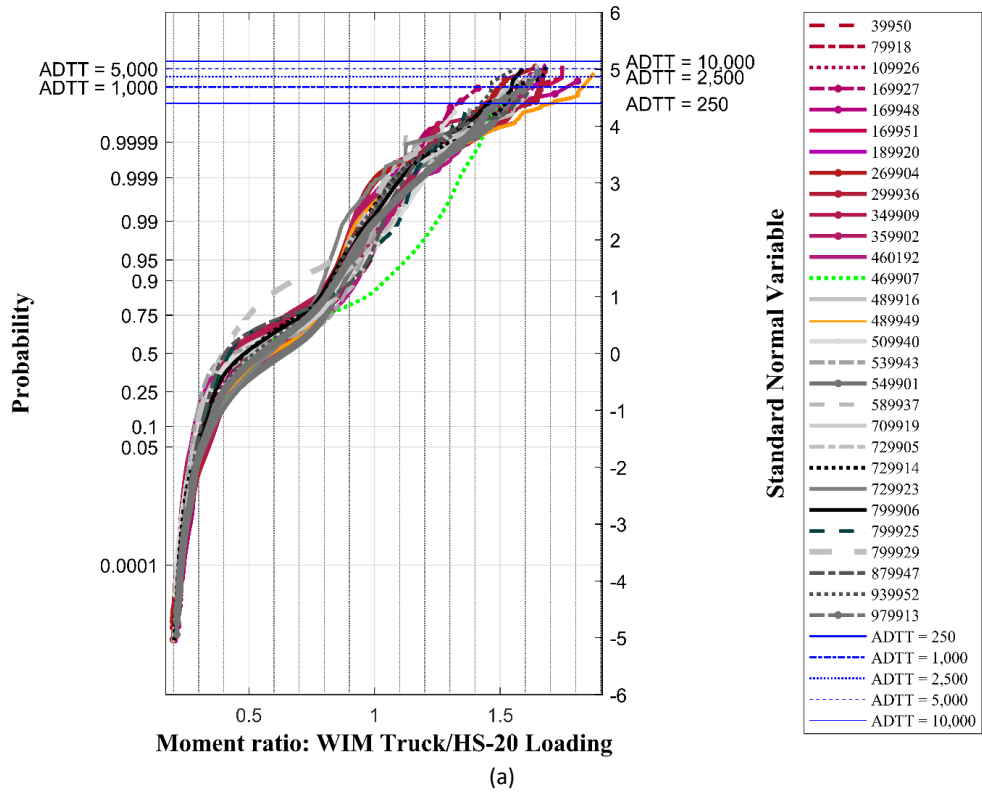
Figure 4-6. CDF plot for the year 2014: (a) Vertical coordinates for different time periods; (b) Mean maximum moment ratios for different ADTT.
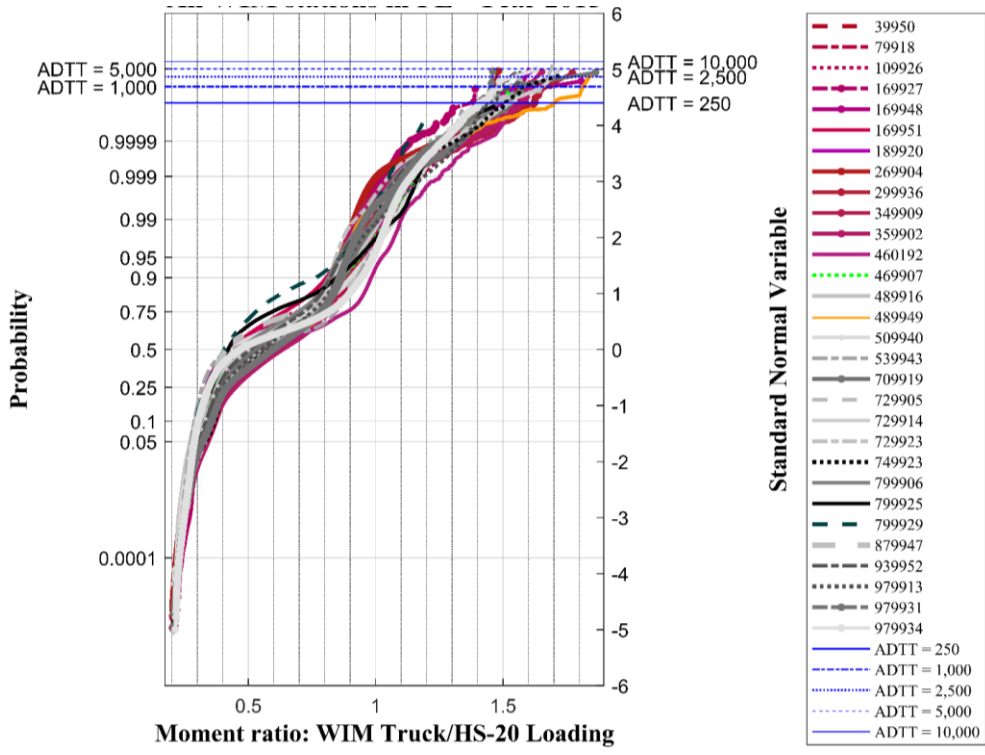
(a)
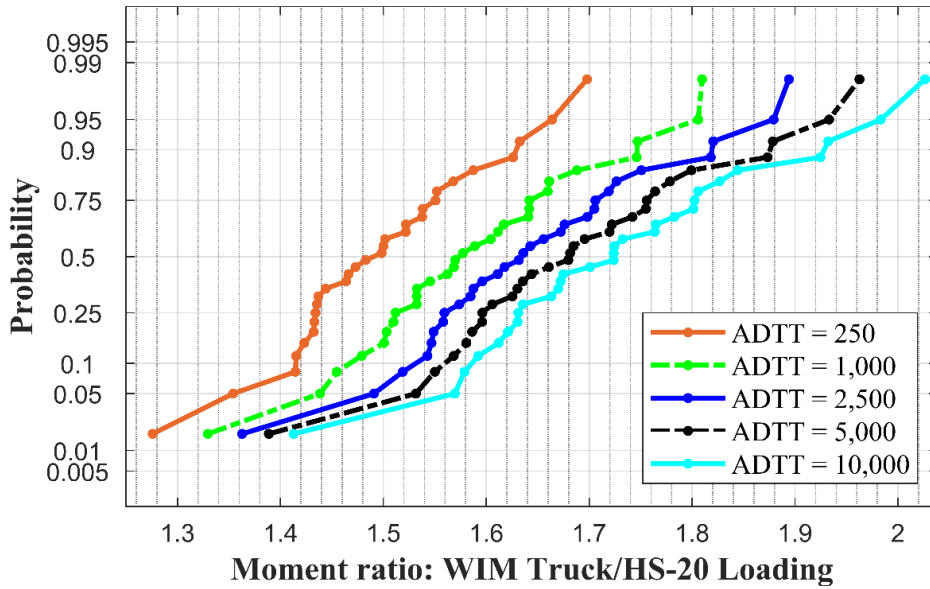
(b)

Figure 4-7. CDF plot for the year 2015 (a) Vertical coordinates for different time periods; (b) Mean maximum moment ratios for different ADTT.
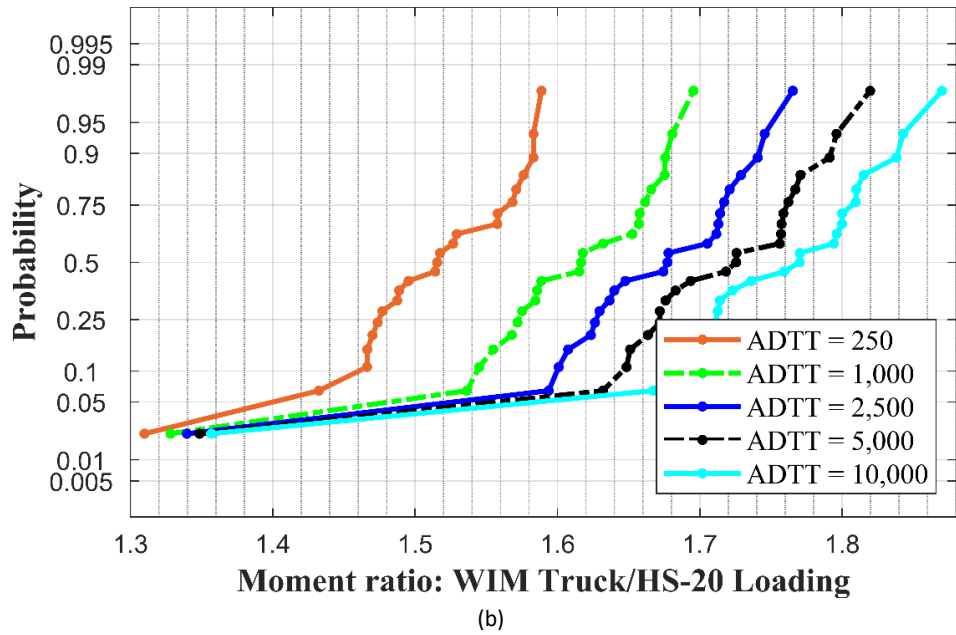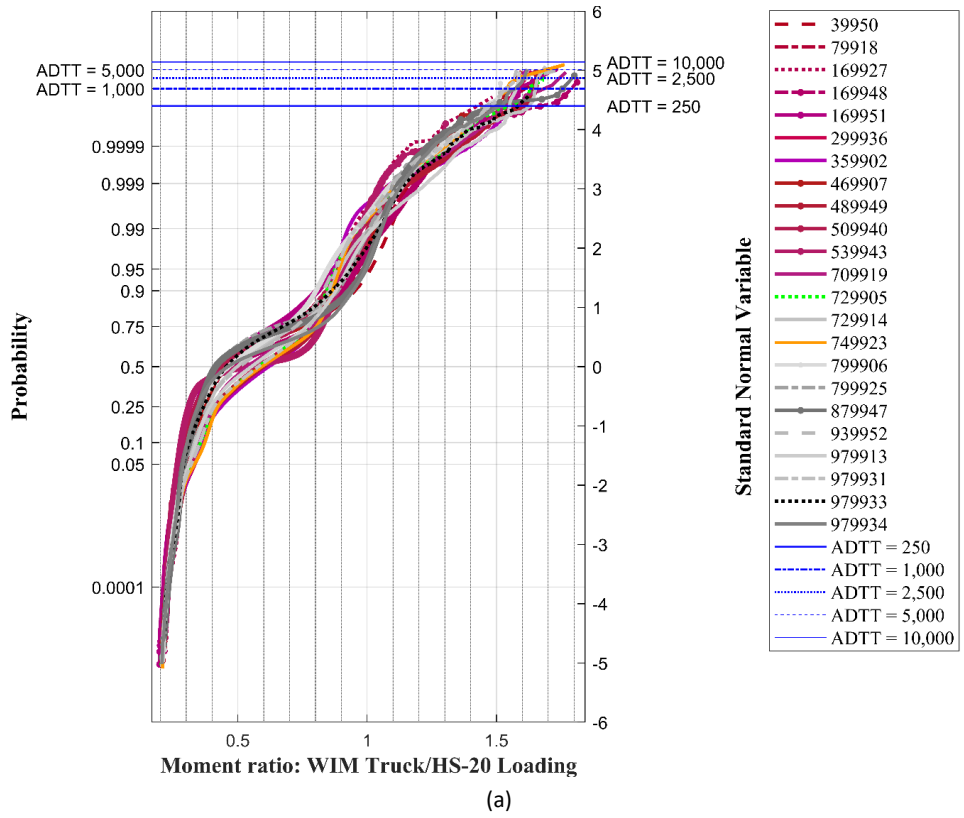
Figure 4-8. CDF plot for the year 2016: (a) Vertical coordinates for different time periods; (b) Mean maximum moment ratios for different ADTT.

Chapter 5   Development and Validation of Finite Element Method

Finite element modeling has been recognized as a means for detailed analysis of steel box girder bridges to investigate their redundancy. Construction of a detailed FE model of the bridge and analysis under loading of various configurations is a time-consuming and costly activity. Modeling of every detail in the bridge is neither economic nor always necessary. Additionally, solution methods available for numerical analysis of FE models are numerous and do not always end to proper convergence and accurate results. Hence, the application of FE modeling and analysis can be quite complex and finding an optimum level of refinement and modeling details, as well as the proper solution method, requires performing some experimentation and validation. Validation can be performed by modeling and analysis of bridges that are tested and for which adequate data in the behavior is available. The finite element (FE) model of a twin steel box girder bridge adopted for this study was created in the environment of ABAQUS [32] to simulate the response of the bridge under the fractured box scenario. A generic model is shown in Figure 5-1. The proper modeling techniques, analysis procedure, and material inputs were investigated thoroughly. The details on element types, material properties, and solution method will be discussed later for each of the bridges modeled.

To date, three bridge specimens for which experimental test results were available were modeled and analyzed for validation of the FE model developed in this study. These bridges are:

- The University of Nebraska–Lincoln Multiple Plate Girder Bridge,
- The University of Texas Twin Steel Box Girder Bridge,
- The Florida International University Twin Steel Box Girder Bridge,

The selected bridges have steel girder concrete deck composite superstructure.

The University of Nebraska-Lincoln bridge [33] is selected as the first model for validation of the FE models for the elastic and ultimate load tests available for this bridge. Although the Nebraska bridge did not use steel box girders and was not subject to fracture of the girder, however, availability of extensive and accurate experimental test results that included failure modes similar to those expected for twin steel box girder bridges were recognized to provide an excellent source for validating FE modeling and analysis technique and its details in general. The bridge has the same combination of steel girder (I-girder) and concrete deck and included failure modes for the deck such as one-way shear and two-way shear (punching shear) and failure limit states for steel girders.

For the second step, The University of Texas Twin Steel Box Girder Bridge was selected to validate the twin steel box girder model for intact and fractured scenarios. The Texas bridge tests included ultimate uniform loading and point loads in terms of simulating the HS-20 truck for the fractured box scenario. Finally, The Florida International University (FIU) Twin Steel Box Girder

Bridge [22] was used to validate the capability of the finite element model for predicting local failure modes such as punching shear and one-way shear in addition to global bridge response. In the FIU bridge tests, a series of elastic tests, a cyclic test, and ultimate load tests were conducted on a small-scale twin steel box girder to evaluate the redundancy of this type of bridge. The results of the experimental tests revealed that punching shear and one-way shear would be the dominant failure modes for both intact and one-girder fractured twin steel box girder bridges subjected to the wheel-simulated loads.

After the model is validated by using experimental results of these three bridges, the twin steel box girder bridge model can then be used for evaluating the redundancy of existing bridges in the state of Florida by analyzing the notional bridges for each group of bridges. The results of these analyses can also be used to determine the dominant failure mode to be considered in the reliability and redundancy analysis.

5.1 Modeling Details

Material nonlinearity for steel and concrete are considered in the models. Traditional metal plasticity is used to represent steel components, and concrete damaged plasticity is used for simulating the cracking and crushing of concrete. Geometric nonlinearity was not deemed to have a significant effect on the results, and for the sake of simplicity, was not included in the modeling. When bridge railing is modeled, Hard contact surface is used for defining the surface contact between the railings. Because there is a gap between each railing segment, there would be no contact between the railing until the gap is closed due to the large deflection of the bridge. In that stage, two sides of the gap will come in contact, and contact force would increase the stiffness of the bridge. As a result, railing contact with a gap needs to be considered in all models. Experimental tests on fractured twin steel box girders show that when there is loading eccentrically over the fractured girder only, torsional moment induced by the loading eccentricity may cause uplift of the intact girder over the supports. Therefore, to consider the possibility of support uplift during the loading, the contact surface is defined between the girders and supports.

Twin steel box girder bridges consist of steel plate girders, brace members, concrete deck, and bridge railings. According to the structural behavior of each component, various type of elements is used to provide a realistic representation of the twin steel box bridges [34]. Eight-node linear brick elements are used for the concrete deck and the railing with a 2-node linear 3-D truss as the reinforcement embedded into the concrete elements. The Four-node shell element (S4R) is used for modeling steel plate girders and stiffeners; all the brace members for diaphragms are modeled using 2-node linear 3-D truss and beam elements. According to results of available tests and analyses, shear studs between girders and deck slab may influence the onset of failure in the deck, and therefore shear stud failure is modeled. In this study, the effect of shear stud failure was investigated by comparing the results of FE analysis in the models where shear studs were modeled

with the result of analysis where shear studs were not modeled (perfect bond between steel and concrete at the girder to deck slab interface).
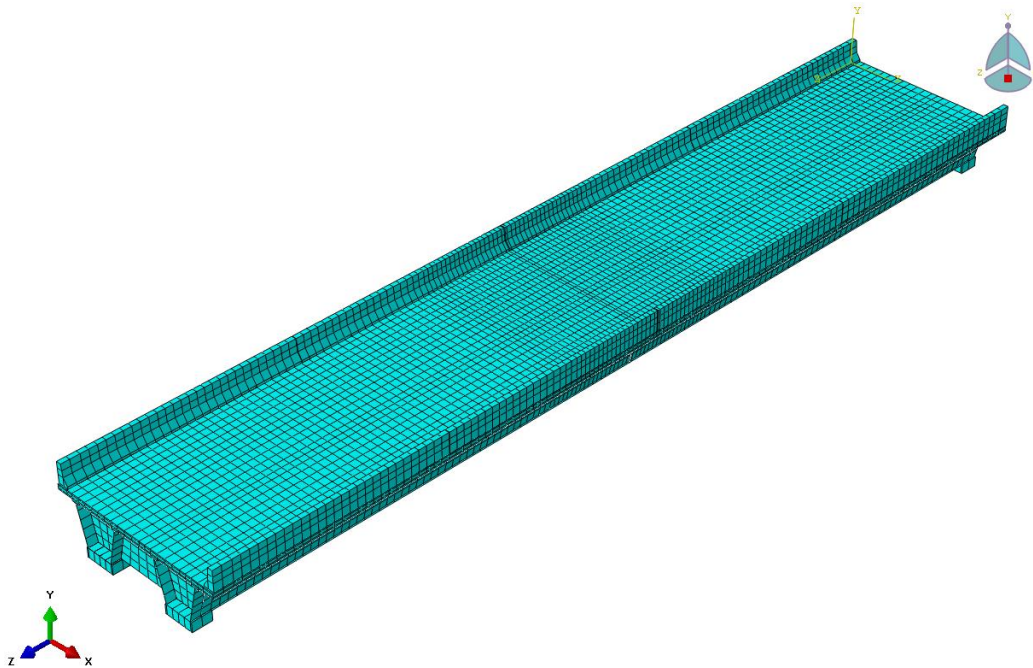
Figure 5-1. Typical finite element model of twin steel box girder bridge.

5.2 Material

5.2.1 Steel Material Model

The multi-linear inelastic material model with isotropic hardening is used for the behavior of steel plates, diaphragms, and reinforcement in both tension and compression [35, 36]. The linear elastic behavior was defined by the specification of the modulus of elasticity and Poisson's ratio, which were 29,000 ksi and 0.3, respectively. Yield and ultimate stress of steel material are considered as the typical value used in the Florida bridges. For the case of the University of Nebraska–Lincoln bridge, the girders were specified as A36 steel with the yield strength of 40 ksi (average obtained from tensile testing), and the concrete reinforcing rebar used in the concrete slab was specified as grade 60 with 60 ksi yield strength, and for the UT bridge, 50 ksi for the steel plates and 60 ksi for the concrete reinforcing bars is assumed as the yield strength of steel material. Figure 5-2 shows the uniaxial representation of the stress-strain relationship for the steel plates and concrete reinforcement used for the UT bridge. According to von Mises theory, the material yields when the equivalent stress exceeded the yield criterion.
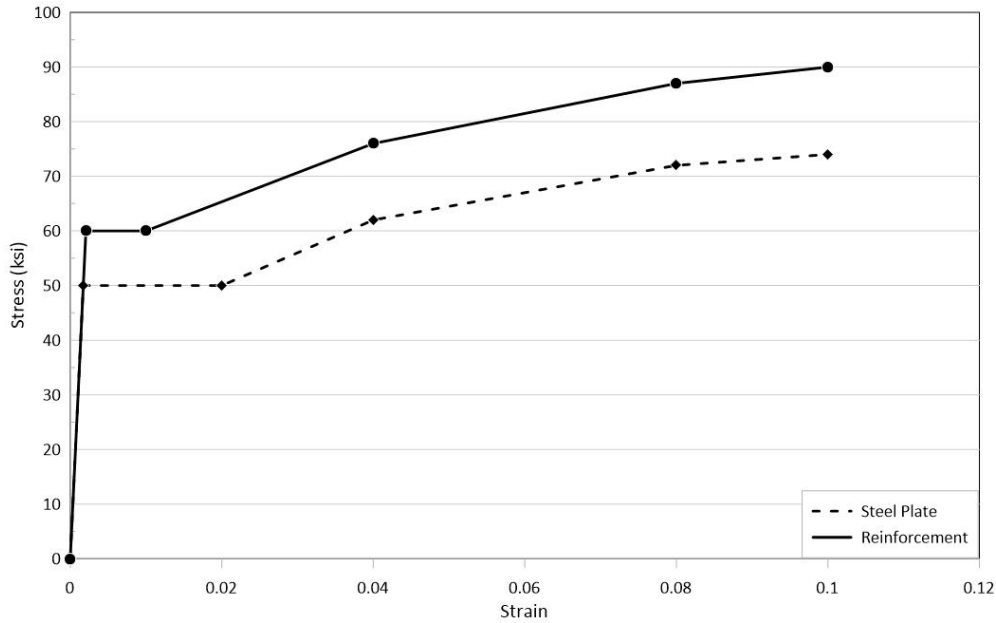
Figure 5-2. Typical steel stress-strain relation.

5.2.2 Concrete Material Model

A linear elasticity with the concrete damage plasticity is used in the FE models [37]. For the initial elastic behavior, the modulus of elasticity is calculated based on the ACI 318-14 [38] ($E_c = 57,000\sqrt{f_c'}$ (in psi) for normal-weight concrete) and a Poisson ratio of 0.2 was used. The concrete damage plasticity is a continuum, plasticity-based, damage model for concrete. It assumes that the main two failure mechanisms are tensile cracking and compressive crushing of the concrete material, and the uniaxial tensile and compressive response of concrete is characterized by damaged plasticity, as shown in Figure 5-3 [32, 39].
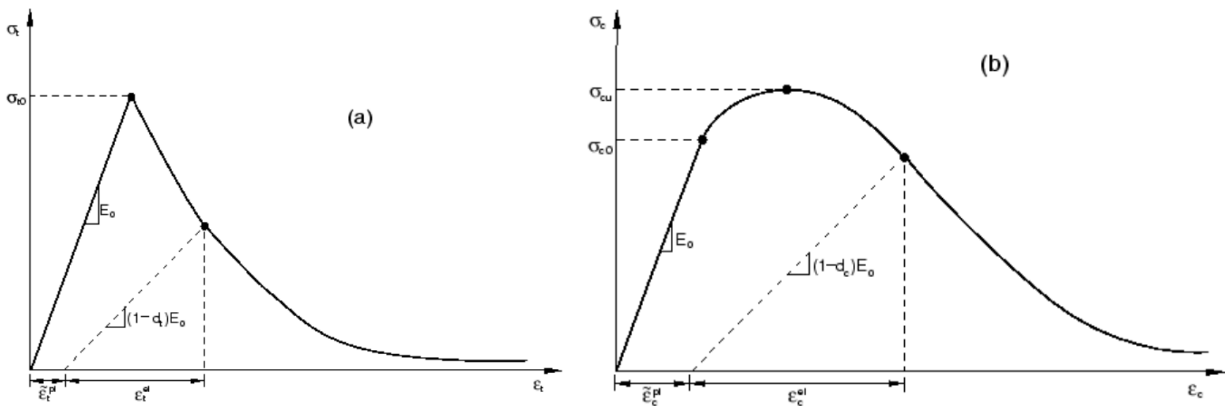
Figure 5-3. Response of concrete to uniaxial loading: (a) in tension; (b) in compression.[32]

28

For uniaxial tension, the stress-strain relationship of concrete is a linear elastic until the point of failure stress, σ_{t0}. After that point, due to micro cracking in the concrete, tensile resistance decreases with a sharp softening stress-strain response, which induces strain localization in the concrete structure. Under uniaxial compression, the response is linear elastic until the point of initial yield, σ_{c0}. In the plastic regime, the response is typically characterized by stress hardening followed by strain-softening beyond the ultimate stress, σ_{cu}. This representation, although somewhat simplified, captures the main features of the response of concrete.

As shown in Figure 5-3, when the concrete specimen is unloaded from any point on the strain-softening branch of the stress-strain curves, the unloading response is weakened: the elastic stiffness of the material appears to be damaged (or degraded). The degradation of the elastic stiffness is characterized by two damage variables, d_t and d_c, which are assumed to be functions of the plastic strains, temperature, and field variables. The damage variables can take values from zero, representing the undamaged material, to one, which represents the total loss of strength.

5.3   Analysis Procedure

For simulating the bridge behavior during construction, finite element analysis is divided into two main steps: bridge construction and final analysis for live loading. For the first step, an initial implicit static analysis is used to incorporate the loading effect through the erection and construction phase when the concrete is not hardened yet, and the section acts non-compositely with only the girders carrying the dead load. During the bridge construction, only the girders carry the deck, and the dead load deflections in the girders remain locked after the concrete deck hardens. For this reason, the stiffness and mass of the concrete and reinforcing rebar are reduced to a very low value during the construction phase, and an equivalent dead load of the deck is applied on the top flange of the girders based on the tributary area. Moreover, the self-weight of the structural steel of the girder components is applied to the model at this stage. By reducing the stiffness of the deck to negligible, only girders carry the load, and there will be no stress and strain on the concrete deck at the end of the construction phase once the concrete deck has hardened.

The results of the first step will be used as an initial predefined state for the final analysis step. In other words, initial states (stresses, strains, displacements, and forces) for the final analysis step is the final state at the completion of bridge construction. From this point on, the girder and slab sections act compositely together. Therefore, the initial equivalent uniform dead load of the concrete on the girders considered in the analysis for the previous step is removed and replaced by concrete with its actual stiffness and mass. The concrete damaged plasticity is also activated. Moreover, based on the construction procedure, railing elements are added at this step, which depending on the railing type, can increase the stiffness of the bridge. To model the sudden girder fracture, tie constraints between the elements of the girder web, and flange on two sides of the fracture assigned at the first step are removed.

At the final step, the flange and webs of one girder are fractured, and an HS-20 truck loading is applied at the middle of the span over the fractured girder with the maximum transverse eccentricity. At this stage, the bridge experiences large deflection and material damage, and the problem becomes highly nonlinear. Because of this, the implicit static solution method for analysis becomes very sensitive and suffers from numerical instability. As a result, the Explicit dynamic solution method that uses the Euler Central Difference scheme is used for the final analysis steps to prevent convergence problems. In Explicit solver, the solution at the end of a time increment is computed based on the state of the system at the beginning of the time increment. The stability of the solution is constrained to a small stable time increment and depends on the mass, stiffness, and size of the finite elements used.

In order to compare the results of dynamic analysis with static test experiments, HS-20 truck loading is applied on the deck slowly to minimize the dynamic effect of sudden fracture and loading on the bridge. The equivalent static deflection is then obtained by averaging the peak dynamic displacements after two periods of oscillation and the maximum. Figure 5-4 shows a typical girder mid-span deflections during dynamic explicit analysis.
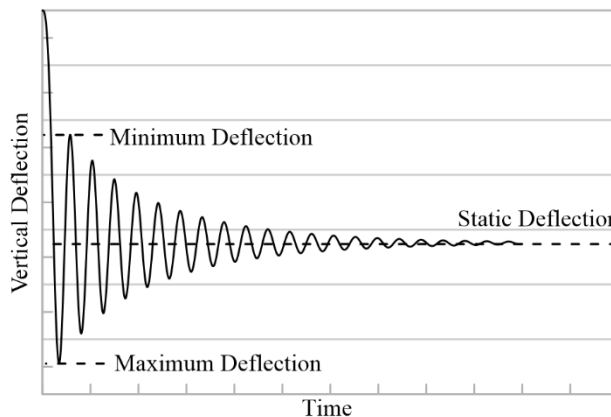
Figure 5-4. Typical dynamic girder deflection due to traffic loading

5.4   Nebraska Bridge Test

The University of Nebraska bridge, whose test results will be used here for validation of the FE model, is a full-scale simple span bridge with a span length of 70 ft and is 26 ft wide (two lanes). The superstructure consists of three welded steel plate girders made composite with a 7 ½ inches reinforced concrete deck, as shown in Figure 5-5. The girders are spaced 10 feet in the center, and the reinforced concrete deck has a 3 feet overhang. As shown in Figure 5-6, the railing system is a typical Nebraska Department of Road (NDOR) open concrete bridge rail, with 11x11 inch posts spaced 8 feet on center. Although the superstructure in this bridge did not contain steel box girders, due to the availability of reliable and extensive experimental results that included service and

30

ultimate load testing and associate failure modes, modeling of this bridge was thought to provide a good background for validation of the FE modeling method adopted for this study.

Figure 5-5. The cross-section of the Nebraska test

Figure 5-6. Details of standard NDOR open concrete bridge rail

Live load testing of this bridge consisted of applying cycles of the equivalent of 2.5 times the weight of AASHTO HS-20-44 truck load on each lane of the bridge. Because of the laboratory limitations, the loading pads were placed at twelve and fifteen feet, instead of ASHTO HS-20 typical spacing of 14 feet. To simulate the typical tire contact area, loads were applied through steel plates having the dimensions of 20"×8"×2" and 10"×4"×2" for the rear and front wheels, respectfully.

Several tests were conducted on this bridge to evaluate the effect of diaphragms, elastic behavior, and ultimate load-carrying capacity of the bridge. The ultimate test, which consisted of loading the bridge to collapse, is selected for validating the capability of FE modeling adopted in this study for predicting the elastic behavior and ultimate capacity and failure modes. During the ultimate load test, all diaphragms except those at the ends were removed to analyze more accurately the response of the steel girder bridge to the applied truck loading. The bridge failure in the laboratory testing is governed by local punching shear failure in the deck under the loading plates. Figure 5-7 shows the loading configuration of the ultimate test.

The strength tests on concrete cylinder samples showed 6000 psi for 221 days after casting, which coincides with the time of ultimate load testing. The steel material used for the girders was specified as A36 steel with the yield strength of 40 ksi, (average obtained from tensile testing), and the concrete reinforcing rebar used in the concrete slab was specified as grade 60 with 60 ksi yield strength. Figure 5-8 shows typical K frame diaphragms used in the ultimate test for the end supports. Deflection measured at mid-span by potentiometers is used to validate the FE model.
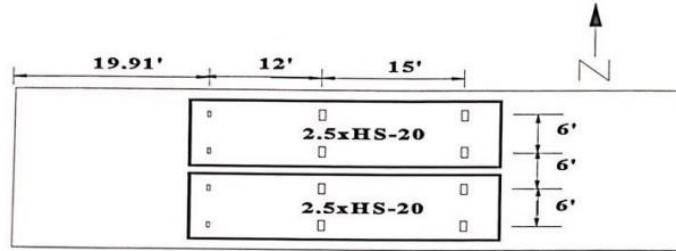
Figure 5-7 The loading configuration of the ultimate test.
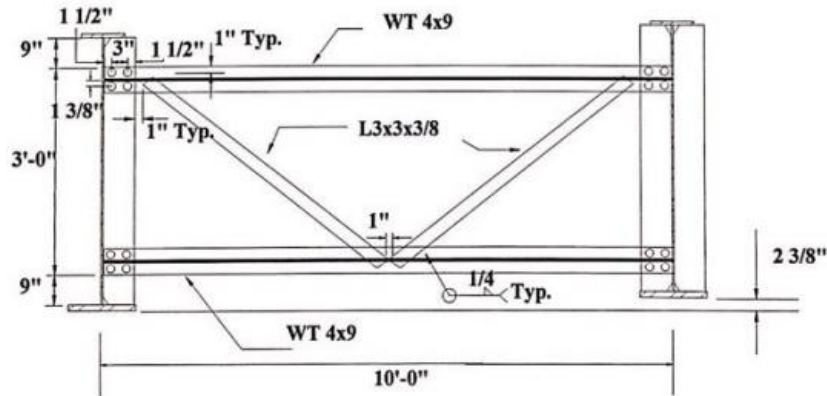
Figure 5-8. Typical K frame detail.

The two-step analysis (bridge construction and load application) was carried out to verify the capability of the FE model for predicting the global behavior and the local punching shear failure for the ultimate test. Figures 5-9 and 5-10 show the location and pattern of local punching shear failure that occurred in the experimental test and the FE concrete damage at the top and bottom of the deck, respectively. Figures 5-11 to 5-13 show the comparison of load-deflection curves between experimental and FE results for exterior and interior girders.
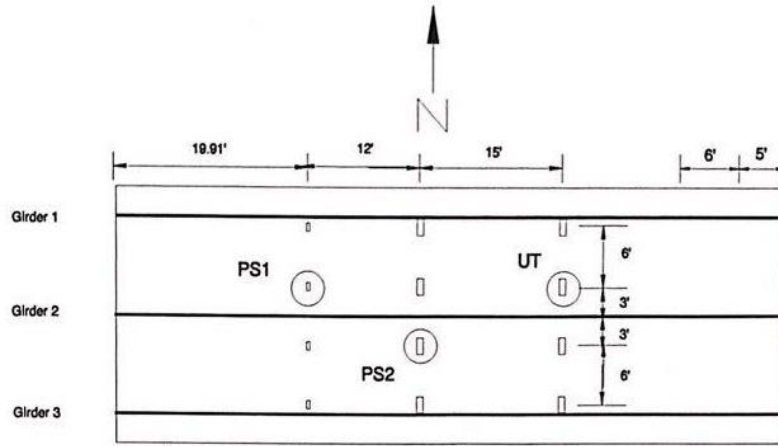
(a)
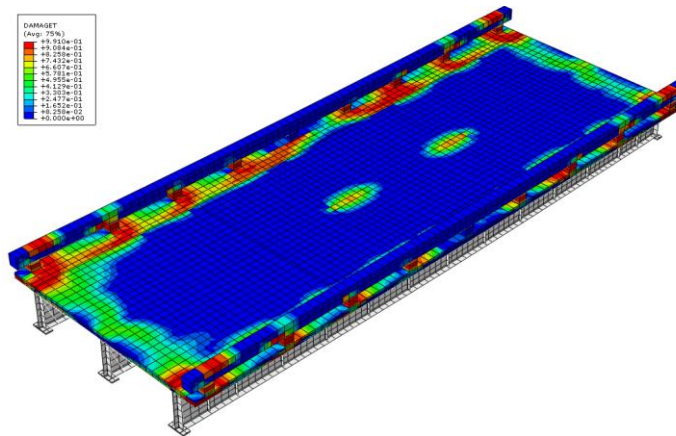
(b)

Figure 5-9. The locations of punching shear failure: (a) Experimental test; (b) Finite Element Model.

(a)
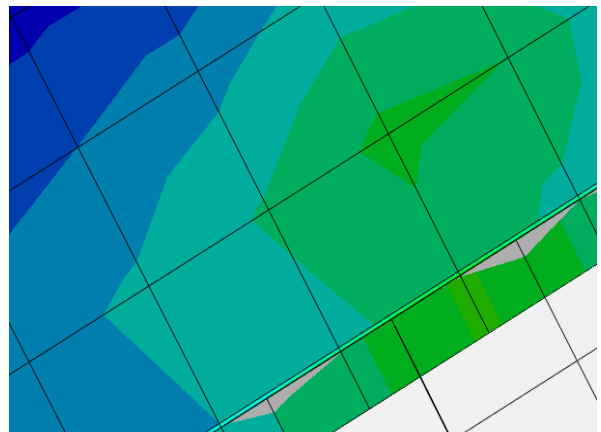
(b)

Figure 5-10. Typical punching shear failure: (a) Experimental test; (b) Finite Element Model.
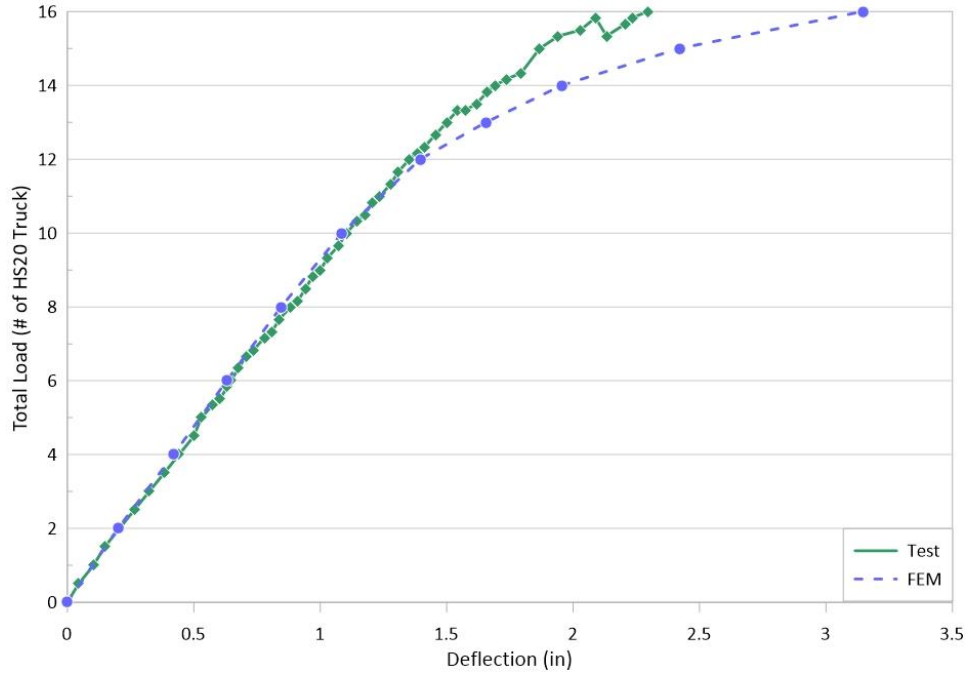
Figure 5-11. Comparison of load-deflection curves for north exterior girder obtained from experiment and FE model.
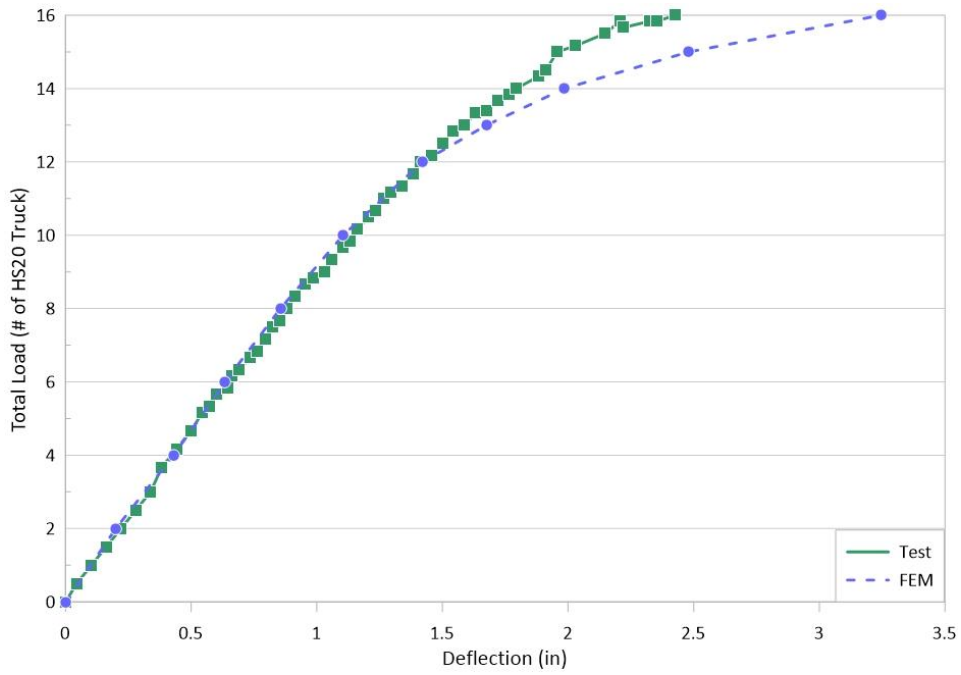
Figure 5-12. Comparison of load-deflection curves for south exterior girder obtained from experiment and FE model.
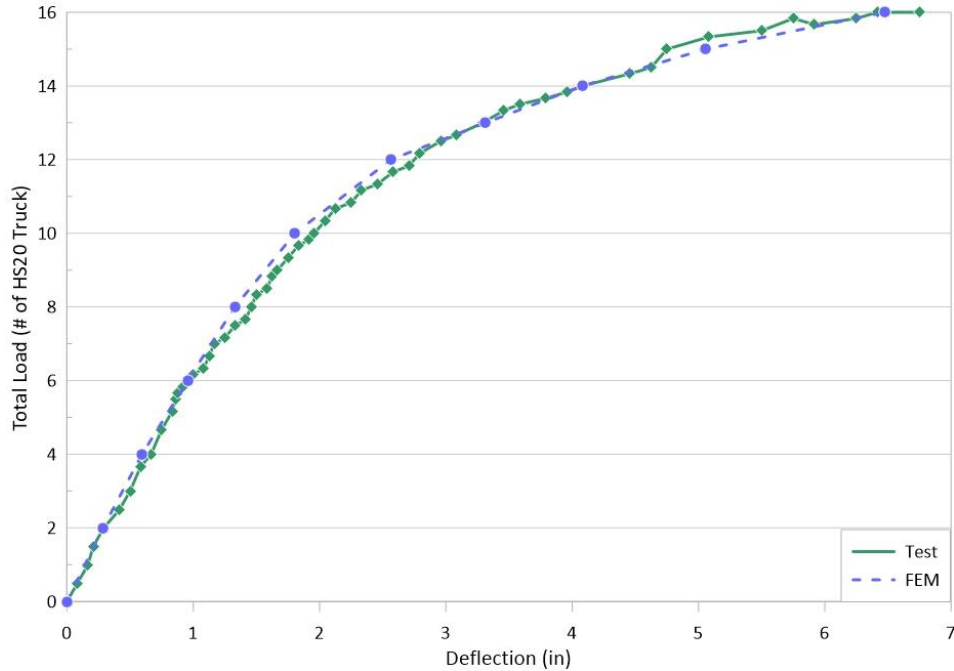
Figure 5-13. Comparison of load-deflection curves for interior girder obtained from experiment and FE model.

Figure 5-14 compares the local cracking in the railing during ultimate load testing for the experimental test and FE model. The results and comparisons show that the FE model can predict the global behavior of the bridge during the elastic and plastic states and simulates the local failure due to punching shear in the deck and cracking in the railing.

| *(a)* | *(b)* |
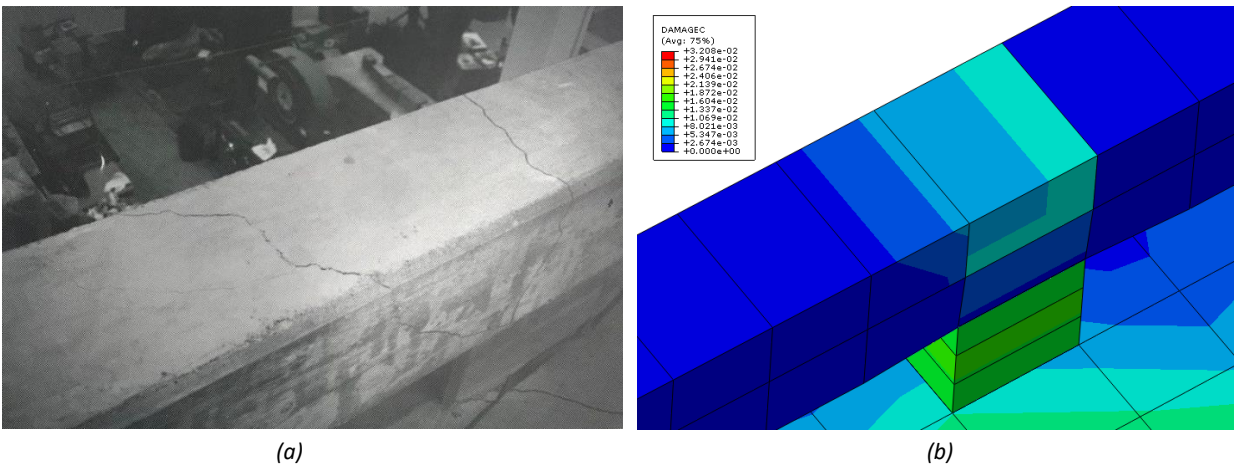
Figure 5-14. Torsional cracks in the rails: (a) Experimental test; (b) Finite Element Model.

5.5   The University of Texas Twin Steel Box Girder Bridge

To further verify the FE model for the case of a bridge with steel box girders, The University of Texas Twin Steel Box Girder bridge was selected. This bridge had been tested in full-scale, with one of its girders having the bottom flange and part of the web fractured, and therefore, offered an excellent opportunity for FE model verification. The UT bridge was a curved 120-ft composite single-span twin box girder bridge. The deck width was 23.3 ft with the radius of curvature of 1,365.4 ft and deck slab thickness of 8 in. The bridge also used 3 in. concrete haunch above the flange of the steel boxes. Figure 5-15 shows the UT bridge that was tested. The deck in this bridge also had erection diaphragms, end stiffeners, intermediate diaphragms, and horizontal bracings.

Three tests were conducted on the full-scale bridge. The first test was performed to evaluate the behavior of the bridge under loading simulated by the weight of concrete blocks (slightly over HS-20 loading and equal to 76 kips total) after a sudden fracture at the bottom flange of the exterior girder. The second test was conducted by cutting the bottom flange and 83% web of the exterior girder to study the fractured bridge behavior under the same loading as Test 1. And finally, the ultimate load test was performed to investigate the ultimate load-carrying capacity of the fractured bridge. The ultimate test was performed by increasing a uniform load applied using sand over the HS-20 truck outline area until the bridge collapsed. These three tests were used for verification of the FE model for the fractured bridge scenario.

Figure 5-15. The University of Texas twin steel box girder bridge.

The steel material used for the girders of this bridge was specified with a yield strength of 50 ksi, and the reinforcing rebar used in the concrete slab was specified as grade 60 with 60 ksi yield strength. Based on the compression tests performed on the concrete cylinder samples, 5.37 ksi for the first test and 6.23 ksi for the second and third test was used as the compressive strength of concrete in the deck.

Similar to the earlier analysis, a two-step analysis (bridge construction and load application) was performed with the FE model for simulating the experimental testing on the UT bridge. Figure 5-16 shows the FE model used for validating the results. Hard contact surfaces were used for defining the surface contact at railing gaps, and girders support bearings in this model. Since there is a gap between each railing segment, there is no contact between railing segments until the gap is closed due to large deflection of the bridge, as shown in Figure 5-17 with the stress and concrete damage rise at railing contact points. After closing the gap, the contact force increases the stiffness of the bridge. As a result, for the first test, since there is a small deflection, the railing does not increase the stiffness of the system. However, for the second and third tests, surface contact between railings increases the stiffness of the bridge.
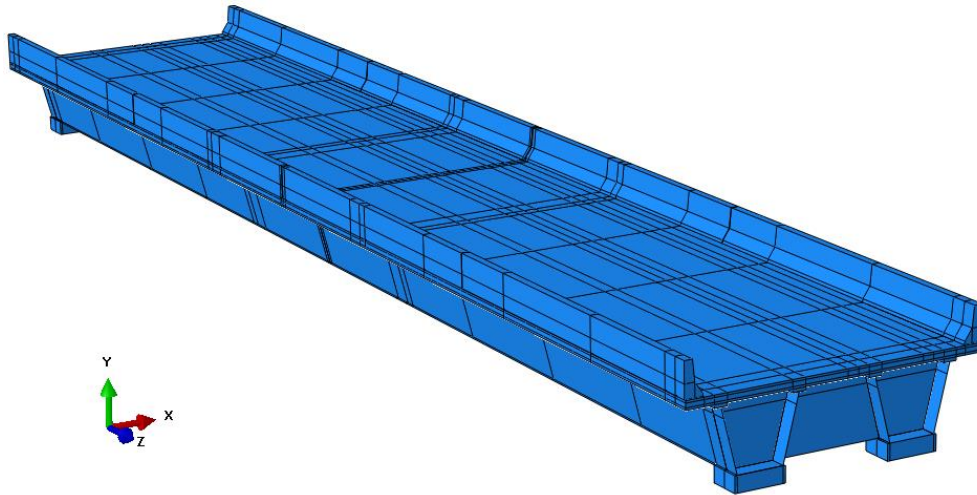
Figure 5-16. The University of Texas FE model.
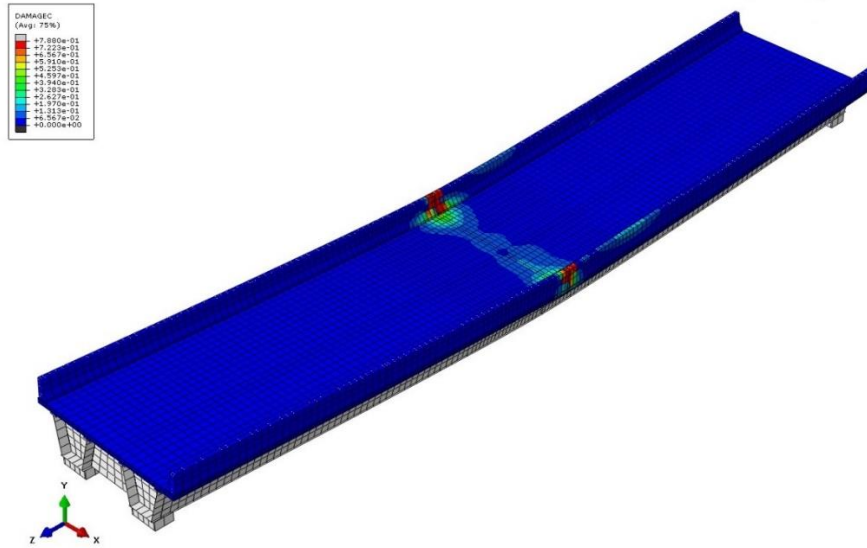
Figure 5-17. Crushing of the railing due to contact surface.

Figures 5-18 and 5-19 show the comparison between experimental and analytical deflection of the fractured girder for the first and second tests, respectively. The horizontal axis in these graphs shows the location along the span, and the vertical axis shows the deflection at the end of the test. As shown in these graphs, the FE model can predict the deflection of the girder along the bridge for both first and second tests. One exception is for Test 2 (Figure 5-19) for deflection at the mid-span. A separation between the top flanges of the fractured girder and the concrete deck due to tension cracking of the concrete was observed during the second experimental test, which caused a sudden deflection at the middle of the span. This may, however, be attributed to post-failure local loss of composite action. By defining the concrete damage plasticity, the FE model can predict the cracking and crushing of the deck due to loading within its capabilities.

Experimental results of the University of Texas test show that extensive cracking developed on the top surface of the concrete deck in the second test. The most prominent cracks were located longitudinally above the intact girder due to one-way shear failure, and the cracks extended toward the supports. Furthermore, some transverse cracks were observed starting from the railing of the fractured girder toward the intact girder. Figures 5-20 and 5-21 show the crack pattern on the surface of the concrete deck from both experimental test and FE analysis. As shown, the FE model can predict the transverse and longitudinal crack pattern of the concrete deck due to load distribution after the fracture.
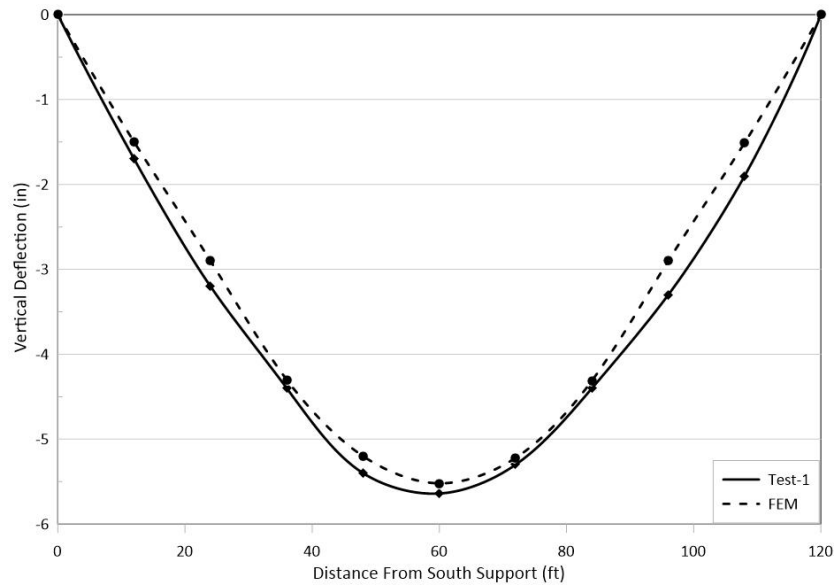
Figure 5-18. Comparison of the deflection curve of the first test for fractured girder obtained from experiment and FE model.
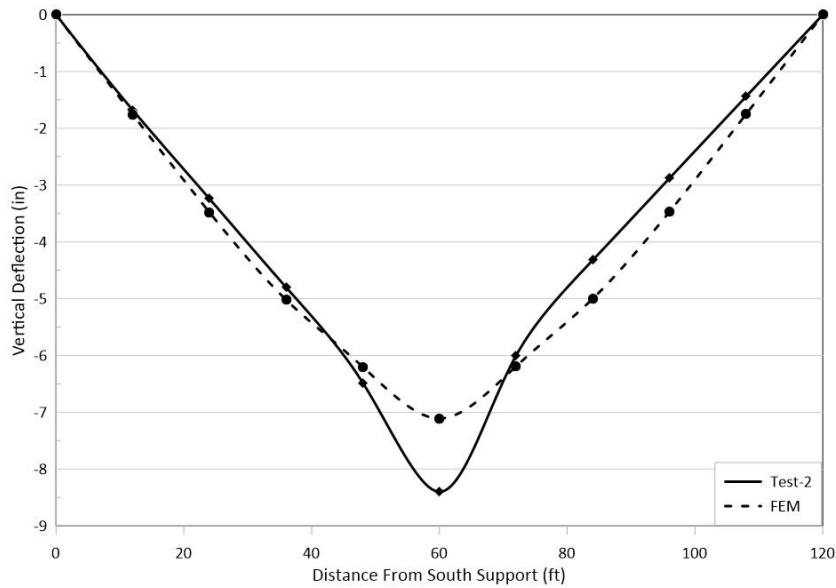
Figure 5-19. Comparison of the deflection curve of the second test for fractured girder obtained from experiment and FE model.

39
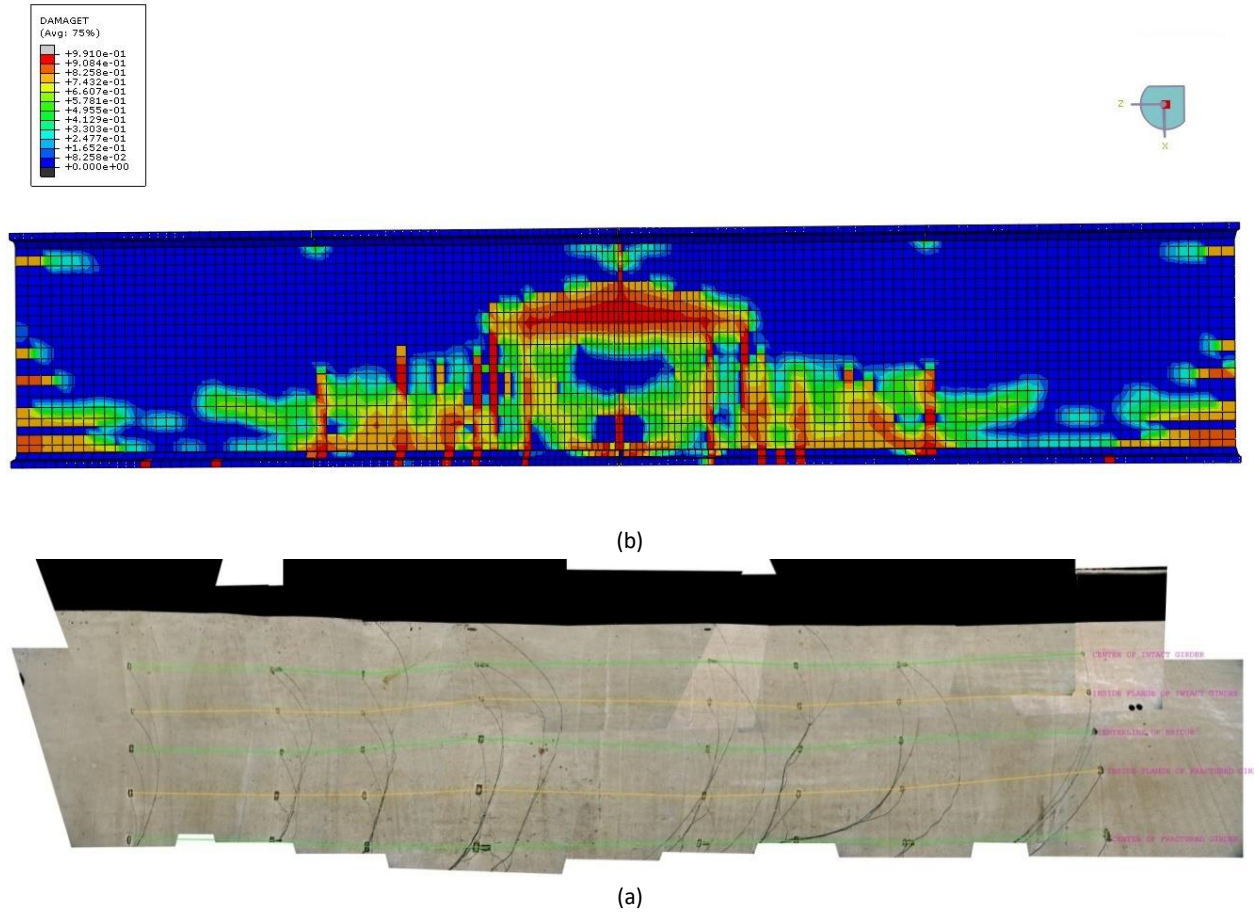
Figure 5-20. Crack patterns on concrete deck: (a) Experimental test; (b) Finite Element Model.

(a)   *(b)*
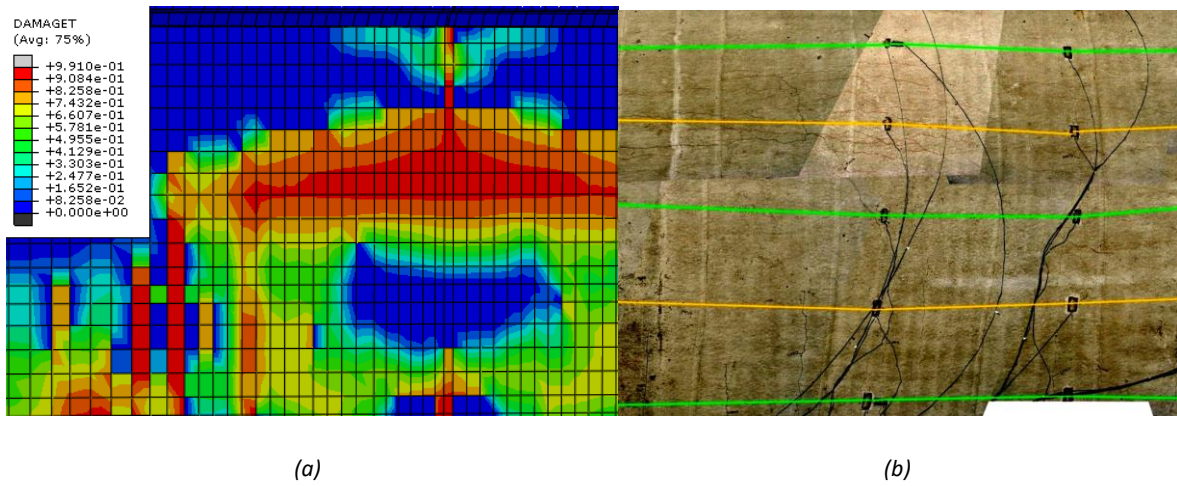
Figure 5-21. Crack patterns above the interior flange of the intact girder: (a) Experimental test; (b) Finite Element Model.

5.6 The Florida International University Twin Steel Box Girder Bridge Specimen

After comparing the results of the FE model with the experimental test results for two full-scale bridges (The Nebraska bridge Test and UT bridge), a twin steel box girder bridge specimen tested by the Florida International University (FIU) (Figures 5-22 and 5-23) was selected to validate the capability of the FE model for predicting local failure modes like punching shear or one-way shear of the concrete slab in addition to predicting the global behavior. The results from the FIU experiments indicate that the bridge with a full fracture in one of the girders has some reserved capacity, and the vertical loads could be transferred to the intact girder through one or more of the railing, continuity, slab, and external cross frames. Moreover, the results show that depending on the loading configuration, the failure mode of the fractured bridge could be punching shear or one-way shear of the deck.
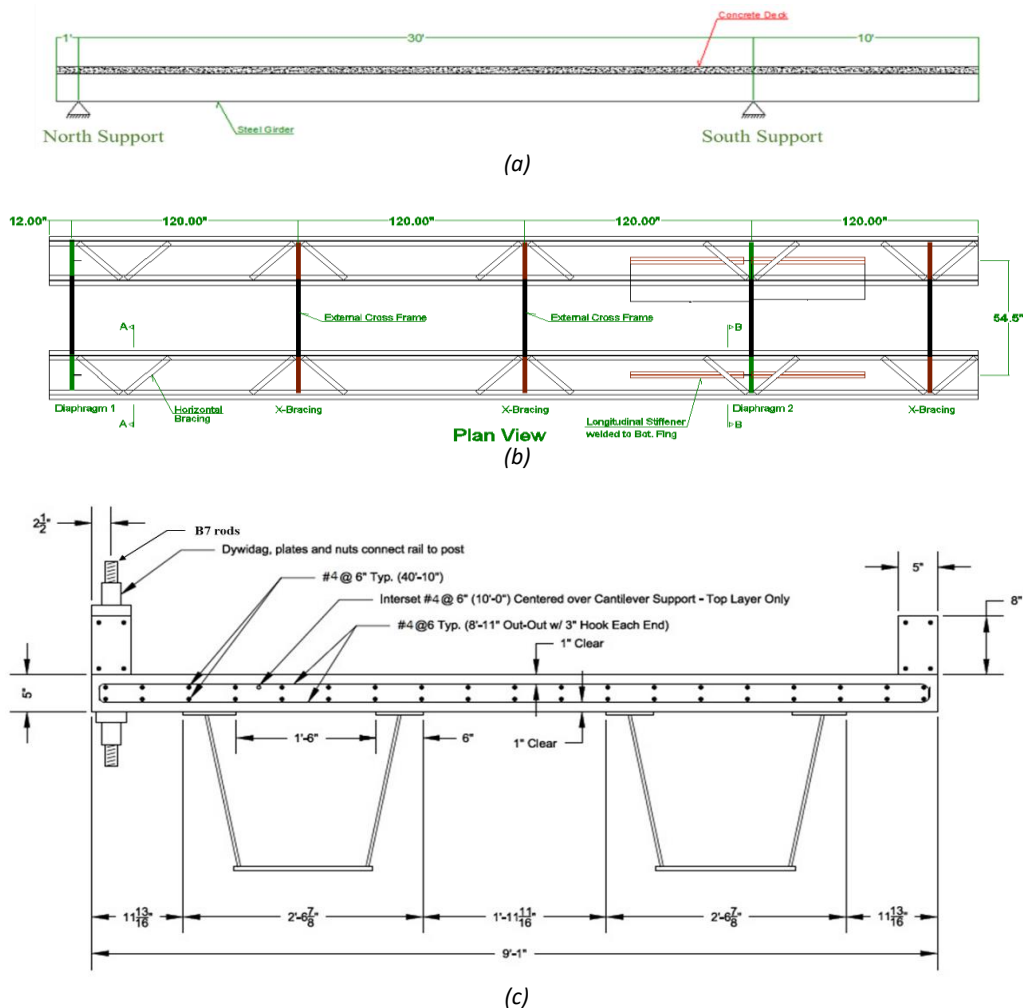
Figure 5-22. The Florida International University bridge: (a) Side view; (b) plan view; (c) cross-section view.

41

Figure 5-23. The FIU test setup: (a) View from cantilever end; (b) View from the simply supported end.
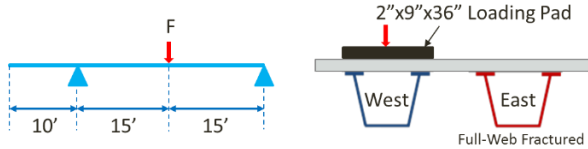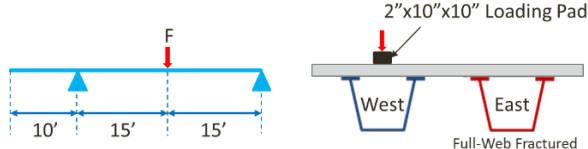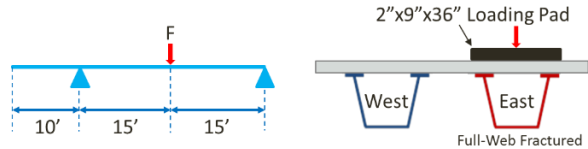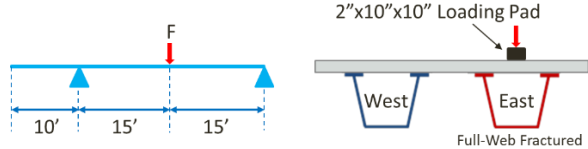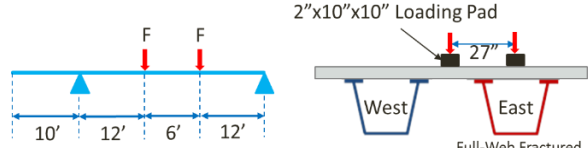
The FIU bridge was an approximately one-third scale straight version of a typical twin steel box girder bridge. The bridge consisted of two spans to consider the effect of continuity on the bridge redundancy with a total length of 41 ft. and width of 109 in. The thickness of the deck was selected and designed to be 5 in. to provide enough space for four mats of #4 reinforcement bars. A removable railing system, including several railing segments, was used to investigate the effect of railing on the behavior of the fractured bridge. Figure 5-22 shows the cross-section and side view of the bridge, and Figure 5-23 shows the FIU test setup.

All the steel plates of the box girders were ASTM A709 Grade 50, and the steel reinforcements were A706 Grade 60 materials. The concrete used for the deck had a compressive strength of 7.8 ksi at the time of the ultimate tests. Several elastic tests, a cyclic test, and five ultimate tests were conducted on this bridge to investigate the behavior of twin steel box girder bridges in both linear and nonlinear range. In order to investigate the failure mode for the fractured bridge, five ultimate tests were performed on the bridge with a full fracture in one of the girders, which are summarized in Table 5-1. Railing segments and continuity were removed for the ultimate tests and different load configuration and locations were used to investigate all the possible failure modes for the fractured bridge.

Tests E-1 and E-2 (Table 5-1) of five ultimate tests performed by FIU were modeled to validate the FE method for predicting local and global failure modes for the one-girder fractured condition. Test E-1 included loading on top of the fractured girder with a single loading pad (2×9×36 in.) placed at the mid-span location, and Test E-2 included a single smaller loading pad (10 in. square) over the fracture in between the steel girder flanges to investigate the punching shear failure. The overall response of the ultimate Test E-1 illustrated that the fractured bridge had a linear elastic response up to 60 kips. After that, by extending longitudinal and transverse cracks at the mid-span, the bridge stiffness greatly reduced, and at the load of 156 kips, the specimen failed due to concrete deck crushing under the loading pad. The test results indicated

42

that a combination of one–way shear and two-way shear was the failure mode of the fractured bridge under a large single loading pad, as shown in Figure 5-24.

Table 5-1. The FIU ultimate load tests.

Test	Loading Configuration	Loading Type
W-1		The load was applied until the plateau in the load-deflection curve was observed. The test was discontinued before the failure.
W-2		The load was applied until the failure occurred
E-1		The load was applied incrementally until failure occurred.
E-2		The load was applied until the failure occurred
E-3		The load was applied through four loading pads until failure occurred.

Since in the ultimate test E-1, the edge of the loading pad was located on the top of the girder flanges, the ultimate test E-2 was conducted to consider the punching shear failure between flanges. The results of test E-2 show that the damaged girder responded linearly up to 30 kips when cracking of concrete started to propagate; however, as shown in Figure 5-25, the intact girder responded linearly for the entire test until the punching shear failure through the loading pad at 83 kips. It is important to note that since this test was conducted after ultimate Tests, W-1 and W-2, and the deck was not reconstructed (only repaired locally), there are some residual deformations in the experimental test results. Therefore, the experimental results of this test are used only for comparing the punching shear capacity predicted by the FE model and the test results.

The FIU bridge specimen was constructed with shoring and then transferred to the test setup. Therefore, the analysis with the FE model was performed only by the application of the load at the loading pad for simulating the experimental testing on the bridge. The displacement control approach was utilized to simulate the test loading by defining a frictionless contact surface between

the loading pad and the bridge deck. Figure 5-26 shows the FE model used for the analysis. Experimental tests of this bridge showed that one-way or (punching) two-way shear failure is the failure mode for the bridge with one fractured girder under wheel simulated loading. To simulate this type of failure, the concrete damage plasticity index for cracking and crushing was calculated over the effective area of one-way shear and (punching) two-way shear, as shown in Figure 5-27. The damage index is indicative of the extent of damage occurring at each stage and can be effectively used to signal shear failure over the effective area/line. In the analysis, damage index along the effective lines and within the slab depth were calculated and averaged.

(a)

(b)

(c)

(d)

(e)

Figure 5-24. Damages in the Test E-1 of FIU bridge.

44

Figure 5-25. Punching shear failure in the Test E-2 of FIU bridge.
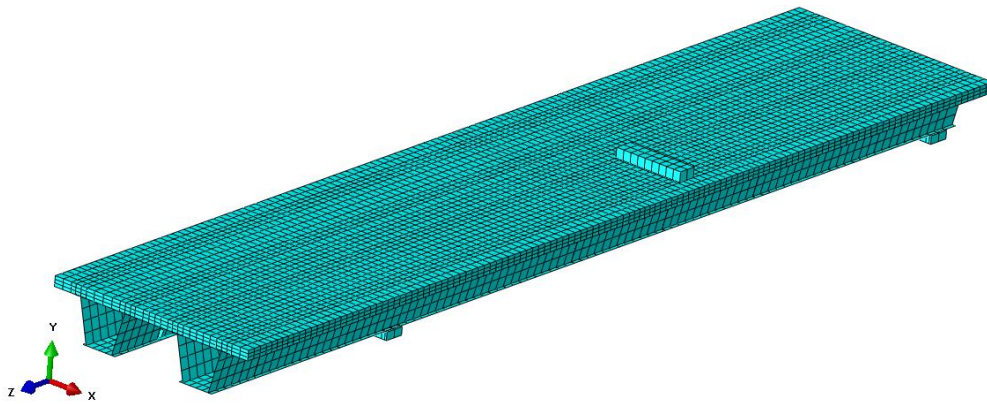
Figure 5-26. The FIU bridge FE model.

In general, shear strength in reinforced concrete slabs can be checked by two approaches. The first approach is to calculate the beam shear capacity over a certain effective width of the support. The second approach is to calculate the punching shear capacity of the slabs over the critical perimeter around the load. ACI 318-14 [38] will be utilized in this study to predict the shear resistance of a damaged twin steel box girder bridge that predominantly failed in one-way or two-way shear. It should be noted that these shear resistance expressions are derived based on results from beam tests. For beams, the maximum shear stress is assumed to be uniform over the entire beam width so that the entire width will be used to compute the shear resistance in the beam. For the slabs, however, the shear resistance should not be calculated over its entire width but over a certain effective width (b_{eff}). The effective width of a one-way slab under a concentrated load can be determined using either a fixed width approach or a horizontal load spreading approach. The horizontal load spreading approach is a more popular approach where the effective width is determined by the projected length of the load onto the face of the support. There are a couple of variations of this horizontal load spreading approach being used depending on the local practice

45

and nature of the problem. Based on the ACI 318-14, the one-way and two-way shear capacity of the deck can be calculated using Equations (3) and (4), respectively.

(a)

(b)

(c)

(d)
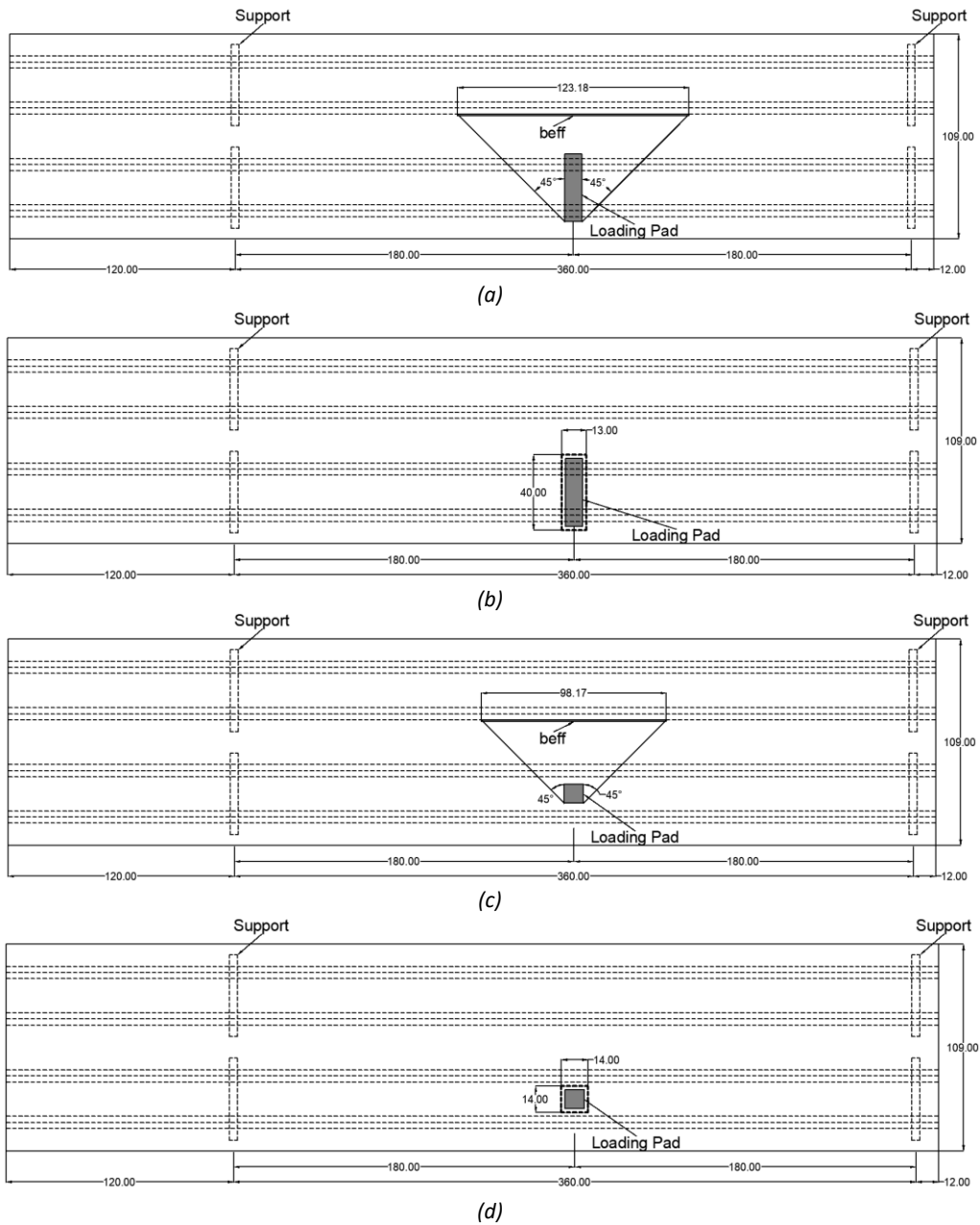
Figure 5-27. Determination of effective width: (a) One-way shear for Test E-1; (b) Two-way shear for Test E-1; (c) One-way shear for Test E-2; (d) Two-way shear for Test E-1.

46

$$V_{ACI} = 2\sqrt{f'_c}b_{eff}d \text{ (psi)} \tag{3}$$
$$P_{ACI} = 4\sqrt{f'_c}b_od \text{ (psi)} \tag{4}$$

These equations were derived from tests on slab-column connections and also applicable to slabs. The effective width for calculating one-way shear is determined using 45° horizontal spreading from the far side of the load, as shown in Figure 5-27. This method was also found to have a better correlation with the experimental results of Lantsoght's study [40]. When the slabs are subjected to multiple concentrated loads, the effective width can be considered by each wheel load separately or by each wheel axle. In ACI 318-14 code, the punching shear stress is assumed to be twice the maximum shear stress of beams failing in the one-way shear manner. The punching shear resistance of the slabs, according to ACI 318-14, is calculated over a critical perimeter, b_o, located at a distance d/2 away from the loading area. It is important to note that the predictions of the punching shear resistance of the bridge slabs in both Tests W-2 and E-2 would be the same using the punching shear provisions above since the load was applied over the same area of the footprint. However, as observed in the experiment, the punching shear failure load in Test W-2 was more than two times greater than the failure load in Test E-2. This significant difference indicated that the fracture damage had a great influence on the punching shear capacity of the deck slab. Critical perimeter and effective width for Test E-1 and E-2 are shown in Figure 5-27.

As was mentioned above, damage indexes along the effective lines and within the slab depth were calculated and averaged as an indication of one-way and two-way shear failure. The average tension damage index for all elements of the effective width and perimeter, as shown in Figures 5-28 and 5-29, is obtained from the FE model to investigate the one-way and two-way shear failure modes of the model. Figure 5-30 (b, d) illustrates the load-tension damage index curve for Test E-1 and E-2. The average damage index of zero in these graphs shows that there is no damage in the effective area. As damage progresses, the damage index increases toward one that would indicate fully damaged elements and complete loss of stiffness in tension. For convergence reasons, however, a smaller upper limit of 0.9 was considered. It is also understood that some portions of element thickness toward the bottom of the deck panel could be in compression and therefore not included in damage index calculation, another reason for the average index to be lower than 0.9. As it can be concluded from the results, the effective one-way shear width starts cracking around 32 kips and 45 kips for the Test E-1 and E-2, respectively. Tension cracks start to propagate from the surface of the mid-span and extend to the supports and depth of the deck. By comparing the damage index of the FE model and experimental test results, it can be concluded that when the average damage index of the effective area reaches about 0.7, the section has lost its capacity in carrying more load, a stage that can be considered as the one-way or two-way shear failure. At this point, the maximum tension damage index for all elements of the effective area in tension is reached to signal negligible capacity. Figure 5-30 (b) indicates that both one-way and two-way shear failure occur at the end of Test E-2 around 160 kips loading. However, Figure 5-30 (d) shows that by decreasing the size of the loading pad in Test E-2, the two-way shear capacity of the section was decreased, and therefore, the FE and experimental Test results show that two-way shear is the

failure mode for Test E-2 with the capacity of around 83 kips. Table 5-2 compares the results of one-way and two-way shear capacity obtained from the Test, FEM, and ACI 318-14.
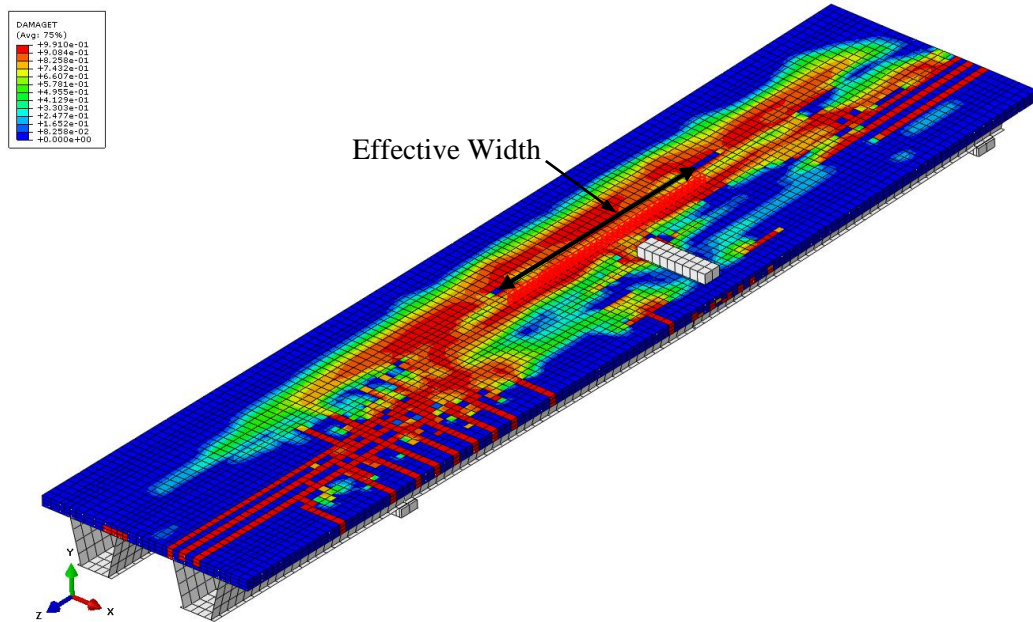
Figure 5-28. One-way shear effective width in the FE model.
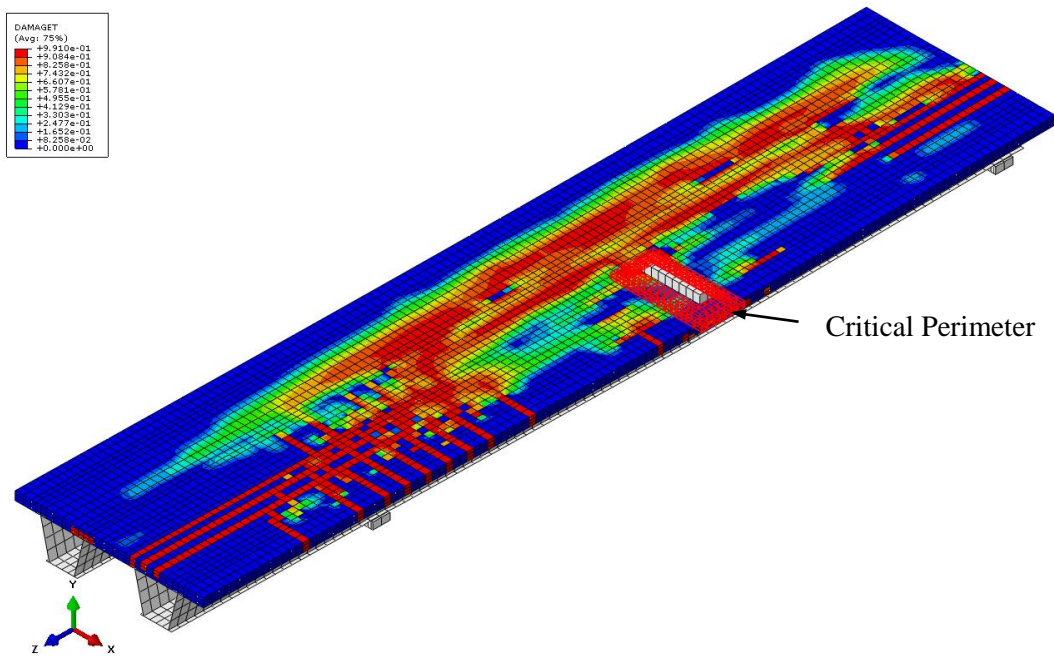
Figure 5-29. Two-way shear critical perimeter in the FE model.

48
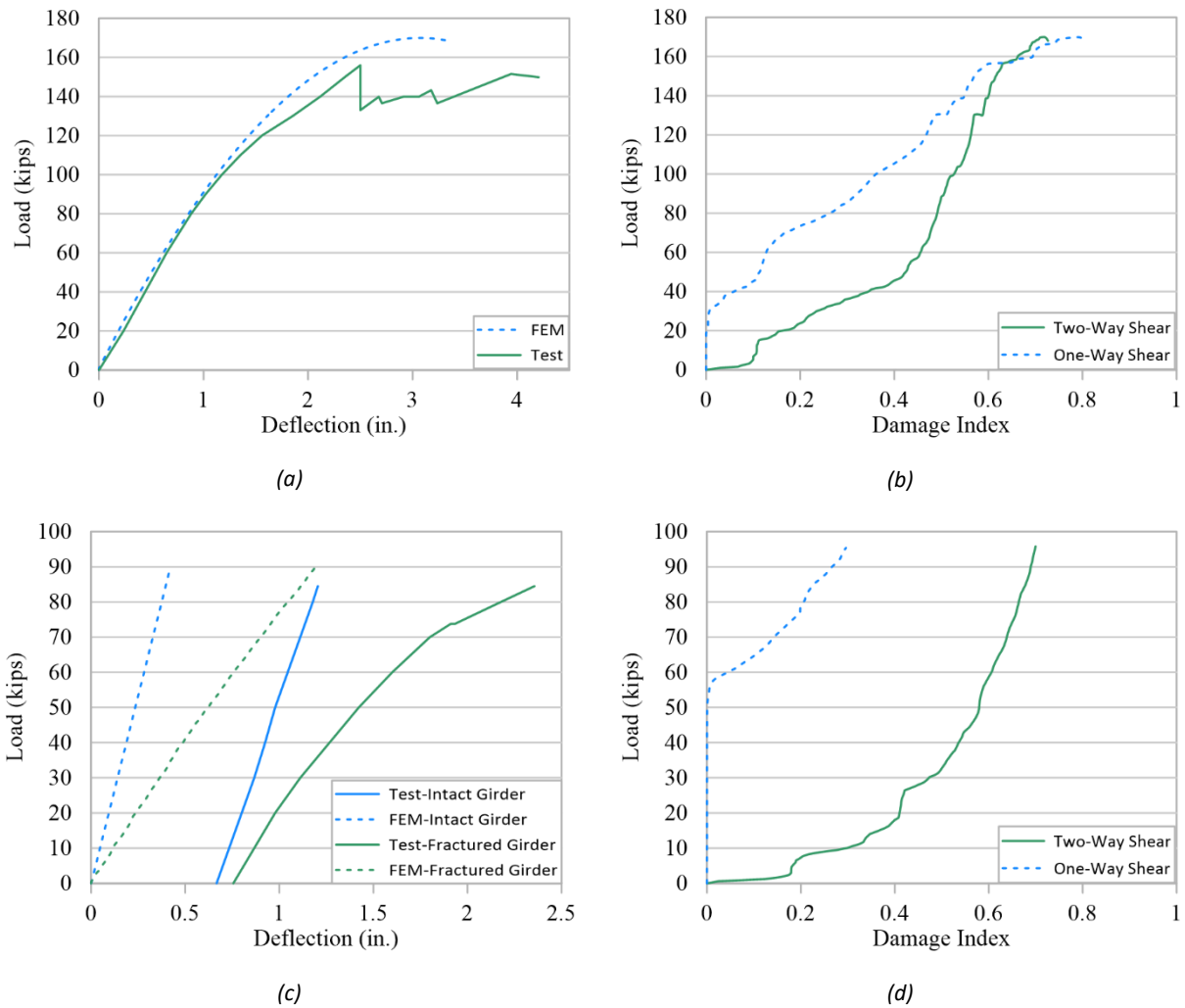
Figure 5-30. Comparison of the FE model with the experimental test: (a) Load-deflection curves of Test E-1; (b) Concrete Damage Plasticity Index of Test E-1; (c) Load- deflection curves of Test E-2; (d) Concrete Damage Plasticity Index of Test E-2.

Table 5-2. Comparison of one-way and two-way shear.

	Test E-1 $f'_c = 7.8\ ksi$		Test E-2 $f'_c = 7.2\ ksi$	
	One-Way (kips)	Two-Way (kips)	One-Way (kips)	Two-Way (kips)
Test	156	156	-	83
FEM	161.9	168.6	159.8	94.17
ACI	87.03	149.79	66.64	76.03

In order to obtain useful data for local behavior of the fractured bridge under point loads in the FIU test, strain gauges and potentiometers were installed along the length of the specimen at different sections, as shown in Figures 5-31 and 5-32. It is important to note that in addition to predicting the global response, the FE model also needs to be validated for simulating the local

49

behavior of the bridge in the ultimate tests to demonstrate its ability for predicting load transferring mechanism and failure modes. To this end, strain results of the FE model for top and bottom flanges of the intact girder at mid-span section and the strain of intact girder bottom flange at section 5 way from the mid-span for the Test E-1 are compared with the experimental results and shown in Figure 5-33 (minor fluctuation in the FE results is due to utilizing the dynamic solution for the damaged bridge). The comparison of the strain data shows that the FE model could predict not only the global behavior and failure mode but also local behavior and load transferring mechanism.
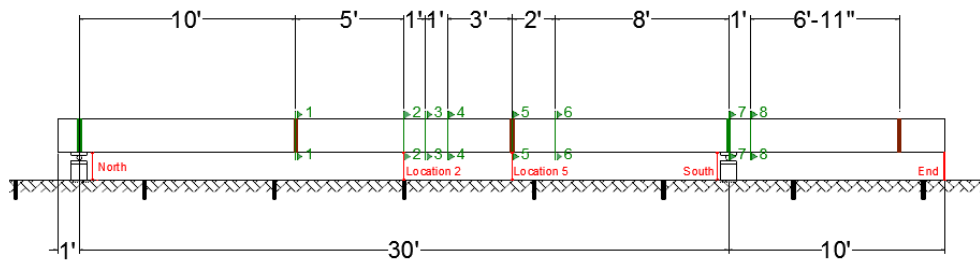
Figure 5-31. Location of strain gauges and potentiometers along the length of the specimen in FIU test.
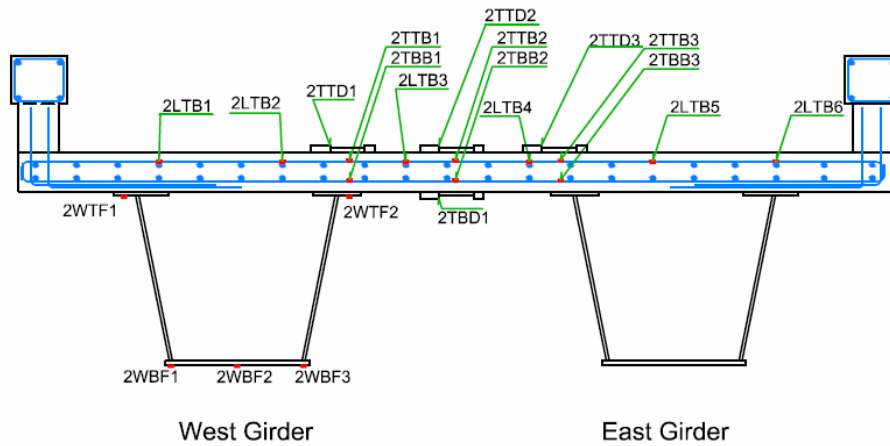
Figure 5-32.Strain gauges in section 2 of the FIU test.
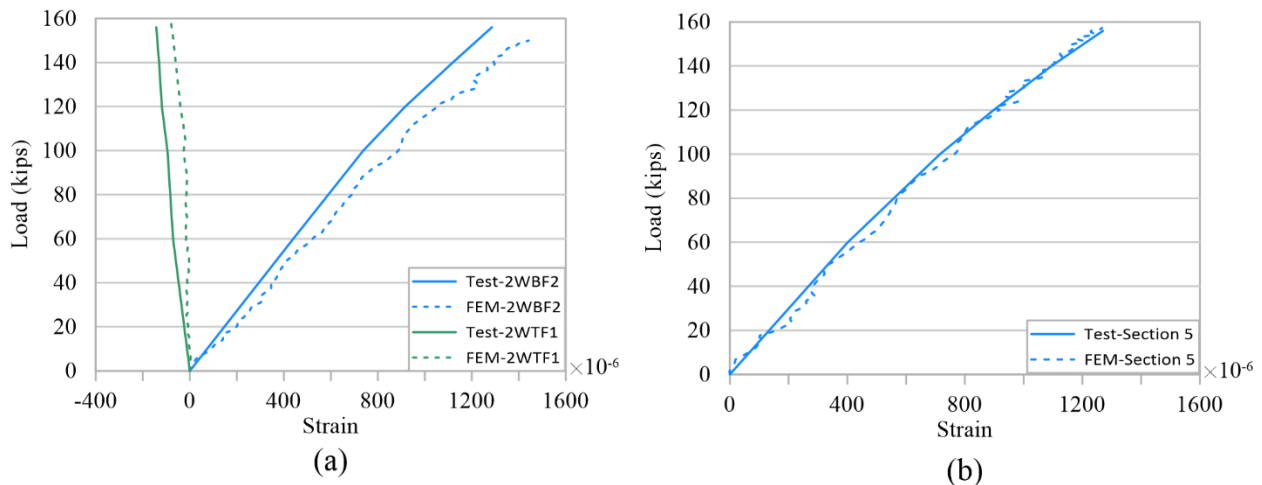
Figure 5-33. Comparison of the longitudinal strain of intact girder: (a) Section 2; (b) Section 5.

50

5.7 FE Analysis for Load-Carrying Capacity of a Baseline Bridge

After verification of the FE model, The University of Texas bridge was selected as a baseline model for developing information for preliminary reliability analysis of twin steel box girder bridges. The bridge was analyzed for two scenarios of the intact bridge, where both girders are intact, and the fractured scenario, where one of the girders is fully fractured. The goal was to develop the response curve and maximum load-carrying capacity under these scenarios and to investigate the local and global behavior of the twin steel box girder bridge under the HS-20 truck loading. The HS-20 truck loading configuration is shown in Figure 5-34. The distance between the front and middle axles shall be varied between 14 ft and 30 ft to produce the maximum loading effect. The tire contact area is assumed to be a single 10-in. square footprint for the front wheels and a single rectangular with 20 in. width and 10 in. length footprint for the rear wheels. In this study, axle distances were considered to be 14 ft, to produce the maximum positive moment and deflection in the middle of the bridge. The truck load is placed in the middle of the bridge (at a position to produce the maximum moment at fracture location) and only in one lane over the left box girder (fractured) to create the worst scenario, i.e., when there is maximum torsion and bending on the bridge due to eccentric loading caused by distributions [41]. The truck load was increased in terms of multiple HS-20 until the bridge reaches its maximum capacity.
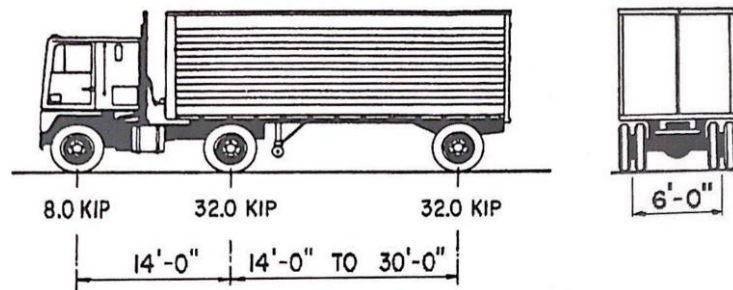
Figure 5-34. Characteristic of the design truck.

5.7.1 Intact Bridge

Figure 5-35 shows the load-deflection curve for the intact bridge scenario at the middle of the span under the center of the girders due to truck loading. The truck loading increased until the load-displacement curve flattened, indicating approaching the maximum load capacity of the bridge. This condition was associated with the development of plastic strain over the entire section of both girders. Before reaching this stage, local failures were in the deck were also observed. The first local failure, as shown in Figure 5-36, was the punching shear pattern under the rear wheels around nine times HS-20, after which one-way shear occurred above the right box. After the local failures, the bridge still continued to carry higher loads until 19 times the HS-20, at which the bridge response (load-deflection curve) plateaued, indicating reaching maximum capacity due to the formation of a hinge in the girders. Figure 5-37 shows the plastic stress over the entire sections at 19 times the HS-20 load.
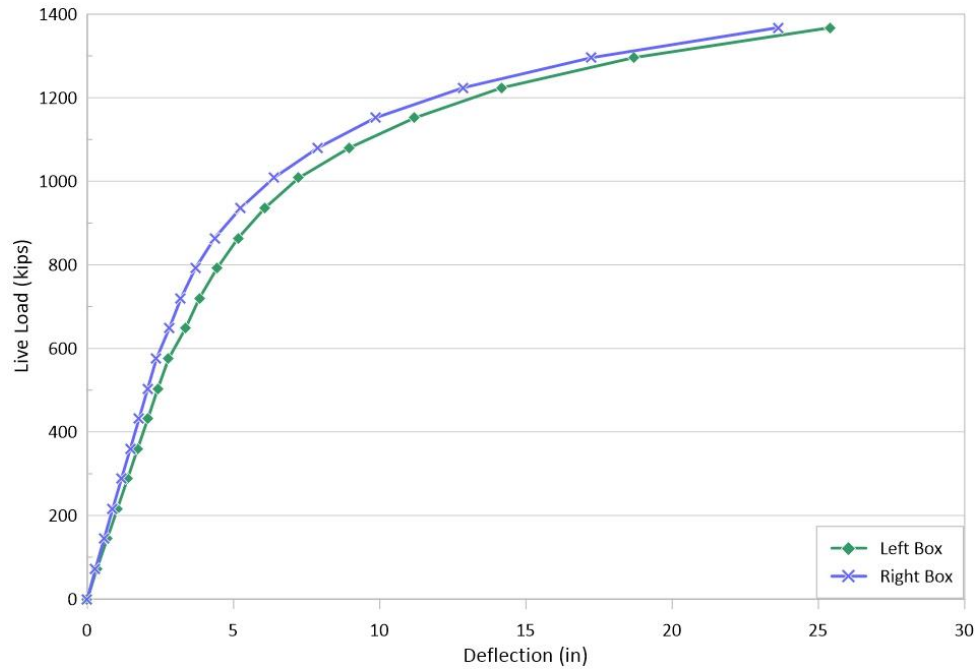
Figure 5-35. Load-deflection curves of intact bridge obtained from the FE model.
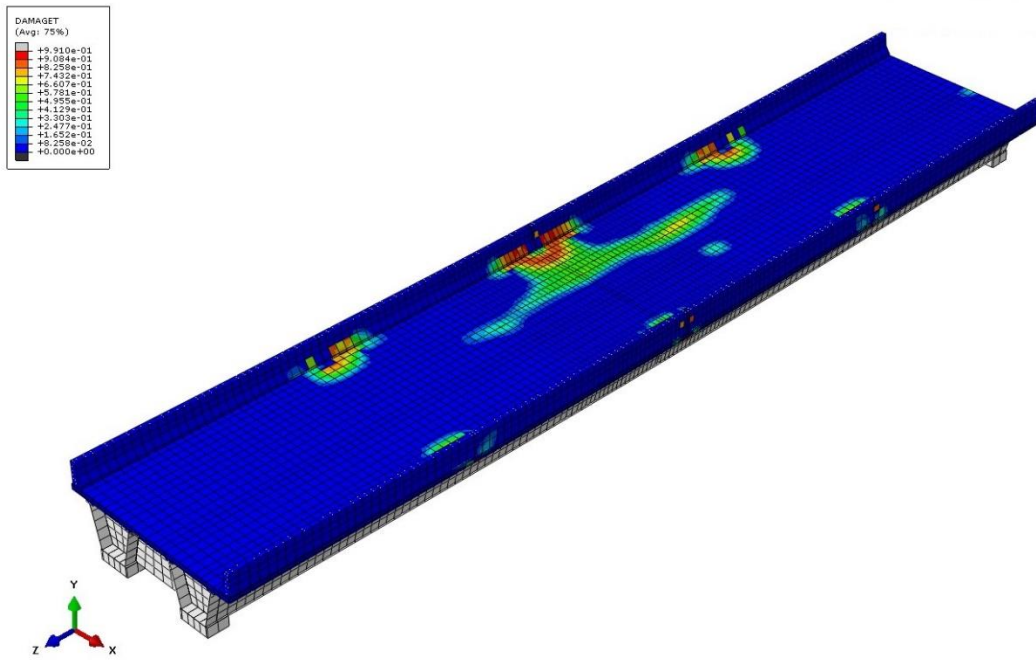
Figure 5-36. The punching shear failure of the concrete deck under 9xHS-20.
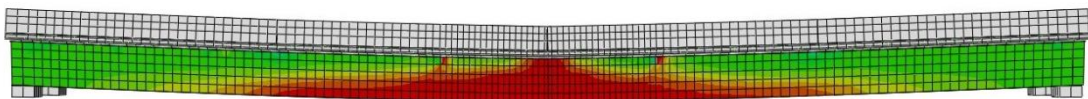
Figure 5-37. Plastic stress of the steel boxes under 19xHS-20.

52

5.7.2 Bridge with One Fractured Girder

The FE results of the damaged bridge show that once the sudden fracture happened, the bridge had a 3.1 in. deflection under the self-weight of the bridge at the mid-span of the fractured girder, and the tension stress at the bottom flange of the intact girder reached the yielding stress. After that, the truck loading increased up to 6 times the HS-20 load, where the middle span deflection of the fractured girder reached 11.51 in. At this level (defined here as failure), the concrete deck experienced extensive damage leading to tension stress at the intact girder due to flexural and torsional moment reaching the yielding point. Figure 5-38 (a) shows the yielding of the intact girder under six times HS-20 loading, and Figure 5-38 (b) shows the concrete tension damage at the top of the deck at this load level.

(a)

(b)

Figure 5-38. Fractured bridge under 6xHS-20: (a) Yielding of the intact girder; (b) Concrete tension damage.

5.7.3   Plastic Moment Capacity of UT Bridge Test

The plastic moment capacity of the UT bridge test for the intact scenario is calculated to compare with the maximum capacity of the bridge obtained from the FE model. The effective flange width of a concrete deck slab in composite or monolithic construction may be taken as the tributary width perpendicular to the axis of the member for determining cross-section stiffness for analysis and for determining flexural resistances. The slab effective flange width in composite girder and/or stringer systems or in the chords of composite deck trusses may be taken as one-half the distance to the adjacent stringer or girder on each side of the component, or one-half the distance to the adjacent stringer or girder plus the full overhang width.

To determine the plastic moment capacity of composite sections, the following assumptions are made:

- Full interaction between steel, reinforcement, and concrete – this is normal practice for bridge design and assumes no slip between the composite components
- The effective area of the structural steel member is stressed to f_{yd}
- The area of reinforcement in compression is ignored
- The effective area of concrete in compression is stressed to $0.85f_c$

Table 5-3 and Figure 5-39 summarize the section properties of the University of Texas bridge for calculating the plastic moment of one girder. The total flexural capacity of the bridge can be obtained by adding the capacity of two girders. Moreover, the FE model is used for obtaining the bridge plastic moment capacity considering all the details, such as reinforcement, as shown in Figure 5-40. Table 5-4 shows the calculation of the plastic moment for two different concrete compressive strength and the result obtained from the FE model. The higher plastic moment obtained from the FE model compared to that obtained by hand calculation can be attributed to the contribution of reinforcement in the FE model and the higher concrete compressive strength (6.2 ksi). In addition, the moment-curvature of the bridge section is illustrated in Figure 5-41.

Figure 5-39.UT Bridge Section.

Table 5-3. Section properties of UT bridge.

Parameter	Value	Unit
f'_c	4 or 6	ksi
f_y steel	50	ksi
f_y reinforcement	60	ksi
Slab Thickness	8	in
Slab Effective Flange Width	140	in
Haunch Thickness	3	in
Haunch Width	12	in
Top Flange Thickness	0.625	in
Top Flange Width	12	in
Web Thickness	0.5	in
Web Height	60	in
Web Height Projected	58.17	in
Bottom Flange Thickness	0.75	in
Bottom Flange Width	47	in
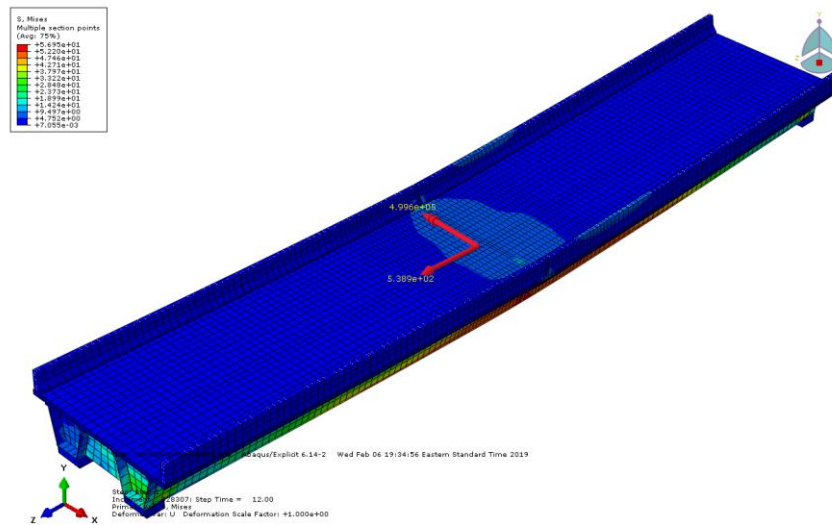
Figure 5-40. Plastic Moment Capacity in FEM.

Table 5-4. Plastic moment capacity.

Compressive Strength of Concrete	P_s kip	P_h kip	P_c kip	P_w kip	P_t kip	Y_{PNA} in	d_t in	d_w in	d_c in	M_p kip. ft
F'c=4 ksi	3808	163.2	750	3000	1687.5	11.6	58.6	29.1	0.3	17972.2
F'c=6 ksi	5712	244.8	750	3000	1687.5	7.6	62.6	33.1	3.7	19026.8
F'c=6.2 ksi- FEM	FEM									20816.7
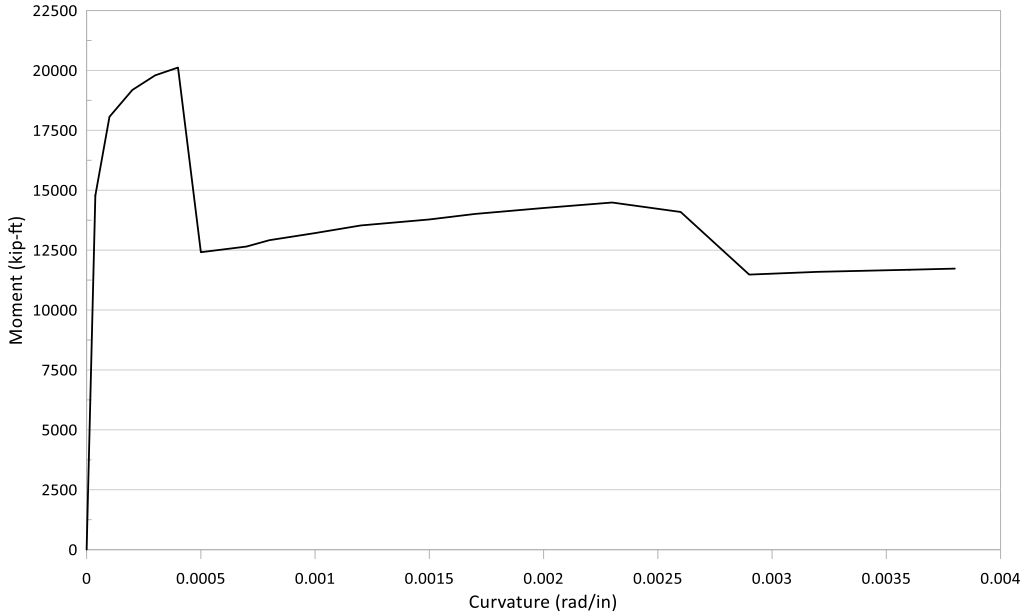
Figure 5-41. Moment curvature curve with nonlinear material properties (f'c=6 ksi).

In order to investigate the effect of railing on the final capacity of the bridge in fracture and intact scenarios, the UT bridge model was loaded until the failure for the intact and fractured bridge considering the effect of the railing. Figure 5-42 shows the results obtained from the FE models for two conditions of the intact bridge (no fracture in the left girder under the load) and the fractured condition (fracture of left girder under the load). It can be concluded from the results that railing could slightly decrease the maximum deflection of the fractured bridge at failure load for up to 8%.
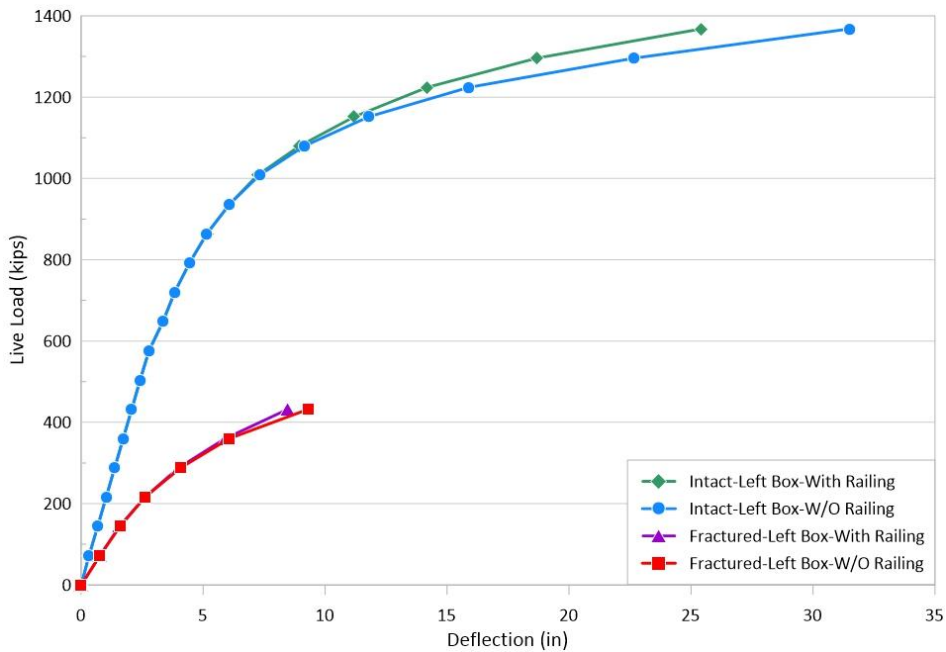
Figure 5-42. The effect of railing on the fractured bridge.

56

Chapter 6   Determining Failure Load Using Simple Analysis for Possible Failure Mechanisms

Based on the finite element analysis and available experimental results, as well as work by others, it is inferred that the failure after fracture of one girder can be one of; a) one-way shear failure of the deck, or b) flexural failure of the deck. The failure of the intact girder under bending and torsion could also be a possible mechanism; however, none of the results from analysis and experiments neither other sources have indicated the occurrence of such mechanism before the failure of the deck. One-way shear failure and flexural failure of the deck are investigated here for the University of Texas bridge.

6.1   Sensitivity Analysis for One-Way Shear Transfer in the University of Texas Twin Steel Box Girder Bridge

The objective of the investigation reported in this section is to perform a sensitivity analysis for one-way shear transfer in the deck slab where the varying parameter is the transverse position of the truck wheels. The main goal is to validate the simple model for one-way shear at the deck in comparison with finite element results and to determine the effective width for the calculation of shear stresses for HS-20 loading. The bridge was loaded in terms of the HS-20 design truck with 14 ft axle spacing positioned at the mid-span over the fractured girder to generate maximum moment at the section with the fracture. Figure 6-1 shows the loading configuration for the parametric study of one-way shear failure. In order to study the effect of truck position on one-way shear effective width and shear stress distribution over the girders, HS-20 truck was positioned in four different locations across the bridge width as shown in Figure 6-2, to constitute four cases, one for each position. Cases 2, 3, and 4 were used for investigating the sensitivity analysis for one-way shear. Case 1, an extraordinary eccentric loading, was used for bending failure investigation later in this report.

Based on the HS-20 design truck location, the shear stress profile was obtained for four sections in the bridge deck slab along the bridge immediately next to the end of steel girder flanges of intact and fractured girders. Figure 6-3 shows the location of shear stress sections. Total shear force transferred longitudinally and transversely was calculated by integrating shear stress profile in longitudinal and transverse across the bridge slab. According to the results, it can be seen that despite the fracture in one girder, a portion of the truck loading is transferred to the fractured girder end supports in the longitudinal direction, and the remaining is transferred transversely to the intact girder. The portion of live load transferred longitudinally by the fractured girder to its support can be calculated by integrating shear stresses along the sections shown in Figure 6-3, and transverse distribution of the live load from the fractured girder to the intact girder can be calculated by subtracting the longitudinally transferred load from the total live load. The proportion of longitudinal and transverse load transfer will depend on the truck location and bridge configuration, i.e., girder spacing, deck thickness, cross-frame spacing, etc.
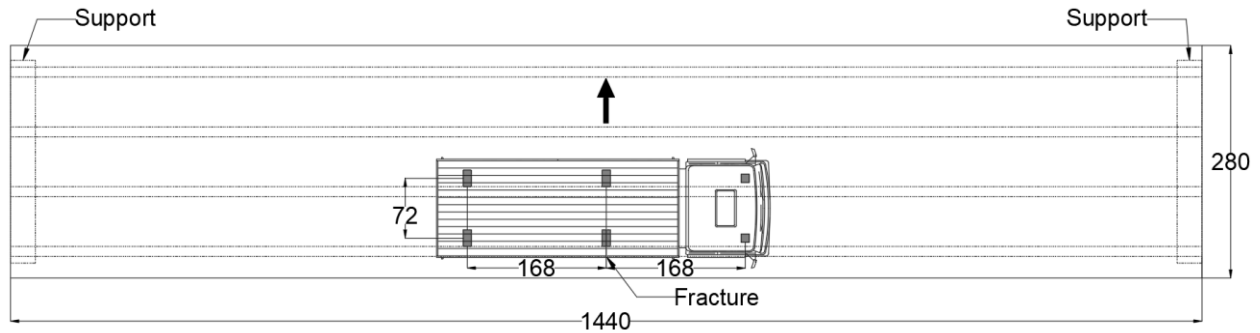
Figure 6-1. Loading Configuration in the one-way shear analysis.
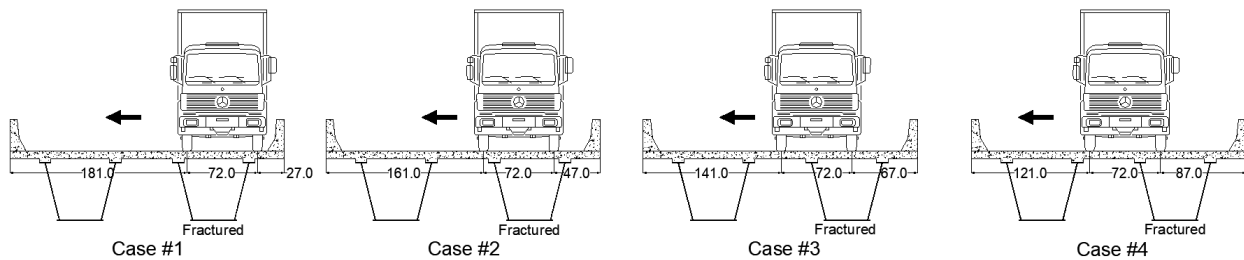
Figure 6-2. HS-20 Truck location in the one-way shear analysis.
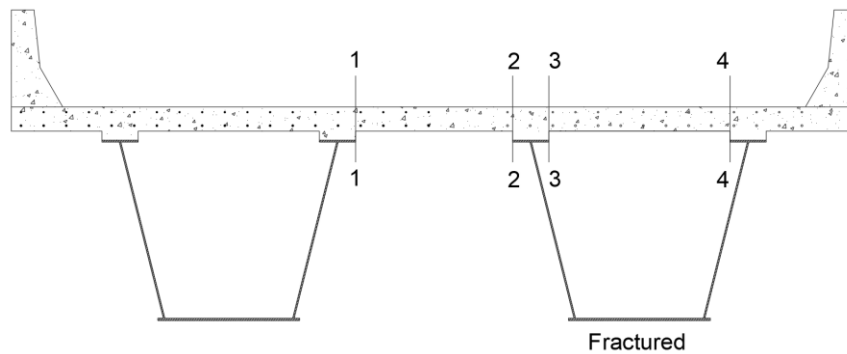
Figure 6-3. Sections in the one-way shear analysis.

For the analysis, the bridge was loaded incrementally until the failure, plateau in the load-deflection curve, and shear stress was captured for all the sections along the bridge in four different truck positions (Cases 1- 4). The results show that shear stress follows a similar pattern for each section and case by increasing the truck loading until the failure stage, where crushing and cracking of the deck changes the initial pattern. Hence, the stress pattern is studied for the failure stage. Figure 6-4 shows the shear stress profile in the slab along the sections for all cases under dead load and twice the HS-20 design truck. Moreover, in order to study the effect of the increasing live load on shear stress pattern and the effective width for one-way shear, shear stress in the slab along Section 1-1 for Case 2 was obtained and is shown in Figure 6-5. The results indicate that by increasing the live load (up to twice HS-20), shear stress follows a similar pattern with negligible changes in one-way shear effective width. Comparison of the shear stress pattern and values in Section 1-1 and Section 2-2 (Figures 6-4 (a) and (b)) indicates that the live load positioned between intact and fractured girder is transferred in both longitudinal and transverse direction. Moreover,

58

the analysis shows that after the fracture, the intact girder (Section 1-1) carries more shear stress than the fractured girder (Section 2-2) because of having a higher stiffness.

(a)

(b)

(c)

(d)
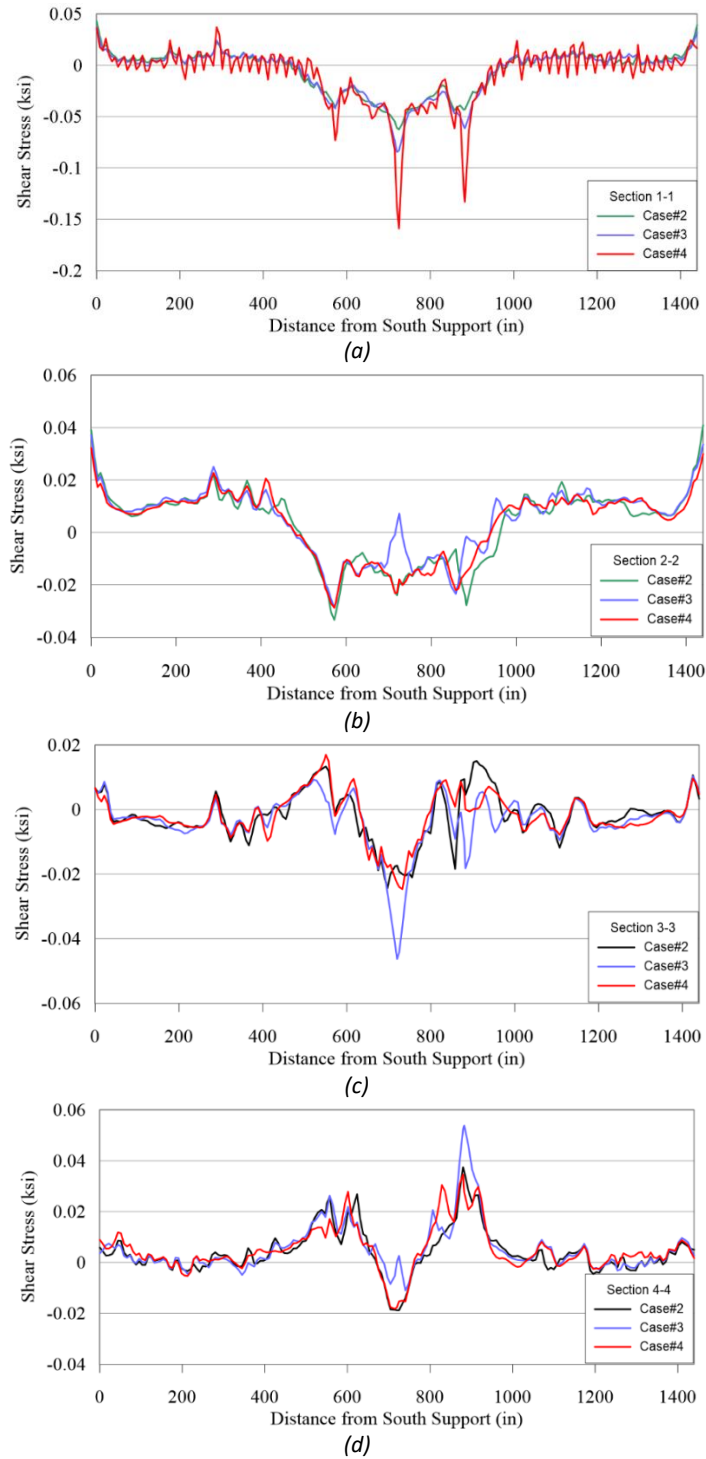
Figure 6-4. Shear stress in the slab along the faces of the intact and fractured girder for all the cases under dead load and two times HS-20 design truck: (a) Section 1-1; (b) Section 2-2; (c) Section 3-3; (d) Section 4-4.

59
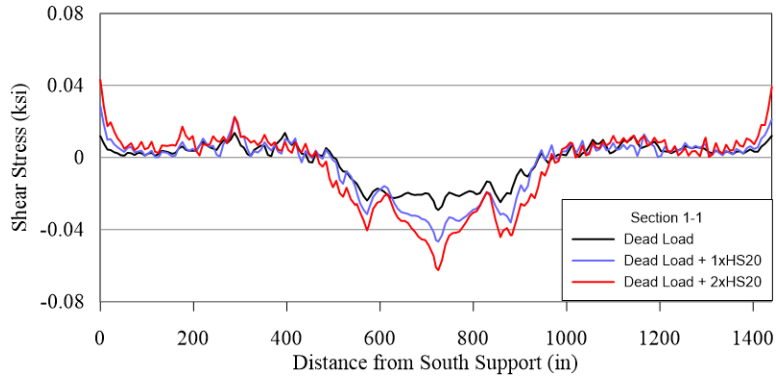
Figure 6-5. Shear stress in the slab along Section 1-1 in case 2 under dead load and increasing HS-20 design truck.

Shear stress analysis of the live load's distribution between Section 3-3 and Section 4-4 (Figures 6-4 (c) and (d)) shows that forces over the fractured girder are mainly transferred transversely to Section 2-2 and then to the Section 1-1 and the remaining is transferred longitudinally to the end supports. Total shear force transferred to the fractured girder was calculated by integrating shear stress along the bridge at each section (Figures 6-4 (c) and (d)). The results reveal that although the local shear transfer is recorded for both Sections 3-3 and 4-4, the total shear force transferred to the fracture girder in the transverse direction is negligible. Therefore, positive and negative shear stress along Section 3-3 and Section 4-4 could be attributed to local deflection after the fracture. The results show pull-out shear forces along Section 3-3 and Section 4-4 in a limited length, which may cause a shear stud failure only at the mid-span. In this region, the bridge deck would not follow the fractured girder deflection at the middle of the span because of its high transverse stiffness, and as a result, pull-out forces will develop between the deck and the fractured girder.

Two methods were used in this study for estimating the effective width and average shear stress transferred transversely to the girders for the approximate simple method (referred hereafter as simple prediction Methods 1 and 2). In the first method (Method 1), the effective width was predicted using 45° spreading line from the far side of the first and last point loads, and total width was considered as the effective width by ignoring gaps between spreading lines. In the second method (Method 2), the effective width was predicted for each point load separately using 45° spreading line from the far side of each point load. See Figure 6-6 for illustration of two different effective widths. Furthermore, the effective width for one-way shear was also calculated using the finite element model for Section 1-1 and Section 2-2 by measuring the length of the negative shear stress to correspond to effective widths estimated using Methods 1 and 2 described for the simple method.

Figures 6-7 (a) and (b) show effective width estimation for the FE method for Method 2. The effective width for Method 1 for FE analysis will be the entire length from the first point on the left to the last point on the right. The effective width for calculating one-way shear from simple prediction methods was compared to the FEM results, as shown in Tables 6-1 and 6-2. The prediction value shows a good agreement with the effective width obtained using the FE model

60

when using Method 1. For Method 1, in all but one case (Case #4, Section 2-2 in method 1), the approximate effective width is smaller than the FE calculated, hence providing for more conservative stress calculation. Method 2 results for simple prediction compare fairly with FE results, the difference to be attributed to the non-distinct variation of stress in the FE results. As a result, the minimum effective width value obtained in this study for Section 1-1 based on the critical live load position (Case 4) can be used for calculating the one-way shear capacity of the fractured bridge.

Tables 6-1 and 6-2 show the maximum and average stress obtained from FEM and simple predication Methods 1 and 2 over the effective width under twice the HS-20 design truck loading. Stresses from the effect of dead load after fracture are subtracted from the total shear stress to obtain live load shear stresses. The difference between average stress in FEM and the simple prediction method can be attributed to two sources. First, because of fracture, in reality, and as captured by FE analysis, the intact girder (Section 1-1) carries more shear stress than the fractured girder (Section 2-2), i.e., a major proportion of the live load will be transferred to intact girder from the fractured girder, where, in the simple predication methods, shear stress is assumed to be transferred only to the intact girder. Moreover, a proportion of live load on fractured girder will be transferred longitudinally to its support, as shown by the FE analysis results. However, in the simple prediction methods, it is assumed that shear stress only will be transferred transversely.

Comparison of results shows that for Method 1 (extended effective width for the entire truck), the average shear stress estimated at Section 1-1 using simple prediction agrees well and is slightly higher than the average shear stress calculated from FE analysis. Results for Method 2 (effective width for individual wheels) show that the average shear stress estimated at Section 1-1 for the rear wheels using the simple prediction method agree very well with the maximum shear stresses calculated by FE analysis. Method 1 is believed to generate results that are more representative of shear stresses when compared with FE analysis results. The effective length obtained from Method 1 is therefore used for calculating the fractured bridge one-way shear capacity in different cases for comparison with bending yield line results. The maximum shear stress is assumed to be uniform over the entire effective width, and the ACI 318-14 equation for one-way shear is used to compute the shear resistance in the deck (Table 6-7).

Table 6-1. One-way shear effective width for Method 1.

	One-Way Shear Effective Width (in)					
	Case#2		Case#3		Case#4	
	FEM	Simple Prediction 1	FEM	Simple Prediction 1	FEM	Simple Prediction 1
Section 1-1	506	461	476	421	440	381
Section 2-2	462	381	447	421	418	461
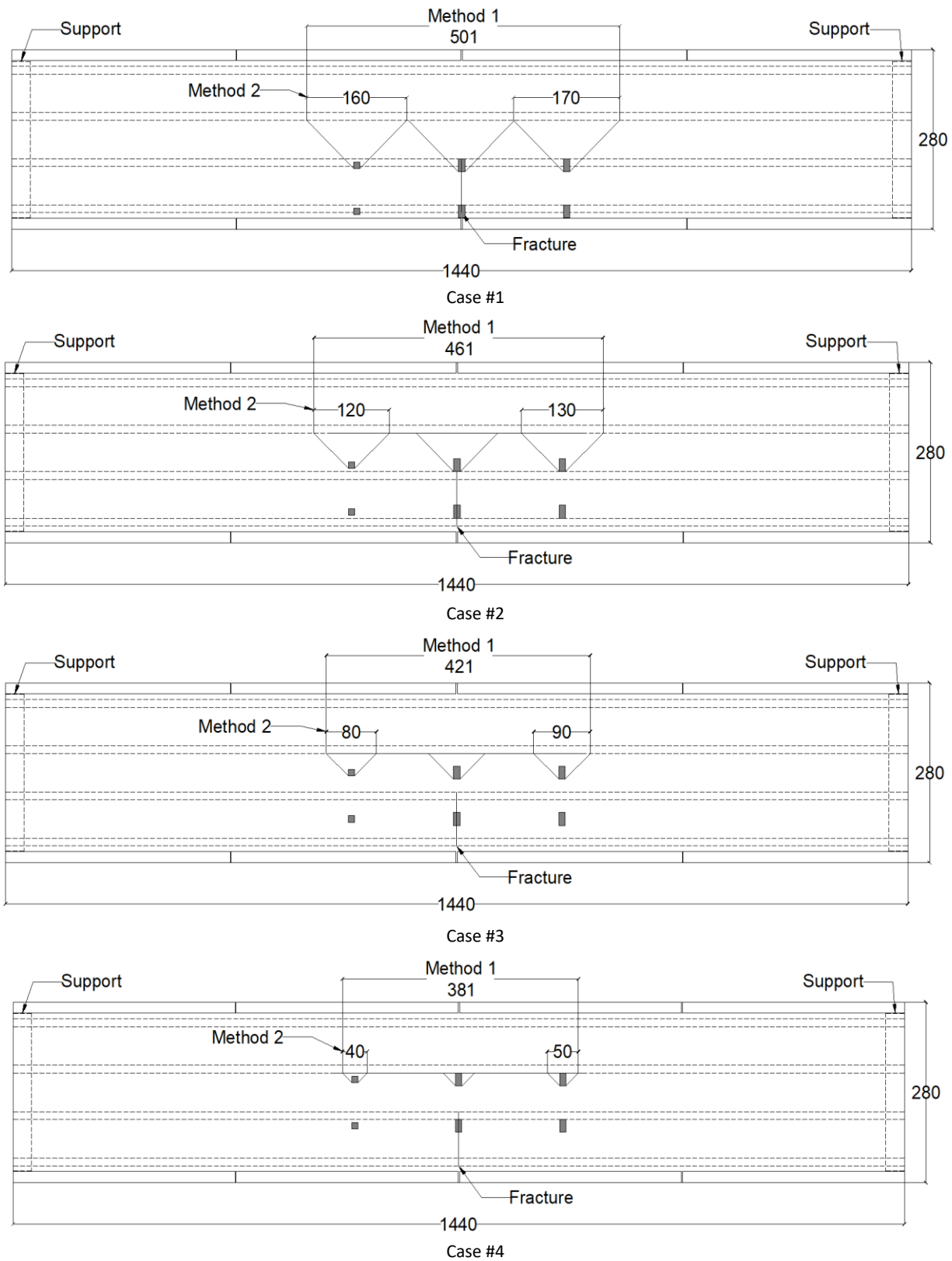
Figure 6-6. The effective width for one-way shear using the simple prediction method.

Table 6-2. One-way shear effective width for Method 2 (Front denotes front wheel; Rear denotes rear wheel).

	One-Way Shear Effective Width (in)											
	Case#2				Case#3				Case#4			
	FEM		Simple Prediction 2		FEM		Simple Prediction 2		FEM		Simple Prediction 2	
	Rear	Front	Rear	Front	Rear	Front	Rear	Front	Rear	Front	Rear	Front
Section 1-1	132	139	130	120	139	139	90	80	110	95	50	40
Section 2-2	119	99	50	40	125	139	90	80	154	137	130	120

(a)

(b)
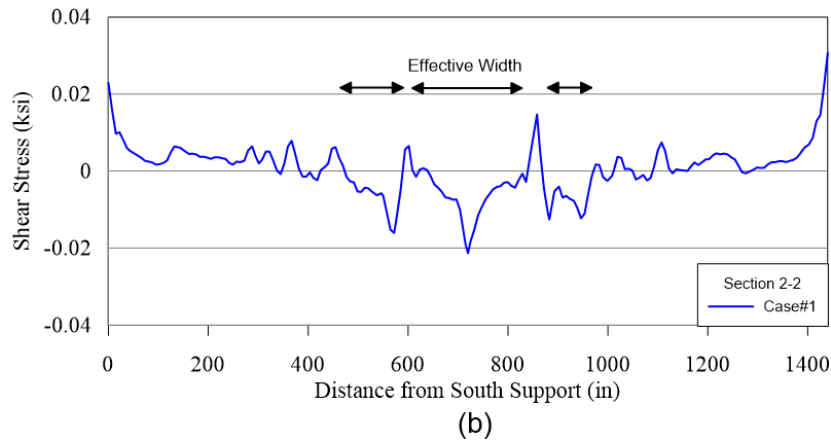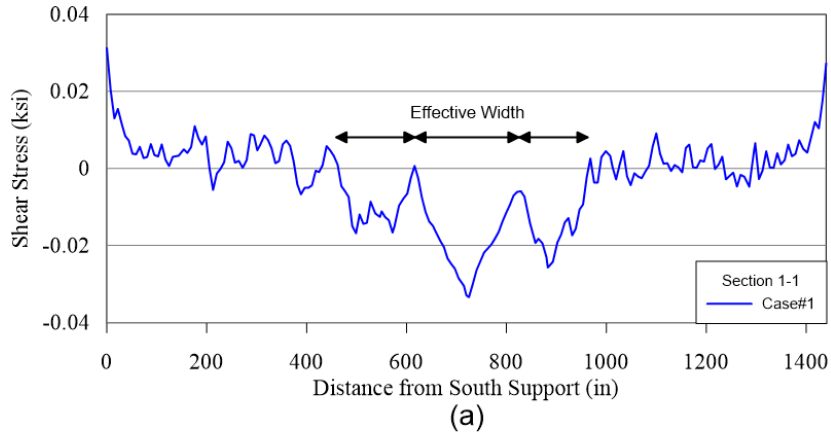
Figure 6-7. The effective width for one-way shear using the finite element model: (a) Section 1-1; (b) Section 2-2.

Table 6-3. One-way shear stress over the effective width under 2xHS-20 for Method 1.

	One-Way Shear Stress (psi)								
	Case#2			Case#3			Case#4		
	FEM		Simple Prediction 1	FEM		Simple Prediction 1	FEM		Simple Prediction 1
	Max.	Avg.	Avg.	Max.	Avg.	Avg.	Max.	Avg.	Avg.
Section 1-1	33.4	14.7	19.5	56.4	18.8	21.4	101.4	20.5	23.6
Section 2-2	21.3	5.76	0	11.3	1.9	0	20.4	5.0	0

	One-Way Shear Stress (psi)														
	Case#2				Case#3				Case#4						
	FEM		Simple Prediction 2			FEM		Simple Prediction 2			FEM		Simple Prediction 2		
	Max.	Avg.		Avg.		Max.	Avg.		Avg.		Max.	Avg.		Avg.	
		R	F	R	F		R	F	R	F		R	F	R	F
Section 1-1	33.4	15.9	10.9	30.8	8.3	56.4	22.4	11.6	44.4	12.5	101.4	28.3	9.8	80.0	25.0
Section 2-2	21.3	7.5	6.9	0	0	11.3	0.1	3.9	0	0	20.4	7.8	5.9	0	0

Note: R= Rear-wheel; F= Front-wheel

6.2 Flexural Failure of the Deck Based on Yield Line Analysis:

The simple yield line model developed by the University of Texas [19] to capture the bending response of a twin steel box girder is investigated here for estimation of the bending capacity deck in the fractured bridge. The proposed yield line pattern of the University of Texas is based on the overall cracking and crushing pattern from the University of Texas bridge test. The experimental results show that the failure in the deck followed the shape of a half-ellipse. Accordingly, a yield line pattern was developed by the University of Texas using a combination of straight lines. Several assumptions were made for developing the pattern. First, it was assumed that a yield line in the deck between the girders closer to the fractured girder (parallel to the girders longitudinal axis) would not form because the shear studs connecting the fractured girder to the deck will fail due to the pull-out force and the fractured girder would not have any contribution. Second, the yield line consisted of straight lines lying on the perimeter of an ellipse along with two diagonal interior fold lines with the linear deflection to its maximum at the edge of the deck at mid-span. The proposed pattern gives the most conservative estimate of capacity by ignoring the contribution of the fractured girder. The yield line pattern is defined by two major parameters; the angle φ between the inner diagonals and the vertical axis and horizontal distance from points at the end of outer diagonal lines to the origin (along the outer edge of the deck over the fractured girder). A series of parametric studies were conducted by the University of Texas to determine these parameters to correspond to minimum capacity under HS-20 truck load.

In the one-way flexural failure of the bridge, plastic hinges will form at the location of the maximum moment, and the hinge lines will rotate plastically with an increase of the load to form the final yield lines. Based on the yield line pattern, the virtual work principle could be used for the calculation of deck bending capacity. The principle of virtual work requires that the external virtual work done by the external forces be equal to the internal virtual work done by the internal forces of each element of a structure. The external virtual work is computed from the summation of the product of the externally applied forces multiplied by the virtual displacement at the load position, which is a function of the assumed virtual displacement. The total internal virtual work due to the virtual displacement is equal to the summation of the product of the bending moment developed at the segment of the yield line multiplied by the hinging rotation of each segment.

Figure 6-8 shows the yield line pattern proposed by the University of Texas. It was assumed that a straight yield line would initiate at the interior top flange of the intact girder, and it would extend diagonally to the edge of the deck above the fractured girder. The yield line needs to be completed by assuming two inner diagonal lines from the end of the interior top flange of the intact girder to the edge of the deck above the fractured girder.

A yield line analysis was performed for the four cases discussed above based on the University of Texas yield line pattern. The finite element model was used for estimating the position and length of the outer yield lines by using concrete damage index in the deck as shown in Figure 6-9, and the ultimate capacity of the bridge was calculated for each case (Tables 6-5 and 6-6). The yield line obtained from the FE analysis closely compares to the yield line suggested by the University of Texas for a similar loading pattern (Case 1). It should be noted that the actual load carried by the University of Texas bridge under uniform loading in term of HS-20 was 363 kips (5 times HS-20). According to the Texas yield line (Table 6-7), the maximum capacity of the bridge in case 1 is 4.2 times HS-20, which is slightly conservative when compared to the maximum capacity of 4.5times HS-20 obtained from the finite element model here in this study. This can be attributed to ignoring the contribution of the fractured girder in the yield line analysis.

Table 6-5. External work calculation of the truck load.

	P	X_{point}	Y_{point}	r_{Load}	r	Delta	EW
Number of HS-20 Design Truck							**4.2**
Front Wheel	16.8	14.0	5.9	6.3	22.5	0.3	4.7
Front Wheel	16.8	14.0	11.9	12.3	26.5	0.5	7.8
Middle Wheel	67.2	0.0	5.9	5.9	14.2	0.4	28.0
Middle Wheel	67.2	0.0	11.9	12.0	14.2	0.8	57.0
Rear Wheel	67.2	-14.0	5.9	6.3	22.5	0.3	18.7
Rear Wheel	67.2	-14.0	11.9	12.3	26.5	0.5	31.2
						EW_{Truck}	147.4
						EW_{DL}	33.3
						EW_{Total}	180.7

Table 6-6. Internal work calculation for the Texas bridge.

	L	α	m_l	m_t	m_b	Rotation	dIW
	33.75	0.00	17.86	17.86	17.86	0.07	42.07
Perimeter	19.30	0.77	17.86	17.86	17.86	0.05	15.64
	19.30	1.05	17.86	17.86	17.86	0.05	15.64
	22.00	0.86	22.68	22.68	22.68	0.05	26.13
Diagonals	22.00	0.97	22.68	22.68	22.68	0.05	26.13
						$IW_{Railing}$	55.22
						IW_{Total}	180.82
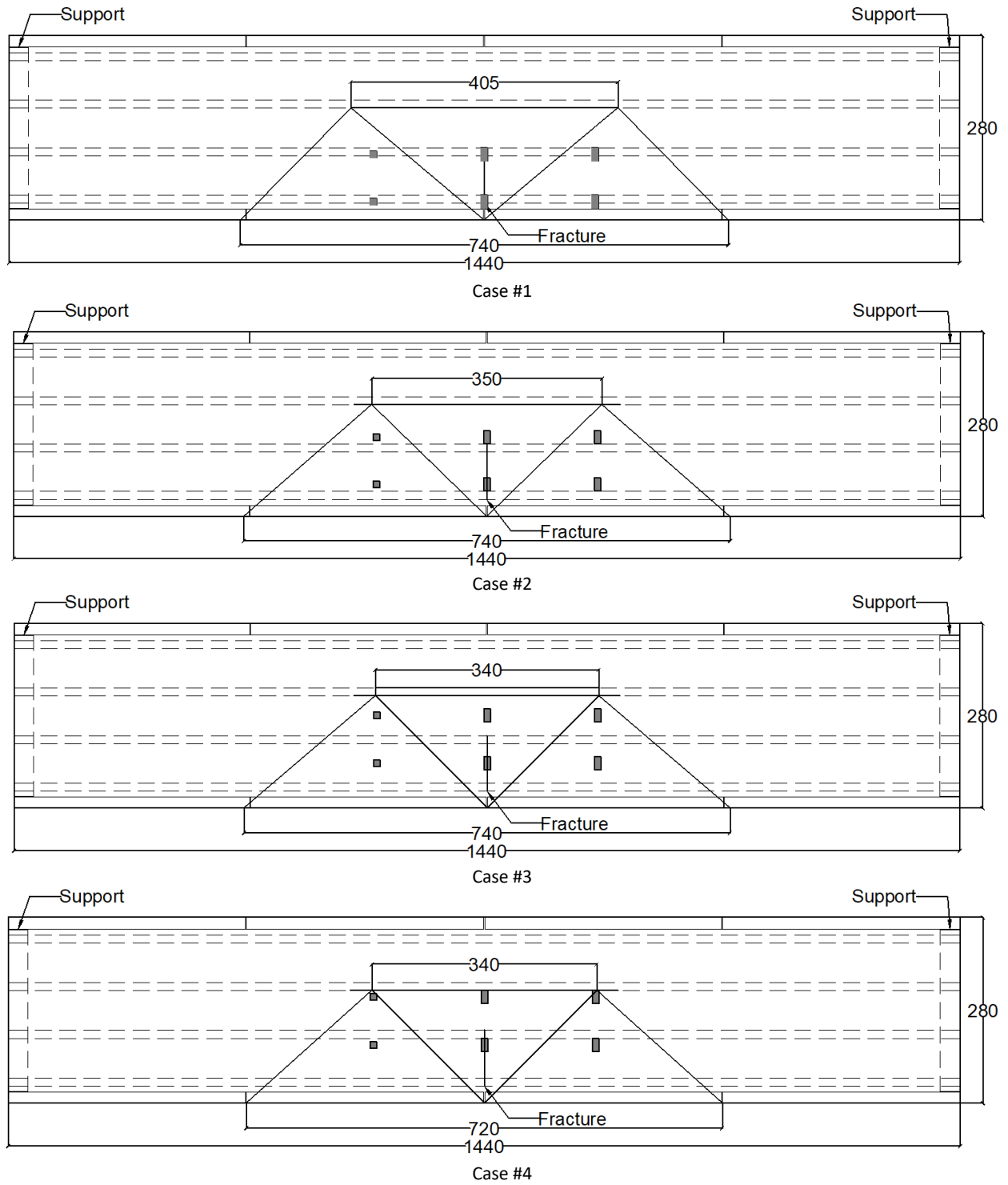
Figure 6-8. The yield line pattern proposed by the University of Texas for cases 1 to 4.

To investigate the effect of shear studs in the load-carrying capacity of the bridge, the interaction between the shear studs and the concrete deck were modeled in the FE analysis. The connector element was utilized for modeling the shear studs. The ultimate shear and tension capacity for the connector elements were assigned based on the shear and pull-out test conducted by Topkaya [42] and the University of Texas [43]. Once the shear or tension force in the shear stud element reaches its capacity, the element would lose its connection to simulate the pull-out or shear failure. The analysis showed that with the connector elements calibrated based on the available stud tests, failure of the studs occurs along a limited length of the deck immediately over the inner edge of the fractured girder just enough to allow the development of the assumed yield line pattern. For comparison purposes, FE analysis was performed on Texas bridges with and without modeling the shear studs. The case of without shear studs assumes perfect composite action with no failure in the studs. Figure 6-9 shows a comparison between the load-displacements curves for Case 1 loading with and without modeling the studs. The response curves are in close agreement until the applied load of about three times HS-20, where the pull-out failure of shear studs begin at the middle of the span over the fractured girder. Stud pull-out extends over a limited length until the maximum capacity is reached. Table 6-7 shows the maximum capacities obtained from FE analysis with stud modeling. For comparison purposes, the maximum capacity for Case 1 is also reported from FE analysis without modeling the shear studs, i.e., assuming full composite action between deck slab and girders.

Another bridge feature influencing the deck bending failure mechanism is bridge railing. In the normal bridge operation, concrete bridge railing is not considered to be a structural component because of the gap between railing segments for expansion joints. When a bridge is subjected to large deflections due to severe damage, two sides of the gap will eventually come into contact, and contact force would increase the stiffness of the bridge. However, in the Finite element model, the railing segments were modeled with no contact force between the segments to eliminate the uncertainty of the railing gap and the force between railing after a large deflection. On the other hand, the simplified yield line model utilized by the University of Texas takes into account the contribution of the railing in the bending resistance along the yield lines wherever applicable.

The finite element analysis incorporating the shear studs shows that the pull-out of studs occurs along a limited length at the mid-span allowing the yield lines to form in a pattern similar to the University of Texas. Moreover, the bridge deflection in the finite element model matches with the proposed pattern when considering the pull-out shear stud failure. Although the yield line pattern proposed by the University of Texas is conservative due to ignoring the contribution of the fractured girder, it can estimate a lower bound capacity for the fractured bridge.

Figures 6-10 (a) and (b) show the yield line pattern obtained from the finite element model using concrete damage plasticity index in the top and bottom view of the deck, respectively. Positive and negative bending lines can be observed in the bottom and top view of the deck. Figure 6-11 shows

the vertical deflection of the deck at the failure in the finite element model and the deflection based on the yield line pattern. It can be seen from the deflected FE model that the bridge deflection in the failure region is approximately linear from the edge of the intact girder to its maximum value at the edge of the deck above the fractured girder at the middle of the span, and the deflection reflects the half-ellipse shape that is the basis for determining the yield line pattern.
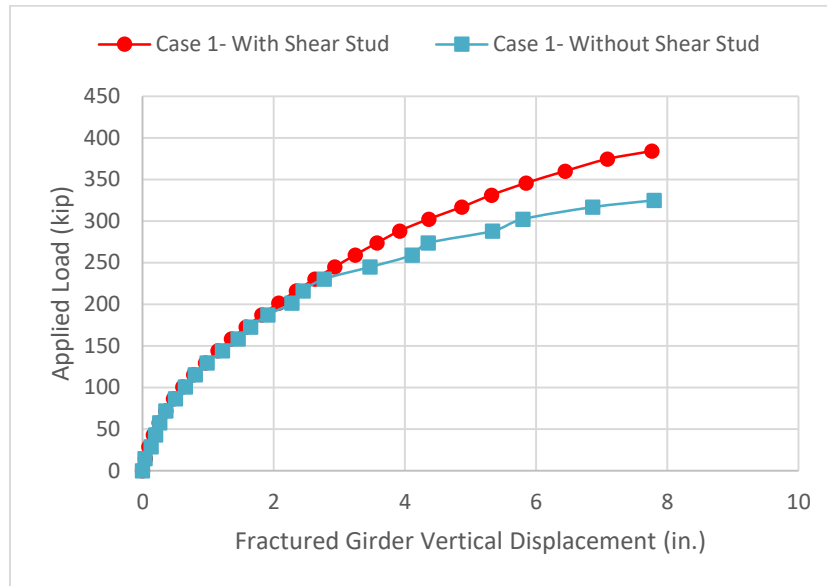
Figure 6-9. Comparison between the load-displacements curves for Case 1 loading with and without modeling the studs.

According to the results shown in Table 6-7, one-way shear is the critical failure mode for Cases 3 and 4 (closest to intact girder), and flexural failure of the deck at the yield lines is the failure mode for Cases 1 and 2 (farthest from intact girder). Accordingly, it can be inferred that the ultimate capacity of the bridge with one fractured girder under HS-20 design truck using simplified method is the smaller value between one-way shear capacity in Case 4 and the deck bending capacity using yield line method in Case 1. Figure 6-12 shows the suggested effective width and yield line pattern for calculating one-way shear and yield line analysis. One-way shear capacity can be estimated using Equation (5) for using the effective width shown in Figure 6-12 (a), and the yield line bending capacity can be estimated using the yield line pattern shown in Figure 6-12 (b) as per the procedure described earlier and shown in Tables 6-5 and 6-6.

$$V_{ACI} = 2\sqrt{f'_c}\,b_{eff}\,d \text{ (psi)} \tag{5}$$
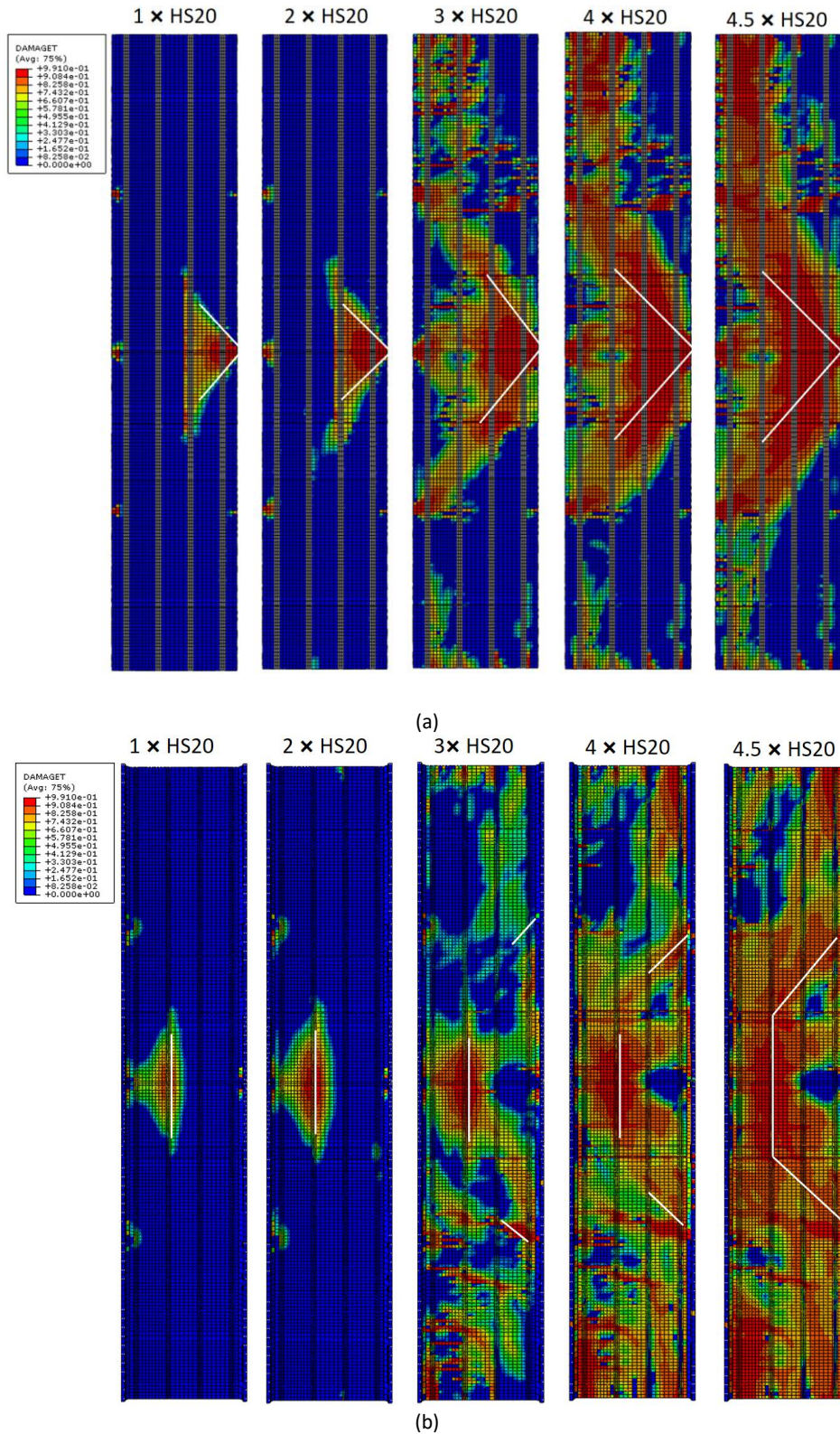
Figure 6-10. The yield line pattern of the deck in the Finite Element Model for Case 1: (a) Bottom view of the deck where positive bending yield lines are shown; (b) Top view of the deck where negative bending yield lines are shown (white lines are added to reflect the idealized yield lines used in simple analysis).
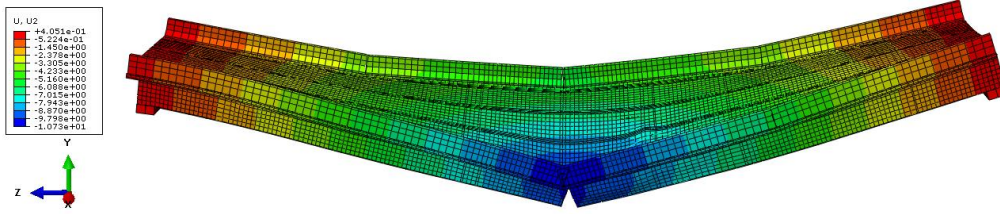
(a)
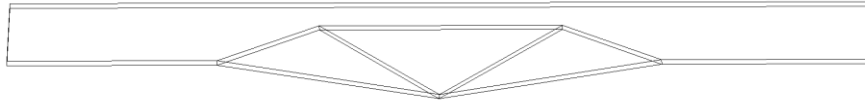
(b)
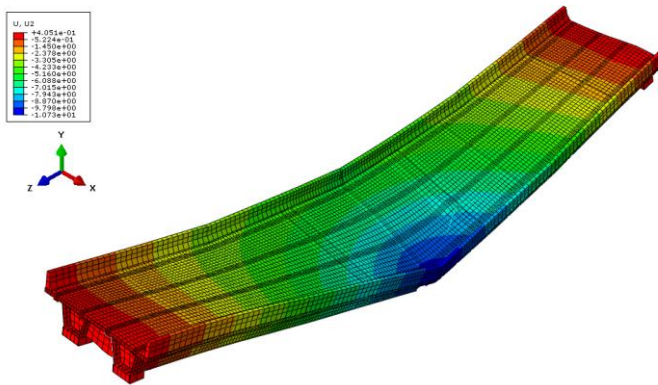
(c)
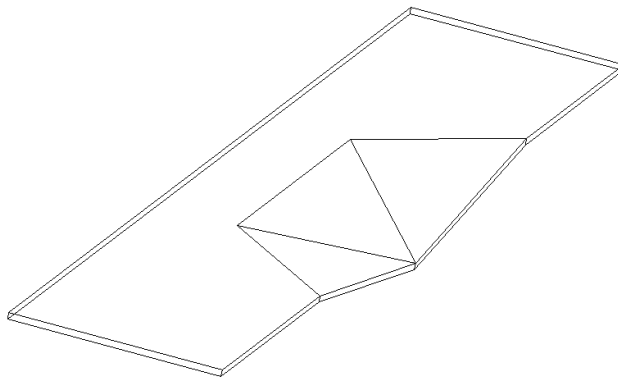
(d)

Figure 6-11. Yield line pattern of the deck: (a,c) Deck deflection contour in FEM; (b,d) Deck deflection based on yield line pattern.
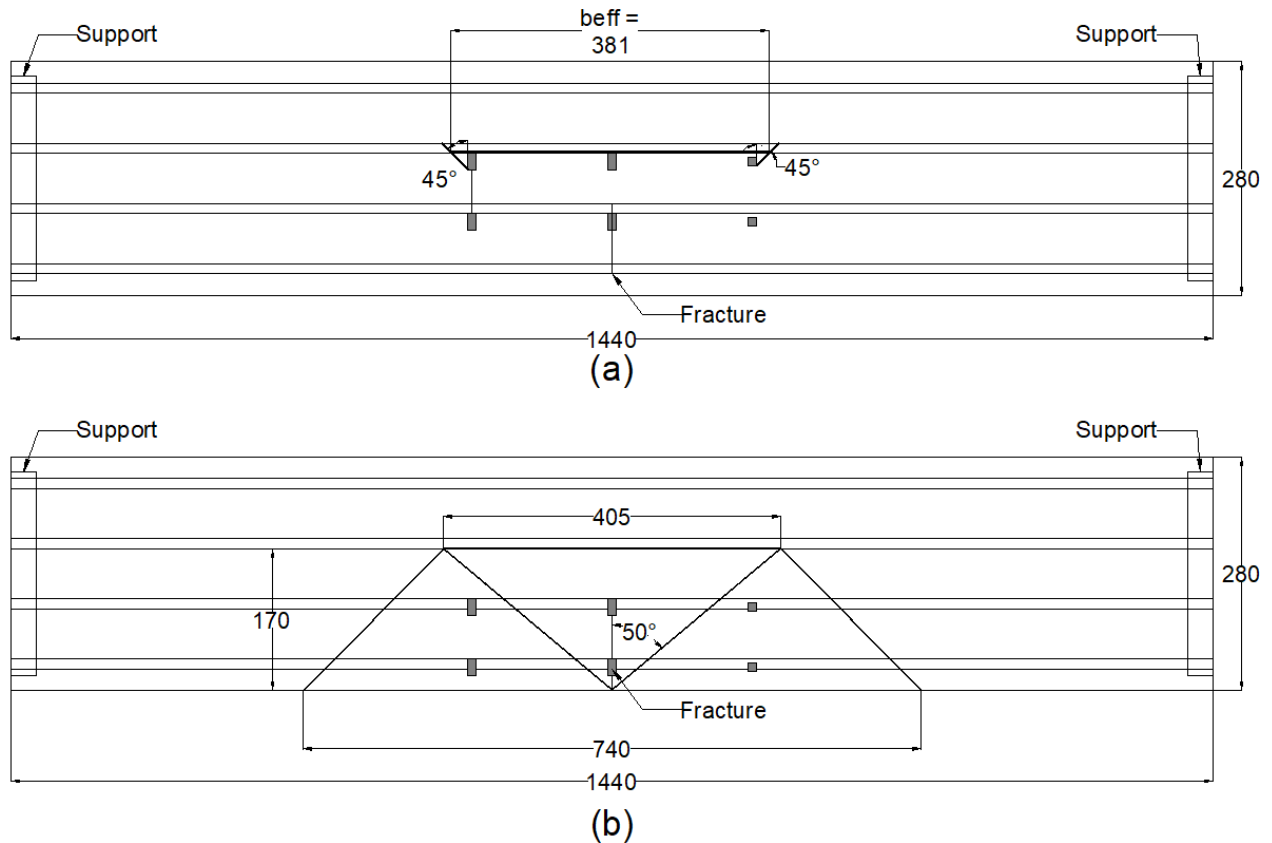
Figure 6-12. The University of Texas bridge failure mechanisms: (a) One-way shear in Case 4; (b) Yield line failure in Case 1.

Table 6-7. Bridge capacity for cases 1 to 4.

Case	One-Way Shear Capacity (kips)	Bending Yield Line capacity (kips)	Max. Capacity from FE analysis- shear studs are modeled (kips)
1	448.7	**301.7**	320
2	412.9	**362.2**	329
3	**377.1**	474.5	335
4	**341.2**	563	340

6.2.1 Sensitivity Analysis for the Concrete Compressive Strength in the University of Texas Twin Steel Box Girder Bridge

Variation in the bridge configuration and material properties, i.e., concrete compressive strength and steel ultimate strength, may result in different failure modes and, therefore, different reserve capacity. In this section, sensitivity analysis for the deck concrete compressive strength is conducted to investigate its effect on the ultimate failure strength and mode.

In the previous analysis, the concrete compressive strength was taken as 6.2 ksi as per reported test results. Accordingly, two other concrete compressive strengths were assigned to the deck in

71

the FE models to investigate the behavior of the bridge with fractured girder under various concrete strengths.

The concrete material parameters used in the presented analyses are: the modulus of elasticity E_0 that is calculated based on the ACI 318-14 [38] ($E_c = 57,000\sqrt{f_c'}$), the Poisson's ratio ν, and the compressive and tensile strengths. The concrete damaged plasticity model was considered in the models. The dilation angle ψ was considered as 36°, the shape factor, $K_c =0.667$, the stress ratio $\sigma_{b0}/\sigma_{c0} =1.16$, and the eccentricity $\varepsilon=0.1$.

Concrete in compression was modeled with the Hognestad parabola [44] (see Figure 6-13). The assumed stress-strain behavior of the concrete under uniaxial compressive loading could be divided into three domains. The first one represents the linear-elastic branch, with the initial modulus of elasticity. The linear branch ends at the stress level of σ_{c0}. The second segment describes the ascending branch of the uniaxial stress-strain relationship for compression loading to the peak load at the corresponding strain level. The third part of the stress-strain curve shows the strength descending part after the peak stress and until the ultimate strain ε_u. Concrete damage was assumed to occur in the softening range in both tension and compression. In compression, the damage was introduced after reaching the load corresponding to the strain level, ε_0.

The uniaxial stress-strain response of concrete in tension is linear elastic up to its tensile strength, f_t'. After cracking, the descending branch is modeled by a softening process, which ends at a tensile strain ε_u, where zero residual tensile strength exists (see Figure 6-14). Sensitivity analyses for the concrete compressive strength for the University of Texas Twin Steel Box Girder bridge were conducted using three different concrete compressive strengths of 4 ksi, 5 ksi, and 6.2 ksi. It should be noted that the concrete compressive strength for the University of Texas bridge at the time of its ultimate test (32 months after casting the deck) was 6.2 ksi and had an average strength of 4.8 ksi at the age of 28 days.

Table 6-8 shows the ultimate bridge capacity obtained from the FE analysis and simplified methods for one-way shear and bending yield line capacity. The results show that by increasing the concrete strength capacity of the deck, the one-way shear capacity increases by the square root of concrete compressive strength according to Equation (5). Moreover, section bending capacity increases by increasing the concrete compressive strength. For example, the section capacity along the yield lines with concrete compressive strength of 4 ksi and 5 ksi is 20 kip. ft/ft and 21.3 kip. ft/ft, respectively. The FE results indicate a similar trend.
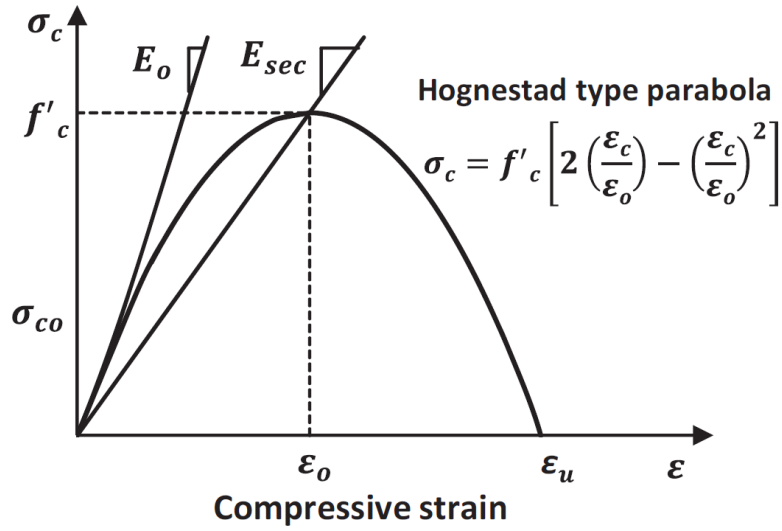
Figure 6-13. The uniaxial compressive stress-strain relationship for concrete.

$$\sigma_c = f'_c \left[2 \left(\frac{\varepsilon_c}{\varepsilon_o} \right) - \left(\frac{\varepsilon_c}{\varepsilon_o} \right)^2 \right]$$
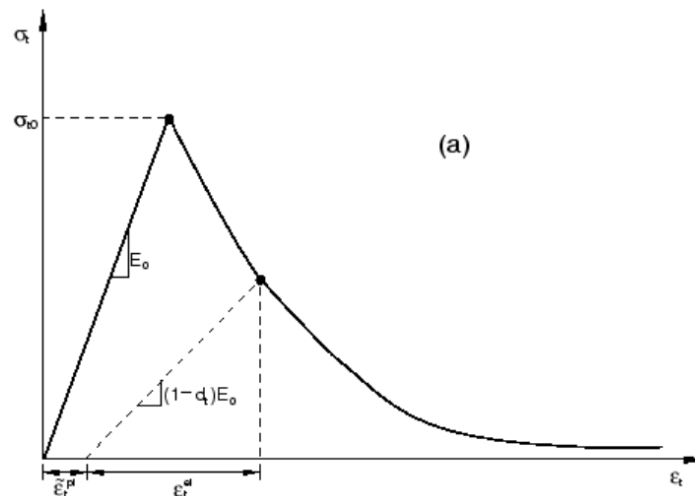
Figure 6-14. The uniaxial tensile stress-strain relationship for concrete.

Table 6-8. Bridge capacity for cases 1 and 4 with different concrete compressive strengths.

Case	concrete compressive strength (ksi)	One-Way Shear Capacity (kips)	Bending Yield Line capacity (kips)	Max. Capacity from FE analysis- shear studs are modeled (kips)
1	6.2	448.7	301.7	320
	5	403.0	288.0	316
	4	360.4	273.6	310
4	6.2	341.2	563	340
	5	306.5	532	335
	4	274.1	506	327

6.2.2 Sensitivity Analysis for the Truck Loading in the University of Texas Twin Steel Box Girder Bridge

The first edition of AASHTO's Standard Specification for Highway Design in 1931, which was based on the 1924 committee report, contained a representation of a design truck and/or a group of trucks with a single unit weighing up to 40 kips, which was known as the H20 truck, and a lane load to be used in specific circumstances. For the HS-20 design truck loading, this consisted of a uniform load of 0.64 kip/ft and a moving concentrated load or loads. A concentrated load of 26 kips was used for shear and for reaction, two 18-kips concentrated loads were used for the negative moment at support and were positioned in two adjacent spans, and a single 18-kips load was used for all other moment calculations.

In the early 1940s, the design truck was extended into a tractor–semi-trailer combination, known in the 1944 Standard Specifications as H20-S16-44 and commonly referred to as simply the HS-20 truck. This vehicle weighed a total of 72 kips and was comprised of a single steering axle weighing 8 kips and two axles that supported the semi-trailer, each weighing 32 kips. The axle spacing on the semi-trailer could vary from 14 to 30 ft, and it was assumed that there was 14 ft between the steering axle and the adjacent axle that formed part of the tractor. The HS-20 design truck is an idealization and did not represent any particular truck. The truck configuration, i.e., axle spacing and weights, is represented to produce moments and shears in the bridge longitudinal direction based on actual truck loading. However, for the fractured bridge in which most of the loads are being transferred transversely, and the failure mode could be one-way shear or flexural failure of the deck, the HS-20 truck may not represent the worst-case scenario for one-way mechanisms. Therefore, sensitivity analysis for the truck loading needs to be conducted for different loading configurations.

In order to consider the effect of truck loading configuration on the bridge failure mode as well as the effect on yield line pattern and one-way shear effective width, three trucks with loading configurations other than HS-20 truck were selected as shown in Figure 6-15. Florida legal loads and emergency vehicles are used for this purpose. The C5 truck that is one of the Florida legal loads weighs a total of 80 kips and with a total length of 36 feet that is longer and heavier than the HS-20 design truck configuration used in this study. EV3 truck loading is one of the Florida emergency vehicles with a total weight of 86 kips (14 kips heavier than HS-20 Truck) and a total length of 19 feet (9 feet shorter than the HS-20 truck configuration used in this study) that creates larger longitudinal and transverse bending moment in the bridge. Moreover, WIM data in the state of Florida was also used for selecting a typical truck, which creates a larger moment and shear for a 120 feet simple span bridge. The selected truck, which is called here WIM Data-FL, has a gross vehicle weight of 120 kips distributed over seven axles (Class 13 based on FHWA vehicle category classification). The ratio of the selected truck moment and shear to HS-20 truck is 1.58 and 1.56, respectively.

74

It should be noted that in all models studied in this section, concrete compressive strength was considered as 6.2 ksi, and the trucks were positioned over the fractured girder in two different locations across the bridge width, to constitute Case 1 for studying the one-way flexural bending failure of the deck and Case 4 for one-way shear failure. In these cases, where most of the truck loading is being transferred transversely to the intact girder, the center of gravity of trucks was positioned at the mid-span for all cases.

Table 6-9 indicates the results of sensitivity analysis for the truck loading. The one-way shear capacity was calculated using the method mentioned in the previous section (The effective width was predicted using 45° spreading line from the far side of the first and last point loads, and total width was considered as the effective width by ignoring gaps between spreading lines.) and the bending yield lines for each case, as shown in Figures 6-16 and 6-17, were captured from the finite element models using the damage indexes, as explained in the previous sections. The bridge yield line capacity and one-way shear capacity were calculated for each case using the yield line pattern and the proposed method for the shear, and the results were compared in Tables 6-9 and 6-10 to the bridge ultimate load capacity obtained from the finite element model.
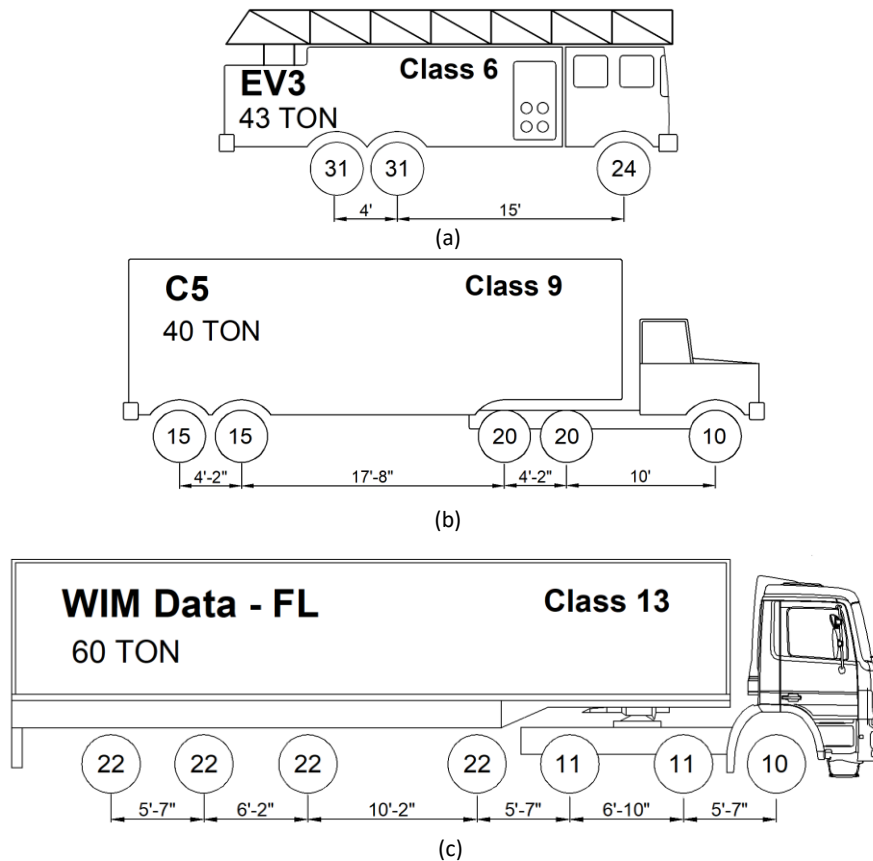
Figure 6-15. Vehicle loading configuration: (a) Florida emergency vehicle (EV3); (b) Florida legal load (C5); (c) Florida typical truck (WIM Data –FL).
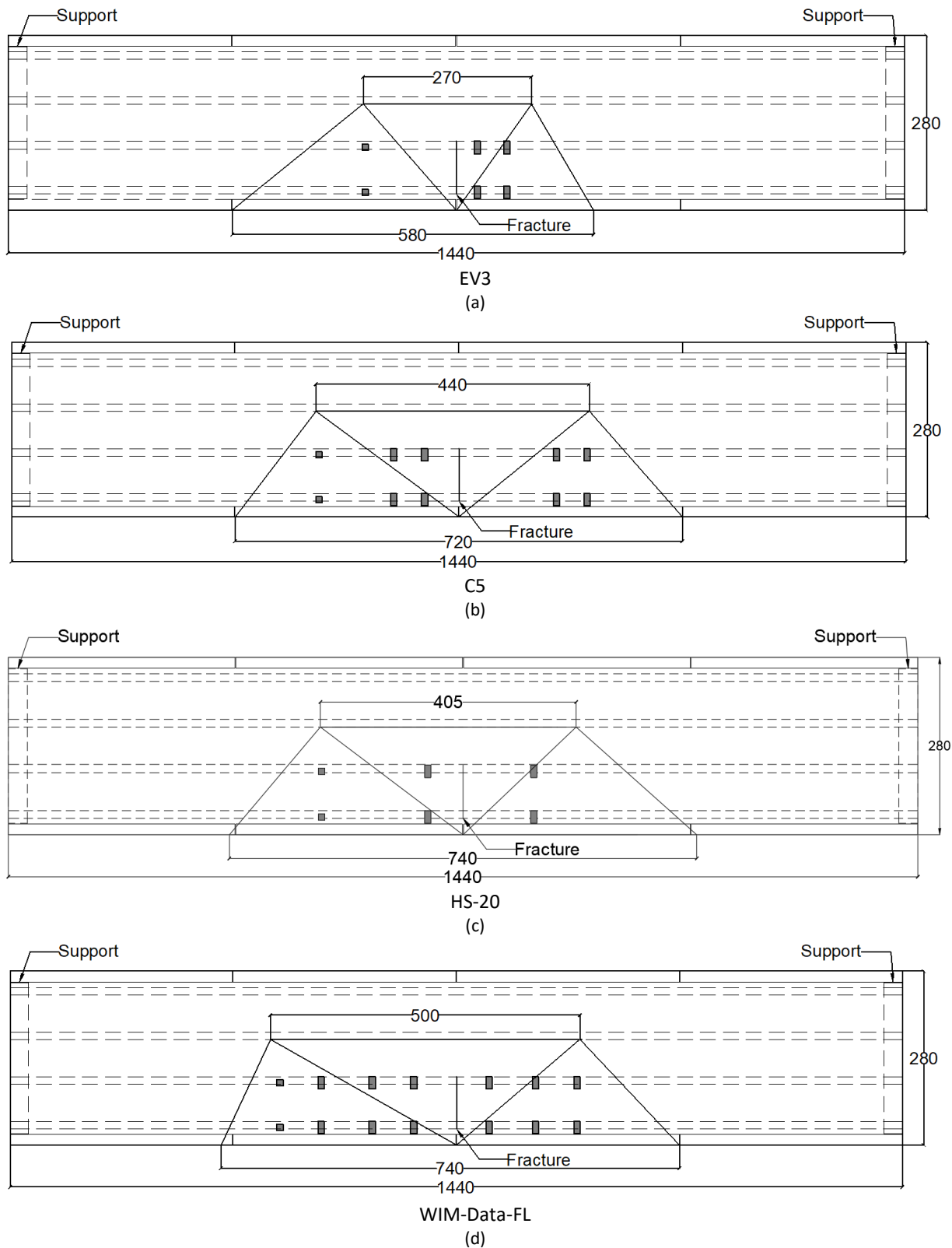
Figure 6-16. University of Texas Bridge Yield Line Failure in case 1 for Different Truck Loading: (a) EV3; (b) C5; (c) HS-20; (d) WIM-Data-FL.
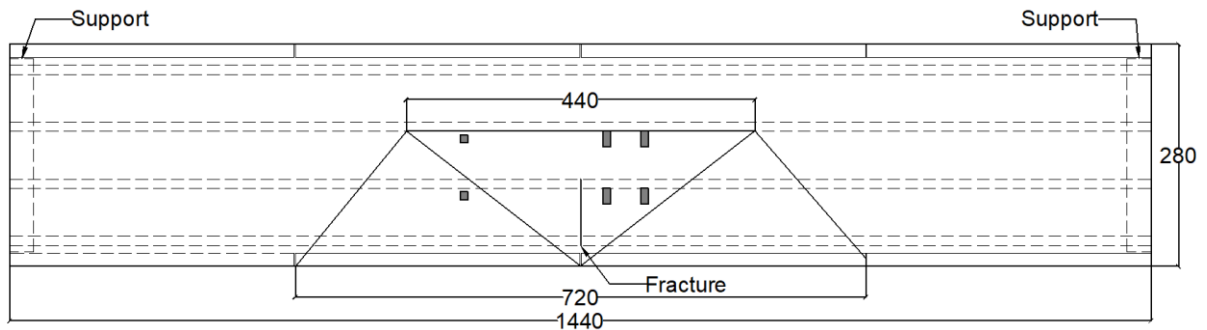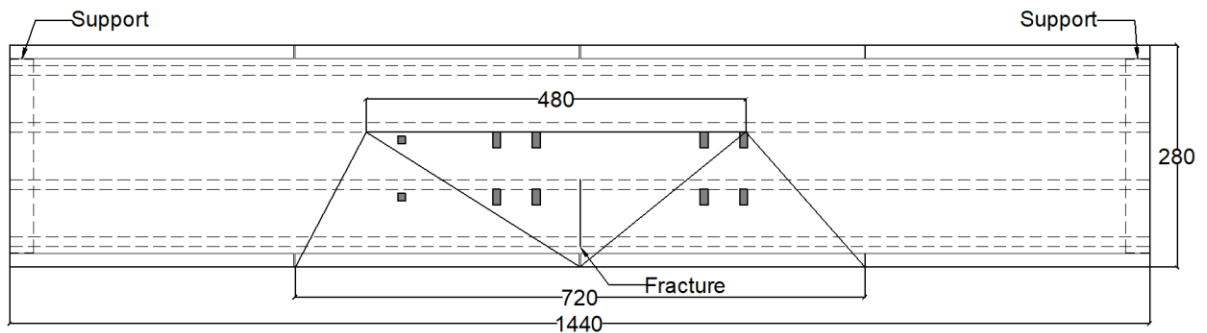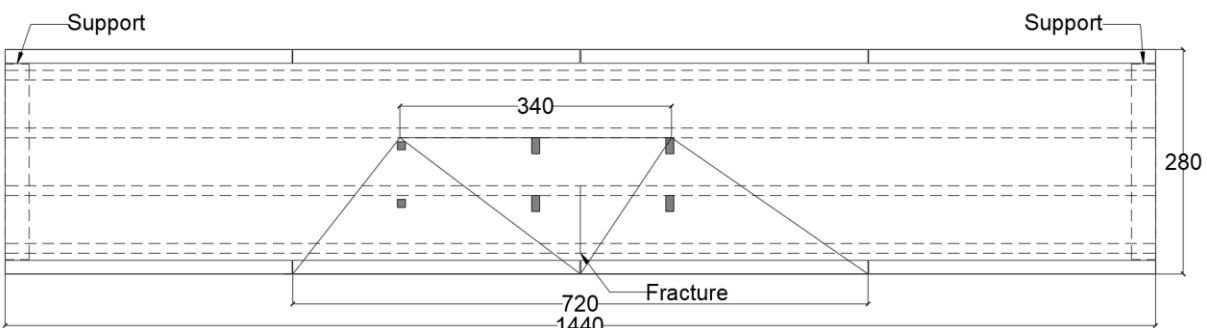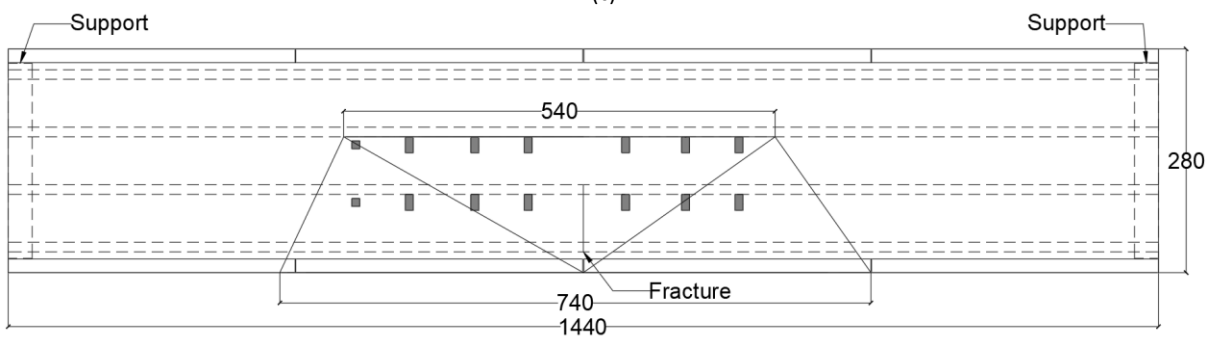
Figure 6-17. The University of Texas bridge yield line failure in case 4 for different truck loading: (a) EV3; (b) C5; (c) HS-20; (d) WIM-Data-FL.

Table 6-9. Bridge capacity for Cases 1 and 4 with different truck configurations.

Case	Truck	One-Way Shear Capacity (kips)	Bending Yield Line capacity (kips)	Max. Capacity from FE analysis- shear studs are modeled (Kips)
1	C5	534.7	**288**	300
	HS-20	448.7	**286.6**	318
	EV3	351.1	309.6	333
	WIM-Data	577.7	**330**	374
4	C5	427.2	620	350
	HS-20	341.2	563	340
	EV3	**243.6**	524	352
	WIM-Data	470.2	668	402

The results show that the bending yield line failure is the failure mode for all the truck configurations in Case 1, where the truck position transversely is farthest from the intact girder, and one-way shear is the failure mode in Case 4, where the trucks were positioned closest to the intact girder. Moreover, the proposed bending yield line can conservatively predict the bridge ultimate load capacity in Case 1 by ignoring the effect of the fractured girder and diaphragms. It is worth mentioning that only for the EV3 truck configuration where the truck length is very short, and the truck weight (86 kips) is much heavier than the HS-20 design truck, the one-way shear capacity of the bridge in Case 4 (243.6 kips) is less than its bending yield line capacity in Case 1 (309.6 kips). In all other truck loadings, Case 1, with the largest eccentricity of loading, is the governing case with the bending yield line as the dominant mode of failure.

In all the above cases, the yield line configuration was determined using the specific finite element damage pattern for each case. Using these results, a unified and simplified method can be developed for predicting the yield line pattern in the deck of a twin steel box girder with one fractured girder for different loading configurations.

Table 6-10. Minimum bridge capacity for all cases with different truck configurations.

Truck	Min. One-Way Shear Capacity (kips)	Min. Bending Yield Line capacity (kips)	Capacity from FE analysis (Kips)
C5	427.2	**288**	300
HS-20	341.2	**286.6**	318
EV3	**243.6**	309.6	333
WIM-Data	470.2	**330**	374

6.3 A Unified Simple Model for Predicting the Reserved Capacity of Twin Steel Box Girder Bridges with A Fracture in One Girder

6.3.1 Simplified Yield Line Pattern for Different Loading Configurations

The results presented in the previous section indicated that the dominant mode of failure for the twin steel box girder bridge considered in this study after a fracture in one girder in all but one case was the bending yield line failure. The exception was the case of EV3, where one-way shear for Case 4 was smaller than bending yield line failure for Case 1 for the same truck. However, even in this case, the capacity indicated by bending yield line failure was noticeably smaller than the capacity obtained from finite element analysis. Also, the simple method adopted in this study for one-way shear failure seems too conservative for the shorter and more compact trucks. Hence, from now on, the simple model based on bending yield line failure will be considered for reliability and redundancy analysis applicable to all truck configurations.

The characteristics and geometry of the yield line pattern for each case have been deducted from the detailed finite element analysis conducted for that specific case (truck loading and position). To simplify the process and avoid the need for FE analysis for each loading case, a simple and unified method of determining the yield line pattern becomes instrumental. This unified pattern, however, has to agree well with the results obtained using FE analysis to satisfy the complex load distribution after the fracture of one girder. Therefore, a parametric analysis was conducted for developing a simplified yield line pattern to be used for calculating the bridge capacity based on the bending yield line failure that would be applicable to different loading configurations. The parametric study on the truck loading configuration shows that when the bridge is loaded over the fractured girder far from the intact girder (Case 1), the deck starts to first crack over the intact girder due to the one-way bending mechanism of the bridge deck. By increasing the load, cracks in the deck will extend along the span, and four diagonal cracks will form to complete the failure mechanism in the deck (Figure 6-16). A comparison between the yield line patterns obtained from the FE analysis for different loading configurations shows that the longitudinal crack over the intact girder extends up to about the truck length in all configurations. Internal diagonal cracks will follow a regular pattern connecting the end of the longitudinal crack to a point on the edge of the deck at the fracture location. However, external diagonal cracks form with different angles from the end of longitudinal cracks to the railing, depending on the loading configuration (see Figure 6-16).

Considering the FE analysis, a simplified yield line pattern was developed, as shown in Figure 6-18. In this pattern, the truck is positioned closest to the railing, where its center of gravity coincides with the mid-span over the fracture. The length of the longitudinal crack is considered equal to the truck length. To find the angle of the diagonal lines (α in Figure 6-18), a parametric analysis was conducted with varying angles. The goal was to find an angle that results in capacity in agreement with previous results using FE derived patterns and capacity obtained from FE analysis. Table 6-11 summarizes the parametric analysis for yield line patterns with different

79

angles varied from 30º by 5º increments. The ratio of the simplified bending yield line capacity to the bridge capacity obtained from the FE analysis is shown in the table for each angle. The results show that the simplified method with the 35º gives the best average capacity ratio (0.92) compared to the bending yield line capacity and ultimate bridge capacity obtained from the FE analysis, and no case produces capacity above the capacity obtained from FE analysis. By decreasing the angle to 30º, the bending yield line analysis gives a higher capacity than the ultimate bridge capacity from FE analysis, and the results for 40º and 45º are too conservative.

Table 6-11. Parametric results on the suggested simplified yield line pattern for different loading configurations.

Truck	Bending Yield Line capacity-FEM (kips)	Ratio	Bending Yield Line Capacity-Simplified Method (kips)								Capacity from FE analysis (Kips)
			$\alpha=30$	Ratio	$\alpha=35$	Ratio	$\alpha=40$	Ratio	$\alpha=45$	Ratio	
C5	288	0.96	329.6	1.10	**300.2**	**1.00**	281.6	0.94	263.2	0.88	300
HS-20	286.6	0.90	329.7	1.04	**298.4**	**0.94**	278.6	0.88	251.6	0.79	318
EV3	309.6	0.93	351.1	1.05	**310.4**	**0.93**	279.1	0.84	254.6	0.76	333
WIM-Data	330	0.88	325.6	0.87	**301**	**0.80**	282.7	0.76	265.2	0.71	374
Average		0.92		1.02		**0.92**		0.85		0.79	
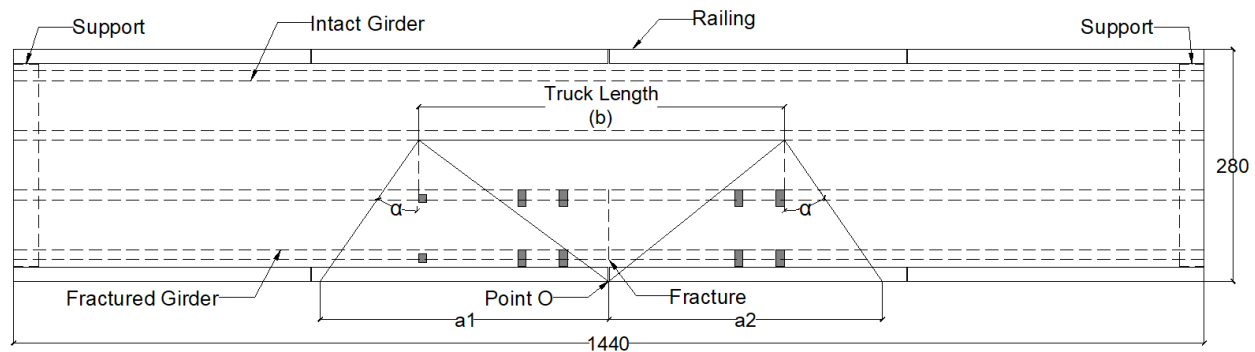
Figure 6-18. Simplified yield line pattern for different loading configurations.

The yield line pattern can be defined for each loading configuration based on the proposed pattern, and the virtual work can be used for computing the fractured bridge capacity. Using fundamental trigonometric relationships, displacement of point loads (Equation (6)), the center of gravity of railing, and the concrete deck triangles (for self-weight) are obtained for calculating the external virtual work (Equations (7-9)). In order to calculate the internal virtual work by the bridge deck, including the deck and railing, the length and rotation of each yield line are calculated using the failure pattern geometry (Equations (10), (11)). Railing can contribute significantly to the ultimate bridge capacity. After a fracture in one of the girders, the railing acts as an edge beam for carrying the loads. The internal work by the railing depends on the type of railing, the location of the hinge lines, and the gaps between railing segments. In the railing system with expansion joints (gap), two sides of the gap will come in contact after a large displacement and increase the internal work depending on the gap size. However, due to uncertainty of gaps size and to be conservative, virtual

work by the railing at the gap (assumed in this study at the fracture location) is not considered in the calculations of the simplified method. Nevertheless, the virtual work by the railing is considered where the yield line intersects the railing by two external diagonal lines.

$$\delta_{load} = r_{load} \cdot \Delta/r \tag{6}$$

$$EW_{Railing} = A_{Railing} \cdot (a_1 + a_2) \cdot 0.15 \cdot \Delta/2 \tag{7}$$

$$EW_{Deck\ Triangles} = A_{Deck\ Triangles} \cdot t \cdot 0.15 \cdot \Delta/3 \tag{8}$$

$$EW_{Truck\ load} = \Sigma\ (load. \delta_{load}) \tag{9}$$

$$IW_{Deck\ Triangles} = \Sigma\ (m_b \cdot l \cdot \theta_{Deck\ Rotation}) \tag{10}$$

$$IW_{Railing} = \Sigma\ (m_b \cdot \theta_{Railing\ Rotation}) \tag{11}$$

Where δ_{load} = Displacement of point loads; r_{load}= Distance from the point load to Point O (see Figure 6-18); r = Distance from Point O to the yield line (passing from the point load); m_b = Bending capacity.

6.3.2 Evaluation of the Simple Model for Various Deck Thickness and Concrete Compressive Strength

The proposed yield line patterns and analysis were used for calculating the ultimate bridge capacity under various truck loading for different concrete deck thickness and compressive strengths separately. The concrete deck thickness varied from 7.5 in. to 8.5 in. and the concrete compressive strength varied from 4 ksi to 7 ksi. Note that for the concrete deck thickness sensitivity analyses, the compressive strength was assumed 6.2 ksi, and for the concrete compressive strength analyses, 8 in. thickness was assumed for the deck. Tables 6-12 and 6-14 summarize the results of sensitivity analysis for the concrete deck thickness and compressive strength, respectively. Moreover, FE analyses were used for comparing the bridge ultimate load-carrying capacity obtained from the FE model and the simple method, as shown in Tables 6-13 and 6-15.

Table 6-12. Ultimate bridge capacity obtained using the yield line analysis for different concrete deck thicknesses (ksi).

	Truck	Concrete Deck Thickness (in)										
		7.5	7.6	7.7	7.8	7.9	8	8.1	8.2	8.3	8.4	8.5
Ultimate Bridge Capacity (kips)	EV3	292	295.8	299.4	303.2	306.7	310.4	314	317.5	321.3	324.9	328.7
	C5	279.4	283.7	287.7	292	296	300.2	304.2	308.5	312.5	316.7	320.8
	WIM	279.7	283.9	288	292.3	296.6	301	305.2	309.5	313.4	317.8	322.1
	HS-20	279.5	283.3	287.1	290.9	294.7	298.4	302.5	306.3	310	313.8	317.7

Table 6-13. Comparison of the ultimate bridge capacity obtained using the simple and FE analysis methods.

		Concrete Deck Thickness (in)			
	Truck	Yield Line Analysis			FEA
		7.5	8	8.5	8
Ultimate Bridge Capacity (kips)	EV3	292	310.4	328.7	333
	C5	279.4	300.2	320.8	300
	WIM	279.7	301	322.1	374
	HS-20	279.5	298.4	317.7	318

81

Table 6-14. Ultimate bridge capacity obtained using the yield line analysis for different concrete compressive strength (ksi).

	Truck	Concrete Compressive Strength (ksi)							
		4	4.5	5	5.5	6	6.2	6.5	7
Ultimate Bridge Capacity (kips)	EV3	287.4	293.4	298.8	303.9	308.3	310.4	312.5	316.3
	C5	273	280.2	286.7	292.6	297.9	300.2	302.8	307.2
	WIM	272.8	280.2	286.9	293	298.4	301	303.6	308
	HS-20	274	280.3	286.2	291.7	296.4	298.4	301	304.8

Table 6-15. Comparison of ultimate bridge capacity obtained using simple and FE analysis methods.

		Concrete Compressive Strength (ksi)					
	Truck	Yield Line Analysis			Finite Element Analysis		
		4	5	6.2	4	5	6.2
Ultimate Bridge Capacity (kips)	HS-20	274	286.2	298.4	308	314	318

It should be pointed out that the amount of reinforcement in the deck was kept the same (#5 bar with 6 inches spacing (Figure 6-19)) for all deck thicknesses. As shown in Figure 6-20, the external/internal work (used in the simple method) and the ultimate bridge capacity in the yield line analysis varies with the section moment capacity, loading configuration, and the yield line patterns. The results indicate that the bridge ultimate load capacity is directly proportional with the deck section moment capacity and deck thicknesses and varies nonlinearly with the concrete compressive strength.

Figures 6-20 (a) and (b) show the moment capacity and the external/internal work (used in yield line analysis) obtained using the simple method for various truck configuration and variation of the deck thickness, where Figures 6-20 (c) and (d) show the same for variation of concrete compressive strength. The results show that the slope of the ultimate bridge capacity and external/internal work varies with each truck because of the difference in the loading configurations and yield line pattern.

Moment capacity analysis using the simple model (Figures 6-20 (c) and (f)) shows that an increase in deck thickness or concrete compressive strength results in an increase in the positive and negative moment capacity. Since the deck configuration used in this study, as shown in Figure 6-19 (#5 bar with 6 inches spacing), is under-reinforced, the rebar reaches yield strain before the concrete reaches crushing strain for all the studied thicknesses. Therefore, increasing the section thickness linearly increases the positive and negative moment capacity of the deck. However, the effect of concrete compressive strength in the section moment capacity is nonlinear.
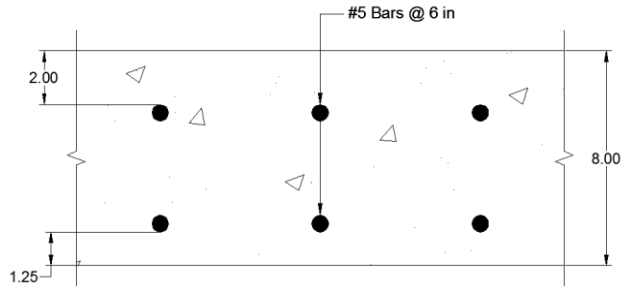
Figure 6-19. The concrete deck section.

Table 6-16. Maximum moment and shear in a simple 120- ft span bridge for different truck loading.

Truck	Moment		Shear	
	Maximum (kip.ft)	Location (Distance from support) (ft)	Maximum (Kip)	Location (Distance from support) (ft)
WIM	2944.3	57.8	103.8	
EV3	2339.3	58.6	81.2	0 and 120
C5	1994.8	57.7	68.5	
HS20	1883.8	57.6	66.4	
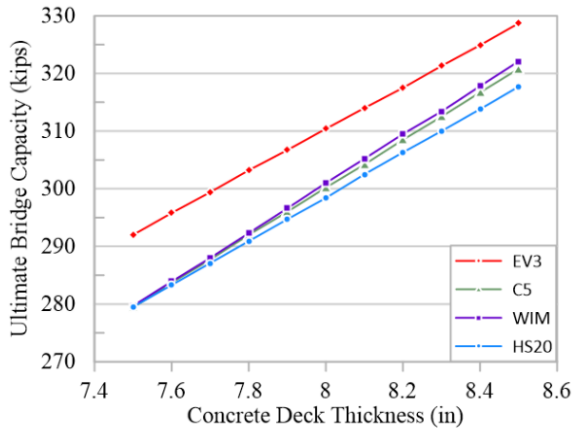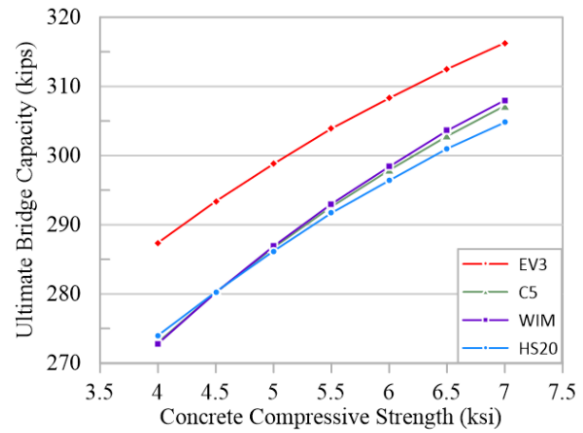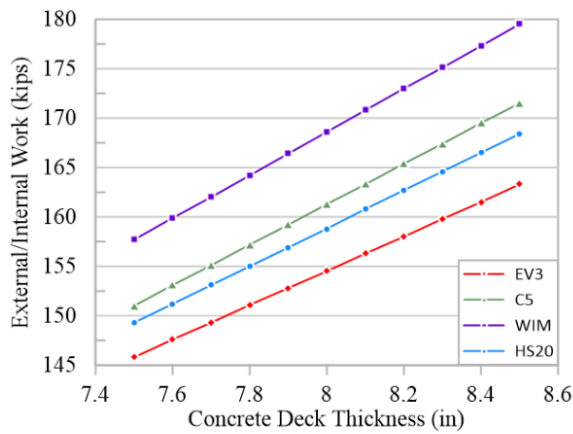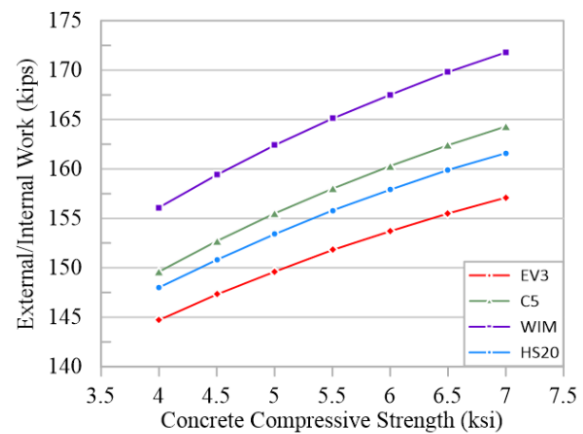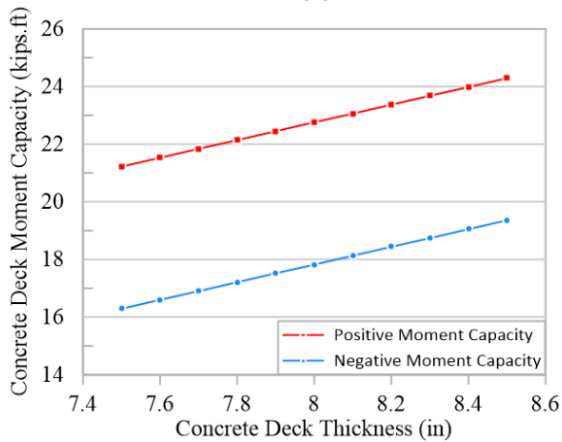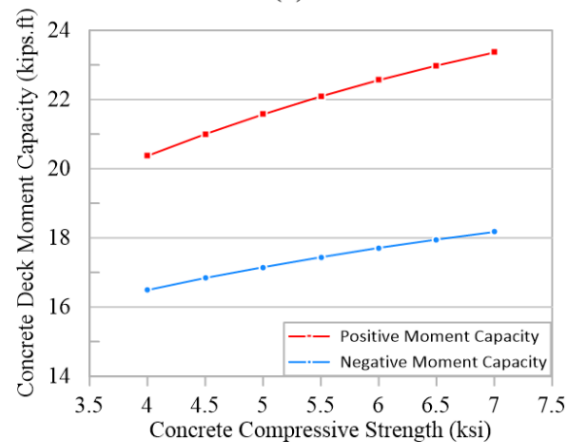
Figure 6-20. Sensitivity analysis of concrete deck thickness: (a-c) and concrete compressive strength; (d-f) using the yield line analysis.

84
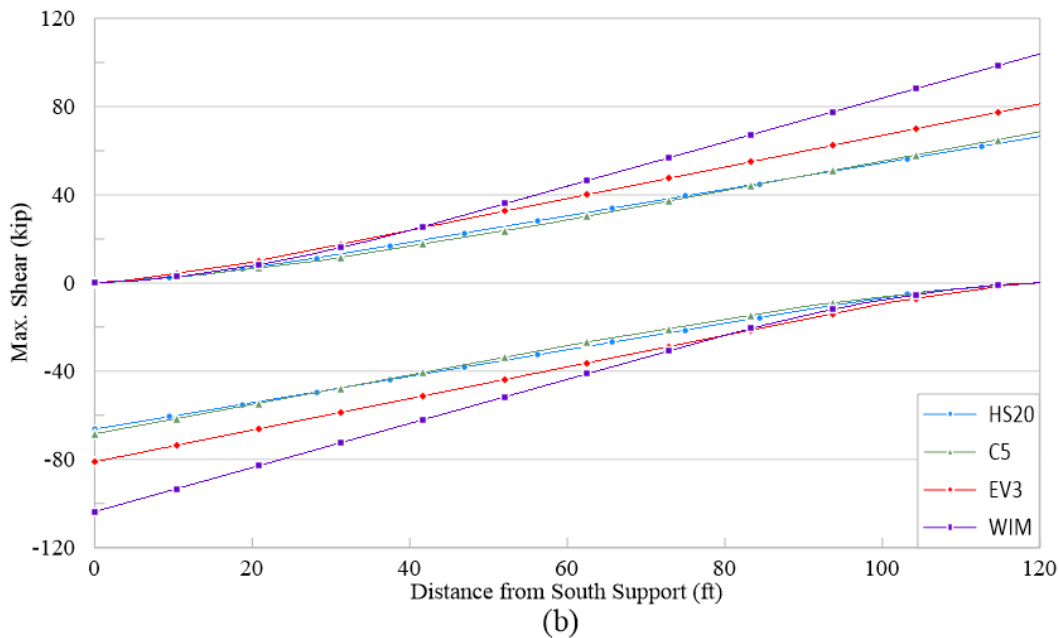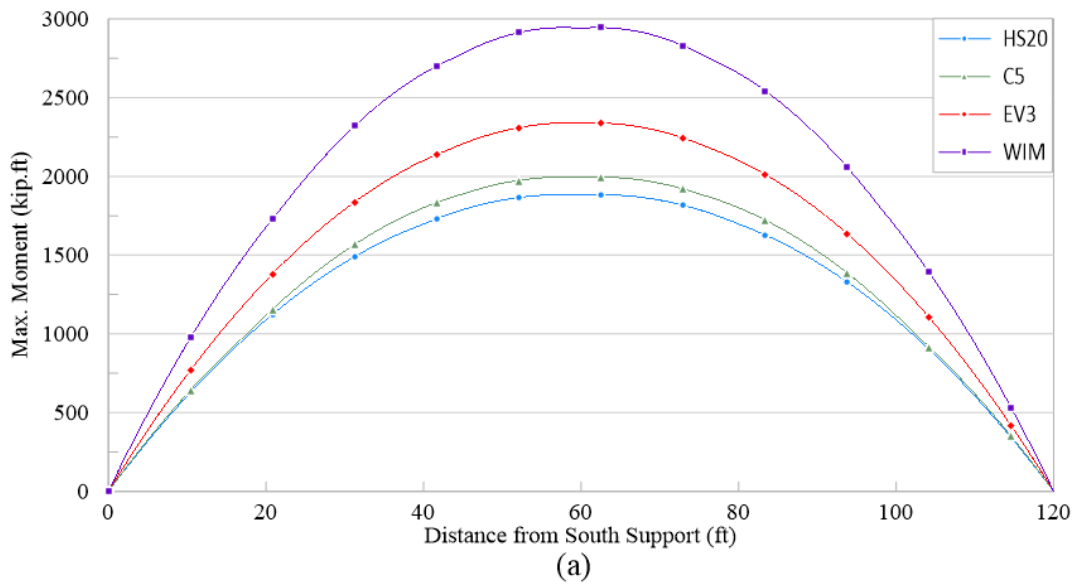
Figure 6-21. Moment and shear diagram in a simple 120 ft span bridge for different truck loading: (a) Maximum moment; (b) Maximum shear.

6.4 Load Distribution Analysis in the University of Texas Twin Steel Box Girder Bridge

A series of analyses are conducted on the bridge to investigate the behavior of the bridge in intact and damaged scenarios under dead and increasing live load. The goal is to determine the distribution of dead and live loads before and after the fracture of one girder. One way to determine the load distribution is by comparing the support reactions of the girders. Unsymmetrical bridge loading like Case #1 in this study creates additional torsional moment over the bridge section that is supported at the bearing as coupling forces (upward and downward forces (T)), which can

85

change the total reaction forces. Depending on the loading eccentricity, bridge configuration, and condition, the torsional force could even lead to uplift at the supports. In the twin steel box girder bridges, since after a fracture in one of the girders, the intact girder needs to transfer the torsional moment created by eccentric loading to the supports, the uplift forces are more pronounced. To this end, the reaction forces at the supports for the intact and damaged bridge subjected to the 1×HS-20 loading (Figures 6-23 and 6-24) are obtained from the FE analysis as shown in Tables 6-17 and 6-18.

The results show that after the fracture in the loaded girder, the reactions at the intact girder supports would increase. However, the girder reactions are affected by both vertical load (R) and an eccentricity torque (T), as shown in Figures 6-22 and 6-23. The torque reduces the total reactions on the right girder and increases the total reaction of the left/loaded girder. The torque is understood to be even larger after fracture when the centroid would move closer to the intact girder. The results show that after a fracture of one girder, a larger portion of the dead load and live load would transfer transversely to the intact girder near the mid-span. A significant portion of the transferred force, however, returns to the fractured girder through the deck and cross-frames that are away from the fracture zone (yield line pattern) therefore reducing the reaction forces on the intact girder to balance the torque.

Table 6-17. Bridge support reaction for the intact bridge obtained from FE analysis.

	Left Girder (Loaded)				Right Girder			
	North	South	Girder Reaction	Ratio to Total	North	South	Girder Reaction	Ratio to Total
Dead Load (R) (kips)	124.7	124.4	249.1	0.50	124.7	124.4	249.1	0.50
1xHS-20 (R) (kips)	30.9	30.5	61.4	0.85	2.3	8.3	10.6	0.15
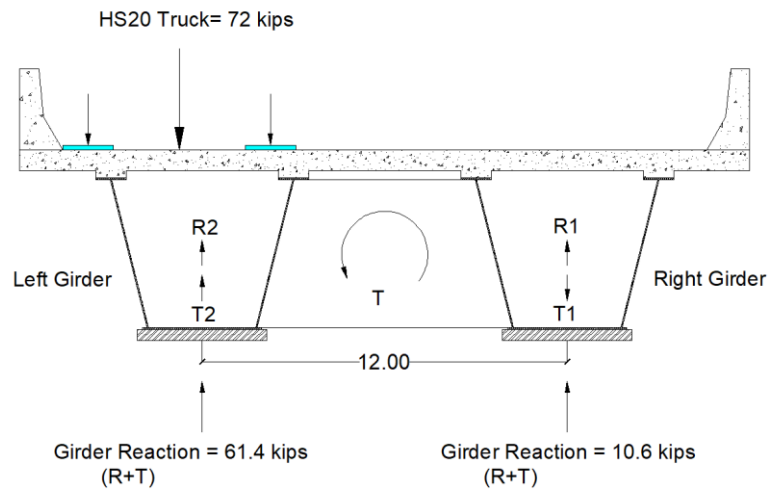
Figure 6-22. Bridge support reaction for the intact bridge obtained from FE analysis.

Table 6-18. Bridge support reaction for dead and live loads after the full-depth fracture obtained from the FE analysis.

	Left Girder (Loaded-Fractured)			Right Girder		
	North	South	Girder Reaction	North	South	Girder Reaction
Dead Load (R+T) (kips)	115.3	116.9	232.2	132.5	133.5	266
1xHS-20 (R+T) (kips)	26.4	30.2	56.6	6.2	9.2	15.4
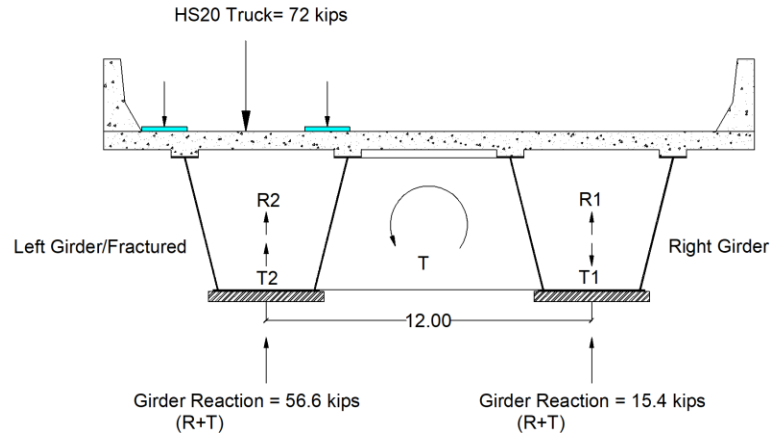
Figure 6-23. Bridge support reaction after the full-depth fracture.

As an alternative way to estimate the live and dead load transfer/distribution to the intact girder after a fracture, shear stress profiles for a section at the face of the intact girder (Figure 6-24) were extracted from the FE analysis. The total shear force from the concrete deck and intermediate cross-frames along the span for the intact and damaged bridge subjected to the dead load and the live load was obtained as shown in Tables 6-19 and 6-20, respectively. It is also realized that the proportion of load transferred due to the fracture of a girder would increase as the level of load increases. This can partly attribute to the damages at the deck to the girder interface (shear studs) and the deck itself, as well as increased torque due to shifting the bridge centroid. To demonstrate this, the damaged bridge was analyzed under 3.2×HS-20 that is closer to the bridge capacity. Table 6-20 shows the transfer of loads because of fracture through shear at the deck and cross-frames from fracture of one girder at Section 1-1.
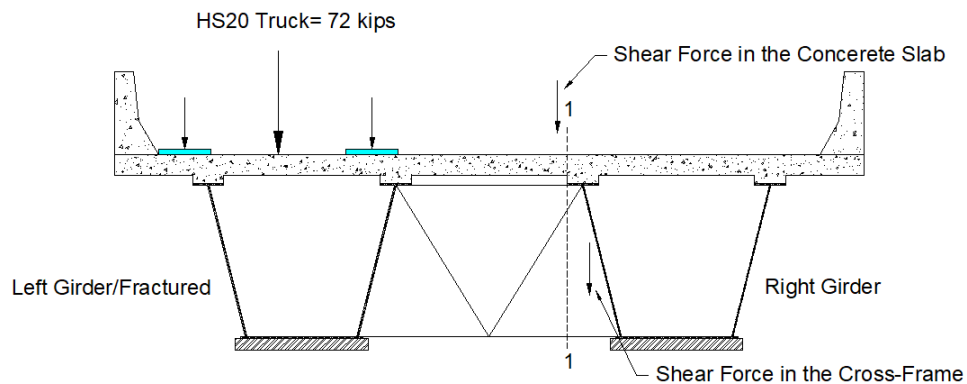
Figure 6-24. Shear force in Section 1-1.

87

Table 6-19. Shear forces transferred to the right girder under dead load and 1 x HS-20 design truck for the intact bridge at section 1-1.

	Shear Forces		
	Concrete Slab	Cross-Frames	Transfer Total
Dead Load (kips)	16.1	0.3	16.4
1x HS-20 (kips)	10.4	15.6	26

Table 6-20. Shear forces transferred due to fracture to the right girder under dead load and 3.2 times HS-20 design truck.

	Shear Forces			
	Concrete Slab	Cross-Frames	Transfer Total	Ratio to Total live load
Dead Load (kips)	31.7	27.8	59.5	
3.2xTime HS-20 (kips)	71.5	85.0	156.5	0.68

The results show that for 3.2×HS-20, 68% of the total live load will be transferred to the intact girder after the fracture of the loaded girder through the concrete deck and cross-frames. Another way for simple estimation of shear transfer is based on the yield line analysis where the live load is assumed to be transferred as shear stress to the intact and fractured girder through the outside yield lines, as shown in Figure 6-25. The live load distribution to the intact and fractured girder for the HS-20 truck loading according to the suggested yield line pattern was calculated as 70% and 30%, respectively; that is a good estimate compared to the FE analysis (68%).
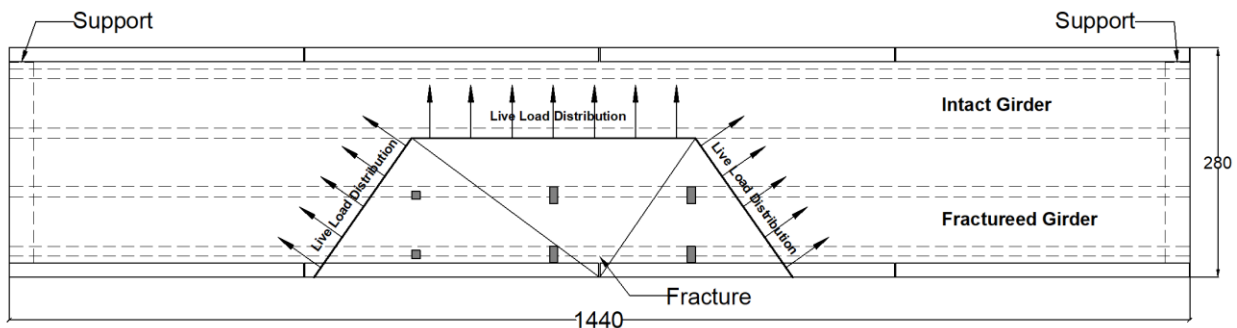
Figure 6-25. Live load distribution based on the yield line analysis for HS-20 loading.

When a fracture occurs, and the deck fails under increasing live load, for the bridge not to collapse, the intact girder has to be able to carry the loads transferred to it, i.e., the intact bridge, to have adequate moment capacity. Accordingly, moment analysis was conducted on the bridge subjected to dead and live load at the middle of the span where the bridge is damaged. Table 6-21 shows sectional moments extracted from finite element analysis for the intact and damaged bridge. According to the results, the dead load moment of each girder in the intact bridge is about 3538.7 kip-ft. However, the moment on intact girder increases by about 50 percent once a fracture occurs in the loaded girder (5618.8 kip. ft). The fractured girder has a very small stiffness at the middle (one can assume hinge or very weak spring), so it attracts only a negligible moment (893 kip. ft) compared to the intact girder.

The live load moment analysis for the intact bridge shows that the left girder (loaded) carries 60%, and the right girder carries 40% of the live load. However, after the fracture, the right girder (intact) carries most of the live load (66%) because of a decrease in stiffness of the fractured girder. Nevertheless, the fractured girder is undamaged through most of its length. Since the truck loads are applied through its wheel footprints, and rear and front wheels are at a distance from the middle, the fracture girder can transfer some portion of live load (34%) through those segments as a cantilever beam. Unlike the live load, the dead load is distributed along the bridge, and the fractured girder is able to transfer a noticeable portion through its undamaged end segments.

In the bridge with one girder fractured, the total moments at the middle of the bridge is not the same as the intact bridge since the girders (or the bridge) cannot be assumed anymore to be separately simply supported. There is a complex interaction between the intact and fractured girder away from the fracture point that can only be simulated with the FE analysis. It should also note that the percentages calculated represent the changes of the moment at mid-span due to the fracture and do not necessarily give a picture of how the load is distributed.

Table 6-21. Moment analysis of the bridge under HS-20 loading (FEM).

| | Moment (kip-ft) | | | | | |
| | Bridge Section | | Right Girder Section | | Left Girder Section | |
	Dead	Dead+ 3.2 HS-20	Dead	Dead+ 3.2 HS-20	Dead	Dead+ 3.2 HS-20
Intact Bridge	7079.6	12636.0	3538.7	5801.7	3541.0	6834.3
Damaged Bridge	6512.2	10792.8	5618.8	9560.7	893.4	1232.1

Chapter 7   Continuous Curved Twin Steel Box Girder Bridge

A continuous curved bridge was analyzed to demonstrate the capability of the finite element modeling methods proposed in Chapter 5 of the report. The possible failure mechanisms and the applicability of the simplified methods presented in Chapter 6 for calculating the bridge ultimate load-carrying capacity will also be investigated. Suggestions will also be made for future work to adapt the methods developed in this study for simple spans to continuous spans.

7.1   Bridge Description

A three-continuous span bridge located in Miami, FL, was selected for this analysis. The bridge was built in 2005 and has an overall length of 682.4 ft. carrying one traffic lane. The length of the first and last span is 210 ft, and the middle span length is equal to 262.4 ft. The first and second spans have a radius of curvature of 492 ft. while the last span is straight. Figures 7-1 and 7-2 show the bridge plan and elevation view. The bridge has diaphragms at supports and horizontal and vertical bracing along the bridge for stability, similar to the University of Texas bridge.
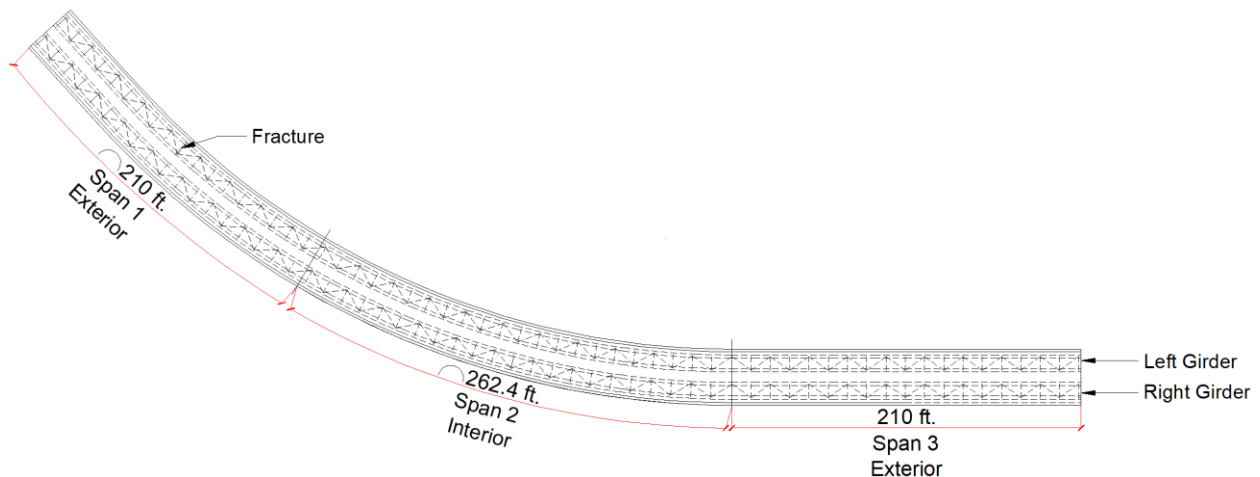
Figure 7-1. Plan view of the three-continuous span bridge.
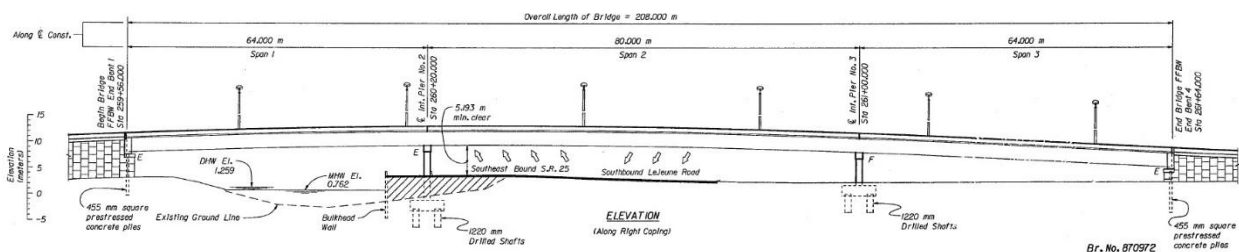
Figure 7-2. Elevation view of the three-continuous span bridge.

7.2   Finite Element Analysis

A finite element model of the bridge was developed to study the bridge behavior after a full-depth fracture at the middle of Span 1 (Figure 7-3). Material properties, contact surfaces, and analysis procedures were assumed the same as the simple span model. In addition to the deck failure mechanisms discussed in this report, a possible failure mechanism in the continuous span bridges is the failure of the intact girder when the bridge is loaded over the fractured girder due to torsion and bending.

In interior spans, two sides of the fracture girder will behave as cantilever beams carrying a large portion of the dead and live load; however, in exterior spans, only one side of the fractured girder can carry the load as a cantilever beam. Therefore, in general, for an equal span length, exterior spans are the critical span for the continuous span bridges, and the only failure in the side span was studied in this report. Since the last span does not have a curvature and has the same length as the first span, the finite element model was developed to consider the fracture in the first span. For the model, a full-depth fracture was assigned to the interior girder (left girder) at the middle of the span, and an increasing load in terms of the HS-20 design truck similar to the simple span bridge was applied over the fractured girder up to the bridge failure.
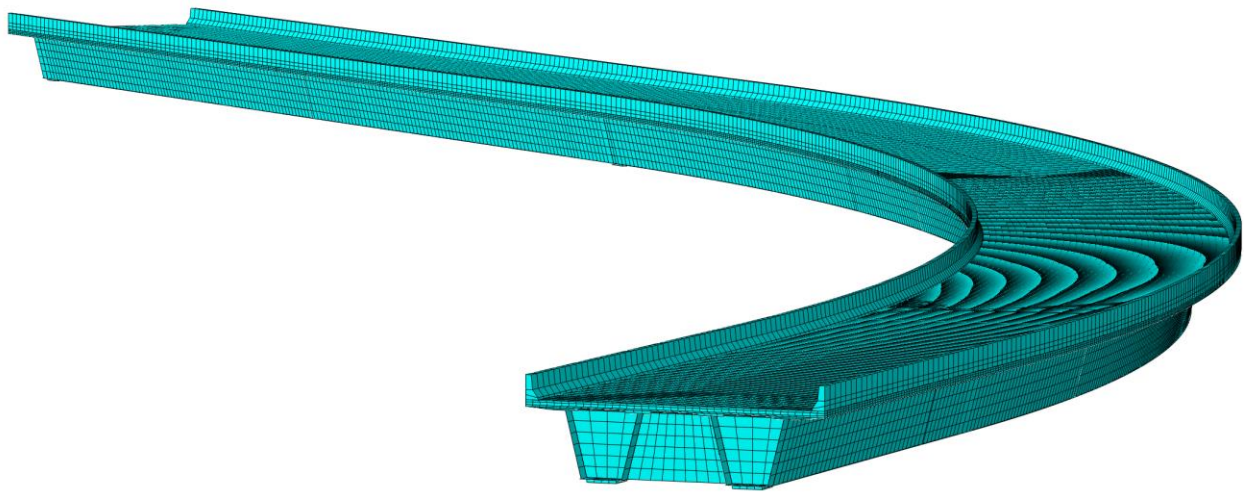
Figure 7-3. Finite element model of the three-continuous span bridge.

7.3   Intact Girder Failure Mechanism

The results show that the intact girder at the middle of Span 1 reaches its plastic moment under dead load and eight times HS-20 design truck loaded over the fractured girder due to a portion of dead load and live load being transferred to the intact girder after the fracture. Moreover, due to the curvature and loading eccentricity, the effect of torsion is more significant in this bridge compared to a straight bridge. Figure 7-4 shows the failure of the intact girder under dead and live loading. Moreover, the results indicate that because of the girder continuity, the fractured girder

91

also carries a large portion of dead load and live load as a cantilever beam more pronounced on the continuous side. This contribution is relatively significant since under eight times HS-20 loading when the intact girder is failed, the stress at the bottom and top flange and a portion of the web of the fractured girder reaches 50 ksi (negative moment). The stress contours in Figure 7-5 show the contribution of the fractured girder in carrying a portion of the loads as a cantilever beam. The FE results also show that after the failure of the intact girder at the middle of Span 1 and with a large deflection, the fractured girder is the only element carrying the load up to the failure at the support due to the negative moment.
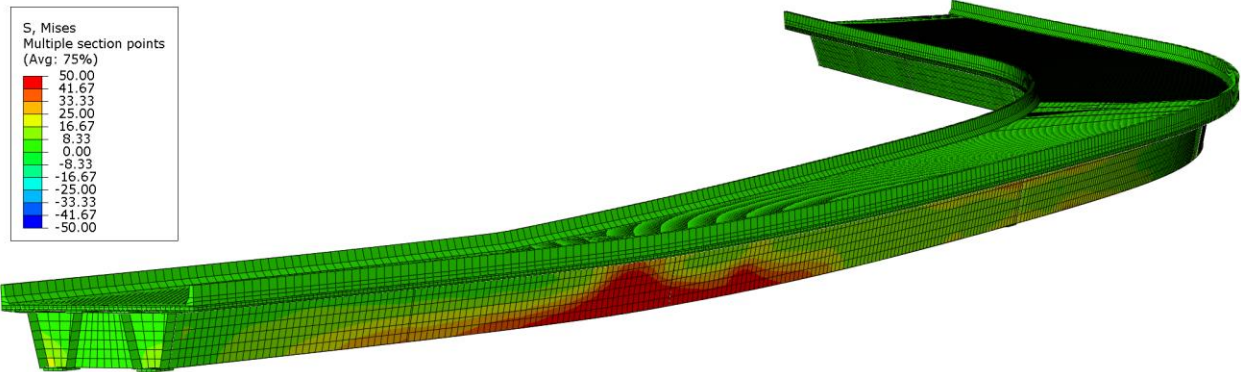
Figure 7-4. Intact girder failure under dead load and eight times HS-20 design truck at the middle of Span 1.
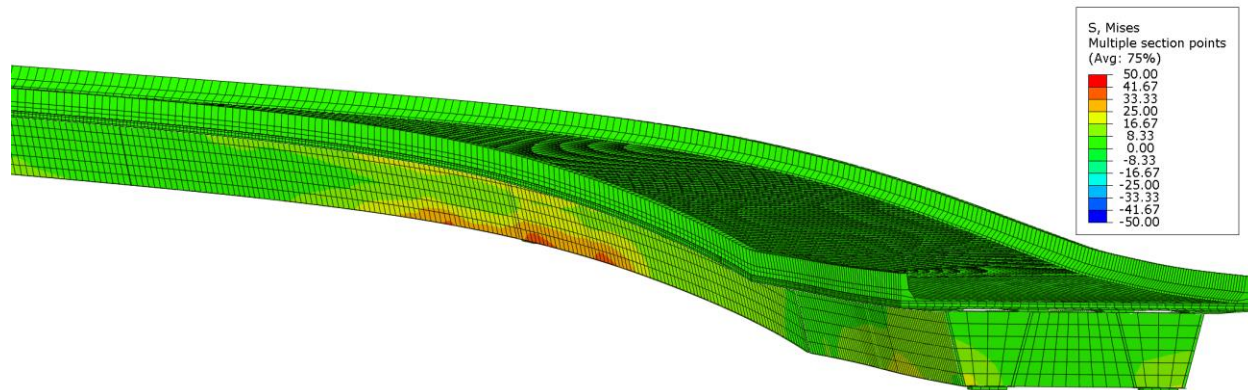
Figure 7-5. Contribution of the fractured girder in carrying a portion of the loads as a cantilever beam.

7.4 Deck Failure Mechanism

Investigation on the deck failure after the fracture using concrete damage plasticity model shows that first cracks will form over the middle supports. After the fracture of one girder, negative moment over the support will increase dramatically since the fractured girder can only carry the load as a cantilever beam (negative moment and partially toward simple support), and some portion of the dead load and live load will transfer to the intact girder which increases the positive moment at the middle of the span and the negative moment over the middle support in the intact girder. Therefore, negative moments over the support will increase for both girders and tension cracks will appear on the top of the deck, as shown in Figure 7-6.

By increasing the live load, longitudinal cracks will form along the intact girder at the middle of the span, and the transverse cracks at the support will be extended. Finally, diagonal cracks will form the half-ellipse failure of the deck, similar to the simple span bridge. Nevertheless, because of the continuity and the contribution of the fractured girder, the angle of the diagonal crack on the continuous span side is much wider than the simple span bridge. Moreover, the fractured girder at the yield line needs to be yielded, as shown in Figure 7-5. (Bottom and a portion of the web in the fractured girder is yielded at the yield line and the support). Therefore, the combination of these factors would result in a higher yield line capacity in the continuous bridge compared to the simple span bridge.
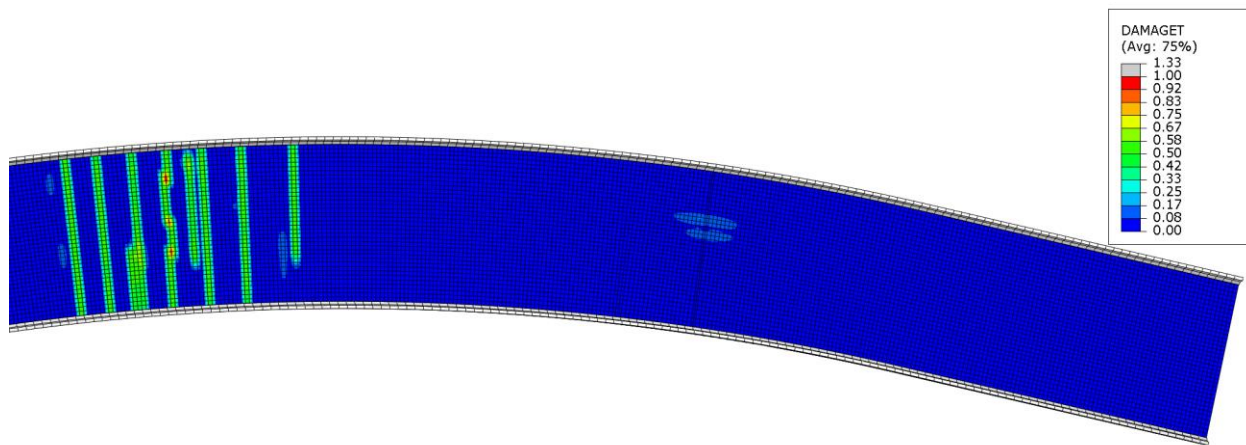
Figure 7-6. Deck crack pattern after a full-depth fracture of one girder in the continuous bridge in Span 1.

The results of the deck failure show that the yield lines will form at dead load plus six times HS-20 before the failure of the intact girder due to the bending and torsion at eight times HS-20 design truck. Figure 7-7 shows the yield line pattern obtained from the FE analysis, which is compared to the proposed yield line pattern for the simple span bridges (Chapter 6) in Figure 7-8. It is evident from the FE results that the continuity of the span has significantly altered the yield line pattern when compared to the simple yield line model developed for simple span bridges. However, it is useful to compare the deck capacity using the simple yield line pattern for comparison purposes only.

The simplified yield line analysis proposed in Chapter 6 for simple span bridges is used to calculate the continuous bridge capacity, as shown in Figure 7-8, Tables 7-1 and 7-2. This bridge has an 8.5 in. deck reinforced longitudinally using two layers of #5 bars with a spacing of 12 in. and 10 in. for top and bottom layers, respectively. In the transverse direction, two layers of #4 with a spacing of 5 in is used for both layers. Noted that the deck moment capacity (concrete only) in this bridge is less than the simple span bridge studied in Chapter 6. (#5 bars with a spacing of 6 in. is used for the simple span bridge for both layers and directions)

In the yield line analysis, only concrete deck capacity was considered in the internal work calculation, and the effect of the fracture girder (continuity) was ignored for simplicity and comparison with Chapter 6. The bridge yield line capacity obtained as 1.9 times HS-20 design truck much less than the capacity obtained from the FE model as six times HS-20 when the yield line pattern formed because of ignoring the girder continuity. Therefore, the simplified method needs to be modified for continuous span bridges by considering the effect of girder continuity in future studies.

(2×HS-20 Design Truck)

(4×HS-20 Design Truck)
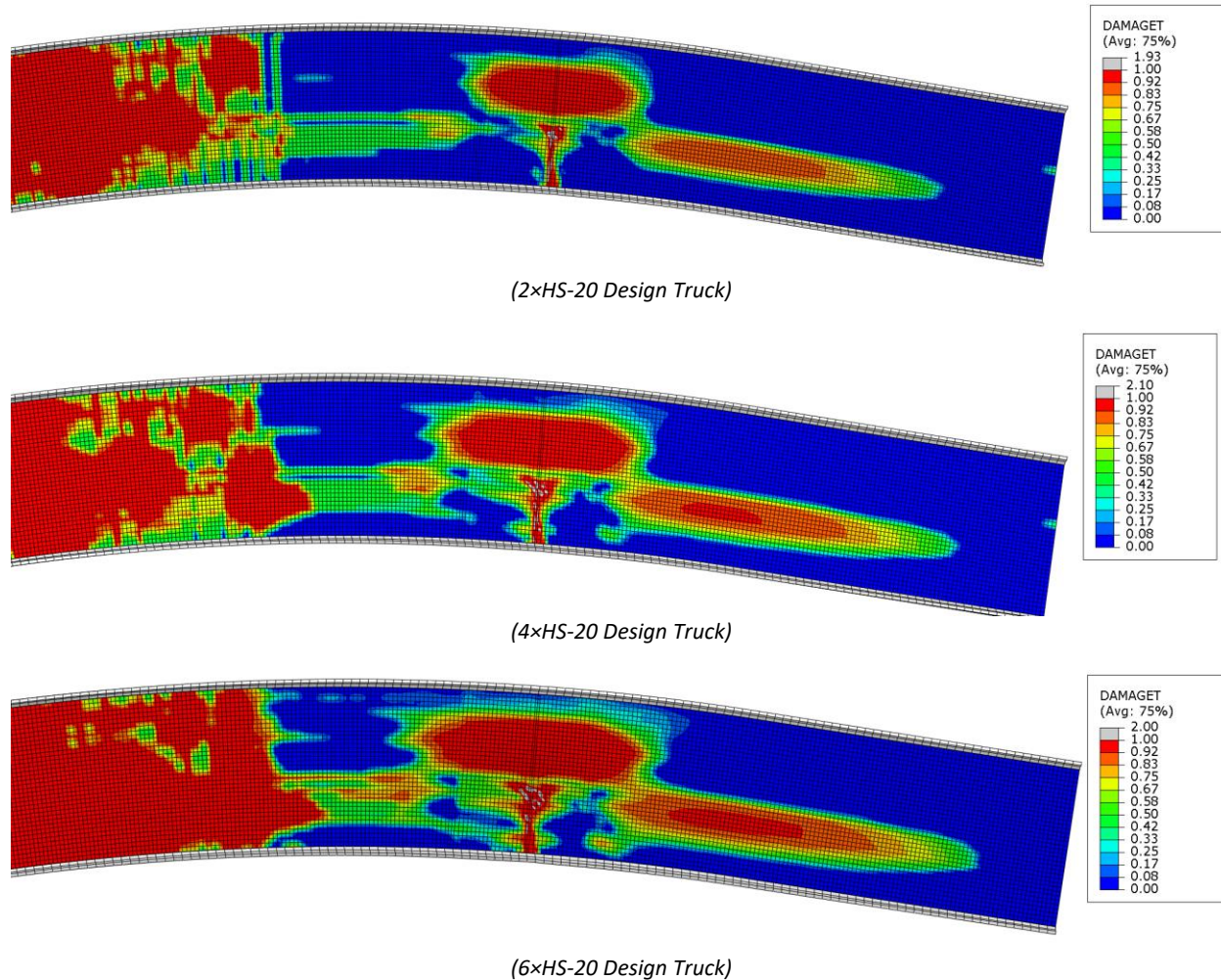
(6×HS-20 Design Truck)

Figure 7-7. The yield line pattern of the deck in the Finite Element Model of the continuous bridge in Span 1.
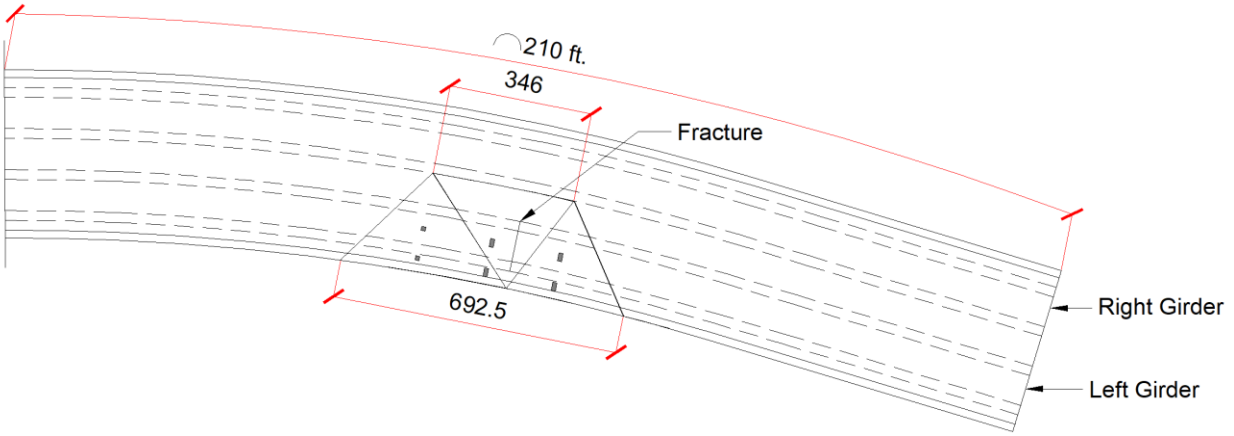
Figure 7-8. The yield line pattern for the continuous span bridge subjected to HS-20 design truck.

Table 7-1. External work calculation of the HS-20 truck load in the continuous span bridge.

	Number of HS-20 Design Truck						**1.9**
	P	X_{point}	Y_{point}	r_{Load}	r	Delta	EW
Front Wheel	7.7	18.7	8.4	6.9	27.3	0.3	2.0
Front Wheel	7.7	18.7	2.4	11.4	30.3	0.4	2.9
Middle Wheel	30.9	4.7	8.4	13.1	22.6	0.6	17.9
Middle Wheel	30.9	4.7	2.4	21.9	27.1	0.8	25.0
Rear Wheel	30.9	-9.3	8.4	7.0	19.5	0.4	11.1
Rear Wheel	30.9	-9.3	2.4	11.1	20.8	0.5	16.5
						EW_{Truck}	75.4
						EW_{DL}	41.1
						EW_{Total}	116.57

Table 7-2. Internal work calculation for the continuous span bridge.

	L	α	m_l	m_t	m_b	Rotation	dIW
Perimeter	28.80	0.00	19.70	16.81	16.81	0.05	24.31
	25.30	0.96	12.99	16.81	14.24	0.04	13.21
	25.00	0.96	12.99	16.81	14.24	0.05	18.65
Diagonals	27.30	0.79	15.05	19.70	17.37	0.04	19.04
	22.10	1.12	15.05	19.70	15.94	0.03	11.68
						$IW_{Railing}$	29.68
						IW_{Total}	116.57

95

7.5   Plastic Moment Capacity

The plastic moment capacity of the bridge for the intact scenario is calculated for the maximum capacity of the bridge. The effective flange width of a concrete deck slab is taken as the tributary width perpendicular to the axis of the member for determining cross-section stiffness for analysis and for determining flexural resistances. The slab effective flange width is taken as one-half the distance to the adjacent girder plus the full overhang width. The cross-section in this bridge varies along the spans based on the demand moments. The plastic moment of one girder at the middle of Span 1 is calculated as 28257 kip. ft. (Figure 7-9). The total flexural capacity of the bridge can be obtained by adding the capacity of two girders.
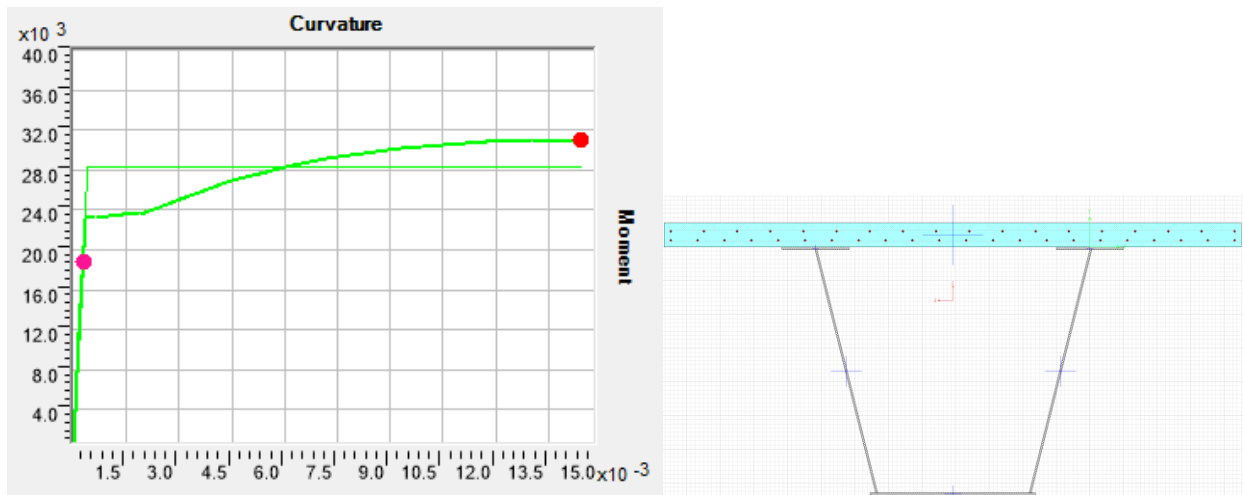
Figure 7-9. Moment curvature curve of one girder at the middle of span 1.

Based on a 3D analysis of the continuous bridge for load condition resulting in the maximum positive moment in the side span, the moment capacity calculated above corresponds to dead load plus 7.2 times HS-20 design truck or 3.1 times HL-93 (Uniform lane load+HS-20 design truck).

7.6   Conclusions

The above analysis results indicate that;
- The finite element modeling developed earlier for the simple span is applicable for the case of continuous bridges.
- The simplified yield line method developed for estimating the load-carrying capacity of the deck for single simply supported bridge spans is not directly applicable to the case of continuous bridges. The yield pattern is most influenced by the continuous end of the span, which brings a significant contribution of the steel girder in the formation and deviation of the external inclined line in the original simple model.
- The yield line pattern and assumptions can be adjusted based on the results of FE analysis to serve the purpose of estimating deck capacity for continuous bridges. This is out of the scope of this work and could be the subject of future work.

- The load-carrying capacity of the intact girder plays a bigger role in the reserve load-carrying capacity of the bridge after the fracture of one girder.
- Distribution of dead and live load between the intact and fractured girder may be far from that assumed for simple span bridges and needs to be determined using the parametric study with the FE model in future work.

Chapter 8 Simplified Reliability Analysis of Fracture-Critical Twin Steel Box Girder Bridge

8.1 Summary

This section presents a simplified reliability analysis of a twin steel box girder bridge superstructure and its deck to estimate the minimum criteria that a deck should satisfy in order to ensure that it can transfer a minimum level of load between the box girders, which one of the girders sustain a severe fracture. The recommendation is made based on meeting a reliability index target, β_{target}=2.5 over a five-year service period. In addition, a list of live load factors is provided for different target reliability levels for the case of a two-year service period.

The calculations are performed assuming that the load-carrying capacity of the deck is modeled using the yield line analysis approach described in Chapter 6, which is similar to the one proposed earlier by the University of Texas. Based on a very limited number of checks, it is observed that the proposed yield line analysis provides a conservative estimate of the deck capacity when compared to the values obtained from nonlinear finite element analysis. However, the level of conservativeness was inconsistent and depended on the truck load configuration. Nevertheless, lacking any additional data, it is herein assumed that the yield line analysis would be applicable for the most heavily loaded trucks that could potentially cross a Florida two-box steel girder bridge that has sustained a severe fracture to one of its box girders.

The yield line analysis process consists of:
- a) Choosing a representative truck configuration. In these analyses, the Florida C5 Semi-Trailer Legal Load (see Figure 6-15(b)) is taken as representative truck because WIM data shows that generally semi-trailers constitute the vast majority of trucks on US highways and the vast majority of overloaded trucks.
- b) Assigning yield lines based on the truck configuration. The yield lines are traced along the edge of the intact box girder that faces the fractured girder for a distance equal to that of the truck centered along a line parallel to that of the truck. Two yield lines then connect the two edges of the first line to the center of gravity of the truck, and another set of two lines flare out from the two edges of the first line along 35° angles towards the damaged box. These five lines enclose three triangular areas within which the truck falls. This yield line pattern was inferred from the nonlinear finite element analysis of the bridge, including the concrete deck, as explained in Chapter 6.
- c) Applying the dead weight with the appropriate dead load factor from the AASHTO LRFD (e.g., γ_{DC}=1.25 for components and γ_{DW}=1.5 for wearing surface. Apply the C5 truck load along with a dynamic amplification IM=1.33 and a live load factor γ_{LL}=2.0 to meet a target reliability β_{target}=2.5 over a 5-year service period.
- d) Verify that the work done by the applied factored loads is less than the work done by the deck after the formation of hinges along the yield lines. The internal work done by the

hinge lines is based on a factored moment capacity of the reinforced concrete deck ϕM_n where $\phi=0.90$ as per the AASHTO LRFD specifications.

Using the models developed in Chapter 6 for the particular bridge and the C5 Class 9 Florida Truck, the deck's safety check takes the form:

$$IW \geq EW \tag{I}$$

with

$$EW = \gamma_{LL} \times IC_{LL} \times IM + \gamma_{DL} \times IC_{deck} \times \omega_{deck} + \gamma_{DL} \times W_{railing} \times IC_{railing} \tag{II}$$

Where $\gamma_{LL}=2.0$, $IC_{LL}=34.35$ kip.ft is the influence coefficient for the C5 nominal truck configuration, IM=1.33 as per AASHTO LRFD, $\gamma_{DL}=1.25$ is the permanent load factor as per the AASHTO LRFD, $IC_{deck}=147.2$ ft^4 is the influence coefficient for the deck, ω_{deck} is the specific weight of reinforced concrete which is usually equal to 0.15 kip/ft^3, $IC_{deck}=147.2$ ft is the influence coefficient for the deck, $W_{railing}$ is the total weight of the railing over the area within the contours of the yield lines and is equal to 20.6, $IC_{railing}=0.5$ is the influence coefficient for the railing.

The internal work done by the concrete deck is equal to

$$IW=IW(\phi M_n) \tag{III}$$

where the resistance factor $\phi=0.90$ is used for consistency with the AASHTO LRFD.

Table I below gives the different live load factors necessary to achieve different reliability levels for the deck of a bridge whose one of its two boxes has fractured. Results for both a five-year rating period and a two-year period are given. As mentioned earlier, to achieve the target reliability, in addition to applying the recommended live load factor, γ_{LL} given in Table I, the yield line analysis implies the application of a dynamic amplification factor IM=1.33, a dead load factor $\gamma_{DL}=1.25$ and a moment resistance factor for the concrete deck equal to $\phi=0.9$.

The analysis of the bridge deck for the 120-ft bridge studied in this report indicates that the bridge deck in its current configuration and concrete strength and ignoring the possible contribution of the railings to help carry some of the load will fail at a live load factor $\gamma_{LL}=1.71$ when the deck's concrete strength is set at f'$_c$=6.23 ksi as determined from the tests. This indicates that its reliability index is on the order of $\beta=2.0$ for a five-year service period, or slightly higher than that for a two-year service period. The live load factors provided in Table I are based on the nominal concrete strength, which is often lower than the actual strength. It is understood that testing the material properties will remove the implicit conservative bias applied during the calibration of the factors in Table I. On the other hand, testing will also reduce the uncertainties in the estimated strength,

and it is often assumed that the reduced uncertainties will offset the removal of the conservative bias implying the final live load factors in Table I are still valid.

Table I. Live load factors for deck analysis necessary to meet different target reliabilities.

Target Reliability index	5-year live load factor, γ_{LL}	2-year live load factor, γ_{LL}
3.50	2.69	2.61
3.00	2.32	2.26
2.50	2.00	1.94
2.25	1.85	1.79
2.00	1.71	1.65
1.50	1.44	1.39
1.00	1.21	1.16

For the bridge to provide sufficient reliability to sustain the possible fracture of one of its two-box girders, it is important that the remaining box girder has sufficient load carrying capacity to withstand the entire live load that may cross the damaged bridge with one fractured box. This can be ensured if the bridge's box girders outside of fracture can satisfy a minimum Rating Factor.

The analysis of fractured bridges is repeated for two scenarios. The first scenario assumes that the fractured bridge will still be able to carry its own dead weight but transfers all the live load to the intact girder. The second scenario assumes that the fractured girder will be able to transfer longitudinally 50% of its own weight away from the critical cross-section due to the action of the deck over the fractured girder and the contribution of the secondary members while the remaining 50% of its weight is transferred laterally to the intact girder's section. Similarly, 34% of the live load traveling in the lane over the fractured girder will transfer longitudinally away from the fractured section while the remaining live load is transferred laterally to the adjacent box girder section. The load transfer mechanism of scenario two was verified through the nonlinear finite element analysis conducted in this study.

Table II gives for the first scenario, the LRFR Inventory Rating Factors required for the box girder members to ensure that the bridge will be able to sustain the fracture of one box girder and yet be able to support sufficient live of loading over a two-year or a 5-year service period until the damage is detected and necessary rehabilitation actions are undertaken. The table shows that an LRFR Inventory Rating on the order of R.F.=1.28 to 1.33 is required to meet a target reliability index $\beta_{target}=2.50$ should one of the two box girders fractures.

Table II. LRFR inventory rating factors for box girders necessary for the fractured bridge to meet different target reliabilities, assuming that all the live load is transferred laterally to the intact girder but none of the dead load.

Target Reliability index, β_{target}	R.F. Inventory Rating for 5-year service life	R.F. Inventory Rating for 2-year service life
3.50	1.73	1.67
3.00	1.52	1.46
2.50	1.33	1.28
2.25	1.24	1.19
2.00	1.16	1.11
1.75	1.07	1.03
1.50	1.00	0.96
1.25	0.92	0.89
1.00	0.85	0.82

Table III gives for the second scenario, the LRFR Inventory Rating Factors required for the box girder members to ensure that the bridge will be able to sustain the fracture of one box girder and yet be able to support sufficient live of loading over a two-year or a 5-year service period until the damage is detected and necessary rehabilitation actions are undertaken. The results shown in Table III require more conservative section strengths because, for these box girder bridges, the dead load is higher than that of a one-lane live load. In this case, an Inventory Rating on the order of R.F.=1.00 is required to meet a target reliability index β_{target} between 1.25 and 1.50.

Table III. LRFR inventory rating factors for box girders necessary for the fractured bridge to meet different target reliabilities assuming that all 50% of the dead load is transferred laterally to the intact girder along with 66% of the live load that was originally carried by the fractured girder.

Target Reliability index, β_{target}	R.F. Inventory Rating for 5-year service life	R.F. Inventory Rating for 2-year service life
3.50	1.74	1.69
3.00	1.55	1.51
2.50	1.38	1.34
2.25	1.30	1.27
2.00	1.23	1.19
1.75	1.15	1.12
1.50	1.08	1.05
1.25	1.01	0.98
1.00	0.95	0.92

The Texas bridge analyzed in this study has an LRFR Inventory Rating R.F.=2.05. Thus, its remaining intact box is capable of sustaining a significant level of the live load as well as a large proportion of the dead load that was original carried over the fractured girder and that the bridge's failure is expected to be due to the failure of the deck as explained earlier. In general, to meet a

target reliability level of β_{target}=2.5, a 120-ft simple span twin steel box girder bridge would need to have a rating factor R.F. on the order of 1.34 to 1.38 to produce a sufficiently high safety level to carry some level of traffic after the fracture of one of its two boxes.

8.2 Assumptions

Several assumptions are made to come up with the recommendation made above. These assumptions need to be supported in future research through a careful review and extensive sensitivity analyses, which are beyond the scope of this particular study. The assumptions made can be summarized as follows:

1. The 120-ft simply supported bridge analyzed in this study is considered to be a typical bridge used in this report to illustrate the process of assessing the after-fracture safety of twin steel box girder bridges and the procedure of calibrating appropriate live load criteria to evaluate their ability to sustain a minimum level of live loading in their damaged state.
2. The Florida WIM truck data used in the modeling of the maximum load effect was truncated at some upper limit. This means that many trucks may produce load effects higher than 1.64 times the effect of one C5 truck, which was used to represent the effects of overloaded trucks that may cross a fractured Florida bridge. Also, the model assumes that the length of the bridge being 120-ft is controlled by one truck in a lane. The loading on longer bridges may be controlled by several trucks following each other in one lane.
3. It is assumed that the C5 truck used for the calculations performed in this report represents the configuration of the heavy critically overloaded trucks crossing over Florida's bridges.
4. It is assumed that the yield line analysis produces similar levels of accuracy as the AASHTO load distribution analysis for girder bridges.
5. It is assumed that the calculation of the deck moment capacity produces similar levels of accuracy as that of the analysis of reinforced concrete beams in bending.
6. Also, it is assumed that after the fracture of one box, the fractured box will still be able to carry some of its own dead weight due to the ability of the deck of closing the gap and transferring some of the live load longitudinally to other sections of the bridges but a significant portion of the dead and live load moments will be transferred laterally and will have to be carried by the remaining intact box.

8.3 Objectives and Approach

The objective of this study is to develop criteria for checking fracture critical two-box steel girder bridges to verify that such fracture-critical bridges provide sufficient levels of safety against collapse should one of the two girders fracture. This section supports the goals of the study in providing a reliability assessment of a typical simply supported two-box steel girder bridge to recommend a set of criteria that will ensure that similar bridges will be able to sustain a potential fracture to one box girder and be able to carry some level of live load in their damaged state. The reliability calculations performed in this section are based on the response of the typical bridge as obtained from a nonlinear finite element analysis and the data provided by the supporting team

102

from Auburn University that studied a set of weigh-in-motion data to project maximum live load effects that the bridge may be subject to over different service periods.

There were several studies conducted in the past by the author and his colleagues to study the redundancy of bridge superstructures and substructures and calibrate methods to assess their capability of carrying some live load after damage to one of their main members [45–47]. Most of these previous studies analyzed bridges assuming complete damage to one entire girder, although the criteria developed in those studies were applied to demonstrate their applicability to the case of the fracture of one girder of a continuous span twin steel box girder bridge [48]. The main focus of these previous studies was on the superstructure, although a sensitivity analysis was performed by Ghosn et al. [46] to analyze the effect of the bridge deck on the load distribution between the intact members of damaged bridges. This current study took a systematic approach to study the nonlinear behavior of the box girder as well as the deck and the possible failure of the deck after the fracture of one box of a 120-ft simple span twin steel box girder bridge. The current analysis, however, does not consider the release of energy associated with the fracture process. A preliminary analysis of the dynamic effects associated with the fracture phenomenon itself was studied by Miao & Ghosn [49]. The extension of the work of Miao & Ghosn [49], however, was outside the scope of this study.

Specifically, the analysis performed during the course of this study focused on analyzing the after fracture load-carrying capacity of a typical two-box steel girder bridge configuration having a simply supported 120-ft span. The bridge has the same configuration as the one tested by the University of Texas at Austin [19, 23]. A detailed finite element analysis of the bridge confirmed the results of the Texas University Study that showed that, after the complete fracture at the mid-span of one girder, this particular bridge exhibited deck failure at high load before the failure of the other originally intact box girder. Thus, this study proposed a simplified approach that engineers could implement in routine engineering practice to verify that the deck will be able to transfer the load from the fractured box girder to the intact girder. The proposed method is based on yield line analysis principles and is consistent with the one proposed in the Texas University study [19, 23]. Because the proposed method is approximate and because it involves parameters whose values are highly uncertain, it is important to associate the proposed method with appropriate safety factors to reduce the probability of failure of the particular bridge being analyzed and, by extension, other fracture-critical bridges with similar configurations.

The objective of this section was to execute a reliability analysis of the fracture-critical box girder bridge analyzed in Chapter 6 and use the reliability results to calibrate appropriate safety factors that can be applied in conjunction with the proposed analysis method. To achieve the objective, this section is divided into the following four subsections:

1. Overview of Reliability Analysis Methodology, which provides a summary of the principles of structural reliability analysis and their application for the calibration of codified safety checking procedures.

2. Live Load Modeling: After giving a quick overview of load modeling principles, this section presents the results of the analysis of the weigh-in-motion data performed by the University of Auburn team as part of this study.

3. Permanent Load Model: The statistical data used to represent the effect of the permanent loads are provided in this section. These data are consistent with the data used by Nowak [26] during the calibration of the AASHTO LRFD Specifications.

4. Load Carrying Capacity Model: In this section, the probabilistic models used for evaluating bridge member capacity, including the analysis of the deck, are presented. These models are consistent with those previously used by Nowak [26] during the calibration of the AASHTO LRFD Specifications.

5. Reliability Analysis of Example Fracture-Critical Box Girder Bridge: The results of the analysis of the bridge configuration are implemented in a simplified reliability analysis procedure to extract the reliability index for the bridge members and its deck and assess its ability to safely transfer the load from the fractured girder to the intact girder. In this section also, the results of the reliability analysis performed in Section 8.5 are used to propose a set of safety factors that can be used by bridge engineers to assess the ability of a twin steel box girder bridge to carry a sufficient level of traffic load for a limited period of service time until a potential fracture is detected and necessary actions undertaken by the authorities.

8.4   Overview of Reliability Analysis Methodology

The aim of structural reliability theory is to account for the uncertainties encountered while evaluating the safety of structural systems or during the calibration of load and resistance factors for structural design and evaluation codes. To account for the uncertainties associated with predicting the load-carrying capacity of a structure, the intensities of the loads expected to be applied, and the effects of these loads on the structural components and entire system, as well as the capacity of structural members and systems to carry these loads, may be represented by random variables.

The value that a random variable can take is described by a probability distribution function. That is, a random variable may take a specific value with a certain probability, and the ensemble of these values and their probabilities are described by the distribution function. In many cases, the most important statistical characteristics of a random variable are its mean value or average and the standard deviation that gives a measure of dispersion or a measure of the uncertainty in

estimating the variable. For example, assuming that R represents the resistance capacity of a structural member or system, the standard deviation of the random variable R, which may have a mean value equal to $\bar{R}$ is represented by σ_R. A dimensionless measure of the uncertainty is the coefficient of variation (COV), which is the ratio of the standard deviation divided by the mean value. For example, the COV of the random variable R is represented by V_R such that:

$$V_R = \frac{\sigma_R}{\bar{R}} \tag{12}$$

Structural design codes and standards often specify nominal or characteristic values for the variables used in design equations. These nominal values are related to the means through bias values. The bias is defined as the ratio of the mean to the nominal value used during the design or evaluation process. For example, if R is the structural member capacity (or resistance), the mean of R, namely, $\bar{R}$ can be related to the nominal or design value, R_n, using a bias factor such that:

$$\bar{R} = b_r R_n \tag{13}$$

where: b_r is the resistance bias, and R_n is the nominal value as specified by the design code. For example, A50 steel has a nominal design yield stress of 50 ksi, but coupon tests show an actual average value close to 56 ksi. Hence, the bias of the yield stress is 56/50 or 1.12.

In structural analysis, safety may be described as the situation where capacity (member strength or resistance) exceeds demand (applied load, moment, or stress). In structural engineering, the probability that a certain limit state criterion is not met is usually referred to as the probability of failure, P_f, which is usually defined as the probability that the capacity is less than applied load effects. There are various simulation and iterative methods that can be used to formally calculate P_f. However, the accuracy of the numerical value depends upon detailed data on the probability distributions of load and resistance variables. Because such data are often not available, approximate models are usually used for calculation.

The reserve margin of safety of a bridge component or system, also known as failure function or limit state equation, can be defined as Z, such that:

$$Z = R - S \tag{14}$$

where R is the structural resistance or capacity, S is the total load effect. Probability of failure, P_f, is the probability that the resistance R is less than or equal to the total applied load effect S or the probability that Z is less or equal to zero. This is symbolized by the equation:

$$P_f = Pr\,[\,R \leq S\,] \tag{15}$$

where Pr is used to symbolize the term probability. If R and S follow independent normal (Gaussian) distributions, then the probability of failure can be obtained based on the mean of Z and its standard deviation, which can be calculated from the mean of R and S and their standard deviations. If these are independent Gaussian or normal random variable, the probability of failure is obtained from:

$$P_f = \Phi\left(\frac{0-\bar{Z}}{\sigma_Z}\right) = \Phi\left(-\frac{\bar{R}-\bar{S}}{\sqrt{\sigma_R^2+\sigma_S^2}}\right) \tag{16}$$

where $\Phi(...)$ is the normal cumulative probability function that gives the probability that the normalized random variable is below a given value. $\bar{Z}$ is the mean safety margin, and σ_Z is the standard deviation of the safety margin. Thus, Equation (16) gives the probability that Z is less than 0.0 (or R is less than S).

To avoid the need to work with very small values of the probability of failure, structural engineers prefer to use the reliability index, β, as a measure of structural safety. The reliability index is related to the probability of failure:

$$P_f = \Phi(-\beta) \tag{17}$$

For example, if the reliability index is $\beta=3.5$, then the implied probability of failure is obtained from the normal probability distribution tables given in most books on statistics as $P_f=2.326\times10^{-4}$. A reliability index $\beta=2.5$ leads to $P_f=6.21\times10^{-3}$. A $\beta=2.0$ implies that $P_f=2.23\times10^{-2}$.

Because it is often difficult to ascertain the type of probability distribution that each variable follows and because it is difficult to collect real data on structural failures, calculated values of probability of failure are often considered to be notional measures of likelihood of failure that are used to compare different structural design options and compare various load capacity evaluation methodologies rather than being considered as actuarial values.

For the independent normal distribution case, the reliability index is obtained from:

$$\beta = \frac{\bar{Z}}{\sigma_Z} = \frac{\bar{R}-\bar{S}}{\sqrt{\sigma_R^2+\sigma_S^2}} \tag{18}$$

Thus, the reliability index, β, which is commonly used as a measure of structural safety, gives in this instance the number of standard deviations that the mean margin of safety falls on the safe side as represented in Figure 8-1.
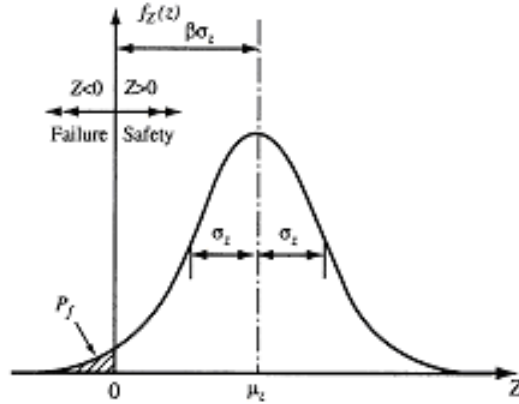
Figure 8-1. Graphical Representation of Reliability Index, β.

The reliability index, β, defined in Equations (17) and (18) provides an exact evaluation of the probability of failure if R and S follow normal distributions. Although β was originally developed for normal distributions, similar calculations can be made if R and S are lognormally distributed (i.e., when the logarithms of the basic variables follow normal distributions). In this case, the reliability index can be calculated as:

$$\beta = \frac{\ln\left(\dfrac{\overline{R}}{\overline{S}}\dfrac{\sqrt{1+V_S^2}}{\sqrt{1+V_R^2}}\right)}{\sqrt{\ln\left[\left(1+V_R^2\right)\left(1+V_S^2\right)\right]}} \tag{19}$$

Which, for small values of V_R and V_S on the order of 20% or less can be approximated as:

$$\beta = \frac{\ln\left(\dfrac{\overline{R}}{\overline{S}}\right)}{\sqrt{V_R^2 + V_S^2}} \tag{20}$$

when R and S are functions of several underlying random variables or when the safety margin equation is not linear, the evaluation of the reliability index β becomes more complicated. In such cases, one can resort to using simulation techniques or "Level II methods". "Level II" methods have also been used to obtain the reliability index for the cases when the basic variables are neither normal nor lognormal. These methods, often referred to as FORM (First Order Reliability Methods) or FOSM (First Order Second Moment), involve an iterative calculation to obtain an estimate to the reliability index and the probability of failure. This is accomplished by approximating the failure equation (i.e., when $Z=0$) by a tangent multi-dimensional plane at the point on the failure surface closest to the mean value. For example, during the calibration of the AASHTO LRFD code, Nowak [26] used the FORM algorithm to calculate the reliability index values when the resistance R is assumed to follow a lognormal distribution and the load S is a normal random variable. More advanced techniques, including SORM (Second Order Methods), have also been developed. In recent years with the advancement in computer capacities, the

implementation of Monte Carlo Simulations, including various variance reduction techniques has become increasingly practical.

The approximate nature of Equation (20) notwithstanding, several previous studies have shown that Equation (20) is sufficiently accurate to produce reliability index values very close to those obtained using FORM algorithms and Monte Carlo Simulations when analyzing the reliability of short to medium span bridges [50].

As observed from this short introduction, evaluating the reliability of bridges requires probabilistic models for all the random variables that control the safety of bridge structures. These can be assembled into three groups: Live loads, Permanent Loads, and Member Resistance.

8.5   Live Load Reliability Model

The factored nominal live load models used in the design and load capacity evaluation of bridges take the form of deterministic simplified formats that do not explicitly include all the parameters that control the effects of live loading on the bridge nor do the models explicitly reflect the random nature of the live load. A more realistic representation of live load effects on bridge members would take the form (see, for example, Ghosn, Sivakumar and Miao [50]; and Sivakumar et al. [51]):

$$LL_T = L_{max} \times L_{HS20} \times IM_{fact} \times \lambda_{max} \times \lambda_{site-to-site} \times \lambda_{data} \tag{21}$$

Where LL_T = total live load effect on the bridge member or on the bridge system, L_{max}= maximum projected load due to the random trucks on the bridge presented in the function of the number of HS-20 equivalent trucks, L_{HS-20} is the load effect of the HS-20 truck used as the base line for analysis, IM_{fac}= dynamic amplification factor of the total load effect, λ_{Lmax} is a variable that reflects the uncertainties in estimating the maximum load effect calculated using the live load projection methodology performed by the team from Auburn University participating in this study and described in Section 4.1, $\lambda_{site-to-site}$ is a variable representing the variation in the projected live load between data collected at different WIM sites, λ_{data} is a variable representing the effect of limitations in the approach taken to perform the live load simulation and the extreme value projection technique utilized.

The live load model presented in Equation (21) can be used to perform reliability calculations of bridge members or systems. Statistical data related to the random variables of Equation (21) are obtained from three sources: a) the analysis of large numbers of WIM data sets assembled from various parts of the state of Florida, which was performed by the Auburn University team and described in Section 4.1, b) the data used in NCHRP 368 during the calibration of the AASHTO LRFD as described in NCHRP 368 by Nowak [26], c)) The analysis of large numbers of WIM

data sets assembled from various parts of the US as described by Sivakumar & Ghosn [52] in the web-based report NCHRP 20-07 Task 285.

8.5.1   Maximum Load Effects

The analyses performed by Azizinamini and his research team in previous studies [22] have shown that the failure of fractured box girder bridges is dominated by loading in the lane closest to the fractured box when the deck slab reaches its limiting capacity, which restricts its ability to transfer the load to the other intact box girder. Therefore, the load simulations performed by the team from Auburn University as described in Section 4.1 provided projections for the expected maximum load effect in a single lane obtained based on projections of truck traffic data collected at a number of Florida weigh-in-motion (WIM) sites. The simulations have shown that, generally speaking, the maximum moment on the 120-ft simply supported bridge approaches a normal distribution with a ratio between the simulated maximum moment as compared to the effect of the AASHTO HS-20 design truck that varies between 1.50 to 1.75 depending on the site and the projection period. These results are summarized in Table 4-3 for the 120-ft simple span bridge. The simulations show that if one lane of traffic on a 120-ft bridge show an Average Daily Truck Traffic ADTT=1250 (thus a total ADTT=2500), the heaviest trucks on the bridge will produce an expected maximum two-year load effect equivalent to the effect of 1.66 times that of the AASHTO HS-20 truck. A five-year projection of the loads on a bridge whose ADTT=2000 will lead to a maximum moment effect equal to 1.76 times that of the HS-20 design truck.

The AASHTO Manual of Bridge Evaluation [5] was calibrated using projections assuming a rating period equal to 5 years. Thus, for the purposes of this study, the variable L_{max} in Equation (21) will take the value of 1.76. The variability in this estimated load effect is on the average equal to 9%. Thus, λ_{Lmax} in Equation (21) is assumed to be a random variable with an average value equal to 1.0 and a COV=8%.

8.5.2   Variability in Results of Simulations

In addition to the expected maximum load effect from the simulation, the reliability analysis requires the consideration of the uncertainties in the maximum load estimate. These uncertainties are represented by the variables λ_{data}, and $\lambda_{site\text{-}to\text{-}site}$. Previous sensitivity analyses such as those performed in NCHRP 368 have indicated that λ_{data} can approximately have a COV on the order of 2% to 5%. These variabilities, for example, represent the differences obtained when comparing the results from different years. A value of 5% is adopted in this study. Finally, the variability in the results between sites having the same ADTT but accounting for different truck weight histograms is represented by $\lambda_{site\text{-}to\text{-}site}$, which in NCHRP Report 20-07 Task 285 have shown variations in COV with a conservative estimate on the order of 20%, which is the value adopted in this study [52].

8.5.3 *Variability in Dynamic Amplification Factors*

The AASHTO LRFD specifies that a nominal dynamic amplification IM=1.33 be used on the truck load effect to account for the increased stresses due to the vibrations of the bridge under moving loads. However, it has been well established that this value is a conservative upper bound. On the average, Nowak [26] indicates that heavily loaded trucks usually produce lower values than the nominal value with a mean value $IM_{fact} = 1.13$ and a COV of V_{IM}=9% for individual truck crossings. For simultaneous crossings in multi-lanes, the average is IM_{fact}=1.09, and the COV is V_{IM}=5.5%.

8.6 Permanent Load Model

Following the approach adopted by Nowak [26], the total permanent load effect, DL is divided into the dead load of pre-fabricated members, DC_1, the dead load of cast-in-place members, DC_2, and the dead load of the wearing surface, DW, such that the mean total dead load is given by:

$$\overline{DL} = \overline{DC}_1 + \overline{DC}_2 + \overline{DW}$$

(22)

The standard deviation of the total dead load, σ_{DL}, is expressed as a function of the standard deviations of each dead load component:

$$\sigma_{DL} = \sqrt{\sigma_{DC_1}^2 + \sigma_{DC_1}^2 + \sigma_{DW}^2}$$

(23)

Following Nowak [26], the dead load effects are assumed to follow Normal probability distributions where the mean values and the COV's of each dead load component are given as:

$$\overline{DC}_1 = 1.03DC_1 \qquad V_{DC_1} = 8\%$$
$$\overline{DC}_2 = 1.05DC_2 \qquad V_{DC_2} = 10\%$$
$$\overline{DW} = DW \qquad V_{DW} = 25\%$$

(24)

Where DC_1, DC_2, and DW are respectively the nominal values of the dead load of pre-fabricated members, cast-in-place *members*, and wearing surface.

The example bridge analyzed in this study has a cast-in-place concrete slab and composite steel box girders where the steel is pre-manufactured, and the concrete is cast in place. Because the weight of the concrete dominates, a bias equal to 1.05 and a COV=10% are used for the effects of all permanent loads.

8.7 Load Carrying Capacity Model

The traditional methods used to calculate the moment and shear capacities of bridge members have been found to lead to conservative estimates of the actual capacities. The data used by Nowak [26] to account for the biases and the variability in the existing current member analysis methods assuming that the member capacities follow lognormal distributions are summarized as follows:

Bending capacity of composite steel beams; $\bar{R} = 1.12 R_n$ $V_R = 10\%$

Bending of prestressed concrete beams; $\bar{R} = 1.05 R_n$ $V_R = 7.5\%$

Bending of reinforced concrete beams; $\bar{R} = 1.14 R_n$ $V_R = 13\%$

(25)

Shear capacity of composite steel beams; $\bar{R} = 1.14 R_n$ $V_R = 10.5\%$

Shear capacity of prestressed concrete beams; $\bar{R} = 1.15 R_n$ $V_R = 14\%$

Shear capacity of reinforced concrete beams; $\bar{R} = 1.20 R_n$ $V_R = 15.5\%$

Of particular interest to this study are the bending capacity of the composite steel box girders and that of the reinforced concrete deck.

The statistical parameters in Equation (25) are for structural member capacities in bending or in shear. There is very little data that provide probabilistic models for the variability and biases between actual bridge system capacities and those estimated using advanced finite element analyses. For the purposes of this study, we will assume that the biases and COV's listed for composite steel members and also valid for steel box girder bridges. Therefore, a bias equal to 1.12 and COV equal to 10% are adopted for the box girders to illustrate the proposed reliability analysis methodology assuming that the mode of failure is related to exceeding the bending capacity of composite members. For the analysis of the failure of the concrete slab in bending, then a bias equal to 1.14 and a COV=13% are adopted.

8.8 Reliability Analysis of 120-ft Twin Steel Box Girder Bridge

8.8.1 Analysis of Nominal Member Strength

The configuration of the steel boxes of the bridge analyzed during the course of this study indicated that each box girder has a nominal moment capacity R_n=19,026.8 kip-ft based on coupon tests of the deck that showed a concrete strength f'_c=6 ksi. Typical design of bridges assumes concrete deck to made of concrete with f'_c=4 ksi or even f'_c=3 ksi is often assumed). If the concrete deck was assumed to have a strength f'_c=4 ksi each box girder would have produced a nominal moment capacity R_n= 17,972.2 kip-ft. The ratio between these two nominal moment capacity values, which is on the order of 6%, is accounted through the bias factor between nominal strength and the mean strength, as explained above.

Even though some other than strength criteria may have dominated the design, such as service limit states or deflection limits, the bridge as-built is clearly overdesigned for the strength limit state, which is of most interest when structural safety is concerned.

The first step of this section is to determine the level of overdesign of main box girders of the bridge and compare the reliability of the box girder members as built to the reliability if they were to be designed to exactly meet the AASHTO Specifications' strength limit state criteria.

According to the AASHTO specifications, the nominal resistance, R_n, of a box girder should meet the criterion set in the following equation:

$$R_n \geq 1.25DC_n + 1.75LL_n \tag{26}$$

where the nominal live load, LL_n, is calculated based on the moment effect of the HS-20 truck, which for this 120-ft span bridge is found to be $L_{HS20} = 1883.8 \, kip.ft$ times the dynamic allowance $IM=1.33$ plus the effect of a lane load $\omega_{lane}= 0.64$ kip/ft, which produces a lane load moment $L_{lane} = 1152 \, kip.ft$. The total live load is multiplied by the lane distribution factor, $D.F.$, so that:

$$LL_n = (L_{HS20} \times IM + L_{lane}) \times D.F. \tag{27}$$

For box girder bridges, $D.F.$ is calculated based on the number of loaded lanes, N_L, and the number of box girders, N_b, using the equation:

$$D.F. = 0.05 + 0.85\frac{N_L}{N_b} + \frac{0.425}{N_L} \tag{28}$$

Which, for two beams carrying two lanes of traffic, produces a lane distribution factor $D.F. = 1.113$.

The final nominal live load is found to be $LL_n = 4071 \, kip.ft$ which when combined with a dead load moment $DC_n = 3650 \, kip.ft$ and implemented in Equation (26) produces a nominal moment capacity $R_n = 11,686 \, kip.ft$. If a wearing surface $DW_n= 553 \, kip.ft$ is added with a load factor equal to 1.5, the strength limit state design would have led to a required nominal resistance $R_n = 12,515 \, kip.ft$. Thus, the calculated moment capacity of the particular bridge analyzed in this study is based on the actual concrete strength f'c=6.23 ksi, which is R_n=19,026.8 kip-ft is 1.53 to1.63 times the value that is required by the Strength limit state of the AASHTO specifications. In the rest of the calculations performed in this report, the weight of the wearing surface is omitted because the finite element analysis performed in this study did not include the weight of the wearing surface.

8.8.2 Box Girder Member Strength Reliability Analysis

Several cases are considered in the reliability analysis performed in this section. Each section also includes a number of sensitivity analyses to study the effect of various factors on the reliability results.

8.8.2.1 *One-Lane Loading on the intact bridge when box girder is designed to exactly meet AASHTO's strength limit state*

The AASHTO Specifications were developed such that the reliability levels of individual members would meet a target member reliability index β=3.5 for a 75-year design life, assuming typical Average Daily Truck Traffic ADTT=2000 trucks per day. In this example, we illustrate the application of Equation (20) in combination with Equation (21) for the reliability analysis of one composite box girder of the 120-ft simple span bridge. In this section, we analyze the reliability of a box girder to verify whether the reliability index of a box girder member designed to strictly satisfy the AASHTO strength limit state will meet the target reliability index.

When studying the loads on the bridge system, the maximum live load is obtained using the live load modeling procedure performed by the Auburn University team, as outlined in Section 4.1. The maximum live loads for different projections are shown in Table 4-3 in terms of HS-20 equivalents. For one-lane loading on the 120-ft simple span bridge, the expected maximum moment will be equivalent to 1.74 HS-20 trucks for a 5-year service period assuming an ADTT=2000 trucks per day, which is equivalent to an ADTT=10,000 as set in Table 4-3. The calculations also show that the expected maximum live load will be associated with a COV for λ_{Lmax}=9%. A variation in the estimate with a COV λ_{data}=5% is also used as recommended by Sivakumar et al. [51] to reflect variations in the expected maximum load associated with the load projection method and the number of data points used to perform the projection. Also, based on previous work by Sivakumar et al. [51], who studied a large number of WIM data sites, it is estimated that the variations due to changes in the WIM data can be associated with $\lambda_{site\text{-}to\text{-}site}$ on the order of 20%. Furthermore, the dynamic load allowance has an average value $\overline{IM}_{fact}$=1.13 and a COV of V_{IM}=9% for individual truck crossings based on Nowak [26].

In the simplified calculations performed in this report, we assume a lognormal model for the resistance, *R*, as well as a lognormal model for the combined effects of all the applied loads represented by the variable, *S* in Equation (20). As mentioned above, previous calculations have shown that the lognormal model produces results similar to those obtained using more advanced models such as FORM or Monte Carlo Simulations for the type of analyses performed for the reliability assessment of bridges (Ghosn, Sivakumar and Miao, [50]).

In this analysis, we also assume that each box girder was designed without the consideration of a future wearing surface because the FEM analysis performed in this study did not consider the weight of the wearing surface. The input data are summarized as follows:

Nominal Resistance: $\qquad$ R_n=11,686 kip.ft

Mean resistance assuming bending failure: $\bar{R} = b_R R_n = 1.12 \times 11,686 = 13,088 \ kip.ft$

COV of bending resistance: $\qquad$ $V_R = 10\%$

Mean of total live load L_{max} in lane 1 $\qquad$ $L_{max} = 1.74 \times L_{HS20} = 1.74 \times 1883.8 = 3278 \ kip.ft$

COV of L_{max}: $\qquad$ V_{Lmax}=9%

COV site-to-site: $\qquad$ $V_{site-to-site} = 20\%$

COV data limitation: $\qquad$ $V_{data} = 5\%$

Mean Dynamic Amplification: $\qquad$ IM_{fact}=1.13

COV Dynamic Amplification: $\qquad$ V_{IM}=9%

Mean of Random Total Live Load Effect on the bridge due to one lane loading:

$$\overline{LL_T} = L_{max} \times L_{HS20} \times IM_{fact} \times \lambda_{max} \times \lambda_{site-to-site} \times \lambda_{data} =$$

$$\overline{LL_T} = 1.74 \times 1883.8 \times 1.13 \times 1 \times 1 \times 1 \quad = 3704 \ kip.ft$$

COV of Applied Random Live Load:

$$V_{LT} = \sqrt{V_{Lmax}^2 + V_{site-to-site}^2 + V_{data}^2 + V_{IM}^2} = \sqrt{9\%^2 + 20\%^2 + 5\%^2 + 9\%^2} = 24\%$$

The AASHTO specifications were developed for a base line of two-lane loadings, and the distribution factor *D.F.* for one lane as specified by AASHTO, which is used in combination with the nominal live load implicitly includes a multiple presence factor *mp*=1.2 to account for the probability that two-lane loadings are on the average lower than two times the loading of one lane. Therefore, when the live load on the bridge is obtained from actual projections of truck data rather than from the nominal design loads, the multiple presence factor must be removed. This is very clear in this situation, where one girder could not possibly carry more than the load of one truck when only a single lane of the bridge is loaded. Therefore, an estimate of the mean of the distribution factor for the box girder bridge loaded by a single lane is obtained as $\overline{D.F.} = \frac{1.113}{1.2} = 0.928$. Ghosn and Moses [53] associated the D.F. with a COV=8% to account for variabilities in measured distribution factors due to different truck configurations and variations in their lateral position within a lane.

Based on the above, the applied live load moment on one box girder is estimated to have a mean value:

$$\overline{LL} = \overline{LL_T} \times \overline{D.F.} = 3704 \times 0.928 = 3437 \ kip.ft$$

The COV for the live load on a girder is obtained from:

$$V_{LL} = \sqrt{V_{LT}^2 + V_{DF}^2} = \sqrt{24\%^2 + 8\%^2} = 25\%$$

The nominal dead load for the bridge member excluding the weight of a future wearing surface is obtained as $DC_n = 3650 \ kip.ft$ with a bias equal to 1.05 and a COV=10%. Hence a mean dead load effect is calculated:

$$\overline{DL} = DC_n \times 1.05 = 3833 \ kip.ft$$

The COV for the live load on a girder is obtained from:

$$V_{DL} = 10\%$$

The total load, including live and dead load its COV, are thus obtained as:

$$\bar{S} = \overline{LL_\square} + \overline{DL} = 3437 + 3833 = 7270 \ kip.ft$$

$$V_S = \frac{\sqrt{(V_{LL} \times \overline{LL})^2 + (V_{DL} \times \overline{DL})^2}}{\bar{S}} = 13\%$$

The reliability index for a box girder member designed to satisfy the AASHTO nominal resistance criteria using Lognormal Model assuming bending failure:

$$\beta = \frac{ln\left(\frac{\bar{R}}{\bar{S}}\right)}{\sqrt{V_R^2 + V_S^2}} = \frac{ln\left(\frac{13088}{7270}\right)}{\sqrt{10\%^2 + 13\%^2}} = 3.59$$

This value is based on the maximum 5-year one-lane loading and not that of the 75-year loading over the entire design life, and it assumes a distribution factor D.F.=0.928.

On the other hand, the finite element analysis performed in this study has shown that, under the effect of one truck, the supports of the loaded girder in the intact configuration carried 85% of the load rather than the assumed 92.8% extracted from the AASHTO tables. In this case, if one assumes that the moment in the girder is proportional to the reaction at the supports and a distribution factor D.F.=0.85 is used, the reliability index would have been equal to 3.88. Subsequent analyses of the moments at the critical cross-section as performed in Section 6.4 show that the moment carried by the critical section is 60% of the total moment, which would produce

a reliability index as high as β=5.11. It is noted that the 60% distribution factor is significantly lower than calculated from the AASHTO LRFD tables for box girder bridges.

The above calculations were based on the maximum 5-year live load, which is appropriate for the operating rating period. For the design of new bridges, the AASHTO LRFD was calibrated for the maximum 75-year live load.   Therefore, the data in Table 4-3 needs to be projected for a longer service period. Given that the maximum load usually follows a Gumbel Type I extreme value distribution as demonstrated by Sivakumar, Ghosn et al. [51], estimating the maximum 75-year live load can be done based on the maximum 5-year load. According to Thoft-Cristensen and Baker [54], the maximum 75-year live load effect, L_{max-75} can be obtained for the 5-year maximum L_{max}=1.74 L_{HS-20} using the relationship:

$$L_{max-75} = L_{max} + \frac{\sqrt{6}}{\pi} \times L_{max} \times V_{Lmax} \times ln\left(\frac{75yrs}{5yrs}\right) \tag{29}$$

$$L_{max-75} = 1.74L_{HS20} + \frac{\sqrt{6}}{\pi} \times 1.74L_{HS20} \times 9\% \times ln\left(\frac{75yrs}{5yrs}\right) = L_{max-75} = 2.07L_{HS20}$$

It is interesting to observe that the calculated $L_{max-75} = 2.07L_{HS20}$ for one lane loading is very close to the value $L_{max-75} = 2.08 \ L_{HS20}$ obtained by Nowak [26] during the calibration of the AASHTO LRFD specifications.

This gives a mean 75-year live load after accounting for the distribution factor and the dynamic amplification:

$$\overline{LL} = 3437 \ kip.ft \times \frac{2.07}{1.74} = 4091 \ kip.ft$$

$$\bar{S} = \overline{LL} + \overline{DL} = 4091 + 3833 = 7924 \ kip.ft$$

And a COV

$$V_s = \frac{\sqrt{(V_{LL} \times \overline{LL})^2 + (V_{DL} \times \overline{DL})^2}}{\bar{S}} = 14\%$$

This leads to a reliability index:

$$\beta = \frac{ln\left(\frac{\bar{R}}{\bar{S}}\right)}{\sqrt{V_R^2 + V_S^2}} = \frac{ln\left(\frac{13088}{7924}\right)}{\sqrt{10\%^2 + 14\%^2}} = 2.92$$

Assuming that the distribution factor is equal to D.F.=0.928 as given in the AASHTO specifications, the calculated reliability index β=2.92, is on the low side compared to the target set in the AASHTO specification for a 75-year design life β_{target}=3.50. On the other hand, using a

distribution factor DF=0.85, which is observed from the distribution of the loads to the supports of the box girder bridge, the reliability index for the box girder under the effect of a single lane of loading is β=3.24, which is closer to the target reliability. When using a distribution factor equal to D.F.=0.60, which is extracted from the moment of the stresses at the critical cross-section of the bridge in its intact configuration, the reliability index becomes as high as β=4.51.

It is noted that the reliability calibration β_{target}=3.50 as executed for the AASHTO specifications considered only I-girder bridges, and the differences in the reliability index values calculated in this report from the target are due to the differences in the load distribution factors between the members of box girder bridges when compared to those for I-girder bridges and for the different dead load to live load ratios for the members of box girder bridges than for the members of I-girder bridges.   It is noted that the distribution factors calculated from the finite element analysis are significantly different than those in the AASHTO LRFD tables.

8.8.2.2   *Two-Lane Loading on Intact Bridge When Box Girder is Designed to Exactly Meet AASHTO's Strength Limit State*

The WIM data from Florida was not analyzed for multiple lane loading. Therefore, in this analysis, we will assume that the observations regarding the relation between one lane and two-lane loadings during the calibration of the AASHTO specifications are valid. Nowak [26] found that when two lanes of the bridge are loaded, each lane will carry 0.85 of the maximum expected loaded projected for a single lane loading. The 0.85 factor accounts for the lower probability of having two very heavy trucks side-by-side on the bridge as compared to having a single heavy truck. Also, Nowak [26] uses a mean dynamic allowance for two-lane loading equal to 1.09 with a COV=5.5% rather than the mean of 1.13 and COV=9% used for one lane. The lower mean dynamic amplification for two lanes is due to the lower probability that trucks moving simultaneously in multiple lanes will have their maximum dynamic components occur at the same instant of time. Hence, the expected 75-year live load in one lane of a bridge under the effect of multi-lane loading is estimated as:

Moment on a girder due to two-lane:

$$\overline{LL}_T = L_{max} \times L_{HS20} \times IM_{fact} \times \lambda_{max} \times \lambda_{site-to-site} \times \lambda_{data} = 0.85 \times 2.07 \times 1883.8 \times 1.09 \times 1 \times 1 \times 1 \quad = 3613 \; kip.ft$$

The distribution factor for the bridge with two lanes loaded is assumed to be equal to the one specified by AASHTO, *D.F.*=1.13. A *D.F.* value slightly greater than 1.0 assumes that the two trucks on the bridge may be slightly shifted laterally to favor one of the two girders.

$$\overline{LL} = \overline{LL}_T \times \overline{D.F.} = 3613 \times 1.113 = 4021 \; kip.ft$$

Thus, the expected 75-year live load moment on one box girder of this bridge due to two-lane loading obtained as 4021 *kip.ft* is slightly lower than the mean 4096 *kip.ft* obtained earlier for one lane loading when we assume the AASHTO distribution factor equal to 0.928 for the single lane loading and a distribution factor equal to D.F.=1.113 when two lanes are loaded as implied in the AASHTO LRFD. The lower load is due to the lower probability of having two very heavily loaded trucks simultaneously on the bridge as compared to having a single heavy truck.

The finite element analysis performed in this study did not consider two-lane loading of the bridge, but we compare the above expected to the results of the FEM one-lane loading, which observed a distribution factor equal to 0.60, then the mean load for one lane loading 2648 *kip.ft* is significantly lower than the moment carried by one girder under the effect of two-lane loading as calculated above.

The total applied load on one beam is:

$$\bar{S} = \overline{LL} + \overline{DL} = 4021 + 3833 = 7854 \; kip.ft$$

And a COV

$$V_S = \frac{\sqrt{(V_{LL} \times \overline{LL})^2 + (V_{DL} \times \overline{DL})^2}}{\bar{S}} = 14\%$$

This leads to a reliability index:

$$\beta = \frac{ln\left(\frac{\bar{R}}{\bar{S}}\right)}{\sqrt{V_R^2 + V_S^2}} = \frac{ln\left(\frac{13088}{7854}\right)}{\sqrt{10\%^2 + 14\%^2}} = 2.97$$

The reliability index for the most critical box girder in a 75-year service period is slightly higher than β=2.92 calculated for a single lane loading assuming the AASHTO distribution factors but still lower than the target reliability index β_{target}=3.5 used for calibration of the AASHTO LRFD. The increase from the single lane loading is primarily due to the difference between the multiple lane loading and the close to doubling of the capacity of the bridge members when both lanes are loaded. However, the calculated β=2.97 is significantly lower than β=4.51 calculated when using a distribution factor equal to D.F.=0.60, which is extracted from the moment of the stresses at the critical cross-section of the bridge in its intact configuration.

The above calculations were based on a total live load of COV=25% for both one-lane and two-lane loadings. However, the AASHTO specifications were based on a COV=20% for two-lane

118

loading. The lower COV for two lanes is justified because the site-to-site variability was found to be lower when studying the maximum 75-year in two lanes of traffic, as observed by Ghosn et al. [50]. Using a COV for live load equal to 20% leads to a higher reliability index β=3.44 for the critical member of an intact twin steel box girder bridge under the effect of two-lane loading, which is closer to the target β*target=3.5*.

8.8.2.3 *Scenario #1: Two-Lane Bridge Loading After Fracture of One Box Assuming the Girders are Designed to Exactly Meet the AASHTO Specifications*

While the main box girders of the bridge in its intact configuration are expected to safely carry the applied maximum single-lane and two-lane loadings, the question that arises is whether a box girder bridge will be able to safely withstand the total loads should one of the box girders fracture. To perform the reliability analysis, two scenarios are considered. The first scenario is based on a commonly used model that assumes that the fractured bridge will be unable to carry any live load. The second scenario will use the load distribution observed from the finite element analysis performed in this study. Both scenarios assume that the deck and secondary members will be able to transfer some of the loads applied over the fractured girder to the intact girder. In fact, the finite element analysis performed for this simply supported bridge shows that if one of the two boxes is fractured, the remaining intact girder is expected to carry a significant portion of loads that were originally carried by the fractured girder. This section considers the first scenario, which assumes that the intact girder will carry all the live load in addition to its own dead weight. The second scenario assumes that the critical section of the intact girder will carry the moment due to its own dead weight plus 50% of the weight of the fractured girder in addition to 66% of the live load that was originally on the lane directly over the fractured girder. This means that the fractured girder will still be able to carry 34% of the moment of the live load traveling in the lane directly above it. The second scenario is analyzed in the next section (8.8.2.4).

To verify that a bridge whose members are designed to satisfy the current AASHTO strength limit state will be able to sustain the maximum live load expected on the bridge during a 5-year service period, the reliability analysis is repeated for the case when the entire two-lane load is to be carried by the only surviving box. The analysis is performed for a 5-year load because a fractured bridge must survive in its damaged configuration for a period of time until the fracture is detected and corrective actions are undertaken. The five-year period is consistent with the rating period used for the AASHTO LRFR calibration (Moses [55], Sivakumar and Ghosn [52]). The calculations are also repeated for a two-year service period, which would be consistent with the two-year biennial inspection cycle.

Given a single lane maximum load equal to $1.74\,L_{HS20}$ and using a multiple presence $=2\times0.85$ as indicated by Nowak [26] and an average dynamic amplification for two lanes $IM_{fact}=1.09$, the projected 5-year maximum two-lane load is obtained as:

$$\overline{LL}_T = mp \times L_{max-one\ lane} \times L_{HS20} \times IM_{fact} \times \lambda_{max} \times \lambda_{site-to-site} \times \lambda_{data} =$$
$$\overline{LL}_T = 2 \times 0.85 \times 1.74 \times 1883.8 \times 1.09 \times 1 \times 1 \times 1 \quad = 6074\ kip.ft$$

In this first scenario, it is assumed that all the load is being carried by one box; the distribution for this case will be $D.F. = 1.0$. Thus, $\overline{LL} = 6074\ kip.ft$. Also, in the first scenario, it is assumed that the fractured member will still be able to carry its own dead weight because the deck and secondary members will be able to bridge the gap over the fracture and transfer the load longitudinally to the cantilevered remaining parts of the box. Thus, this first scenario assumes that the surviving box will only need to carry its own dead weight.

For this first scenario, it is assumed that the dead load over the fractured beams will still be carried by the slab and that the composite intact beam will have to carry the total live load and only its own dead load. Thus, the mean applied load on the intact beam and its COV become:

The total applied load on one beam is

$$\bar{S} = \overline{LL}_\square + \overline{DL} = 6074 + 3833 = 9907\ kip.ft$$

And the COV is:

$$V_s = \frac{\sqrt{(V_{LL} \times \overline{LL})^2 + (V_{DL} \times \overline{DL})^2}}{\bar{S}} = 16\%$$

This leads to a reliability index for the five-year load assuming a COV=25% on live load:

$$\beta = \frac{ln\left(\frac{\bar{R}}{\bar{S}}\right)}{\sqrt{V_R^2 + V_S^2}} = \frac{ln\left(\frac{13088}{9907}\right)}{\sqrt{10\%^2 + 16\%^2}} = 1.48$$

When a COV=20% is assumed for the live load, the reliability index increases slightly to β=1.70; this constitutes a significant reduction from β=2.97 and 2.92 calculated for the 75-year reliability when the entire bridge is intact at its AASHTO strength limit state and is carrying two lanes of traffic. It is noted that the reliability index β=1.48 is lower than the target β_target=2.50 used during the calibration of the AASHTO LRFR procedures [55].

The reliability index β=1.48 was based on using the maximum live load for a 5-year service period, which is the recommended service period between rating cycles as per Moses [55] and Sivakumar and Ghosn [52]. However, regular inspections are conducted at 2-year intervals, and one would expect that any severe damage as that assumed herein would be detected during the routine biennial inspection. In such cases, as shown in Table 4-3, the projection of the maximum expected load in

a two-year period would reduce from 1.74 times an AASHTO truck load to 1.68 obtained by interpolating the results of Table 4-3 assuming 2000 trucks per day which, for a two-year period according to Table 4-3, would be equivalent to an ADTT=4000. In that case, the total live load moment on the bridge is LL_T=5865 kip.ft, and the reliability index increases respectively to β=1.62 for COV of live load equal to 25%.

These reliability index values would be reached only if the box girders rate at *R.F.*=1.0 at the LRFR inventory level, which for the first scenario assumes that the deck remains sound and capable of transferring the live load to the intact girder while it simultaneously remains capable of carrying the weight of the fractured girder longitudinally to the supports rather than transferring those loads to the remaining intact girder. It is also noted that the damaged system offers no additional reserve strength meaning that the bridge will collapse when the intact member reaches its limit capacity.

To find what rating factor would be required to achieve the target reliability index β_{target}=2.5 set for the AASHTO LRFR and assuming this first load distribution scenario, a live load COV=25%, over a two-year service period, which produces a total applied moment equal to 9698 kip.ft rather than the 9907 kip.ft associated with a five-year period, a reliability index β=2.50 would be reached if the mean resistance $\bar{R} = 15378\ kip.ft$ as obtained from the equation:

$$\beta = \frac{ln\left(\frac{\bar{R}}{\bar{S}}\right)}{\sqrt{V_R^2 + V_S^2}} = \frac{ln\left(\frac{\bar{R}}{9698}\right)}{\sqrt{10\%^2 + 16\%^2}} = 2.50$$

This corresponds to a nominal resistance R_n=13,730 kip.ft or a rating factor R.F.=1.29 at the LRFR Inventory level.

Assuming a live load COV=20%, a reliability index β=2.50 over a two-year service period would be reached when the nominal resistance R_n=13,047 kip.ft or a rating factor R.F.=1.19 at the LRFR Inventory level.

8.8.2.4 *Scenario #2: Two-Lane Bridge Loading After Fracture of One Box Assuming the Girders Are Designed to Exactly Meet the AASHTO Specifications*

In this scenario, it is assumed that the deck and secondary members will transfer an even more significant portion of the loads from the fractured girder to the intact girder. Specifically, the second scenario assumes that the critical section of the intact girder will carry the moment due to its own dead weight plus 50% of the weight of the fractured girder in addition to 100% of the load from the lane over the intact girder plus 66% of the live load that was originally on the lane directly over the fractured girder. These distributions were inferred from the FEM analysis performed in this study on the Texas University bridge and are assumed to be valid for different lateral positions of the trucks and for different strengths of bridges having the same configuration as the Texas University bridge.

The analysis performed in this section is meant to verify that a bridge whose members are designed to satisfy the current AASHTO strength limit state will be able to sustain the maximum live load expected on the bridge during a 5-year service period. The analysis is performed for a 5-year load because a fractured bridge must survive in its damaged configuration for a period of time until the fracture is detected and corrective actions are undertaken. The five-year period is consistent with the rating period used for the AASHTO LRFR calibration [55]. The calculations are also repeated for a two-year service period to be consistent with the two-year biennial inspection period.

Given a single lane maximum load equal to $1.74 \, L_{HS20}$ and using a multiple presence factor equal to 0.85 x 2 as inferred by the work of Nowak [26], and an average dynamic amplification for two lanes $IM_{fact} = 1.09$, the projected 5-year maximum two-lane load is obtained as:

$$\overline{LL_T} = mp \times L_{max-one\,lane} \times L_{HS20} \times IM_{fact} \times \lambda_{max} \times \lambda_{site-to-site} \times \lambda_{data} =$$
$$\overline{LL_T} = 2 \times 0.85 \times 1.74 \times 1883.8 \times 1.09 \times 1 \times 1 \times 1 \quad = 6074 \, kip.ft$$

In this second scenario, a large portion of this live load moment is assumed to transfer to the intact girder as shown from the finite element analysis, which showed that the deck in combination with the cross bracings were able to transfer only a portion of the moment longitudinally over the fractured section. Following Nowak [26], it is assumed that the total load is caused by two correlated trucks such that each lane would produce a moment equal to 3037 kip.ft (6074/2). Thus, the intact girder will carry 5041 kip.ft (=3037+0.66x3037 kip.ft). Furthermore, in this second scenario, it is assumed that the intact girder will carry its own dead weight moment (3833 kip.ft) plus 50% of the moment that was originally on the fractured girder = 1916.5 kip.ft (=3833x0.5). Thus, the total applied load on the intact girder is:

$$\bar{S} = \overline{LL} + \overline{DL} = 5041 + 5750 = 10791 \, kip.ft$$

And a COV

$$V_s = \frac{\sqrt{(V_{LL} \times \overline{LL})^2 + (V_{DL} \times \overline{DL})^2}}{\bar{S}} = 12\%$$

This leads to a reliability index:

$$\beta = \frac{ln\left(\frac{\bar{R}}{\bar{S}}\right)}{\sqrt{V_R^2 + V_S^2}} = \frac{ln\left(\frac{13088}{10791}\right)}{\sqrt{10\%^2 + 12\%^2}} = 1.24$$

This constitutes a further reduction from β=1.48, which was obtained from scenario 1. It is noted that both these values are significantly lower than the target β_{target}=2.50 used during the calibration of the AASHTO LRFR procedures [52, 55].

The calculations above are based on a COV for live load effect e1ual to 25%. If a COV on live load is reduced to 20%, then the reliability index increases to β=1.30.

Furthermore, the reliability index β=1.24 was calculated for a 5-year service period, which is the recommended service period between rating cycles as per Moses [55] and Sivakumar and Ghosn [52]. However, regular bridge inspections are conducted at 2-year intervals, and one would expect that any severe damage as that assumed herein would be detected during the routine biennial inspection. In such cases, as shown in Table 4-3, the projection of the maximum expected load in a two-year period would reduce from 1.74 times an AASHTO truck load to 1.68 obtained by interpolating the results of Table 4-3 assuming 2000 trucks per day, which for a two-year period according to Table 4-3 would be equivalent to an ADTT=4000. In that case, the reliability index increases slightly to β=1.28 and 1.40 for COV of live load equal to 25% and 20%, respectively.

These reliability index values would be reached only if the box girders rate at $R.F.$=1.0 at the LRFR inventory level, which for the first scenario assumes that the deck remains capable of transferring a significant portion of the live and dead loads to the intact girder while simultaneously the deck remains capable of carrying 50% of its own weight and 34% of the live load from one lane. It is also noted that the damaged system offers no additional reserve strength meaning that the bridge will collapse when the intact member reaches its limit capacity.

Assuming a live load COV=25%, a reliability index β=2.50 over a five-year service period would be reached if the mean resistance $\bar{R} = 16260\ kip.ft$ as obtained from the equation:

$$\beta = \frac{ln\left(\frac{\bar{R}}{\bar{S}}\right)}{\sqrt{V_R^2 + V_S^2}} = \frac{ln\left(\frac{\bar{R}}{10791}\right)}{\sqrt{10\%^2 + 12\%^2}} = 2.50$$

This corresponds to a nominal resistance R_n=14,518 kip.ft or a rating factor R.F.=1.40 at the LRFR Inventory level.

Assuming a live load COV=25%, a reliability index β=2.50 over a two-year service period would be reached when the nominal resistance R_n=14,285 kip.ft or a rating factor R.F.=1.36 at the LRFR Inventory level.

8.8.3 Reliability Analysis of Box Girder Bridge Analyzed in This Study

The above analysis was performed assuming that the box girders were designed to exactly satisfy the AASHTO strength limit state. In this section, we repeat the analyses by applying Equation (20) in combination with Equation (21) to calculate the reliability index for the 120-ft simple span bridge having the actual section properties of the bridge tested by the University of Texas and analyzed during this study.

The cross-section of one composite steel box is calculated to have a bending strength capacity R=19,027 *kip-ft* when considering the actual concrete strength f'c=6.23 ksi. This calculated capacity when compared to the expected mean value of $\bar{R} = 13,088 \, kip.ft$ shows an overcapacity of 1.45 over the expected mean value that would be obtained if the bridge were to be designed to exactly meet the AASHTO specifications. The overcapacity is by a ratio of 1.63 if compared to the design requirement $R_n = 11,686 \, kip.ft$ if the design requirement does not include the weight of a wearing, which the bridge analyzed in this study did not have.

As shown in Figure 5-42, the finite element analysis of the Texas University Bridge, when still intact, indicates that the entire system's capacity is about 1350 kips or 18.75 times the HS-20 truck load (18.75=1350/72 kips). Given that the HS-20 truck gives a moment $L_{HS20} = 1883.8 \, kip.ft$, the capacity of the entire intact bridge system to carry the live load, is found to be $18.75 \times 1883.8 = 35321 \, kip.ft$. Given an estimated dead load moment per beam $\overline{DL} = DC_n \times 1.05 = 3833 \, kip.ft$, the total bridge system capacity is estimated to be $R = 35,321 + 2 \times 3833 = 42,987 \, kip.f$t. This shows a bias in the system's capacity equal to $1.13 = \frac{42,987}{2 \times 19,027}$. This 1.13 ratio is the bridge overstrength, which gives a measure of the actual capacity of the entire system as compared to the methods we use to find the capacity of each individual member. The 1.13 ratio is very close to the bias b_R=1.12 assumed during the reliability analysis performed above, as recommended by Nowak (1999). Therefore, in these calculations, we assume that the mean strength capacity of the bridge members are each equal to $\bar{R} = \frac{42,987}{2} = 21,494 \, kip.f$t.

The results in Figure 5-42 for the analysis of the bridge with a fractured box shows that the damaged bridge can carry its own weight in addition to 430 kips before it fails. Even though this analysis was performed when the truck was not placed at the extreme edge of the bridge and thus may not be for the most critical loading condition, it indicates that failure of the fractured bridge is due to deck failure rather than the failure of the intact box. The failure of the damaged bridge corresponds to 6 HS-20 trucks (=430 kips/72 kips). When the truck is moved to the most critical lateral position, the analysis results shown in Figure 6-9 indicate that the deck fails at a load equal to 320 kips or 4.44 HS-20 trucks.

The finite element analysis shows that the deck of this bridge fails first. However, because the bridge is overdesigned, it would be of interest to study the reliability of the actual bridge and the

ability of the bridge members and that of the system to carry the entire live load before and after-fracture if the deck capacity is so high that the deck itself does not fail and will remain capable of transferring the load between the members. This is done to assess the reliability of the bridge system in cases where the deck is also overdesigned. Specifically, the analysis assumes a mean box girder resistance equal to 21494 *kip.ft,* which is equivalent to an LRFR Inventory Rating equal to 2.38. If one removes the overstrength factor equal to 1.13, the Inventory rating based on its calculated nominal member capacity becomes 2.03.

8.8.3.1 *One-Lane Loading of Intact Texas Bridge*

Using a mean resistance $\bar{R} = 21,494\ kip.ft$ as estimated from the finite element analysis, the reliability of the most critically loaded box girder when the bridge is loaded by the maximum 75-year one-lane load and assuming the AASHTO load distribution factor equal to D.F. =0.928 is obtained as:

$$\beta = \frac{ln\left(\frac{\bar{R}}{\bar{S}}\right)}{\sqrt{V_R^2 + V_S^2}} = \frac{ln\left(\frac{21,494}{7924}\right)}{\sqrt{10\%^2 + 14\%^2}} = 5.80$$

This is close to double the reliability index that would have been obtained if the bridge members were designed to exactly meet the AASHTO strength design requirements, which were originally found to produce a reliability index β= 2.92. If we assume a COV for live load equal to 20%, the reliability index for the intact member is equal to β=6.58.

When using a distribution factor equal to D.F.=0.60, which is extracted from the moment of the stresses at the critical cross-section of the bridge in its intact configuration as obtained through the finite element analysis, the live load moment on the girder under the loaded lane becomes:

$$\overline{LL}_T = L_{max} \times L_{HS20} \times IM_{fact} \times \lambda_{max} \times \lambda_{site-to-site} \times \lambda_{data} =$$

$$\overline{LL}_T = 1.74 \times 1883.8 \times 1.13 \times 1 \times 1 \times 1\ \ = 3704\ kip.ft$$

$$\overline{LL} = \overline{LL}_T \times \overline{D.F.} = 3704 \times 0.60 = 2222\ kip.ft$$

The COV for the live load on a girder is obtained from:

The total load, including live and dead load its COV, are thus obtained as:

$$\bar{S} = \overline{LL}_{\square} + \overline{DL} = 2222 + 3833 = 6055\ kip.ft$$

$$V_s = \frac{\sqrt{(V_{LL} \times \overline{LL})^2 + (V_{DL} \times \overline{DL})^2}}{\bar{S}} = 11\%$$

The reliability index for the box girder member of the Texas University bridge assuming bending failure:

$$\beta = \frac{ln\left(\frac{\bar{R}}{\bar{S}}\right)}{\sqrt{V_R^2 + V_S^2}} = \frac{ln\left(\frac{21494}{6055}\right)}{\sqrt{10\%^2 + 11\%^2}} = 8.52$$

This is a very high-reliability index reflecting the over strength of the actual girders used in the Texas University bridge.

8.8.3.2 *Two-Lane Bridge Loading of the Intact Texas University Bridge*

As explained earlier, the moment on a girder due to two-lane loading is calculated as

$$two\ lane\ \overline{LL}_T = L_{max} \times L_{HS20} \times IM_{fact} \times \lambda_{max} \times \lambda_{site-to-site} \times \lambda_{data} =$$

$$\overline{LL}_T = 0.85 \times 2.07 \times 1883.8 \times 1.09 \times 1 \times 1 \times 1 = 3613\ kip.ft$$

The distribution factor for the bridge with two lanes loaded is assumed to be equal to the one specified by AASHTO, *D.F.*=1.13. A *D.F.* value slightly greater than 1.0 assumes that the two trucks on the bridge may be slightly shifted laterally to favor one of the two girders.

$$\overline{LL} = \overline{LL}_T \times \overline{D.F.} = 3613 \times 1.113 = 4021\ kip.ft$$
The total applied load on one beam is:

$$\bar{S} = \overline{LL} + \overline{DL} = 4021 + 3833 = 7854\ kip.ft$$

And a COV

$$V_s = \frac{\sqrt{(V_{LL} \times \overline{LL})^2 + (V_{DL} \times \overline{DL})^2}}{\bar{S}} = 14\%$$

This leads to a reliability index:

If the bridge is analyzed for the 75-year two-lane loading, the reliability index of one box girder is obtained as:

$$\beta = \frac{ln\left(\frac{\bar{R}}{\bar{S}}\right)}{\sqrt{V_R^2 + V_S^2}} = \frac{ln\left(\frac{21,494}{7854}\right)}{\sqrt{10\%^2 + 14\%^2}} = 5.85$$

This value is based on the maximum 75-year two-lane loading and is compared to the reliability β=2.97, which was calculated for a bridge designed to exactly satisfy the AASHTO specifications for member strength. The higher reliability calculated herein reflects the over strength of the Texas University bridge as compared to a bridge that would have built to exactly meet the AASHTO strength limit state.

8.8.3.3 *Two-Lane Bridge Loading After the Fracture of One Box of the Texas University Bridge*

The analysis performed in this section is meant to verify that the Texas bridge would have been able to sustain the maximum live load expected on the bridge during a 5-year service period after the fracture of one of its two-box girders if the deck did not fail. The analysis is first performed for a 5-year load because a fractured bridge must survive in its damaged configuration for a period of time until the fracture is detected and corrective actions are undertaken. The five-year period is consistent with the rating period used for the AASHTO LRFR calibration [55]. The calculations are also repeated for a two-year service period to be consistent with the two-year biennial inspection period.

Given a single lane maximum load equal to $1.74\ L_{HS20}$ and using a multiple presence factor equal to 0.85 x 2 as inferred by the work of Nowak [26], and an average dynamic amplification for two lanes $IM_{fact} = 1.09$, the projected 5-year maximum two-lane load is obtained as:

$$\overline{LL}_T = mp \times L_{max-one\ lane} \times L_{HS20} \times IM_{fact} \times \lambda_{max} \times \lambda_{site-to-site} \times \lambda_{data} =$$
$$\overline{LL}_T = 2 \times 0.85 \times 1.74 \times 1883.8 \times 1.09 \times 1 \times 1 \times 1 \quad = 6074\ kip.ft$$

In this second scenario, a large portion of this live load moment is assumed to transfer to the intact girder as shown from the finite element analysis, which showed that the deck in combination with the cross bracings were able to transfer only a portion of the moment longitudinally over the fractured section. Following Nowak [26], it is assumed that the total load is caused by two correlated trucks such that each lane would produce a moment equal to 3037 kip.ft (6074/2). Thus, the intact girder will carry 5041 kip.ft (=3037+0.66x3037 kip.ft). Furthermore, in this second scenario, it is assumed that the intact girder will carry its own dead weight moment (3833 kip.ft) plus 50% of the moment that was originally on the fractured girder = 1916.5 kip.ft (=3833x0.5). Thus, the total applied load on the intact girder is:

$$\bar{S} = \overline{LL}_{□} + \overline{DL} = 5041 + 5750 = 10791\ kip.ft$$

And a COV

$$V_s = \frac{\sqrt{(V_{LL} \times \overline{LL})^2 + (V_{DL} \times \overline{DL})^2}}{\bar{S}} = 12\%$$

Taking a mean resistance value for the intact girder of the Texas University bridge $\bar{R} = 21{,}494$
This leads to a reliability index:

$$\beta = \frac{ln\left(\frac{\bar{R}}{\bar{S}}\right)}{\sqrt{V_R^2 + V_S^2}} = \frac{ln\left(\frac{21494}{10791}\right)}{\sqrt{10\%^2 + 12\%^2}} = 4.41$$

This constitutes a high probability of survival in case of fracture of this over strength bridge.

The calculations above are based on a COV for live load effect e1ual to 25% for the maximum 5-year live load. The reliability index is repeated for the 2-year maximum two-lane loading assuming that after the fracture of one box girder, the fractured member is still able to carry 50% of its own dead weight and that the weight of 83% one lane load plus 0.66 of the load of the lane immediately over the fracture box of the entire two-lane live load is shifted to the intact box.

Given a live load for two loaded lanes

$$\overline{LL}_T = mp \times L_{max-one\ lane} \times L_{HS20} \times IM_{fact} \times \lambda_{max} \times \lambda_{site-to-site} \times \lambda_{data} =$$
$$\overline{LL}_T = 2 \times 0.85 \times 1.68 \times 1883.8 \times 1.09 \times 1 \times 1 \times 1 \quad = 5864\ kip.ft$$

The live load per one lane is 2932 kip.ft (=5864/2). The live load on the intact girder becomes 4867 kip.ft (=2932+0.66x2932 kip.ft). Furthermore, the intact girder will carry its own dead weight moment (3833 kip.ft) plus 50% of the moment that was originally on the fractured girder = 1916.5 kip.ft (=3833x0.5). Thus, the total applied load on the intact girder is:

$$\bar{S} = \overline{LL} + \overline{DL} = 4867 + 5750 = 10617\ kip.ft$$

And a COV

$$V_s = \frac{\sqrt{(V_{LL} \times \overline{LL})^2 + (V_{DL} \times \overline{DL})^2}}{\bar{S}} = 13\%$$

Taking a mean resistance value for the intact girder of the Texas University bridge $\bar{R} = 21{,}494$
This leads to a reliability index:$\beta = \frac{ln\left(\frac{\bar{R}}{\bar{S}}\right)}{\sqrt{V_R^2 + V_S^2}} = \frac{ln\left(\frac{21{,}494}{10617}\right)}{\sqrt{10\%^2 + 13\%^2}} = 4.30$

This reliability value β=4.30 is significantly higher than the reliability index β=1.28 that would have been obtained if the bridge members were designed to exactly meet the AASHTO strength design requirements. Actually, the bridge tested by Texas University and analyzed in this study would have rated at $R.F. = 2.05$ if the nominal capacity R_n=19191 $kip.ft$ is used to find the rating at the AASHTO LRFR Inventory level.

$$R.F. = \frac{R_n - 1.25 DC_n}{1.75 L_n} = \frac{19{,}191 - 1.25 \times 3650}{1.75 \times 4071} = 2.05$$

8.8.4 Generalization to Two-Lane Loading of 120-Ft Twin Steel Box Girder Bridges After the Fracture of One Box

The analysis of fractured bridges is repeated for two scenarios. The first scenario assumes, as done earlier that the fractured bridge will still be able to carry its own dead weight but transfers all the live load to the intact girder. The second scenario assumes that the fractured girder will be able to transfer longitudinally 50% of its own weight away from the critical cross-section while the remaining 50% of its weight is transferred laterally to the intact girder's section. Similarly, 34% of the live load traveling in the lane over the fractured girder will transfer longitudinally away from the fractured section, while the remaining 66% of the live load is transferred laterally to the adjacent box girder section. The load transfer mechanism of scenario two was based on the nonlinear finite element analysis conducted in this study.

Table 8-1 gives for the first scenario, the LRFR Inventory Rating Factors required for the box girder members to ensure that the bridge will be able to sustain the fracture of one box girder and yet be able to support sufficient live of loading over a two-year or a 5-year service period until the damage is detected and necessary rehabilitation actions are undertaken. The table shows that an LRFR Inventory Rating on the order of R.F.=1.28 to 1.33 is required to meet a target reliability index β_{target}=2.50 should one of the two box girders fractures.

Table 8-1. LRFR inventory rating factors for box girders necessary for the fractured bridge to meet different target reliabilities, assuming that all the live load is transferred laterally to the intact girder but none of the dead load.

Target Reliability index, β_{target}	R.F. Inventory Rating for 5-year service life	R.F. Inventory Rating for 2-year service life
3.50	1.73	1.67
3.00	1.52	1.46
2.50	1.33	1.28
2.25	1.24	1.19
2.00	1.16	1.11
1.75	1.07	1.03
1.50	1.00	0.96
1.25	0.92	0.89
1.00	0.85	0.82

Table 8-2 gives for the second scenario, the LRFR Inventory Rating Factors required for the box girder members to ensure that the bridge will be able to sustain the fracture of one box girder and yet be able to support sufficient live of loading over a two-year or a 5-year service period until the damage is detected and necessary rehabilitation actions are undertaken. The results shown in Table

8-2 require more conservative section strengths because, for these box girder bridges, the dead load is higher than that of a one-lane live load. In this case, an Inventory Rating on the order of R.F.=1.00 is required to meet a target reliability index β_{target} on the order of 1.25. A target β_{target} = 2.50 would require an inventory rating on the order of 1.34 to 1.38.

Table 8-2. LRFR inventory rating factors for box girders necessary for the fractured bridge to meet different target reliabilities, assuming that all 50% of the dead load is transferred laterally to the intact girder along with 66% of the live load that was originally carried by the fractured girder.

Target Reliability index, β_{target}	R.F. Inventory Rating for 5-year service life	R.F. Inventory Rating for 2-year service life
3.50	1.74	1.69
3.00	1.55	1.51
2.50	1.38	1.34
2.25	1.30	1.27
2.00	1.23	1.19
1.75	1.15	1.12
1.50	1.08	1.05
1.25	1.01	0.98
1.00	0.95	0.92

8.8.5 Deck Strength Reliability Analysis

The finite element analysis as summarized in Figure 6-9 indicates that the bridge, after the fracture of one girder, was able to carry 4.44 HS-20 trucks before its deck fails when it is no longer able to transfer the applied load to the intact girder. At failure, the finite element analysis showed that the fractured girder was able to transfer 34% of its live load longitudinally across the fracture and 50% of its own weight. This means that up to this point, the intact girder carried at least 11,220 *kip.ft* in bending ($11,220\ kip.ft = 4.4 \times 0.66 \times L_{HS20} + 1.5 \times self\ weight = 4.4 \times 0.66 \times 1883.8 + 1.5 \times 3833\ kip.ft$). This value is significantly lower than the actual capacity of each of the box girders in the analyzed bridge but is only slightly lower than the nominal resistance R_n=11,686 kip.ft by a margin of only 4%. On the other hand, the applied load remains lower than the expected value $\bar{R} = 13,088\ kip.ft$ which would have been obtained if the girder were designed to exactly meet the AASHTO strength limit state. But, the margin of safety would have been extremely low

In this section, a simplified reliability analysis of the deck is performed to estimate the minimum criteria that the deck should satisfy in order to ensure that it will be able to transfer a minimum level of the load from the fractured box girder to the intact box.

The calculations are performed assuming that the load-carrying capacity of the deck is modeled using the yield line analysis approach described in Chapter 6, which is similar to the one proposed

130

earlier by the University of Texas. Based on a very limited number of checks, it is observed that the proposed yield line analysis provides a conservative estimate of the deck capacity when compared to the values obtained from the nonlinear finite element analysis. However, the level of conservativeness was inconsistent and depended on the applied truck configuration. Nevertheless, lacking any additional data, it is herein assumed that the yield line analysis would be applicable for the most heavily loaded trucks that could potentially cross a Florida two-box girder bridge that has sustained a severe fracture to one of its box girders.

As explained in Chapter 6, the yield line analysis process consists of the following steps:

a) Choosing a representative truck
b) Assigning yield lines based on the truck configuration. The yield lines are traced along the edge of the intact box closest to the fractured girder for a distance equal to the truck length and then connecting the two ends of that line to the center of gravity of the truck. Another set of two lines flare from the two ends of the line that runs along the intact box at 35° angles towards the damaged box to enclose three triangular areas within which the truck falls. This yield line pattern was inferred from the nonlinear finite element analysis of the bridge, including the concrete deck, as explained in Chapter 6.
c) Applying the dead weight and a truck load on the deck.
d) Incrementing the truck's load until a yield line failure takes place when the internal work from the yield line hinge rotations is equal to the work done by the weight of the portion of the deck inscribed within the yield lines and the incremented truck load.
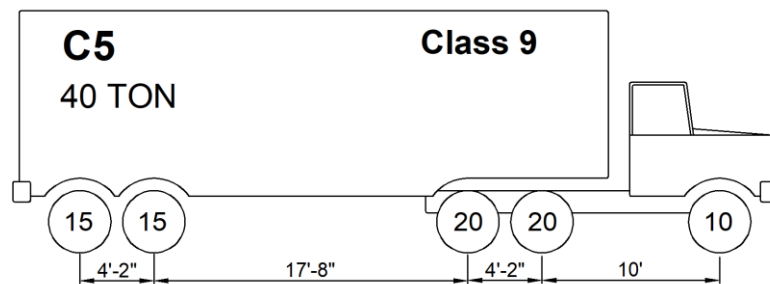
Figure 8-2. Representative semi-trailer truck.

The yield analysis was performed for several representative truck configurations. In these reliability calculations, we adopt the yield line pattern for Florida C5 load rating truck shown in Figure 8-2. This truck is selected because semi-trailer trucks are known to represent the vast majority of trucks on US highways. It is herein assumed that the maximum 5-year truck load and the maximum 2-year truck load are due to trucks having the C5 truck configuration. This truck produces a maximum moment equal to *1994.8 kip.ft* on the simple 120-ft bridge. This means that the 5-year L_{max}=1.74 L_{HS-20}=*1.74×1883.8=3278 kip.ft* maximum load effect as projected from the WIM data by the Auburn University team is equivalent to 1.64 times the weight of one C5 truck. On the other hand, the 2-year L_{max}=1.68 L_{HS-20}=*1.68×1883.8=3165 kip.ft* maximum load effect as

projected from the WIM data by the Auburn University team is equivalent to 1.59 times the weight of one C5 truck.

The yield line analysis indicates that the work done by one C5 truck is equal to 34.35 *kip-ft/ft* and that it is linearly related to the load factor. This indicates that the total work done by the maximum 5-year projected load is $L_{max} = 1.64 \times 34.35 = 56.33\ kip.ft/ft$. For the two-year load, $L_{max} = 1.59 \times 34.35 = 54.62\ kip.ft/ft$ This applied work done by the truck weight is then entered along with a mean value for the dynamic amplification $IM_{fact} = 1.13$ to find the mean applied load.

$$\overline{LL} = L_{max} \times IM_{fact} \times \lambda_{max} \times \lambda_{site-to-site} \times \lambda_{data} =$$

The five-year load gives: $\overline{LL} = 56.33 \times 1.13 \times 1 \times 1 \times 1 = 63.7\ kip.ft/ft$

The two-year load gives: $\overline{LL} = 54.62 \times 1.13 \times 1 \times 1 \times 1 = 61.7\ kip.ft/ft$

The COV for the applied random live load effect:

$$V_{LT} = \sqrt{V_{Lmax}^2 + V_{site-to-site}^2 + V_{data}^2 + V_{IM}^2} = \sqrt{9\%^2 + 20\%^2 + 5\%^2 + 9\%^2} = 24\%$$

No statistical information is available on the accuracy and variability in the yield line analysis process. The few sensitivity analysis performed in Chapter 6 show very large variations depending on the truck configuration. As a minimum, one can apply the same COV adopted above for the load distribution factor and account for these using:

The COV for the live load on a girder is obtained from:

$$V_{LL} = \sqrt{V_{LT}^2 + V_{DF}^2} = \sqrt{24\%^2 + 8\%^2} = 25\%$$

The work done by the weight of the 8-in deck is found to be 22.1 *kip.ft/ft* when the concrete weighs 0.15 *kip/ft³*, and it varies linearly with the weight. The work done by the weight of the railing is found to be 10.3 *kip.ft/ft* for a total work due to the nominal dead weight equal to DC_n=32.4 *kip.ft/ft*. The mean value of the dead load is thus:

$$\overline{DL} = DC_n \times 1.05 = 34.0\ kip.ft/ft$$

The COV for the live load on a girder is obtained from:

$$V_{DL} = 10\%$$

The total work done by the applied load, including live and dead load and its COV, are thus obtained as:

For the five-year load: $\bar{S} = \overline{LL} + \overline{DL} = 63.7 + 34 = 97.7 \; kip.ft/ft$

$$V_s = \frac{\sqrt{(V_{LL} \times \overline{LL})^2 + (V_{DL} \times \overline{DL})^2}}{\bar{S}} = 17\%$$

For the two-year load: $\bar{S} = \overline{LL} + \overline{DL} = 61.7 + 34 = 95.7 \; kip.ft/ft$

$$V_s = \frac{\sqrt{(V_{LL} \times \overline{LL})^2 + (V_{DL} \times \overline{DL})^2}}{\bar{S}} = 17\%$$

The analysis of the capacity of the yield line to carry the applied load is based on the moment capacity of the reinforced concrete deck. No statistical data is currently available on the moment capacity of concrete decks. Therefore, in this analysis, we will adopt the bias and COV used by Nowak [26] during the calibration of the AASHTO LRFD specifications.

Bending of reinforced concrete beams; $\quad\quad\quad\quad \overline{R} = 1.14 R_n \quad\quad V_R = 13\%$

It has been recommended that an engineer interested in verifying the ability of a concrete deck to transfer the applied vehicular load to the intact box girder of a two-girder bridge whose one of its two girders has fractured to perform a yield analysis similar to the one developed by this study after applying an adequate live load, dead load and resistance factors. The object of the yield analysis would be to verify that the external work done by the factored applied loads is lower than the factored internal work that would be done by the concrete deck. Based on the data provided in Chapter 6, this indicates that for this particular bridge configuration, the external work can be calculated following the steps a) through d) listed above with the understanding that a live load factor γ_{LL}, yet to be determined, be applied on the nominal live load represented by the truck shown in Figure 8-2 after applying an impact factor IM=1.3. The engineer should also apply a dead load factor γ_{DL}= 1.25 and a resistance factor ϕ=0.90.

Using the models developed in this study for this particular bridge and the C5 Class 9 truck shown in Figure 8-2, the safety check will be based on ensuring that the external work done by the factored applied loads exceeds the internal work done by the factored deck moment capacity. This safety check takes the form:

$IW \geq EW$

$EW = \gamma_{LL} \times IC_{LL} \times IM + \gamma_{DL} \times IC_{deck} \times \omega_{deck} + \gamma_{DL} \times W_{railing} \times IC_{railing}$

Where γ_{LL} is to be determined, IC_{LL}=34.35 is the influence coefficient for the C5 nominal truck configuration, IM=1.33 for consistency with AASHTO LRFD, γ_{DL}=1.25 is permanent load factor to be consistent with AASHTO LRFD, IC_{deck}=147.2 is the influence coefficient for the deck, ω_{deck}

is the specific weight of reinforced concrete which is usually equal to 0.15 kip/ft^3. IC$_{deck}$=147.2 is the influence coefficient for the deck, W$_{railing}$ is the total weight of the railing over the area within the contours of the yield lines and is 20.6, IC$_{railing}$ is the influence coefficient for the railing taken as 0.5. Thus, for a typical bridge, the external work is equal to:

$$EW = \gamma_{LL} \times 34.35 \times 1.33 + 1.25 \times 147 \times 0.15 + 1.25 \times 20.6 \times 0.5$$

The beam is considered to be safe if the internal work done by the concrete deck is equal to:

$IW=EW/\phi$

where the resistance factor ϕ=0.90 for the reinforced concrete deck in bending is used for consistency with the AASHTO LRFD.

$$IW = \frac{(\gamma_{LL} \times 34.35 \times 1.33 + 1.25 \times 147 \times 0.15 + 1.25 \times 20.6 \times 0.5)}{0.9}$$

$$IW = \gamma_{LL} 50.76 + 44.93$$

The mean bending capacity is

$$\overline{IW} = 1.14 \times IW = \gamma_{LL} \times 57.87 + 51.22$$

The reliability index for a box girder member designed to satisfy the AASHTO nominal resistance criteria using Lognormal Model assuming bending failure:

$$\beta = \frac{ln\left(\frac{\overline{IW}}{\overline{EW}}\right)}{\sqrt{V_{IW}^2 + V_{EW}^2}} = \frac{ln\left(\frac{\gamma_{LL} \times 57.87 + 51.22}{97.7}\right)}{\sqrt{13\%^2 + 17\%^2}}$$

To achieve a reliability β_{target}=2.5 when $\bar{S} = 97.7 \; kip.ft$ calculated for the 5-year load as currently adopted for the AASHTO LRFR, we should require a live load factor γ_{LL}=2.0.

For a two-year reliability β_{target}=2.5 when $\bar{S} = 95.7 \; kip.ft,$ the live load factor can be reduced to γ_{LL}=1.94.

$$\beta = \frac{ln\left(\frac{\overline{IW}}{\overline{EW}}\right)}{\sqrt{V_{IW}^2 + V_{EW}^2}} = \frac{ln\left(\frac{\gamma_{LL} \times 57.87 + 51.22}{95.7}\right)}{\sqrt{13\%^2 + 17\%^2}}$$

Table 8-3 gives the different live load factors necessary to achieve different reliability levels for the deck. Results for both a five-year rating period and a two-year bridge inspection cycle are given. As mentioned earlier, to achieve the target reliability, in addition to applying the

recommended live load factor, γ_{LL} given in Table 8-3, the yield line analysis implies the application of a dynamic amplification factor IM=1.33, a dead load factor γ_{DL}=1.25 and a moment resistance factor for the concrete deck equal to ϕ=0.9.

The analysis of the bridge deck for the 120-ft bridge studied in Chapter 6 indicates that the bridge deck in its current configuration and concrete strength will fail at a live load factor γ_{LL}=1.71. This indicates that its reliability index is on the order of β=2.0 for a five-year service period, or slightly higher than that for a two-year service period.

Table 8-3. Live load factors for deck analysis necessary to meet different target reliabilities.

Target Reliability index	5-year live load factor, γ_{LL}	2-year live load factor, γ_{LL}
3.50	2.69	2.61
3.00	2.32	2.26
2.50	2.00	1.94
2.25	1.85	1.79
2.00	1.71	1.65
1.50	1.44	1.39
1.00	1.21	1.16

Chapter 9   Summary and Discussion

In steel girder bridges, fatigue cracking is one of the most important phenomena affecting structural performance and integrity. In general, fatigue cracks are the result of out-of-plane distortion or other unanticipated secondary stresses at low fatigue resistance members. Development of fatigue cracking may lead in time to a full-depth fracture of one girder without noticeable bridge profile changes. It is critical to ensure that the bridge will have adequate capacity to prevent collapse until the next cycle of inspection discovers the damage. Bridges that a failure in an individual member could result in the total collapse of the structure are classified as fracture critical by AASHTO. It is required that inspection of these bridges be carried out using "arms-length" approach, which is costly and is a drain on the state's total bridge budget.

Currently, twin steel box girder bridges are classified as bridges with fracture critical members. However, recent research results indicate that these bridges could be redundant because of their high torsional resistance even after a full-depth fracture of one girder. The most notable study is the series of full-scale tests carried out by the University of Texas-Austin that demonstrated a high level of internal redundancy of twin steel box girder bridges. The main question as to what load level should be used and established using a scientific approach still remains as a task to be accomplished. Further, many questions remain on the expected failure mode of the damaged twin steel box girder bridges and the methods for assessing the bridge performance, before these bridges could be removed from the non-redundant list. An upcoming specification developed by Purdue researchers establishes a set of requirements for redundancy of twin steel box girder bridges that could be considered at the design stage to assure redundancy. This specification applies only to bridges with continuous spans.

The objective of this project is to establish a design target performance and safety level for twin steel box girder bridges, and outline a methodology and approach for assessing the redundancy of these bridges of simple and continuous spans. The Florida Bridge Inventory was statistically analyzed to determine the available range of each functional and geometric parameter like span length, number of spans, number of lanes, deck width, and radius of curvature in existing twin steel box girder bridges, and at the end, the bridge tested at the University of Texas with the span length of 120 ft was selected as a baseline model for developing information for preliminary reliability analysis of twin steel box girder bridges. Furthermore, Weight-in-Motion (WIM) data from 32 stations collected throughout four years (2013-2016) in the state of Florida was used to develop a live load model the bridge would be subjected to during two-year inspection intervals. The data left after filtering out vehicles less than 20-kip gross vehicle weight (GVW) were used for further analysis.

Since the controlling design criteria in the design are moments and shears, the load effects, i.e., moment and shear created by these vehicles, are important. Each vehicle in the database was run over an influence line for the considered span length of 120 ft, and moment and shear were

calculated. For a better interpretation of results, the moment and shear produced by each vehicle were divided by the corresponding load effects of the HS-20 design truck. It was assumed that 32 WIM stations in Florida have representative truck traffic for Florida. The statistical parameters of mean maximum and coefficient of variation (CV) of live load (moment) were presented and were used for reliability analysis calculations.

A detailed finite element model was developed to simulate the local and global behavior of bridge superstructure using steel girder made composite with concrete deck slabs. The model was validated with a series of available test results on full-scale and scaled bridges. These included the full-scale, University of Nebraska bridge consisting of three I-shaped steel girders and the FIU scaled twin steel box girders. The finite element models were shown to simulate very well both the global and local behavior of the tested bridges in their intact condition as well as after one girder fracture (FIU bridge). The University of Texas bridge was then modeled to investigate the failure mode and ultimate load-carrying capacity of the bridge subjected to truck loading after a full-depth fracture in one of the girders. Material nonlinearity and concrete damage plasticity were used to consider tensile cracking and compressive crushing of the concrete deck in the model. Contact surface was used for defining the surface contact between the railings and also to consider the possibility of support uplift during the loading. Moreover, according to the results of available tests and analyses, shear studs between girders and deck slab may influence the onset of failure in the deck, and therefore shear studs were also modeled. A large number of analyses were performed on this bridge chosen as a case study for reliability analysis.

Three tests were conducted by the University of Texas on the full-scale bridge. The first test was performed to evaluate the behavior of the bridge under loading simulated by the weight of concrete blocks (slightly over HS-20 loading and equal to 76 kips total) after a sudden fracture at the bottom flange of the exterior girder. The second test was conducted by cutting the bottom flange and 83% web of the exterior girder to study the fractured bridge behavior under the same loading as Test 1. And finally, the ultimate load test was performed to investigate the ultimate load-carrying capacity of the fractured bridge. The ultimate test was performed by increasing a uniform load applied using sand over the HS-20 truck outline area until the bridge collapsed. The finite element model was validated against these available experimental test results conducted by the University of Texas. In addition to global behavior, the model was capable of simulating the local behavior, including the development of the deck yield line pattern.

After verification of the FE model, the bridge was analyzed for two scenarios of the intact and fractured bridge. The bridge was loaded in terms of the HS-20 design truck positioned at the mid-span over the fractured girder to generate maximum moment at the section with fracture (one lane loading). In order to study the effect of truck position on the failure mode and the ultimate load-carrying capacity, the HS-20 truck was positioned in four different locations across the bridge width. The results showed that concrete deck failure is the governing failure mode of the fractured

bridge subjected to truck loading at different positions. The sensitivity analysis indicated that one-way shear is the bridge failure mode when the truck is positioned closest to the intact girder, and concrete deck bending is the bridge failure mode when the truck position transversely is farthest from the intact girder. Nevertheless, the truck position at farthest from the intact girder with the concrete deck bending failure resulted in the lowest bridge load carrying capacity and was considered as the dominant failure mode.

In order to consider the effect of variation in bridge configurations and material properties, as well as truck loading configuration on the bridge failure mode, sensitivity analysis for the deck concrete compressive, deck thickness, and truck configuration was conducted. Different concrete compressive strength and deck thickness varying from 4 ksi to 6.2 ksi and 7.5 in. to 8.5 in., respectively, and three trucks with loading configurations other than HS-20 truck were selected for this purpose. The C5 truck that weighs a total of 80 kips and with a total length of 36 feet that is longer and heavier than the HS-20 design truck configuration and EV3 truck with a total weight of 86 kips (14 kips heavier than HS-20 Truck) and a total length of 19 feet (9 feet shorter than the HS-20 truck configuration used in this study) that creates larger longitudinal and transverse bending moment in the bridge were selected as Florida legal and emergency vehicles. Moreover, WIM data in the state of Florida was also used for selecting a typical truck, which creates a larger moment and shear for a 120 ft simple span bridge. The selected truck, which is called here WIM Data-FL, has a gross vehicle weight of 120 kips distributed over seven axles (Class 13 based on FHWA vehicle category classification).

The results showed that variation in material properties and truck loading configuration would not change the dominant mode of failure for the twin steel box girder bridge considered in this study after a fracture in one girder. Therefore, to simplify the process and avoid the need for FE analysis for each loading case, a simple and unified yield line analysis based on the concrete deck damage pattern observed in the FE analysis to determine the bridge load carrying capacity subjected to different truck configurations. This model is an improvement to a model proposed earlier by the University of Texas that was developed based on limited test and analysis results. In this newly proposed pattern, the truck is positioned closest to the railing, where its center of gravity coincides with the mid-span over the fracture. The length of the longitudinal yield line (b) is considered equal to the truck length. To find the angle of the diagonal lines (α in Figure 6-18), a parametric analysis was conducted to find an angle that results in capacity in agreement with patterns and capacity obtained from FE analysis. The results show that the simplified method with the 35° gives the best average capacity ratio compared to the FE analysis. This unified pattern, however, provides a conservative estimate of the deck capacity when compared to the values obtained from nonlinear finite element analysis.

Moreover, a series of analyses were conducted on the bridge to investigate the behavior of the bridge in intact and damaged scenarios under dead and increasing live load. The goal was to

determine the distribution of dead and live loads before and after the fracture of one girder. According to the results, the dead load moment on the intact girder increases by about 50 percent once a fracture occurs. The fractured girder has a very small stiffness at the middle (one can assume hinge or very weak spring), so it attracts only a negligible moment compared to the intact girder. The live load moment analysis for the intact bridge shows that the left girder (loaded) carries 60%, and the right girder carries 40% of the live load. However, after the fracture, the right girder (intact) carries most of the live load (66%) because of a decrease in stiffness of the fractured girder. Nevertheless, the fractured girder is undamaged through most of its length. Since the truck loads are applied through its wheel footprints, and rear and front wheels are at a distance from the middle, the fracture girder can transfer some portion of live load (34%) through those segments as a cantilever beam. Unlike the live load, the dead load is distributed along the bridge, and the fractured girder is able to transfer a noticeable portion through its undamaged end segments.

A simplified reliability analysis of a twin steel box girder bridge superstructure and its deck was presented to estimate the minimum criteria that a deck should satisfy in order to ensure that it can transfer a minimum level of load between the box girders, which one of the girders sustain a severe fracture. The recommendation was made based on meeting a reliability index target, β_{target}=2.5 over a five-year service period. In addition, a list of live load factors was provided for different target reliability levels for the case of the two-year service period. The calculations are performed assuming that the load-carrying capacity of the deck is modeled using the yield line analysis approach presented in this study that provides a conservative estimate of the deck capacity compared to FE analysis. Nevertheless, lacking any additional data, it is herein assumed that the yield line analysis would be applicable for the most heavily loaded trucks that could potentially cross a Florida twin steel box girder bridge that has sustained a severe fracture to one of its box girders. In addition to applying the recommended live load factor, the yield line analysis implies the application of a dynamic amplification factor IM=1.33, a dead load factor γ_{DL}=1.25 and a moment resistance factor for the concrete deck equal to ϕ=0.9.

A reliability analysis was carried out to estimate the reliability index corresponding to various live load levels based on the simplified yield line bending failure of the deck only. The analysis of the bridge deck for the 120-ft bridge studied in this report, therefore, indicates that the bridge deck in its current configuration and concrete strength and ignoring the possible contribution of the railings to help carry some of the load will fail at a live load factor γ_{LL}=1.71 when the deck's concrete strength is set at f'$_c$=6.23 ksi as determined from the tests. This indicates that its reliability index is on the order of β=2.0 for a five-year service period, or slightly higher than that for a two-year service period. However, For the bridge to provide sufficient reliability to sustain the possible fracture of one of its two-box girders, it is important that the remaining box girder has sufficient load carrying capacity to withstand the entire live load that may cross the damaged bridge with one fractured box. This can be ensured if the bridge's box girders outside of fracture can satisfy a minimum Rating Factor.

The analysis of fractured bridges was repeated for two scenarios. The first scenario assumes that the fractured bridge will still be able to carry its own dead weight but transfers all the live load to the intact girder. The second scenario assumes that the load distribution follows the nonlinear FE analysis conducted in this study that the bending moment of the intact girder will increase by 50% under dead load, and 66% of the live load in the lane over the fractured girder will transfer to the intact girder. Based on the assumed scenarios, the LRFR Inventory Rating Factors required for the box girder members to ensure that the bridge will be able to sustain the fracture of one box girder and yet be able to support sufficient live of loading over a two-year or a 5-year service period until the damage is detected. The results show that an LRFR Inventory Rating on the order of R.F.=1.28 to 1.33 and R.F.= 1.34 to 1.38 is required for scenarios I and II, respectively, to meet a target reliability index β_{target}=2.50 should one of the two box girders fractures.

The bridge analyzed in this study has an LRFR Inventory Rating of R.F.=2.05. Thus, the intact box girder is capable of sustaining a significant level of the live load as well as a large proportion of the dead load that was originally carried by the fractured girder, and that the bridge failure is definitely expected to be due to the failure of the deck as explained earlier. It should be noted that in simple span steel bridges, service limit states are normally the governing design limit states, and the strength LRFR Inventory Rating is considerably greater than one and in the order of the bridge considered in this study.

9.1 Reliability and Safety Analysis of Twin Steel Box Girder Bridges with One Fractured Girder: Case Study

The objectives of this study included developing a simple analytical method for estimating the capacity of twin steel box girder bridges following the fracture of one girder and estimating the reliability index associated with the system after the fracture of one girder. The methodology described here uses one particular case study. It should be noted that aspects of the methodology described below are universal and apply to all twin steel box girder bridges. As it is described in the report, the methodology involves three major steps as elaborated below;

1- Determining the loading expected on the bridge in the time interval between routine inspections. For the case of bridges in Florida, this was performed according to the analysis of WIM data from 32 stations across the state for the time frame between 2013-2016. The results were presented in the form of Cumulative Distribution Functions (CDF) per Gross Vehicle Weights (GVW). The CDFs were translated into CDFs per multiple HS-20 truck weights that would generate the same moment in the bridge under consideration. Calculate statistical data as mean and coefficient of variation for various ADTT for a two-year interval.

2- Estimating the load-carrying capacity of the bridge after fracture of on girder. Based on the results of experiments performed by others and finite element analysis, it was determined that the dominant failure mechanism after fracture of one girder is deck bending failure. A

140

simple method for determining the yield line pattern for bending failure of the deck was developed that is an improvement to the existing model proposed by the University of Texas. The simple model can predict the bridge deck capacity after the fracture of one girder for various truck configurations, with or without the contribution of the railing. It was shown that truck configuration, deck thickness, and concrete material properties would not change the dominant failure mechanism.

3- Reliability analysis for the safety of the bridge after the fracture of the girder. A representative truck configuration was first selected for reliability analysis. The reliability index was calculated in the range of 1 to 3.5 for variation of live load factor that would fail the bridge deck. The live load factor was calculated using the simple analytical method for bridge deck bending capacity and AASHTO LRFD factors. The Live load factor can then be used to determine the reliability index for bridge deck failure. For the bridge considered in this study, the live load factor was calculated to be 1.71 that corresponds to a reliability index of 2.1 when a 2-year interval is considered. To assure that the intact girder will not fail before the bridge deck, reliability analysis was performed considering the potential for bending failure of the intact girder. Reliability index in the range of 1 to 3.5 was calculated for variation of inventory rating factor for the intact girder. Distribution of dead and live load after fracture of one girder was assumed to follow two scenarios, the more conservative and straight forward of which anticipating for the intact girder to carry its own dead weight and all the live load. For the bridge under consideration, the inventory rating factor was 2.05, corresponding to a reliability index higher than 3.5, indicating that the girder is capable of sustaining a significant level of live load and allowing for deck failure to occur first. For the bridge under consideration with its 120-ft span length, one truck in each lane and two trucks side-by-side was considered as the critical case for the moment capacity of the intact girder.

Application of the three general steps described above to one particular case study was achieved using the following ten steps;

1- As-built drawings for the bridge under consideration were obtained and reviewed.
2- Information on truck live loading was gathered, and CDFs per GVW were developed. Representative truck configuration was identified and translated the CDF for a multiple of representative truck weights that would produce equivalent bending moments. Mean and coefficient of variation for various ADTT for a two-year interval were calculated (Section 4.1.5).
3- Using the simple analysis method developed in this study for yield line bending capacity, the bridge deck capacity after fracture of one girder was estimated for the representative truck configuration (Section 6.3).
4- Using AASHTO LRFD factors, the live load factor that would result in the failure of the deck was calculated.
5- Using the reliability analysis method, as described in Section 8.8.5 of the report or Table 8-3, the reliability index controlled by the bridge deck capacity was calculated.

6- The critical loading configuration was determined for the moment along the span in the bridge in the form of single or multiple truck loading, or truck and uniform loading in each lane, and/or truck in one lane or multiple lanes transversely.

7- It was assumed that after the fracture of one girder, the intact girder has to carry its self-weight and all the live load, and calculated the moment acting on the intact girder (Section 8.8.2.3).

8- The reliability index for the intact girder after one girder fracture was calculated using the procedure described in Section 8.8.4 of the report.

9- The least of reliability index between the index for the intact girder (calculated in Item 8) and that for the deck capacity (calculated in Item 5) is controlling.

10- In this case, the controlling reliability indexes are deemed to be indicating the bridge will be safe after the fracture of one girder until the next inspection period, and the bridge can be taken as redundant or not fracture critical.

Among the conclusions of this study obtained by conducting experimental, numerical, and analytical investigations is that simple-span twin steel box girder bridges have a reserve capacity to carry the traffic loads following the complete fracture of one girder.

The steps described above are also illustrated in Figure 9-1.

Figure 9-1. Reliability and safety analysis of twin steel box girder bridges with one fractured girder: A case study.

143

References

[1]   J. Yu, P. Ziehl, B. Zrate, and J. Caicedo, "Prediction of fatigue crack growth in steel bridge components using acoustic emission," *J. Constr. Steel Res.*, vol. 67, no. 8, pp. 1254–1260, 2011.

[2]   C. F. Scheffey, "PT pleasant bridge collapse-conclusions of federal study," *Civ. Eng.*, vol. 41, no. 7, p. 41, 1971.

[3]   AASHTO, *AASHTO LRFD Bridge Design Specifications* (8th ed.). Washington, D.C.: American Association of State Highway and Transportation Officials, 2017.

[4]   AASHTO and AWS, "AASHTO/AWS D1.5M/D1.5: Bridge Welding Code,." Washington, DC, Miami, FL, 2015.

[5]   AASHTO, "The Manual for Bridge Evaluation," American Association of State Highway and Transportation Officials. *Washington, D.C.*, 2011.

[6]   M. Abedin, S. Farhangdoust, and A. B. Mehrabi, "Fracture detection in steel girder bridges using self-powered wireless sensors," in *In Risk-Based Bridge Engineering: Proceedings of the 10th New York City Bridge Conference, August 26-27, 2019*, 2019, p. 216.

[7]   M. Abedin and A. B. Mehrabi, "Novel Approaches for Fracture Detection in Steel Girder Bridges," *Infrastructures*, vol. 4, no. 3, p. 42, 2019.

[8]   R. J. Conner, R. J. Dexter, and H. Mahmoud, *Inspection and management of bridges with fracture-critical details: A synthesis of highway practice*, vol. 354. Transportation Research Board, 2005.

[9]   R. L. Idriss, K. R. White, C. B. Woodward, and D. V Jauregui, "After-fracture redundancy of two-girder bridge: Testing I-40 bridges over Rio Grande," in *Proceedings of the Fourth International Bridge Engineering Conference*, 1995, pp. 316–326.

[10]   Y. Park, W. Joe, J. Park, M. Hwang, and B. H. Choi, "An experimental study on after-fracture redundancy of continuous span two-girder bridges," *Int. J. Steel Struct.*, vol. 12, no. 1, pp. 1–13, 2012.

[11]   R. J. Connor, F. J. B. Martín, A. Varma, Z. Lai, and C. Korkmaz, *Fracture-Critical System Analysis for Steel Bridges*. Washington, D.C.: Transportation Research Board, 2018.

[12]   M. Irfaee and H. Mahmoud, "Mixed-Mode Fatigue and Fracture Assessment of a Steel Twin Box-Girder Bridge," *J. Bridg. Eng.*, vol. 24, no. 7, article no. 4019056, 2019.

[13]   C. G. Hovell, *Evaluation of Redundancy in Trapezoidal Box-Girder Bridges Using Finite Element Analysis*, University of Texas at Austin (Doctoral dissertation), TX, USA, 2007.

[14]   V. A. Samaras, J. P. Sutton, E. B. Williamson, and K. H. Frank, "Simplified method for evaluating the redundancy of twin steel box-girder bridges," *J. Bridg. Eng.*, vol. 17, no. 3, pp. 470–480, 2012.

[15]   W. Lin, T. Yoda, Y. Kumagai, and T. Saigyo, "Numerical study on post-fracture redundancy of the two-girder steel-concrete composite highway bridges," *Int. J. Steel Struct.*, vol. 13, no. 4, pp. 671–681, 2013.

[16]   W. Lin, T. Yoda, N. Taniguchi, H. Lam, and K. Nakabayashi, "Post-Fracture redundancy evaluation of a twin box-girder shinkansen bridge in Japan," in *IABSE Conference, Guangzhou 2016: Bridges and Structures Sustainability - Seeking Intelligent Solutions - Report*, 2016, vol. 106, no. 6, pp. 675–682.

[17]   J. W. Fisher, A. W. Pense, and R. Roberts, "Evaluation of fracture of Lafayette Street bridge," *J. Struct. Div.*, vol. 103, no. ASCE 13051 Proceeding, 1977.

[18]   S. Quiel, *Forensic analysis of the steel girder fracture in the I-95 Brandywine River Bridge*, *Res. Exp. Undergraduates Report, Univ. Notre Dame*, 2003.

[19]   B. J. Neuman, "Evaluating the Redundancy of Steel Bridges: Full-Scale Destructive Testing of a Fracture Critical Twin Box-Girder Steel Bridge," University of Texas at Austin (Doctoral Dissertation), TX, USA, 2009.

[20]   J. Kim and E. B. Williamson, "Finite-element modeling of twin steel box-girder bridges for redundancy evaluation," *J. Bridg. Eng.*, vol. 20, no. 10, article no. 4014106, 2015.

[21]   J. Peterson and P. Cashin, "Design Solutions for Steel Bridges in Milwaukee's Marquette Interchange," in *New Horizons and Better Practices*, 2007, pp. 1–9.

[22]   H. V Pham, "Evaluation of Redundancy of Twin Steel Box-Girder Bridges," Florida International University (Doctoral dissertation), FL, USA, 2016.

[23]   E. B. Williamson, J. Kim, and K. H. Frank, "Redundancy evaluation of twin steel box-girder bridges using finite element analyses," in *Structures Congress 2010*, 2010, pp. 2793–2802.

[24]   R. L. Idriss, K. R. White, C. B. Woodward, and D. V Jauregui, "Evaluation and testing of a fracture critical bridge," *NDT E Int.*, vol. 28, no. 6, pp. 339–347, 1995.

[25]   J. H. Daniels, W. Kim, and J. L. Wilson, "Guidelines for redundancy design and rating of two-girder steel bridges, Final Report, November 1988, 365p.," 1988.

[26]   A. S. Nowak, "Calibration of LRFD bridge design code," 1999.

[27]   Federal Highway Administration, "Traffic Monitoring Guide," *Fhwa*, 2001.

[28]   J. M. Kulicki, W. G. Wasser, D. R. Mertz, and A. S. Nowak, "Bridges for Service Life Beyond 100 Years: Service Limit State Design." Washington, D.C., 2015.

[29]   A. Ramesh Babu, O. Iatsko, and A. S. Nowak, "Comparison of Bridge Live Loads in US and Europe," *Struct. Eng. Int.*, pp. 1–10, 2018.

[30]   Federal Highway Administration, "Traffic Monitoring Guide," *Fhwa*, 2016.

[31]   R. Babu and A. Mogali, "Quantifying the Fatigue Damage Accumulation in Bridges," 2019.

[32]   Dassault, "ABAQUS Documentation," *ABAQUS/CAE Doc.*, 2016.

[33]   S. Kathol, A. Azizinamini, and J. Luedke, *Strength Capacity of Steel Girder Bridges. Final Report*. Washington, DC: Transportation Research Board, 1995.

[34]   M. Abedin and A. B. Mehrabi, "Effect of Cross-Frames on Load Distribution of Steel Bridges with Fractured Girder," *Infrastructures*, vol. 5, no. 4, p. 32, 2020.

[35]   M. Abedin, S. Maleki, N. Kiani, and E. Shahrokhinasab, "Shear lag effects in angles welded at both legs," *Adv. Civ. Eng.*, vol. 2019, 2019.

[36]   M. Abedin, N. Kiani, E. Shahrokhinasab, and S. Mokhtari, "Net section fracture assessment of welded rectangular hollow structural sections," *Civ. Eng. J*, vol. 6, no. 7, pp. 1243–1254, 2020.

[37]   J. Lubliner, J. Oliver, S. Oller, and E. Onate, "A plastic-damage model for concrete," *Int. J. Solids Struct.*, vol. 25, no. 3, pp. 299–326, 1989.

[38]   ACI Committee, "318, Building Code Requirements for Structural Concrete (ACI 318–14) and Commentary (ACI 318R–14)," *Am. Concr. Institute, Farmingt. Hills, MI*, p. 519, 2014.

[39]   N. Naeimi and M. A. Moustafa, "Three-Dimensional Finite Element Modeling of UHPC Using Total Strain Crack Models," in *AFGC-ACI-fib-RILEM Int. Symposium on Ultra-High Performance Fibre-Reinforced Concrete, UHPFRC*, 2017, pp. 2–4.

[40]   E. O. L. Lantsoght, A. de Boer, C. van der Veen, and J. C. Walraven, "Effective shear width of concrete slab bridges," *Proc. Inst. Civ. Eng. - Bridg. Eng.*, vol. 168, no. 4, pp. 287–298, Dec. 2015.

[41]   E. Rahimi, A. Shamshiripour, R. Shabanpour, A. Mohammadian, and J. Auld, "Analysis of

Transit Users' Response Behavior in Case of Unplanned Service Disruptions," *Transp. Res. Rec.*, p. 0361198120911921, 2020.

[42] C. Topkaya, E. B. Williamson, and K. H. Frank, "Behavior of curved steel trapezoidal box-girders during construction," *Engineering Structures*, vol. 26, no. 6. pp. 721–733, 2004.

[43] J. P. Sutton, J. M. Mouras, V. A. Samaras, E. B. Williamson, and K. H. Frank, "Strength and ductility of shear studs under tensile loading," *J. Bridg. Eng.*, vol. 19, no. 2, pp. 245–253, 2014.

[44] E. Hognestad, "A Study of Combined Bending and Axial Load in Reinforced Concrete Members," University of Illinois at Urbana Champaign, College of Engineering …, 1951.

[45] M. Ghosn and F. Moses, *Redundancy in highway bridge superstructures*, vol. 406. Transportation Research Board, 1998.

[46] M. Ghosn, J. Yang, D. Beal, and B. Sivakumar, *Bridge system safety and redundancy*, no. Project 12-86. 2014.

[47] M. Ghosn, F. Moses, and D. M. Frangopol, "Redundancy and robustness of highway bridge superstructures and substructures," *Struct. Infrastruct. Eng.*, vol. 6, no. 1–2, pp. 257–278, 2010.

[48] G. Fiorillo, F. Miao, and M. Ghosn, "Direct Redundancy Evaluation of Bridges Designated as Fracture-Critical," *J. Perform. Constr. Facil.*, vol. 30, no. 3, p. 4015045, 2016.

[49] F. Miao and M. Ghosn, "Reliability-based progressive collapse analysis of highway bridges," *Struct. Saf.*, vol. 63, pp. 33–46, 2016.

[50] M. Ghosn, B. Sivakumar, and F. Miao, "Development of state-specific load and resistance factor rating method," *J. Bridg. Eng.*, vol. 18, no. 5, pp. 351–361, 2013.

[51] B. Sivakumar, M. Ghosn, and F. Moses, *Protocols for collecting and using traffic data in bridge design*, vol. 683. Transportation Research Board, 2011.

[52] B. Sivakumar and M. Ghosn, "Recalibration of LRFR live load factors in the AASHTO manual for bridge evaluation," *NCHRP Proj.*, no. 20–07, 2011.

[53] M. Ghosn and F. Moses, "Reliability calibration of bridge design code," *J. Struct. Eng.*, vol. 112, no. 4, pp. 745–763, 1986.

[54] P. Thoft-Cristensen and M. J. Baker, *Structural reliability theory and its applications*. Springer Science & Business Media, 2012.

[55] F. Moses, *Calibration of load factors for LRFR bridge evaluation*, no. Project C12-46 FY'97. 2001.

Appendix A. Florida Bridge Inventory

Table A- 1. Florida Bridge Inventory.

Brkey	Year built	Year recon.	Design Load	Service Type	No. Main Spans	Max. Span (ft)	Length (ft)	Skew	Deck Width (ft)	Level service	Lanes	Road Width (ft)	No. of Box Girders	Radius of Curvature (ft)
870725	1991	0	HS 20+ Mod	Highway	5	113.19	1605.2	99	44.6	Ramp	2	41.9	2	440.74
860521	1989	0	HS 20	Overpass	3	120	272	13	29.5	Ramp	1	27	2	F3-3,778.719 ft /F4-5770.578 ft
755926	1989	0	HS 20	Highway	3	125	309.3	12	47.4	Service	2	44.9	2	300
170113	1980	0	HS 20+ Mod	Highway	7	131.89	850.1	44	42.6	Mainline	2	39.6	2	unknown
860526	1990	0	HS 20	3rd Level	5	132	623.6	99	38.8	Ramp	1	36	2	11385.156
860527	1990	0	HS 20	3rd Level	5	132	625.8	99	38.9	Ramp	2	36	2	5729.578
874643	2008	0	A	Highway	5	136	610	0	44.1	Ramp	2	36	2	175
480159	1979	0	HS 20	Highway	5	140.1	649.9	0	38.7	Mainline	2	36	2	1968.5
480165	1979	0	HS 20	Highway	10	144	1343	0	29.8	Ramp	1	30	2	430
480163	1980	0	HS 20	Highway	10	150	7746	0	42.7	Spur	2	40.2	2	1809.859
480162	1979	0	HS 20	Highway	8	152	984	0	29.7	Ramp	1	27	2	8094.224
750724	2012	0	Railroad	Highway	2	153.5	301.9	99	36.1	Ramp	1	32.7	2	694.49
720580	1991	0	HS 20+ Mod	Highway	7	154.86	1631.89	0	79.72	Ramp	4	70.87	2	Spans 1 - 3, 5729.58; ; Spans 4 - 7, 280.14
480164	1980	0	HS 20	Highway	16	156	8136	0	42.8	Spur	2	40	2	880
750589	2010	0	Railroad	Highway	2	160.2	272.2	99	35.1	Ramp	1	32	2	286.48
860563	1990	0	HS 20+ Mod	Overpass	3	163.44	780.8	0	46.6	Ramp	2	44	2	C1-11459.16 / C2 440.74
860525	1990	0	A	Overpass	2	164.3	302.3	17	29.8	Ramp	1	27	2	not available
755929	1989	0	HS 20	Highway	1	166.7	166.7	0	43	Service	2	40	2	400
750729	2007	0	Railroad	Highway	2	172	292	10	36	Ramp	1	33	2	5560
860628	1994	0	A	Overpass	9	175	1275	0	31.1	Ramp	1	28	2	C1-205 / C2-320
860523	1990	0	HS 20	Overpass	1	175	175	16	71.3	Mainline	4	68.5	2	18093.404
860540	1988	0	HS 20+ Mod	Overpass	6	177.8	830.2	0	42.8	Ramp	2	40	2	954.9297

147

Brkey	Year built	Year recon.	Design Load	Service Type	No. Main Spans	Max. Span (ft)	Length (ft)	Skew	Deck Width (ft)	Level service	Lanes	Road Width (ft)	No. of Box Girders	Radius of Curvature (ft)
860561	1990	0	HS 20+ Mod	3rd Level	7	181.1	1077	0	46.5	Ramp	2	44	2	C1-11459.16 / C2 440.74
860539	1990	0	HS 20+ Mod	Overpass	5	183.3	769.8	0	42.8	Ramp	2	40	2	716.1972
720706	2007	0	HS 20	Highway	2	186.25	325.9	0	36.1	Ramp	1	33	2	775
750402	1990	0	HS 20	Overpass	8	186.5	1249	0	29.8	Ramp	1	27	2	1150
871007	2006	0	HS 20	Highway	3	186.5	454.5	0	45	Ramp	2	42	2	1146
720701	2007	0	HS 20	Highway	2	186.6	353.5	0	36.1	Ramp	1	32.9	2	775
720697	2004	0	HS 20+ Mod	Highway	2	188.46	364.67	11	43.08	Mainline	2	40	2	straight
720698	2004	0	HS 20+ Mod	Highway	2	188.46	364.67	11	43.08	Mainline	2	40	2	straight
750515	2006	0	Railroad	Highway	10	190	1629	0	45.6	Ramp	2	42	2	432.42
720502	1982	0	HS 20	Highway	4	191.93	574.15	0	41.99	Alternative	2	39.7	2	1647.168
720503	1982	0	HS 20	Highway	4	195.87	576.12	0	41.99	Mainline	2	39.7	2	1647.168
100634	2015	0	A	Overpass	2	196	392	0	36.5	Ramp	1	33	2	424
720705	2007	0	HS 20	Highway	2	196.6	353.3	0	36.1	Ramp	1	32.6	2	775
720702	2007	0	HS 20	Highway	2	198.4	346.7	0	36.1	Ramp	1	33	2	775
720519	1999	0	HS 20+ Mod	Highway	3	199.48	399	0	43.31	Mainline	2	40	2	straight
720520	1999	0	HS 20+ Mod	Highway	3	199.48	399	0	43.31	Mainline	2	40	2	straight
871008	2006	0	Railroad	Highway	4	200	724.5	0	29.75	Ramp	1	26.8	2	1869
874641	2006	0	A	Highway	4	200	606.6	0	42	Ramp	2	39	2	520.87
754128	2003	0	HS 20+ Mod	Highway+p	5	201	946.8	99	42	Mainline	2	30.5	2	400
750730	2007	0	Railroad	Highway	1	201.5	201.5	0	36.1	Mainline	1	33	2	440.74
860542	1990	0	HS 20	3rd Level	12	203.7	1964.8	0	42.6	Ramp	2	40	2	1145.9156
860541	1990	0	HS 20+ Mod	3rd Level	10	206.3	1639	99	42.8	Ramp	2	40	2	818.5111
860667	2012	0	A	Highway	3	206.3	579.5	99	62.5	Ramp	3	59.5	2	C1-620 / C2-14714
861000	1998	−1	HS 20+ Mod	Overpass	3	208	525	99	43	Ramp	2	40	2	440.737
860598	1994	0	HS 20	3rd Level	9	210	1458.5	0	31.1	Ramp	1	28	2	C1-1145.92 / C2-352.95 / C3-694.49
930469	2001	0	HS 20+ Mod	Highway	5	210.8	863.1	0	36.3	Ramp	1	33.1	2	492

148

Brkey	Year built	Year recon.	Design Load	Service Type	No. Main Spans	Max. Span (ft)	Length (ft)	Skew	Deck Width (ft)	Level service	Lanes	Road Width (ft)	No. of Box Girders	Radius of Curvature (ft)
860538	1990	0	HS 20+ Mod	4th Level	21	210.8	4055.3	0	42.8	Ramp	2	39.8	2	2864.789
920169	1996	0	HS 20+ Mod	Overpass	4	212.93	627.62	0	49.5	Ramp	2	46.5	2	1273.24
860537	1989	0	HS 20+ Mod	Overpass	5	213	695	0	42.8	Ramp	2	40	2	716.1972
920195	2007	0	HS 20	Highway	9	215.8	1678	15	36.6	Mainline	1	36.6	2	818.51
750723	2012	0	Railroad	Highway	5	217	877.1	99	36.1	Ramp	1	32.8	2	1320
874639	2008	0	HS 20	Highway	6	217	1248.5	0	43.1	Ramp	2	40	3,4,2	395.14
720707	2007	0	HS 20	Highway	10	217	1777.7	0	49.1	Ramp	2	45.6	2	775
860393	1989	0	HS 20	3rd Level	4	223	779	0	29.8	Ramp	1	27	2	690
860337	1982	0	HS 20	Overpass	2	225.07	438.6	0	42.6	Ramp	2	39.6	2	2864.789
860338	1982	0	HS 20	Overpass	2	225.07	438.65	0	42.6	Mainline	2	39.6	2	852
750571	2008	−1	A	Highway	7	230	1447	0	36.6	Ramp	1	33.8	2	710
874640	2007	0	HS 20+ Mod	Highway	5	230	968.1	0	36.6	Ramp	1	27	2	545.67
860390	1989	2013	A	3rd Level	5	233	976.3	0	29.8	Ramp	1	27	2	600
920602	2006	0	HS 20+ Mod	Overpass	7	233	1167.8	0	49.1	Ramp	1	46	2	1120
860652	2013	0	A	Highway	2	239.1	400.9	0	59.6	Ramp	4	56.6	2	855.16
550122	1997	0	HS 20+ Mod	Highway	6	243	994	0	43	Bypass	2	40	2	5729.578
750561	2010	0	A	Highway	3	246.3	518.9	34	58.6	Mainline	3	47.5	2	6000
750804	2016	0	A	Highway	4	246.9	957.3	0	43.3	Ramp	2	40	2	1145.916
860601	1994	0	A	Overpass	8	250	1275	0	31.1	Ramp	1	28	2	C1-205 / C2-320
720685	2007	0	HS 20	Highway	2	251	420	0	35.59	Ramp	1	32.4	2	578.576
480201	2007	0	HS 20	Highway	8	251.3	1685.5	0	47.1	Ramp	2	44	2	954.93
860638	1995	0	HS 20	Overpass	7	255	1305	0	31.1	Ramp	1	28	2	C1-22963.31 / C2-600 / C3-330
920601	2006	−1	HS 20+ Mod	3rd Level	5	255.4	1038	99	49.1	Ramp	1	46	2	1359
750560	2010	−1	A	Highway	3	258.3	518.75	34	58.5	Mainline	3	47.5	2	6000
870972	2005	0	HS 20	Highway	3	262.47	682.41	42	33.63	Mainline	1	30.51	2	150
871024	2008	0	A	Highway	11	265.5	2167.5	0	27	Ramp	1	27	2	4584

Brkey	Year built	Year recon.	Design Load	Service Type	No. Main Spans	Max. Span (ft)	Length (ft)	Skew	Deck Width (ft)	Level service	Lanes	Road Width (ft)	No. of Box Girders	Radius of Curvature (ft)
100491	1985	0	HS 20+ Mod	Overpass	1	266	266	0	43.6	Ramp	2	40	2	3,819.72
870996	2004	0	A	Highway	2	273	528	32	75.08	Ramp	4	72	2	11459
860600	1995	0	HS 20	Overpass	7	275	1305	0	31.1	Ramp	1	28	2	C1-22963.31 / C2-600 / C3-330
750825	2012	0	A	Overpass	7	281	1564	99	46.5	Ramp	2	43	2	890
720704	2007	0	HS 20	Highway	8	282.5	1714.7	0	36.1	Ramp	1	33.06	2	775
100498	1987	0	HS 20+ Mod	Overpass	1	285.9	285.9	0	43.3	Ramp	2	40.3	2	1,145.92
930493	2004	0	HS 20+ Mod	Highway	3	297.8	657	0	33.6	Ramp	1	30.5	2	656
860654	2013	0	A	Overpass	7	301	1691	0	36.1	Ramp	1	33	2	855.16
860653	2013	−1	A	Highway	9	304	2092.9	0	36.1	Ramp	1	33	2	C1-22918 / 1145.92
100712	2008	−1	Railroad	3rd Level	7	324	1759	99	49.5	Ramp	2	46	2	774.00
720686	2007	0	HS 20	Highway	5	372	1552	0	33.6	Ramp	1	30.5	2	Span 1, Straight; Spans 2 & 3, 531.988; Spans 4 & 5 , straight

Appendix B. Design of the University of Texas Twin Steel Box Girder Bridge Based on *AASHTO LRFD*

In this section, the University of Texas bridge is designed based on AASHTO LRDF speciation for different limit states to determine the level of overdesign and compare the reliability of the bridge main box girder members as built to the reliability if it were to be designed to exactly meet the AASHTO Specifications' strength limit state criteria. According to the AASHTO specifications, the nominal resistance, R_n, of a box girder should meet the criterion set in the following equation:

Strength I:

$$R_n \geq 1.25DC_n + 1.5\, DW_n + 1.75LL_n \tag{B-1}$$

where the nominal live load, LL_n, is calculated based on the moment effect of the HS-20 truck, which for this 120-ft span bridge is found to be $L_{HS20} = 1883.8\, kip.ft$ times the dynamic allowance IM=1.33 plus the effect of a lane load ω_{lane}= 0.64 kip/ft, which produces a lane load moment $L_{lane} = 1152\, kip.ft$. The total live load is multiplied by the lane distribution factor ($D.F.$) so that:

$$LL_n = (L_{HS20} \times IM + L_{lane}) \times D.F. \tag{B-2}$$

which for box girder bridges is calculated based on the number of loaded lanes, N_L, and the number of box girders, N_b, using the equation:

$$D.F. = 0.05 + 0.85\frac{N_L}{N_b} + \frac{0.425}{N_L} \tag{B-3}$$

which produces a lane distribution factor $D.F. = 1.113$.

The final nominal live load is found to be $L_n = 4071\, kip.ft$ which when combined with a dead load moment $DC_n = 3649.8\, kip.ft$, $DW_n = 553\, kip.ft$ and implemented in Equation (B-1) produces a nominal moment capacity $R_n = 12516.2\, kip.ft$. Thus, the nominal moment capacity of the particular bridge analyzed in this study, which is R_n=17972.2 kip-ft is 1.44 times the value that is required by the AASHTO specifications. The bridge is design for the following limit states: Demand/Capacity ratio: 12516.2/17972.2=**0.69**

Strength IV:

$$R_n \geq 1.5DC_n + 1.5\, DW_n \tag{B-4}$$
$$1.5 \times 3649.8 + 1.5 \times 553 = 6304.4\, kip.ft$$

Demand/Capacity ratio: 6304.4/17972.2= **0.35**

Service I:

The girder must be checked for service limit state control of permanent deflection. This check is intended to prevent objectionable permanent deflections due to expected severe traffic loadings.

$$\Delta_{allowable}= (Span/800)\times(12\ in./1ft)=1.8\ in. \tag{B-5}$$

The bridge deflection is taken as the larger of the deflection resulting from the design truck alone (1.24 in.) and the deflection resulting from 25 percent of the design truck taken together with the design lane load (1.18 in.).
The live load portion of Load Combination Service I is used, including the dynamic load allowance.

Demand/Capacity ratio: 1.24/1.8= **0.69**

Service II:

The flange stresses for both steel flanges of composite sections must satisfy the following requirement:

$$f_f \leq 0.95R_hF_{yf} \tag{B-6}$$

$f_{bot\text{-}girder} = 43.17$ ksi
$f_{top\text{-}girder} = -37.9$ ksi
$0.95R_hF_{yf} = 47.5$

Demand/Capacity ratio: 43.17/47.5= **0.91**

Table A- 2. The University of Texas bridge design summary.

Limit State	Demand/Capacity Ratio			
	Strength I	Strength IV	Service I	Service II
UT bridge	0.69	0.35	0.69	0.91

Dead load assumptions for calculating the moments:
$D_{Railing} = 653.4$ kip.ft
$D_{Girder\ and\ Diaphragms}= 761.4$ kip.ft
$D_{Concrete\ Slab}= 2235$ kip.ft
The total dead load of structural components and Non-structural attachments (DC) = 3649.8
Future wearing surface: $W_{fws} = 0.140$ kcf
Future wearing surface thickness: $t_{fws} = 2.5$ in. (assumed)
$D_w= 553$ kip.ft